Comparative evaluation of methanol production processes using natural gas: A thermodynamic and economic assessment

vorgelegt von
M.Sc.

Timo Dominik Blumberg

geb. in Berlin

von der Fakultät III - Prozesswissenschaften
der Technischen Universität Berlin
zur Erlangung des akademischen Grades

Doktor der Ingenieurwissenschaften
-Dr.-Ing.-

genehmigte Dissertation

Promotionsausschuss
Vorsitzender: Prof. Dr. F. Behrendt
Gutachter: Prof. Dr.-Ing. G. Tsatsaronis
Gutachterin: Prof. Dr. T. Morozyuk
Gutachter: Dr.-Ing. Y.D. Lee

Tag der wissenschaftlichen Aussprache: 27.07.2018

Berlin 2018

Acknowledgement

Berlin, 2018

Timo Blumberg

Zusammenfassung

In der vorliegenden Arbeit werden verschiedene erdgasbasierte Prozesse für die Erzeugung von Methanol aus thermodynamischer und ökonomischer Sicht analysiert. Kommerziell verfügbare Technologien sowie vielversprechende Zukunftsalternativen für erhöhte Effizienz, eine verbesserte Wirtschaftlichkeit sowie reduzierte Treibhausgasemissionen werden bewertet und miteinander verglichen. Die untersuchten Prozesse basieren auf der indirekten Synthese mit dem Zwischenschritt der Synthesegaserzeugung. Die einzelnen Prozesse sind durch eine unterschiedliche Reformierungstechnologie sowie einen isothermen Synthesereaktor gekennzeichnet. Die Auswahl geeigneter Reformer- und Reaktortechnologien sowie deren Betrieb ist entscheidend für das thermodynamische Verhalten einer Methanolanlage. Parameterstudien werden für die Basistechnologien durchgeführt um vorteilhafte Betriebsparameter für hohe Umsätze und Ausbeuten zu bestimmen. Die kommerziell gängige Nutzung einfacher Reformertechnologien erzielt nur geringe Produktausbeuten. Eine Kombination verschiedener Reformer- und Gaskonditionierungstechnologien ermöglicht die Bereitstellung eines hochreaktiven Synthesegases für höhere Produktausbeuten. Eine Untersuchung der beiden kommerziell erfolgreichsten Reaktortechnologien weist wesentlich höhere Methanolausbeuten für die isotherme Reaktortechnologie als für die adiabate Mehrbett-Quench-Technologie aus. Eine Energieanalyse zeigt, dass die Prozesse mit endothermer Reformertechnolgie zwangsläufig eine Koproduktion von Methanol und Elektrizität für hohe Effizienz ermöglichen müssen. Die CO_2 Nutzung durch trockene Reformierung und Hydrierung im Synthesereaktor wird erfolgreich für eine Verringerung der Emissionen und des Brennstoffbedarfs eingesetzt. Im Rahmen einer Exergieanalyse werden die größten irreversibilitäten für die Prozesse mit endothermer Reformierung ermittelt. Diese können der Verbrennung zur Prozesswärmebereitstellung zugeordnet werden. Mit Hilfe der Ertragsbedarfsmethode werden Kostenvorteile für die Prozesse mit autothermer Technologie aufgedeckt. Die Ergebnisse der exergoökonomischen Analyse zeigen, dass der Zwei-Stufen-Reformierungsprozess die Produkte zu den niedrigsten Kosten bereitstellen kann, während das Methanol im konventionellen Dampfreformierungsprozess am teuersten produziert wird. Auf der Komponentenebene haben die Verbrennungseinheiten aufgrund von Irreversibilitäten und der Luftkompressor als kapitalintensivste Komponente den größten Kosteinfluss. Im Falle einer Monetarisierung des integrierten CO_2 steigen die Produktkosten an, wobei der Trockenreformierungsprozess von der größten Kostensteigerung betroffen ist. Eine erweiterte Exergieanalyse für den Zwei-Stufen-Reformierungsprozess zeigt, dass der Großteil der Exergievernichtung endogen und für einige wichtige Komponenten vermeidbar ist.

Abstract

In the work, different processes for the production of methanol from natural gas are analysed from a thermodynamic and an economic point of view. Commercially available processes and promising future alternatives for increased thermodynamic efficiency, improved economics and reduced greenhouse gas emissions are assessed and compared. The analysed processes are based on the indirect synthesis route via syngas production. Each design features a different reforming technology in conjunction with an isothermal synthesis reactor. The choice of suitable reformer and reactor technologies and their operation are decisive for the thermodynamic performance of a methanol plant. Parameter studies are conducted for the basic technologies to determine favorable operation conditions for high reactant conversion and product yield. The commercial use of simple reforming technologies only enables for a low methanol yield. A combination of different reforming technologies with application of syngas conditioning units generates a highly reactive syngas for improved methanol yield. The two main reactor technologies in commercial use are investigated - the isothermal reactor technology allows much higher conversion rates than the adiabatic multi-bed quench reactor technology. An analysis of the energy distribution shows that the processes with endothermic reforming inevitably feature a co-production of electricity for a high efficiency. CO_2 utilization by dry reforming and direct hydrogenation in the synthesis unit is successfully used for an reduction of the emissions and the fuel demand. A conventional exergetic analysis identifies the highest inefficiencies for processes with endothermic reforming technology, these being primarily related to the combustion unit for process heat supply. The application of the total revenue requirement method identifies economic advantages of the processes with autothermal reforming caused by a low fuel consumption. Furthermore, the results of an exergoeconomic analysis show, that the two-step reforming process can generate the products at the lowest cost, while methanol obtained from a conventional steam methane reforming process is associated with the highest cost. On a component level, the combustion units and the air compressor have the highest cost significance due to the cost rate associated with irreversibilities and the investment, respectively. In case of a monetization of the integrated CO_2, the product cost increase. In particular in the dry reforming process, the product costs are affected by the cost of CO_2. An advanced exergetic analysis of the two-step reforming process reveals that the major part of the inefficiencies is endogenous and avoidable for some important components.

Contents

List of Figures

List of Tables

Nomenclature

E_A	activation energy	J
f	exergoeconomic factor	%
h	specific enthalpy	J/kg
$\dot{H}$	enthalpy flow rate	W
i	interest rate	%
k	heat transfer coefficient	W/m^{2}K
ke	kinetic energy	J/kg
KE	total kinetic energy	J
$\dot{m}$	mass flow rate	kg/s
$\dot{n}$	mole flow rate	mol
p	pressure	bar
pe	specific potential energy	J/kg
PE	potential energy	J
$\dot{Q}$	rate of heat transfer	J
r	relative cost difference	%
R	reaction rate	
R	ideal gas constant	J/molK
T	temperature	°C, K
U	internal energy	J
U	overall heat transfer coefficient	W/(m^{2}K)
V	volume	m^3
$\dot{W}$	power	W
x	mole fraction	mol/mol
x	steam quality	kg$_{steam}$/kg$_{tot}$
y_D, y_D^*	exergy destruction ratio	%

Greek symbols

α	scaling exponent	—
Δ	difference	—
ε	exergetic efficiency	%

η_s	isentropic efficiency	%
η_{pol}	polytropic efficiency	%
τ	time/ residence time / annual full load hours	s / h
ρ	density	kg/m^3

Superscripts

$\cdot$	time derivative	
$\sim$	mole related	
ads	adsorption	
AV	avoidable	
CH	chemical	
EN	endogenous	
EX	exogenous	
PH	physical	
UN	unavoidable	
0	refers to ambient conditions	
C	compressor	
ch	chemical	
cv	control volume	
D	destruction	
el	electrical	
F	fuel	
gen	general	
i, j	running indicies	
in	inlet	
k	*k*-th plant component	
l	length of tube	
L	levelized	

Subscripts

L	loss	
n	nominal, number of years	
out	outlet	

pol	polytropic
PE	purchased equipment
s	isentropic
sys	subsystem
tot	overall system
T	turbine/ expander
X	capacity of the amount X
Y	capacity of the amount Y

Abbreviations

AFUDC	allowance for funds during construction time
AGR	acid gas removal
ASU	air separation unit
ATR	autothermal reforming
C	distillation column in flowsheet
CC	carrying charges
CCS	carbon capture and storage
CCU	carbon capture and utilization
CELF	constant escalation levelization factor
CEPCI	chemical engineering plant cost index
CM	compressor in flowsheet
CMR	combined methane reforming
CtL	coal to liquid
D	drum in flowsheet
DISTL	distillation subsystem
DMR	dry methane reforming
DMT	Dimethylterephtalat
ECO	economizer
EVA	evaporator
FC	fuel cost
FCI	fixed capital investment
GtL	gas to liquid
HEX	heat exchanger in flowsheet
HHV	higher heating value
HP	high pressure

Abbreviations

HRSG	heat recovery steam generator
ICI	Imperial Chemical Industries
IP	intermediate pressure
LHV	lower heating value
LCOE	levelized cost of electricity
LCOM	levelized cost of methanol
LP	low pressure
LPM	liquid phase methanation
MEA	Monoethanolamine
MC	minimum cost
MTBE	methyl-tert-butylether
MTO	Methanol-to-olefins process
MTP	Methanol-to-propylene process
mtpd	metric tons per day
NIST	National Institute of Standard and Technology
O/C	oxygen to carbon ratio
OMC	operation and maintenance cost
PC-SAFT	perturbed chain statistical association fluid theory
PEC	purchased equipment cost
R	reactor in flowsheet
RE	subsystem reforming unit
RKS-BM	Redlich-Kwong-Soave with Boston-Matthias alpha function
RTFR	recycle to feed ratio
S/C	steam to carbon ratio
SH	superheater
SPECO	specific exergy costing
SMR	steam methane reforming
SYN	subsystem synthesis unit
T	turbine in flowsheet
TCI	total capital investment
WGS	water-gas shift

Chapter 1

Introduction

The rising standard of living of an evermore growing world population requires a steady economic growth, which can only be ensured by covering the demand for energy and other essential products. The use of fossil feedstock currently is the only mean to cope with rapid increasing consumption. Coal, oil and natural gas are still considered as a reliable and relatively inexpensive primary resource of energy for most industrialized countries. In 2017 fossil fuels accounted for 82.7% of the global energy supply [1, 2]. Besides being the major energy source, fossil substances also serve as a feedstock for a great variety of derived hydrocarbon materials and products. The range comprises petrochemical and chemical products, including plastics, pharmaceuticals and synthetic fuels, as well as diesel oil or gasoline [3]. The chemicals and petrochemicals sector is one of the fastest growing industries and by far the largest industrial energy consumer accounting for 10% of the global final energy consumption in 2014 [4]. The strong demand growth for hydrocarbon derived products, in particular methanol, increases the pressure on the diminishing fossil resources.

A problem closely linked to the intensive use of fossil fuels refers to the emissions of greenhouse gases. Utilization of coal, oil and natural gas in the energy and industrial sector significantly contributes to anthropogenic greenhouse gas emissions. For example, the chemicals and petrochemicals sector accounted for 13% of the direct industrial CO_2 emissions in 2014 [4]. Carbon capture and storage (CCS) and carbon capture and utilization (CCU) represent the two major strategies to reduce these emissions [5]. While CCS technologies are developed with a focus on capturing and storing CO_2 in large quantities, novel concepts for the chemical valorization of CO_2 are developed simultaneously. Although the former technology is currently considered as the most promising avoidance mechanism, the CCU appears to be more beneficial, due to the abatement of CO_2 emissions in conjunction with an effective production of valuable fuels and chemicals [6].

In the last decade, new carbon utilization concepts were proposed for the integration of CO_2 as an auxiliary feedstock or commodity into Gas-to-Liquids (GtL) processes [7, 8]. The large-scale production of methanol from its predominating feedstock natural gas (NG) attracted particular attention, due to the increasing product demand and abundant gas resources [9–12].

A promising approach to reduce the dependence from fossil fuels is based on a successive substitution by methanol and its variety of hydrocarbonecous derivates. In 2005, this approach has been suggested by George Olah, USA, who entitled the concept as the *Methanol Economy* [13–15]. Thus, methanol as an integral part of life not only would constitute a partial replacement of fossil fuels, but also could act as a CO_2 sink when chemical recycling is integrated into future and retrofitting manufacture concepts.

Methanol is rated among the most important feedstock for the chemical, petrochemical and energy industries, with a worldwide demand of 83 million metric tons in 2016 [16, 17]. At present, the bulk chemical is almost exclusively produced from synthesis gas derived by catalytic reforming and gasification of natural gas and coal. Commercial synthesis routes are associated with technological complexity, energy intensity and costly operation. However, only fossil-based processes enable a large-scale production which can hold pace with the rising demand. The derivation from biomass, biogas, municipal waste and agricultural by-products is of minor significance [3]. Alternative direct conversion processes without the initial and cost intensive step of syngas production may economically be more viable but up to now industrially not feasible.

Fig. 1.1 shows the distribution of the methanol demand in millions of metric tons and is based on data obtained from [18]. The global production capacity is represented by a solid line, while the dashed line refers to the average annual operation rate of the facilities. The capacity is forecasted to grow annually by an average rate of 5% to reach approximately 140 million metric tons in 2020 [16, 19]. Within the last decade, China became by far the biggest consumer of methanol [19]. Furthermore, the highest growth rates are predicted for the Chinese market [20]. The low operation rate of 63% in 2015 is forecasted to increase to 80% in 2020. This improvement is caused by the decommissioning of small coal-based plants and their substitution by modern gas-based large-scale plants. The graphs show that the available production capacity at high operation rates is sufficient to cover the worldwide methanol demand.
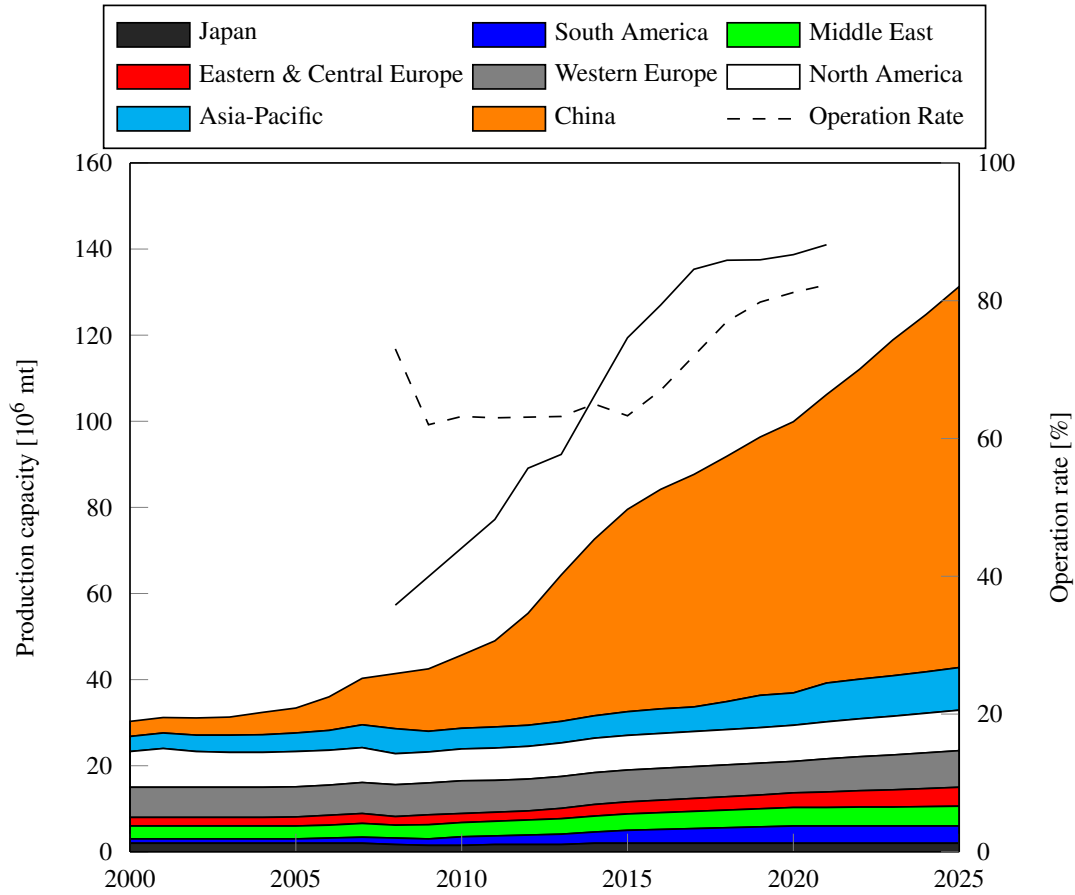
Figure 1.1: Methanol demand forecast (based on [18]).

Methanol is produced worldwide in about 90 plants which are mainly located in Asia, the Middle East, North and South America, and Europe [21]. In the recent past, a variety of production facilities moved from the consuming regions to the countries of the raw material extraction, which thus could incorporate a further step in the value chain [3]. At present the majority of the methanol plants in commercial operation has a capacity below 3,000 metric tons per day (mtpd) [6]. The increase in demand and the economies of scale drive the progress towards higher single plant capacities of up to 10,000 mtpd [22–24]. Depending on the region, the predominant feedstock for methanol generation is natural gas or coal. The Middle East and Asia have become the largest methanol-producing regions, due to abundant reserves of raw materials [6]. While large-scale production facilities are established in regions with large reserves of low-cost natural gas (the Middle East, North America), small coal-based plants are installed in the Asian-pacific region. The major part of the global methanol production capacity is based on natural gas, due to lower complexity of the synthesis route, higher operation rate, and reduced investment

and operation cost [25]. Most likely, gas will continue to be the main feedstock in the near future, due to recent advances in shale gas production [26, 27].

The construction of a variety of new plants with large capacities increases the competition and in general the pressure on the market price. During the past 20 years, the methanol market price was subject to large temporal and regional volatilities [28]. Considering the time period since 1975, the average methanol wholesale price amounts to 175 US$/mt [25]. Between 1998 and 2018, methanol was traded on different markets for 100 - 850 US-$ per metric ton. Generally, due to a variety of impact factors an estimation and prediction of the production cost and market price is difficult. A study conducted by Masih et al. [29] suggests that the natural gas price is the driving force for the methanol price level in Europe and North America, while the prices on the Asian continent are determined by the growing market of derivative products. Lastly, the increasing availability of shale gas in the United States resulted in a significant drop of natural gas prices, leading to a higher profitability of the domestic methanol production [6]. Independent of market conditions, the production cost can actively be reduced by the selection of suitable technology and the associated advantages through upscaling.
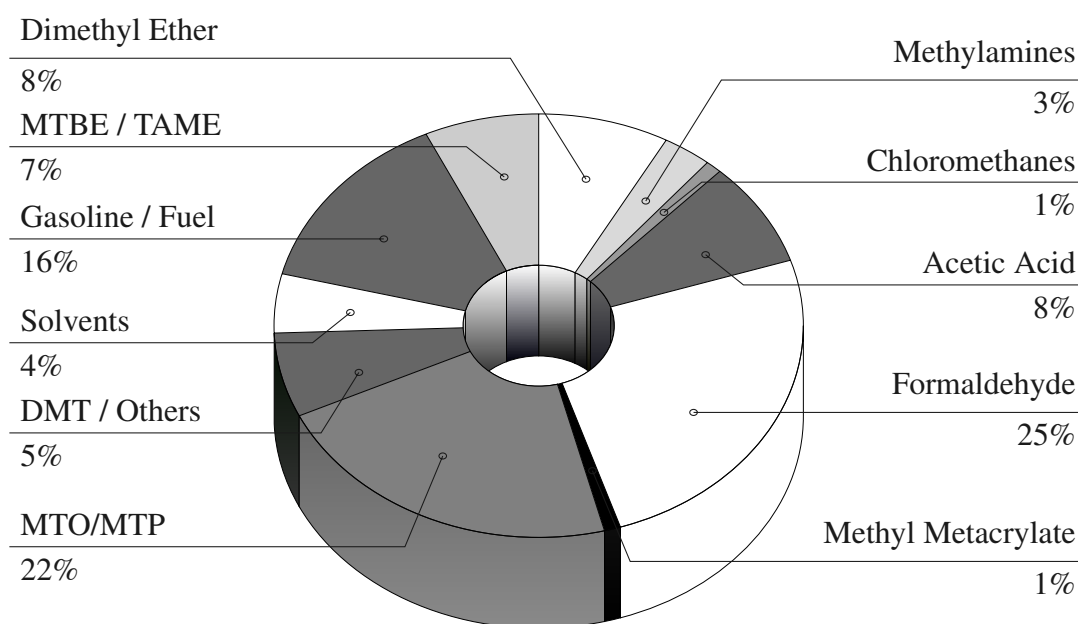
Figure 1.2: Methanol product distribution in 2016 (based on [25]).

Methanol plays an integral role in the global economy. Since it is the starting material for many chemical industries, the profits of a variety of derivative markets, and in general the availability of products, directly depend on the price of the feedstock [6]. The industrial applications range from the further processing to bulk chemicals, e.g.,

formaldehyde and acetic acid, to the production of synthetic fuels [18]. The piechart in Figure 1.2 shows the distribution of methanol applications in the year 2016 based on data obtained from [25]. About 69% of methanol is produced for the chemical market, wherein the focus in on the production olefins (alkenes) and formaldehyde as downstream intermediate chemicals. In particular, the methanol-to-olefins process (MTO), which allows the production of consumer plastics like polypropylene and polyethylene, is associated with high growth rates. As there are other competing processes for their production (e.g. steam cracking), the methanol price is crucial for the spread of the MTO technology in this segment. Formaldehyde as the largest single consumer of methanol is used for the production of plastics and resins, pharmaceuticals, chemical fibres, paint and pesticides [6, 30].

In addition to the significance as a basic chemical, methanol is required for the production of a variety of synthetic fuels like dimethyl ether (DME), methyl-tert-butylether (MTBE), TAME (tert-amyl methyl ether) and gasoline [6, 16, 17]. Furthermore, methanol/gasoline blends also have a large significance for the transport sector. Approximately one third of the total methanol production is processed to synthetic fuels, whereby the relative share of end-products in total methanol use stagnated or slightly decreased over the past decade [31]. For an improved overview, the flowsheet of the entire methanol value chain is presented in Figure 1.3.

Against the background of an energetic use, the properties of easy storage and transportability make methanol a favourable and competitive energy carrier. In contrast to electricity, methanol can be transported over long distances without significant energy losses. At the consumer, methanol can be directly converted into electricity by means of a direct methanol fuel cell (DMFC). Moreover, despite of the recent advancements of battery technology, there is still no large-scale storage of electricity possible [3]. In regard to crude oil and other fossil fuels, methanol has the potential to displace these materials, since the entire chain of hydrocarbon fuels can be derived from methanol. Since methanol can be produced from any hydrocarbon source, price imbalancies and shortages in conventional fossil fuels can be used to gain opportunity revenues for the end products. Furthermore, ethanol and hydrogen are often considered as a direct competitor to methanol.

The main advantage of methanol over ethanol is that the latter relies exclusively on agricultural resources. Regarding a hydrogen economy, substantial disadvantages refer to a high volatility, explosion risk and limitations in terms of storage and transportation [3].

For a more efficient, economically and ecologically more viable use of resources in the methanol production industry, three main goals can be defined:

1. Innovative and more efficient processes based on indirect synthesis routes with a special focus on new reforming and alternative gasification technologies for a reduction of capital investment and fuel cost.

2. Further development of sustainable production concepts for reduced fuel consumption through chemical valorization of carbon dioxide.

3. Maximization of single train capacities to increase the economic attraction through scale effects.
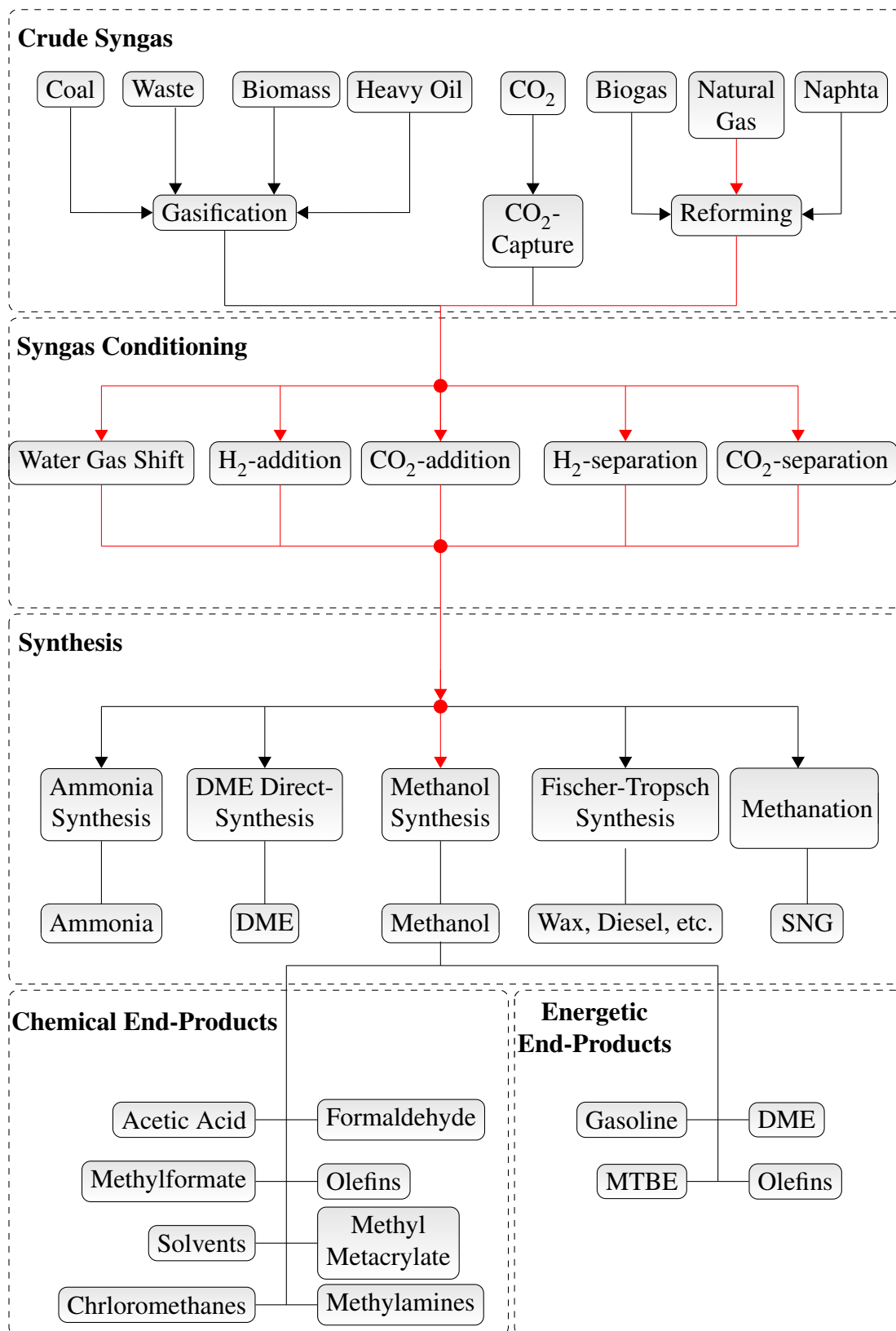
Figure 1.3: Overview of the methanol value chain.

Scope of work

The focus of this research is to approach the objectives of a more efficient, ecologically friendly and economically more viable methanol production. An endless variety of synthesis routes for the indirect conversion from natural gas has to be considered in order to reach a final plant design. Profound investigations are performed for the syngas generation unit and the synthesis reactor technology, since the operation of these units is decisive for the selection of a plant design, the overall performance and consequently also for the economics of a process. By application of sensitivity analyses, favourable operation parameters for high conversion and large yield are determined. Finally, the analyses enable for a synthesis of advanced designs with improved efficiency. Two reactor technologies dominating the methanol market are investigated - the isothermal reactor design and the adiabatic reactor technology with direct and indirect cooling. Taking into account the findings, six final process designs are subject to further investigations. These include three basic processes which use a single reformer technology for medium capacities of up to 3,000 mtpd. Furthermore, three advanced processes with mixed reforming technology and syngas conditioning for higher capacity are examined. First, the overall process performance is investigated by key operating parameters, such as the methanol yield, the recycle-to-feed-ratio and the methane intensity. Four process designs integrate CO_2 for utilization at different locations of the synthesis routes. The utilization strategies are quantitatively assessed in terms of CO_2 integration potential, overall CO_2 abatement and the saving of fuel. Subsequently, an exergetic analysis is conducted for all designs to identify the main sources and the magnitude of the irreversibilities. Furthermore, an economic analysis serves for an investigation of the influences of external market conditions on the revenues and the contribution margin and shows the interactions of the wholesale prices of generated products. The combination of these two analyses in an exergoeconomic analysis allows an identification of the internal cost distribution within the components of each process. The analysis results in a calculation of the levelized cost of the generated products methanol and electricity. Subsequently, the impact of economic uncertainties on the product cost is studied. Finally, an advanced exergetic analysis is conducted for an outstanding two-step reforming process to analyse exemplary the interactions and the improvement potential of the components.

Chapter 2

State of Research

In general, Gas-to-Liquids-processes (GtL) can be divided into direct and indirect liquefaction processes. Indirect processes involve the intermediate step of producing a synthesis gas (syngas), consisting mainly of CO and H_2, before this mixture is further processed to liquid end-products by means of catalysis. Large-scale applications of methanol generation are exclusively based on the indirect synthesis route [25]. These processes (in particular the syngas generation) are energy intensive and costly in terms of investment and operation. The disadvantages have led to studies on processes that allow for a direct synthesis of methanol, avoiding the undesired step of syngas generation. Although direct conversion has been thoroughly investigated over the past few decades, there are still barriers to an industrial implementation. The main obstacle for their spread refers to weak characteristics (low selectivity to CH_3OH, low conversion of CH_4) of the catalyst materials which make an upscaling too cost-intensive or impossible. The processes for direct conversion of CH_4 to methanol are briefly given in the following list:

1. Direct oxidation of methane to methanol [32–35]

2. Catalytic gas-phase oxidation of methane [25, 36]

3. Liquid-phase oxidation of methane to methanol [25, 37]

4. Methane into methanol conversion through monohalogenated methanes [25, 38]

5. Microbial or photochemical conversion of methane into methanol [25]

An overview of various indirect synthesis routes for the production of methanol is given in Fig. 2.1. The processes differ in terms of syngas generation and conditioning applications, synthesis reactor technology and crude product purification. The processing steps of an indirect synthesis route for methanol production from natural gas will be introduced in the following.

2.1 Syngas Generation from Natural Gas

A variety of technologies is available to produce a syngas from natural gas. The choice of an adequate syngas production technology has to consider a number of factors: feedstock availability and composition, cost of the feedstock and the fuel, plant location, complexity of integration with existing facilities, required reliability and environmental constraints and capital cost considerations. The common objective to all syngas production technologies is the provision of a synthesis gas with a stoichiometric composition for the respective synthesis.

Methanol in general can be produced with high selectivity (99.9%) via hydrogenation of CO or CO_2, as shown in reaction Eqs. 2.25 and 2.26. The reaction mechanism is not definitively understood since there is a disagreement whether methanol is mainly produced via reaction 2.25 or 2.26 [39]. Three different parameters are used to describe the stoichiometry and reactivity of a syngas and thus also the efficiency of the synthesis. Several studies characterize the composition of a syngas simply by using the H_2/CO ratio, which has ideally a value of 2 with respect to the synthesis of methanol [40]. This approach neglects the hydrogenation of CO_2 via Eq. 2.26 in the stoichiometric consideration. Although the methanol synthesis mainly proceeds over CO, the reaction is 100 times faster in the presence of CO_2 [41]. Taking into consideration the role of CO_2, an extension of the H_2/CO ratio by a second parameter referred to as stoichiometric module S is proposed to describe the composition for covering the stoichiometry of both reactions [3, 42–45]. With respect to the synthesis of methanol over commercially copper-based catalysts, the S module ideally has a value of slightly above 2. Typically, the feed gas composition for the methanol synthesis contains 4-10 mole-% CO_2 for high conversion and yield [6, 46]. Using an energy-intensive acid gas removal (AGR), the CO_2-content can be further decreased to 1 - 3 mole-% to achieve maximum methanol yield [39].

Stoichiometric module S

$$S = \frac{\dot{n}_{H_2} - \dot{n}_{CO_2}}{\dot{n}_{CO} + \dot{n}_{CO_2}} \tag{2.1}$$

Commercially used catalysts show a high activity in reaction equation 2.27, whereby CO is involved in the reverse water gas shift (RWGS). Dybkjaer et al. [26] oppose that the stoichiometric module S is not adequate to describe the reactivity of a syngas in methanol synthesis, since the module is independent of the water gas shift reaction 2.27.

Instead they suggest to use the CO/CO_2 ratio for this purpose. A high ratio increases the reaction rate and the per pass conversion in methanol synthesis, since the CO is preferred over CO_2 as a reactant by copper based catalysts. Moreover the production of water is decreased, which prolongs the lifetime of the catalyst and reduces the water content in the crude product.

A less common measure to describe the stoichiometry of a syngas is given by the stoichiometric ratio R in Eq. 2.2. A stoichiometric syngas for methanol synthesis has a R value close to unity. Accordingly a carbon rich syngas has a R value below one, while a hydrogen rich gas has a ratio above unity.

Stoichiometric ratio R

$$R = \frac{\dot{n}_{H_2}}{2\dot{n}_{CO} + 3\dot{n}_{CO_2}} \tag{2.2}$$

Depending on the adopted raw material, the applied syngas generation technology and the used reforming agents, the composition and therefore the values of the stoichiometric modules can widely vary [47]. The most widely used technology for the conversion of natural gas to a synthesis gas in industrial methanol applications is steam reforming by H_2O (SMR), including gas heated reforming (GHR) and heat exchange reforming (HER). Furthermore, autothermal reforming (ATR), two-step reforming, and to a minor extent catalytic and thermal partial oxidation (CPOX and TPOX) also found commercial application. Mixed or combined reforming (CMR) by integration of various reforming agents can be mentioned as a separate category. The dry reforming (DRM) using CO_2 as a reactant is considered as a pre-commercial technology. The variety of different process routes is shown schematically in Fig. 2.1.
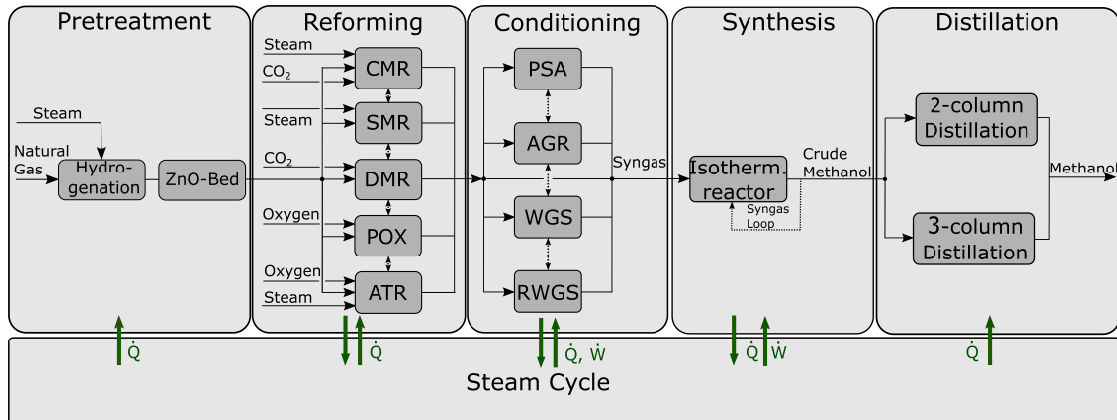
Figure 2.1: Schematic of the synthesis routes for the production of methanol from natural gas.

The process units of each of these synthesis routes can be assigned to six major subsystems: a pretreatment unit for the removal of sulfur impurities, a reforming unit serving for the syngas generation, a conditioning section for syngas adjustment, a synthesis unit for the conversion of syngas to methanol, a purification section for refining the crude methanol, and a steam cycle for balancing the overall heat and electricity supply and demand of the process units. In the following detailed information will be provided for the technologies of the subsystems.

2.1.1 Pretreatment

Natural gas typically contains several organic sulfur species, which are potentially poisonous to the catalysts used in methanol production processes [48]. The catalysts used in the reforming unit and the synthesis become quickly deactivated in their presence, which decreases the performance of the overall plant. An upper sulfur level of 0.002 ppmv for the processing of natural gas in reformers is recommended in [49]. Most common applications use a serial arrangement of two absorption beds to decrease the sulfur level to an acceptable level. The organic sulfur components, particularly carbonyl sulfide (COS), are first hydrolysed to hydrogen sulfide (H_2S) in a temperature range of 250 - 400 °C, and a pressure range of 5 - 40 bar [50] (reaction Eq. 2.3). Typically, the hydrogenation step is carried out over nickel or cobalt molybdenum catalysts. Subsequently, the H_2S is absorbed on a zinc oxide bed to produce zinc sulphide ZnS according to reaction 2.4.

$$COS + H_2O \rightleftharpoons CO_2 + H_2S \tag{2.3}$$

$$ZnO + H_2S \rightleftharpoons ZnS + H_2O \tag{2.4}$$

2.1.2 Pre-reforming

Natural gas inherently contains long-chained hydrocarbons, which can be beneficial for the production of methanol but detrimental to the operation of the reformer. Higher hydrocarbons are characterised by a high ratio of carbon to hydrogen and allow a generation of a stoichiometric more suitable synthesis gas than obtained by steam reforming of methane. An adiabatic reformer prior to the main reforming unit permits the use of heavier feedstock and reduces the load on the main reformer, thus allowing higher throughput and improved efficiency [51]. The pre-reformer is operated within a temperature range of 350 - 550 °C, which requires a preheating of the two reactants

steam and natural gas [52]. The mixture passes through a bed of catalyst pellets, which are typically based on nickel that is dispersed on an alumina stabilizer. The reactions are carried out adiabatically, whereby all higher hydrocarbons are converted to methane. A portion of the methane is further reformed to hydrogen and carbon monoxide. The process gas cools as the endothermic reactions proceed, and the pre-reformer effluent is then reheated before entering the main reforming section. The inclusion of a pre-reformer reduces the size of main reforming unit, since all energy added to the pre-reformer does not have to be supplied to the following reformers. For example, the reduction in a tubular steam methane reformer duty is 10 - 15% corresponding to about 75 reformer tubes.

2.1.3 Hydrocarbon Reforming

The reforming unit in general has a high impact on the overall process performance. A careful selection of a specific technology based on defined criteria therefore is essential for the overall thermodynamic performance and the economics of a plant. After the reforming technologies will be introduced in this chapter, a variety of selection criteria will be outlined which assist in finding a suitable reforming technology.

2.1.4 Steam Reforming

Catalytic steam reforming of methane (SMR) is the industrially most common used technology for synthesis gas production from natural gas. Large-scale applications not only refer to the production of methanol, but also include the manufacture of other precursors like hydrogen and ammonia. In SMR, natural gas is converted in highly endothermic and irreversible reactions (see Eqs. 2.5 and 2.6) with steam over catalyst pellets, typically based on Ni/Al_2O_3, at high temperatures and low pressures [53]. The process conditions are in the range of 20 - 40 bar with inlet temperatures of 300 - 650 °C and outlet temperatures of 700 - 1000 °C [33, 47, 52]. A large amount of steam according to a steam-to-carbon mole ratio (S/C ratio) of 3-5 is supplied to achieve a high conversion of natural gas. This typically results in large flow rates downstream the reforming unit. The stoichiometry of the product gas is highly sensitive to a variety of factors, such as the reaction temperature, pressure and the S/C ratio. The SMR reaction in Eq. 2.5 is inevitably accompanied by the water-gas-shift in Eq. 2.6. In particular for a high operation temperature, the conversion via the WGS is reduced, decreasing the amount of undesired CO_2 in the product gas [47].

$$CH_4 + H_2O \rightleftharpoons CO + 3H_2 \qquad\qquad \Delta H_{298K} = 206 \frac{kJ}{mol} \qquad (2.5)$$

$$CO + H_2O \rightleftharpoons CO_2 + H_2 \qquad\qquad \Delta H_{298K} = -42 \frac{kJ}{mol} \qquad (2.6)$$

The endothermic character of the main reaction requires an intense heat supply to the reaction zone. Industrial SMR is commonly performed in a fixed bed reactor, consisting of a variety of catalyst-filled tubes, which are located in the radiant section of a firebox. The process heat is supplied by a number of burners, which are fuelled with natural gas and a vent gas recycled from the synthesis. To ensure an effective heat transport in radial direction, the tubes are characterized by a low diameter-to-height ratio. The tubes typically have a length of 10-14 m and an outer diameter of 10-12 cm [26]. The variety of available firebox designs differs in terms of burner configuration - they can be located on the roof, on the bottom, on levelled terraces at the walls or as side burners on the walls. The design has an implication on the heat flux and the temperature profile and consequently also on the operation and the material stresses. Further information on different firebox designs is reported in [54, 55].

Since only about 50% of the fired energy is directly absorbed by the tubes, a heat recovery section is located downstream of the refractory lined zone. The thermal efficiency of the entire unit is increased to approximately 90%, by using the waste heat for preheating the reactants and for electricity generation in a steam cycle. An effective heat recovery reduces the flue gas temperature to about 150 °C, whereby values below 100 °C are possible in case of low sulfur species content.

A typical composition of a syngas obtained by SMR has a stoichiometric module of S equals 3 and yields a H_2/CO ratio of the same range. The composition is far away from the desired stoichiometry required by the methanol synthesis (S = 2.05 and H_2/CO ratio = 2). Due to the hydrogen surplus, a large amount of syngas is carried out unreacted from the synthesis and therefore agglomerates as a ballast in the recycle loop [6]. Unlike other reforming technologies, the product gas from SMR has a low content of carbon species, in particular CO_2. Therefore, integration of CO_2 as a conditioning measure to increase the methanol yield by direct hydrogenation via reaction 2.6 is discussed as an option for carbon utilization [3, 56]. Typically, about 1 mole of CO_2 has to be added to 4 moles of natural gas feed to achieve a nearly stoichiometric syngas as it enters the methanol loop [42]. However, according to Klier et al. [57] an optimal syngas composition for methanol synthesis is fixed for a CO_2 mole fraction of 2%. At much higher CO_2-levels, the methanol yield would be reduced.

Furthermore, other syngas conditioning measures could be applied to achieve an H_2/CO ratio $= 2$. Since typical ratios for SMR are far above this value, a composition adjustment by reverse water gas shift (RWGS) or a removal of H_2 by pressure swing absorption (PSA) would be beneficial. A conditioning by blending the syngas with CO_2 upstream a RWGS unit increases the amount of CO and H_2O to adjust the H_2/CO ratio to the stoichiometric requirements. However, this carbon utilization measure can only be applied for a low content of CO_2 in the synthesis gas.

2.1.5 Heat Exchange Reforming / Gas Heated Reforming

The heat exchange reforming technology was developed to reduce the investment cost of syngas-based processes [6]. In a heat exchange reformer, natural gas and other reactants are exposed to convective heat that is supplied by a flue gas or process gas. The design is similar to that of a tubular gas/gas heat exchanger. In contrast to fired reformers, the heat within heat exchange reformers is mainly transferred by convection. Various types of heat exchange reformers have been developed by several companies [52, 54] in the 80s and 90s. The technologies differ in terms of the heat source (process gas or flue gas), the tube design (bayonet or straight through), the maximum heat flux, and in operation parameters. A schematic of the three main heat exchange reformer types is provided in Figure 2.2. Further information on the different designs is reported in [54].
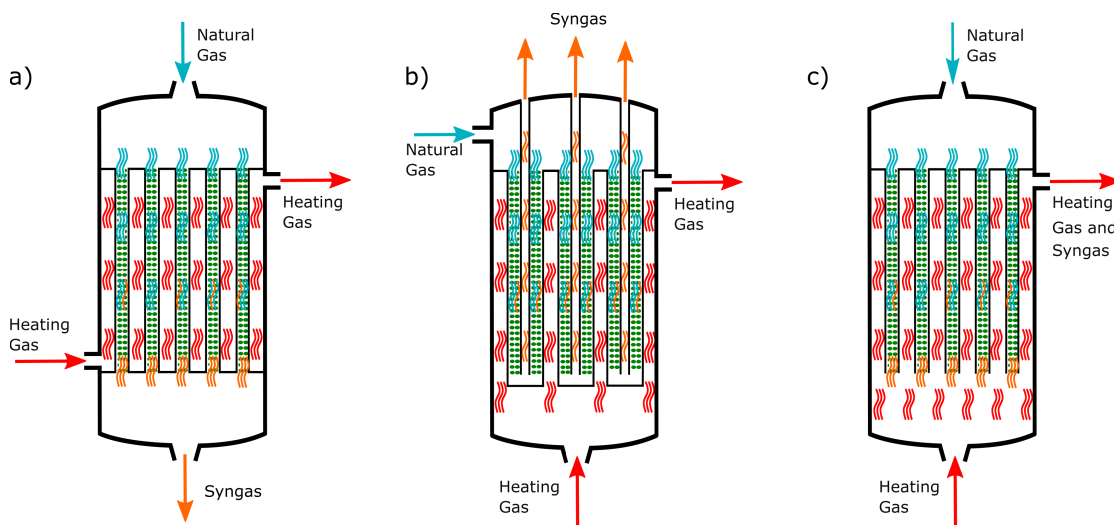
Figure 2.2: Types of heat exchange reformer a) with "straight-through" tubes, b) with bayonet tubes, c) with mixing of heating gas and product gas before heat exchange.

The GHR technology can be combined with an autothermal reformer (ATR, see Section 2.1.8) or oxygen blown reformer in serial or parallel configurations. A GHR based on SMR is often used in revamp projects with a stand-alone ATR to increase the plant capacity and the carbon efficiency [52].

For a combination of GHR and ATR, the endothermic reactions within the primary gas heated steam reformer consume the excess heat released by the secondary exothermic ATR. The heat is transferred by recycling the hot effluent from the ATR to the shell-side of the GHR. In two-step reforming concepts the majority of the methane feed is converted within the ATR (60 - 80%) while the remainder is completed by the GHR. The main advantages of a GHR (in two-step reforming) over conventional tubular SMR refer to a small size, lower investment costs and reduced steam utility. The technological progress drove the S/C ratio down to values of 0.6 - 1.5. The GHR types a) and b) can be used in a serial or parallel arrangement, while type c) only can be used in a parallel configuration. The gas heated reformer technology has been successfully demonstrated on a large scale in the Sasol Synfuel Complex in Secunda, South Africa, and in a GtL plant in Nigeria [52, 58].

2.1.6 Partial Oxidation

The carbon content of a syngas produced by conventional steam reforming technology is below the stoichiometric requirement of the methanol synthesis. The surplus in hydrogen requires an addition carbon components, which can either be supplied by an integration of a recycled CO_2 stream or alternatively by application of the partial oxidation technology (POX). POX refers to a substoichiometric combustion, which can be carried out with or without the use of a catalyst (catalytic partial oxidation CPOX and thermal partial oxidation TPOX) [59, 60]. The operation can be conducted in a wide temperature range of 800 - 1500 °C at elevated pressures [59, 61, 62]. Eqs. 2.7 - 2.9 show the main reactions occuring in the partial oxidation of methane.

$$CH_4 + 0.5\,O_2 \rightleftharpoons CO + 2H_2 \qquad \Delta H_{298K} = -36\frac{kJ}{mol} \qquad (2.7)$$

$$2\,CO \rightleftharpoons C + CO_2 \qquad \Delta H_{298K} = -172.5\frac{kJ}{mol} \qquad (2.8)$$

$$H_2 + 0.5\,O_2 \rightleftharpoons H_2O \qquad \Delta H_{298K} = -241.8\frac{kJ}{mol} \qquad (2.9)$$
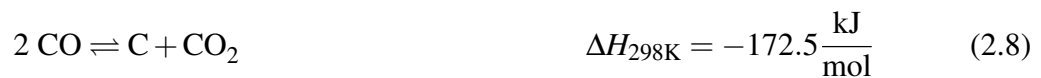
The partial oxidation of methane is a highly exothermic process, which yields a syngas with a low H_2/CO ratio of around 1.6 - 2 (see reaction Eq. 2.7). The composition of the process gas can be adjusted by controlling the mole ratio of oxygen to methane [59], which is also termed as O/C ratio. Depending on the operation parameters, the POX reaction is accompanied by undesired carbon deposition according to the Boudouard reaction in Eq. 2.8. The excess heat of the hot process gas may be recovered as steam for electricity generation or for supply to other units [3]. In this study, only the non-catalytic partial oxidation is considered as a part of the autothermal reforming unit.

2.1.7 Autothermal Reforming

The use of autothermal reforming (ATR) for syngas generation in methanol and ammonia production started in the middle of the 20th century. Since then, ATR has been incorporated in various application fields for the manufacture of a variety of products. Today, large scale applications can be found in Europe (2002), South Africa (2004), Qatar (2006) and other parts of the world [26, 63]. The ATR technology is preferentially used for methanol production capactes above 5,000 mtpd due to the economies of scale effect. In 2012, an ATR based methanol plant with a single-train capacity of 10,000 mtpd started operation in Nigeria [23].

ATR merges steam reforming and partial oxidation in one compact pressure vessel. As shown in Figure 2.3, the reactor consists of a combustion chamber (combustion zone) and a fixed catalyst bed within a refractory lined pressure shell (catalytic zone) [56, 64]. The burner arrangement allows a soot-free combustion, a homogenous gas and temperature distribution, and protects the vessel and nozzles from the hot flame core.

The hydrocarbon feedstock is blended with steam and reacts substoichiometrically with highly concentrated oxygen in a variety of combustion reactions that proceed along with steam reforming and the shift reaction [26, 64]. The set of reactions carried out within the combustion and catalytic zone of the ATR is shown in Eqs. 2.10 - 2.12.
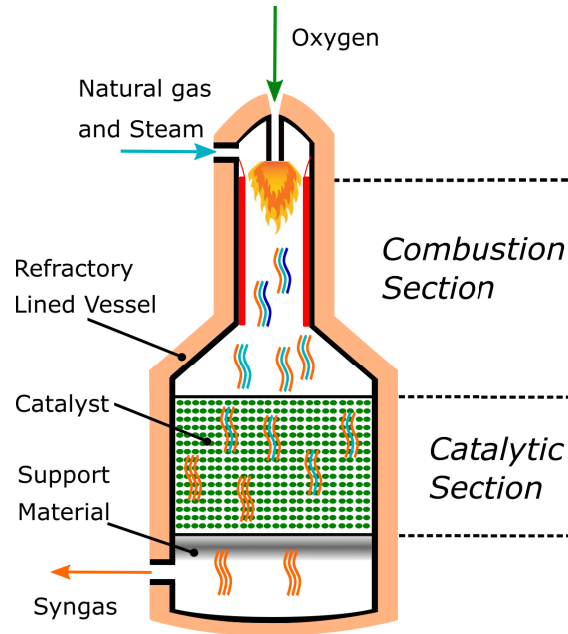
Figure 2.3: Design of a autothermal reformer (own presentation based on [65]).

Combustion zone:

$$CH_4 + 1.5\,O_2 \rightleftharpoons CO + 2\,H_2O \qquad \Delta H_{298K} = -520\,\frac{kJ}{mol} \tag{2.10}$$

Combustion and catalytic zone:

$$CH_4 + H_2O \rightleftharpoons CO + 3\,H_2 \qquad \Delta H_{298K} = 206\,\frac{kJ}{mol} \tag{2.11}$$

$$CO + H_2O \rightleftharpoons CO_2 + H_2 \qquad \Delta H_{298K} = -42\,\frac{kJ}{mol} \tag{2.12}$$
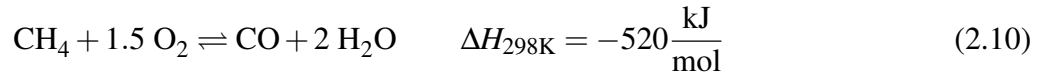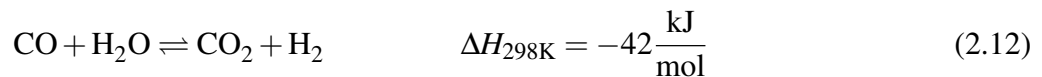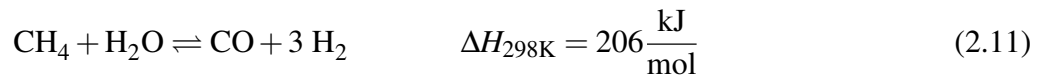
The partial oxidation of methane (reaction Eq. 2.10) can cause an increased temperature up to 3000 °C within the flame core in the upper part of the combustion zone. The vessel temperature is limited by the thermal stability of the catalyst and of the interior refractory lining [6]. After leaving the combustion zone, the mixture is equilibrated in the catalytic zone. The size and shape of the catalyst pellets are optimized for high activity and a low pressure drop to enable a compact design. Small sintering effects on the catalyst material are tolerated.

Industrial autothermal reformers are operated in a pressure range of 30 - 50 bar with outlet stream temperatures between 950 - 1100 °C [6, 66]. Due to the higher suction pressure, the electricity demand of the syngas compression is only about 50% compared to the energy demand in a conventional plant using steam reforming [6]. In oder to

keep the temperature in a moderate range and to allow a higher hydrogen content, steam is injected to initiate the endothermic steam methane reforming according to reaction Eq. 2.11. The ATR offers great flexibility in terms of operation, which adjusted to the respective downstream application. ATR is operated with a low S/C ratio, thus reducing the flow rate through the plant and dimishing the investment cost. Manufacturers of ATR report a steam-to-carbon mole ratio (S/C ratio) of 0.5 - 1.5, while the oxygen-to-carbon mole ratio (O/C ratio) is in the range of 0.6 - 1.0 [22, 66].

The process gas produced by ATR typically is of high temperature and therefore requires intensive cooling before further processing. The thermal energy is used for medium pressure steam generation. With respect to the composition, the syngas module S is in the range of 1 - 2, and has a CO/CO_2 ratio of 2.5 - 5.5 [22, 56, 66].

The fraction of unconverted methane in the effluent (methane slip) is below 3 mole-% [65]. The high carbon monoxide content results in a high reactivity of the syngas. Even though the high CO content makes the syngas highly reactive, further syngas conditioning steps might be necessary to increase hydrogen content while lowering the carbon dioxide fraction. Approaches to increase the hydrogen content are typically realized by hydrogen recovery from the purge gas within the synthesis loop through application of a pressure swing absorption unit [56, 66]. Other possibilities refer to a WGS unit which can be used in conjunction with carbon dioxide removal by application of industrially proven physical absorption processes (Selexol$^{®}$, Rectisol$^{®}$).

2.1.8 Two-step Reforming

Two-step reforming refers to a proven process that has been applied commercially by several companies for the production of a variety of products [56]. The reforming concept comprises a serial or parallel arrangement of a primary tubular steam reformer and an oxygen enhanced secondary reformer (POX) or alternatively an autothermal reformer [35, 42, 56]. The primary reformer can be designed as a fired reformer or a gas heated reformer, using the effluent of the secondary reformer as a heat source (see Section 2.1.5). The two basic configurations are presented in Fig. 2.4.

In the serial arrangement (2.4 a)), the entire fuel stream is fed to the inlet of the primary reformer and passes through both reactors. This concept is often used for retrofitting conventional plants based on SMR to debottleneck the reforming unit. In many configurations, the hot effluent from the secondary reformer is recycled to the primary reformer for heat supply to the SMR (see Section 2.1.5). The primary reformer can be operated with a significant leakage of methane, thus requiring a low S/C ratio and

a low operation temperature. Compared with stand-alone SMR, a reduction of 60% in the transferred duty and of 75 - 80% in the reformer tube weight is obtained. The savings thus obtained more than compensate the investment expenditures for the air separation unit, which is required to supply oxygen to the ATR [67]. Compared to stand-alone ATR, the demand for oxygen and therefore the size of the ASU is reduced due to lower O/C ratio and partial conversion of methane in the primary reformer. The main disadvantage of the serial configuration refers to the inflexibility of the operation pressure due to direct coupling of the reactors. The syngas composition can be controlled by the outlet temperature of the primary refomer, which is typically operated in a low temperature range of 700 - 800 °C and pressures of 35 - 40 bar [66].

In the parallel arrangement (Fig. 2.4 b)), the fuel is divided into two fractions whereby the first fraction is reformed at high pressure and moderate temperature in the SMR unit. Subsequently, the effluent from the primary reformer is mixed with the second fraction of the feedstock before supplying it to the secondary reactor. A small component size and an independent setting of the operation parameters are the major benefits of the parallel arrangement. The main disadvantage refers to the need of additional components compared to the serial arrangement.

In general, the combination of endothermic SMR and exothermic ATR can ensure a thermoneutral generation of a syngas with favorable (nearly stoichiometric) composition for high methanol yield [3, 42]. Furthermore, two-step reforming concepts allow increased fuel flexibility with regard to the production of a stoichiometric synthesis gas. The methane slip of two-step reforming concepts is relatively low, thus reducing the ballast of unconverted CH_4 in the synthesis unit. Exemplary plants based on two-step reforming started up in Norway in 1997 (2,400 MTPD) and in Saudi Arabia in 2008 (5,000 MTPD)[56].

a)

Natural Gas & Steam

Serial Gas-heated Reformer (GHR-s)

Autothermal Reformer (ATR)

Oxygen

Syngas, Steam & Methane (reactant ATR)

Syngas (CO,H$_2$,CO$_2$)

Combustion Section

Catalytic Section

Syngas (Product ATR)

b)

Natural Gas & Steam

Natural Gas & Steam

Parallel Gas-heated Reformer (GHR-p)

Autothermal Reformer (ATR)

oxygen

Syngas, Steam & Methane (Reactant ATR)

Syngas (CO,H$_2$,CO$_2$)

Combustion Section

Catalytic Section

Syngas (product ATR)

Figure 2.4: Serial a) and parallel b) configuration of the two-step reforming process (own presentation based on [54]).

2.1.9 Dry and Mixed Reforming

Dry reforming of methane (DMR), also termed as CO_2-reforming, is a well known conversion process which attracts many research efforts due to various environmental and economic incentives [6, 12, 68–70]. The technology is considered a promising carbon utilization concept which shall be used primarily for the production of methanol and urea. Incentives for the implementation not only refer to the mitigation of CO_2-emissions but also aim at reducing the amount of used feedstock to decrease the operation expenses. Despite these attractive features, there are no commercial applications for pure DMR. The major disadvantages are related to the poor catalyst performance and the energy intensity of the reforming process [69]. For instance, the import of CO_2 may need compression and purification of an extra feedstock, which requires further unit operations and a higher investment. According to Holm-Larsen et al. [71] CO_2-reforming is only economically feasible at locations where a large and relatively pure amount of methanol is accessible.

The conversion of methane by carbon dioxide is inevitably associated with catalyst deactivation by carbon deposition. DMR is a highly endothermic reaction, which requires an operation temperature in the range of 800 - 1000 °C to attain satisfying equilibrium conversions and to minimize the driving force for undesired carbon production [68, 69]. Catalysts used in DMR are typically based on Ni (e.g. Ni/MgO, Ni/MgAl$_2$O$_4$), whereby other nobel metals are preferable with respect to carbon desposition, but still are uneconomically in large quantities as used in industrial applications. Reaction Eq. 2.13 shows that DMR generates a syngas with an equimolar amount of CO and H_2 [68].

$$CH_4 + CO_2 \rightleftharpoons 2CO + 2H_2 \qquad\qquad \Delta H_{298K} = 247\frac{kJ}{mol} \qquad (2.13)$$

Dry reforming can also be combined with steam reforming (also named combined reforming) and partial oxidation to adjust the syngas composition towards the stoichiometric requirement of the synthesis. A combined use of the reforming agents O_2, CO_2, and H_2O is termed mixed reforming or bi-reforming and tri-reforming, respectively. An addition of O_2 is typically used to compensate the heat deficit of the DMR in reaction Eq. 2.14 by the exothermicity of the oxidation reaction in Eq. 2.15.

$$CH_4 + 0.5O_2 \rightleftharpoons CO + 2H_2 \qquad\qquad \Delta H_{298K} = -36\frac{kJ}{mol} \qquad (2.14)$$

$$CH_4 + 2O_2 \rightleftharpoons CO_2 + 2H_2O \qquad\qquad \Delta H_{298K} = -802\frac{kJ}{mol} \qquad (2.15)$$

The injection of H_2O is a tool to increase and control the hydrogen content of the synthesis gas from mixed reforming. The process gas obtained from dry reforming typically is lean in hydrogen, being unsuitable as a metgas (syngas for methanol synthesis). The supply of steam initiates the SMR, which can compensate for the deficit of hydrogen. The supply of both reforming agents therefore most likely will result in a syngas with a S module of equal to two. The catalysts applied to combined reforming have the same characteristics as in SMR.

$$CH_4 + H_2O \rightleftharpoons CO + 3H_2 \qquad \Delta H_{298K} = 206 \frac{kJ}{mol} \qquad (2.16)$$

$$3\,CH_4 + CO_2 + 2\,H_2O \rightleftharpoons 4\,CO + 8\,H_2 \qquad \Delta H_{696K} = 206 \qquad (2.17)$$
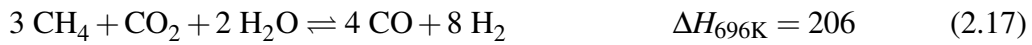
DMR inherently is accompanied by the decomposition of methane as well as the Boudouard reaction to produce harmful carbon on the catalyst surface as shown by Eq. 2.18 and Eq. 2.19. In addition to a careful selection of operation parameters, the supply of H_2O in bi- and tri-reforming is a successful measure to avoid carbon formation and therefore catalyst deactivation [12].

$$CH_4 \rightleftharpoons C(s) + 2\,H_2 \qquad \Delta H_{298K} = 75\frac{kJ}{mol} \qquad (2.18)$$

$$2\,CO \rightleftharpoons C(s) + CO_2 \qquad \Delta H_{298K} = -172.5\frac{kJ}{mol} \qquad (2.19)$$
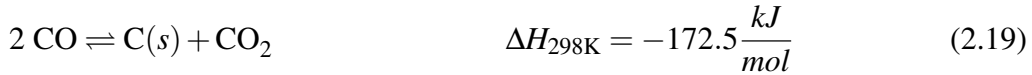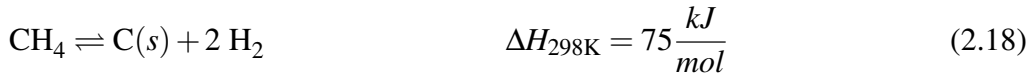
In case steam is used as a reforming agent, the RWGS reaction simultaneously is initiated, decreasing the H_2/CO ratio to a value below one [68]. The RWGS is only present at temperatures below 820 °C while DMR proceeds in the foward direction above 640 °C [72]. Carbon formation according to reaction 2.18 and 2.19 occurs above 560 °C and below 700 °C, respectively. Within this temperature range, carbon formation reaches a maximum due to simultaneous occurence of both mechanisms. Thus, bi-reforming should also be carried out above temperatures of 800 °C to obtain a syngas with an improved composition for the methanol synthesis.

2.1.10 Process Selection Criteria for Methanol Generation

A careful selection of a suitable reforming technology is essential for the thermodynamic efficiency and the profitability of a methanol plant. The syngas generation unit is the most expensive unit, accounting for approximately 60% of the overall investment cost.

Moreover, the performance of the reforming unit determines the demand for fuel, which constitutes the major cost contributor to the variable cost. According to [6], a cost breakdown for a natural gas based methanol plant shows that the fuel cost account for 50 - 75% of the overall cost. The following selection criteria can be defined:

1. Single-train capacity

2. Economies of scale

3. Composition of the syngas product

4. Heat integration and co-generation of electricity

5. Cost of the feedstock

6. Investment cost

7. Availability of utilities

The selection of a specific reforming technology primarily depends on the single-train capacity and cost reduction effects associated with an upscaling of the unit. Several studies presented a capacity range demarcation for the use of reforming technologies in methanol plants [6, 56]. The operation of SMR-based methanol production is economically justifiable only for a single-train capacity of up to 2,500 mtpd [55]. Above this capacity, large steam reformers become progressively more expensive and thus nearly show no economies of scale [6]. Two-step reforming concepts are economically beneficial in the intermediate capacity range of 2,500 to 5,000 mtpd. For large-scale capacities above 5,000 mtpd, ATR is the preferred technology, as higher cost reductions are associated with the upscaling of an air separation unit (ASU) than with tubular reforming. However, there are no absolute limits for the application of different reforming technologies but certain ranges of preference [6]. The typical capacity range for the reforming technologies is presented in Fig. 2.5. DMR and mixed-reforming cannot be shown as no applications exist on an industrial scale. Generally, single POX is not used for syngas generation in the production of methanol, due to high cost associated with the large oxygen supply.
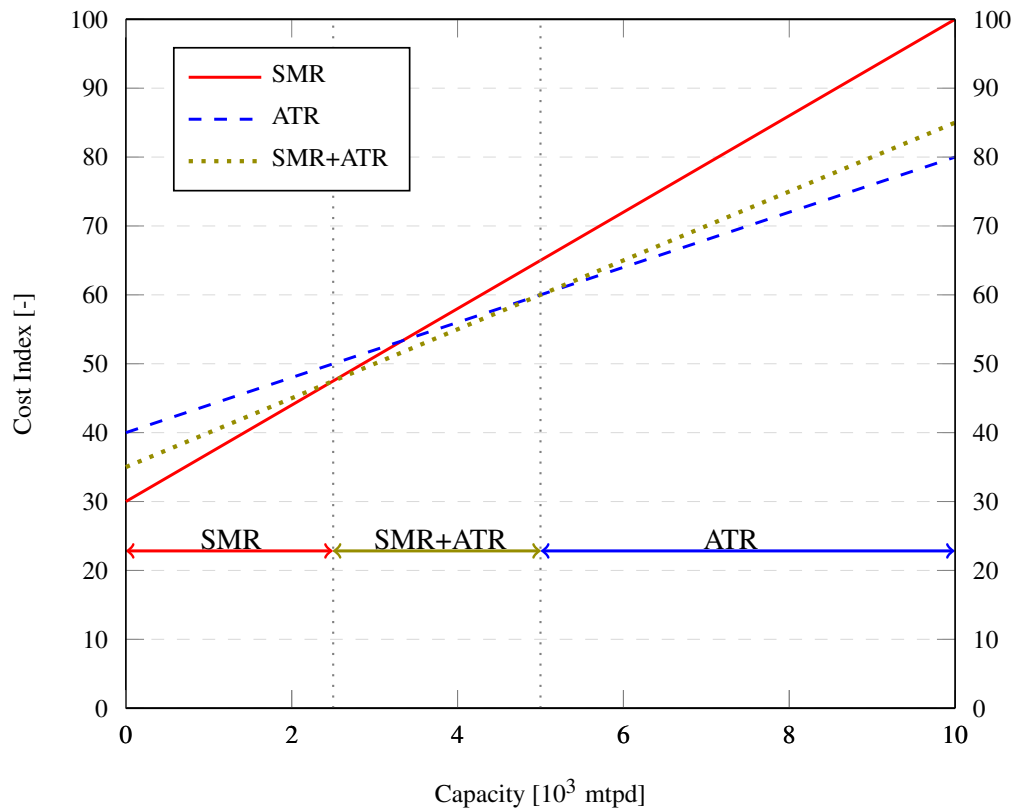
Figure 2.5: Capacity range of the commercial reforming technologies.

The reforming technology also has an impact on the size and the investment cost of downstream components through the composition and the flow rate of the provided synthesis gas. Depending on the composition, the size of downstream components in the synthesis and purification unit are determined and further syngas conditioning steps may be required.

Although the methane slip is generally in a low range, small differences in inert content can have a significant impact on the size of the synthesis unit as the inert components agglomerate in the synthesis loop. Furthermore, the CO_2 content of the process gas (typically 2 - 10 %) on one hand acts as a reaction promoter and on the other hand causes a production of undesired water. The high water content inevitably leads to an increase of the number and size of distillation columns and the heat duty required for product purification. Since the syngas composition is considered as a key parameter for the design layout and the operation of a methanol plant, special attention will be given to this selection criterion in Section 4.1.

Furthermore, the endothermic or exothermic character of the reaction mechanism is decisive for the fuel supply, the heat integration management and eventually a co-

generation of electricity. The operation of a SMR and DMR unit requires the supply of high temperature process heat which is typically generated by combustion of natural gas. A use of low temperature waste heat by recovery as steam for co-generation of electricity is essential for a high efficiency of those processes. In contrast, exothermic ATR can dispense with the supply of process heat and additional fuel. However, process integration of the ATR also requires and heat management system.

Significant differences also exist in terms of operating pressure. An energy-intensive syngas compression downstream of the reforming unit is required to compress the syngas to the pressure level of the synthesis unit. Depending on the reforming technology, the energy demand of the multi-compressor unit significantly varies. In particular for DMR, the compressor unit constitutes a large energy consumer, while the energy demand of a compressor after a pressurized ATR is comparatively low. The cost of supplied feedstock is the key to an economic success of a natural gas based methanol plant. In addition to the cost for natural gas, the cost of the reforming agents oxygen and carbon dioxide also have a significant impact on the product cost. Economic advantages for ATR and DMR particularly occur, when oxygen is or carbon dioxide is available at low cost.

2.2 Conditioning of Synthesis Gas

2.2.1 Carbon Utilization Measures in the Production of Methanol

Two major concepts for the utilization of carbon dioxide in a methanol production process via syngas production are of scientific and industrial interest [11, 44]. In general, the utilization of CO_2 is a promising approach to valorize a waste product for the generation of valuable fuels while reducing the CO_2 emissions and the demand for fossil feedstock. The CO_2 may either be added as a reforming agent for syngas production (see Section 2.1.9) or within the loop of the synthesis unit for direct hydrogenation in the synthesis reactor [44, 68, 72–76]. From a mass balance point of view, the location of the injection does not make a difference. However, from the perspective of the plant units the difference is significant. For instance, the reaction rate in the methanol synthesis is highly dependent on the CO/CO_2 ratio and increases with increasing ratio. Therefore, the synthesis unit significantly benefits when CO_2 is added before the reformer, where most of it is converted to CO by the reverse water-gas-shift reaction. Other drawbacks associated with dry reforming refer to the high coke production and the lack of experience

regarding the upsclaing of the technology [74].

Alternatively, CO_2 can be directly injected into the synthesis unit to produce methanol by the catalysed hydrogenation according to the reaction in Eq. 2.26. The main advantage of this carbon utilization option can be seen in the reduction of the reformer load. Since a highly concentrated CO_2 stream is directly fed to the loop or the inlet of the syngas compressor, less syngas needs to be produced in the reforming section. An injection downstream of the syngas generation unit results in high CO_2 mole fractions of the reactor feed gas, which may decrease the product yield and the efficiency of the overall plant. This is caused by the low activity and selectivity of commercial three component catalysts in the hydrogenation of CO_2. Thus, the potential for CO_2 integration is limited by catalytic constraints. Efforts have been made to develop catalysts that are better adapted to high CO_2 feed. The proposed catalysts are based on Cu-Zn oxides (with additives such as ZrO_2, GaO_3 and SiO_2) and show a low selectivity in reverse water-gas shift reaction while having a high selectivity for the hydrogenation [74, 77]. This direct hydrogenation constitutes a solution for the production of green methanol, when the required hydrogen is produced by electrolysis, which is driven by electricity from renewable energy sources. In 2010, Carbon Recycling International [78] installed such a system with an annual capacity of 3,000 t/a in Iceland.CO_2 is supplied by an aluminium production facility and a geothermal plant, while H_2 is generated from an electrolysis. Approximately 10 tons of methanol are produced from 18 tons of CO_2. Furthermore, Mitsui Chemicals Inc. [79] installed a unit in Japan, having an annual methanol capacity 100 t [80]. Here, the CO_2 is supplied as a waste product from an ethylene production plant.

For an assessment of the carbon utilization measures, the analysed processes are benchmarked against a conventional process based on steam methane reforming. Some key figures are introduced to evaluate the characteristics and the impact of the CO_2 integration. These measures include the CO_2-emission intensity, the CO_2-feed intensity, the relative CH_4-reduction and the CO_2-abatement. In Eqs. 2.22 and 2.23 the subscript 0 refers to the benchmarking process. The overall exergy of product $\dot{E}_{P,tot}$ (see Section 3.1.2) is taken as a basis for comparison, since different products of different energetic quality are generated by the processes.

$$CO_2 - \text{emission intensity} = \frac{CO_{2,\text{emis}}}{\dot{E}_{P,tot}} \tag{2.20}$$

$$CO_2 - \text{feed intensity} = \frac{CO_{2,\text{feed}}}{\dot{E}_{P,tot}} \tag{2.21}$$

$$CH_4 - reduction = \frac{CH_{4,tot,0}}{\dot{E}_{P,tot,0}} \cdot \dot{E}_{P,tot} - CH_{4,tot} \tag{2.22}$$

$$CO_2 - abatement = \frac{CO_{2,emis,0}}{\dot{E}_{P,tot,0}} - \frac{CO_{2,emis} - CO_{2,feed}}{\dot{E}_{P,tot}} \tag{2.23}$$

2.2.2 (Reverse) Water-gas Shift Reaction

Almost without exception, the synthesis gas from the reforming unit does not meet the stoichiometric requirements of the synthesis. SMR typically provides a syngas with excess hydrogen, while DMR and ATR technology most likely generate a syngas with a hydrogen deficiency. An efficient and economic measure to adjust the syngas composition to the corresponding stoichiometry of the synthesis refers to the use of a water-gas shift unit. A distinction can be made between the clean gas conversion and the sour gas conversion. In clean gas conversion, the unit is preceded by a purification section to remove the major part of the sulfur components and higher hydrocarbons that may be present in the gas, while the sour shift accepts an untreated feed gas. Depending on the temperature level, a second distinction is made between the high temperature shift conversion (300 - 500 °C) and the low temperature shift conversion (180 - 280 °C) [39]. The low temperature shift is only applied to obtain a syngas with very low CO content, which is not of interest for the synthesis of methanol.

The water-gas shift equilibrium defines a firm relationship between CO, CO_2, H_2 and H_2O which is independent of the pressure and determined by the temperature. The reaction shown in 2.24 is typically catalysed via iron oxide with heat release.

$$CO + H_2O \rightleftharpoons H_2 + CO_2 \qquad \Delta H_{298K} = -41.47 \frac{kJ}{mol} \tag{2.24}$$
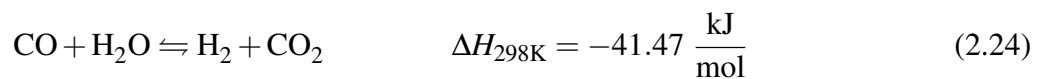
The temperature range of the shift conversion is determined by the thermal resistance of the catalyst material and the activation energy of the reaction. In case of a CO deficiency, as given for SMR and possibly for ATR, the reaction can be reversed (reverse water-gas shift RWGS). According to the endothermic nature, the conversion of the reverse reaction is favoured at high temperatures. Furthermore, a separation of water from the feed gas shifts the equilibrium towards high CO yield [81].

2.3 Methanol Synthesis Process

2.3.1 Chemistry and Thermodynamics

In methanol synthesis, a syngas consisting mainly of CO, H_2 and CO_2 is catalytically converted to produce raw methanol. The synthesis comprises a set of exothermic reactions that proceed selectively to give a single product. CO and CO_2 react with H_2 according to the reaction Eqs. 2.25 and 2.26. Additionally the reactants are involved in the water-gas shift reaction 2.27, which strongly influences the synthesis by offering a mechanism for the interconversion between CO and CO_2 [82].

$$CO + 2H_2 \rightleftharpoons CH_3OH \qquad \Delta H_{298K} = -90.64 \ \frac{kJ}{mol} \qquad (2.25)$$

$$CO_2 + 3H_2 \rightleftharpoons CH_3OH + H_2O \qquad \Delta H_{298K} = -49.67 \ \frac{kJ}{mol} \qquad (2.26)$$

$$CO + H_2O \rightarrow CO_2 + H_2 \qquad \Delta H_{298K} = -41.47 \ \frac{kJ}{mol} \qquad (2.27)$$

The conversion rate of the reactants is restricted by chemical equilibrium and the kinetic characteristics of the synthesis. Due to the exothermic and non-equimolar character of the reactions with fewer molecules on the product side than on the reactant side, high conversion to methanol is favored at low temperature and high pressure. The synthetic reactions cause a remarkable volume reduction. In order to achieve moderate reaction rates, the synthesis typically is conducted in the presence of a copper-zinc based catalyst ($CuO/ZnO/Al_2O_3$) at temperatures between 200 - 300 °C and pressures in the range of 50 - 100 bar, resulting in a yield of 5 - 15 mole-% methanol at the outlet [3, 23, 30, 46, 56]. The commercial catalysts have a high selectivity to methanol of above 99.5% [6]. Additional information on commercially used catalysts is reported in [25, 30].

Different measures exist to evaluate the performance of the synthesis. The carbon efficiency *CE* measures the incorporation of carbon atoms of the reactant into the final product. The component conversion *X* is the ratio of the difference of the amounts of a reactant at the inlet and outlet to the amount of the reactant at the inlet. The selectivity *S* is calculated as the ratio of the desired product and the converted feedstock that is used to generate the product.

Carbon efficiency

$$CE = \frac{\dot{n}_{CH_3OH}}{\dot{n}_{CO} + \dot{n}_{CO_2}} \tag{2.28}$$

Component conversion

$$X_m = \frac{\dot{n}_{m,in} - \dot{n}_{m,out}}{\dot{n}_{m,in}} \qquad \text{for m} = CO, CO_2 \text{ and } H_2 \tag{2.29}$$

Product selectivity

$$S = \frac{\dot{n}_{CH_3OH}}{\dot{n}_{CO^+CO_2,in} - \dot{n}_{CO^+CO_2,out}} \tag{2.30}$$

2.3.2 Methanol Reactor Technology and Synthesis Configuration

The high pressure methanol synthesis developed in the 1920s used a $ZnO/Cr_2O_3/Al_2O_3$ catalyst which favored conversion at temperatures between 320 - 450 °C, and a pressure in the range of 250 - 350 bar [40, 83]. Advances in catalyst technology and the switch from coal to natural gas as a predominant feedstock led to the development of the low-pressure methanol synthesis during the 1960s. Today, the worldwide methanol production is based on the low-pressure methanol process, which allows a conversion of syngas at 25 - 100 bar [84]. Consideration of the chemistry and thermodynamics of the methanol synthesis led to the development of a variety of processes with different reactor technologies. In addition to the conventional gas phase reactor technology, liquid phase reactors have attracted particular attention due to superior temperature control and high conversion efficiency. However, the LPMEOH^{TM} technology by the company air products only has been used on an industrial scale in the Eastman Chemical's coal gasification complex [40, 85]. Thus, only gas phase reactors found commercial applications in worldwide methanol plants. The gas phase technology can be subdivided into two main categories, including isothermal reactors and adiabatic quench reactors with direct and indirect cooling. Fig. 2.6 lists the processes according to the technology licensor.

The majority of the methanol production processes is based on the ICI-Synetix[*] and the Lurgi[†] reactor technology [30]. ICI-Synetix has a outstanding market share of 60%, while 27% of the licensed processes are based on Lurgi technology. To complete the polypolistic market, Mitsubishi Gas Chemcial Co., Inc. has a share of 8%, KBR, Inc.

---

[*]Today Johnson Matthey plc, Great Britain
[†]Today Air Liquide Global E&C Solutions, Germany

of 3% and all others 2%. The indirect pseudo-isothermal reactor developed by Lurgi [22, 52, 86] and the direct-cooled adiabatic quench reactor licensed by ICI Synetix / Johnson Matthey [87] are in the focus of this work. These corresponding synthesis configurations mainly differ in heat integration, make-up gas introduction and reactor design. An overview of their features is provided in Table 2.1.

Gas Phase Reactor Technologies

Isothermal reactors	**Adiabatic reactors**
• Linde converter [40, 47, 88]	**Multi-bed quench configuration with direct cooling** • ICI Quench Converter [87, 91–93]
• Lurgi isothermal reactor [89] One-step reactor [22, 47, 52, 86] Two-step reactor [47]	• Casale Advanced Reactor [47, 94] • Haldor Topsoe Collect Mixed Distribute Reactor [47]
• Mitsubishi Heavy Industries MGC/MHI Superconverter [40, 90]	**Multi-bed quench configuration with indirect cooling** • Kellogg Brown and Johnson Spherical Reactor [40, 47] • Toyo Engineering Corporation MRF-Z [40, 95]

Figure 2.6: Overview of commercial methanol reactor technologies.

Common industrial solutions for methanol production are exclusively based on the low-pressure synthesis. These processes tend to low conversion rates of the synthesis gas per pass. Therefore the synthesis reactor in general is used in conjunction with a recycle loop to achieve adequate yields [40]. Typically, the loop is equipped with a purge to remove inert and hazardous components that would otherwise build up in the process and reduce the partial pressure of the active components [71]. For instance, a methane slip of 2.5% in the reforming unit may result in a loop concentration of 25%.

The purge gas is either used for combustion in a furnace to generate process heat or the contained hydrogen can be recovered by an PSA for syngas conditioning. The purge ratio is typically in the range of 5-10%, depending on the stoichiometric ratio of the reactants and the internal heat or hydrogen demand [40]. The pressure level results from a trade off between energy demand for compression of the syngas feed and the amount of produced methanol. Generally, a high operation pressure favors the production of methanol due to an increase of the reactants partial pressures. In consequence, the required amount of the catalyst and the reactor size are decreased which reduces the capital investment. On the other hand, the operation and investment cost of the synthesis gas compression progressively increase. The compression of the make-up gas and the unconverted recycled syngas can be accomplished in one compressor or independent compressors [96]. Catalysts are developed to allow for adequate conversion rates at a pressure of even below 50 bar to further reduce the energy intensity and the operation costs of the syngas compression [40].

Table 2.1: Features of the isothermal reactor technology and the adiabatic multi-bed quench reactor technology.

Reactor Type	adiabatic quench	isothermal
Company	ICI / Johnson Matthey plc [97]	Lurgi / Air Liquide S.A. [98]
Temperature [°C]	250-300 [91]	230 - 265 [65, 86]
Pressure [bar]	50-100 [87, 91]	50-60 [86]
Catalyst	$Cu/ZnO/Al_2O_3$	$Cu/ZnO/Al_2O_3$
Capacity [mtpd]	1,350 - 3,000 [92, 93]	1,200-5,000 [47]

The commercial reactors are designed for an economically and efficient heat removal. [56]. A sensitive temperature control is required to allow an operation within a defined range. The temperature limits are determined by sufficient activity and thermal stability of the catalyst material. Detailed information on the characteristics of the considered reactor concepts will be given in the following section. An overview of their characteristics and operation parameters is provided in Table 2.1. Furthermore, the reactor technologies are depicted in Fig. 2.7, while the process operation lines are schematically shown in Fig. 2.8.

2.3.2.1 Adiabatic Reactor / Multi-Bed Converter

The adiabatic synthesis concept comprises a number of catalyst beds installed in a series of reactors or within a common pressure shell. Typically, the temperature increases linearly with the conversion for an adiabatic operation of an exothermic reaction [30]. The reaction pathway shown in Fig. 2.8 therefore is represented by a typical sawtooth profile. In general, the reactor and bed sizes are designed to allow the synthesis reaction to reach equilibrium. The temperature rise requires a control, which is provided by cooling devices inbetween the separated catalyst beds[40]. Intermediate or integrated cooling concepts are used for damage prevention and displacement of the gas temperature in direction of higher equilibrium conversion [99]. Two adiabatic synthesis concepts can be distinguished. The first comprises a series of adiabatic reactors with indirect cooling by application of intermediate heat exchangers. The second concept refers to a single shell containing multiple beds with direct cooling through injection of cold syngas (quench gas). The quench configuration has a maximum single-train capacity of 3,000 mtpd [56, 93]. Thus, in large-scale plants a parallel structure of several quench reactors is required.

In this work, only the quench technology is taken into consideration for process integration (see Fig. 2.7). In particular, the quench reactor developed by ICI Synetix in the 1960s is investigated. Worldwide, this quench converter is the most widespread technology among the low-pressure methanol synthesis processes. Compared with other commercially available technology, the reactor design is very simple and consequently features a low financial investment. The reactor feed is split into several fractions, which are supplied to the synthesis reactor between four individual catalyst beds by means of effective distribution devices [47, 100]. A successive addition of cold quench gas allows sufficient temperature control. Compared with other designs, the catalyst utilization is poor since not the entire amount of reactants passes through the total catalyst volume. Another disadvantage of the design refers to the fact that heat is not recovered at all or ineffectively [43]. The synthesis reactor is typically operated in a temperature range of 220 - 270 °C and a pressure range of 50 - 100 bar using a classic catalyst based on Cu/Zn/Al$_2$O$_3$ [93]. Due to irregular flow distribution and variable void fraction along the bed, the catalyst pellets do not receive the same gas flow. The uneven distribution may cause cold and hot reaction zones, which result in low reaction rates and catalyst deactivation [47]. Today, several further developments of the ICI technology exist for advanced quench gas distribution [92, 93].
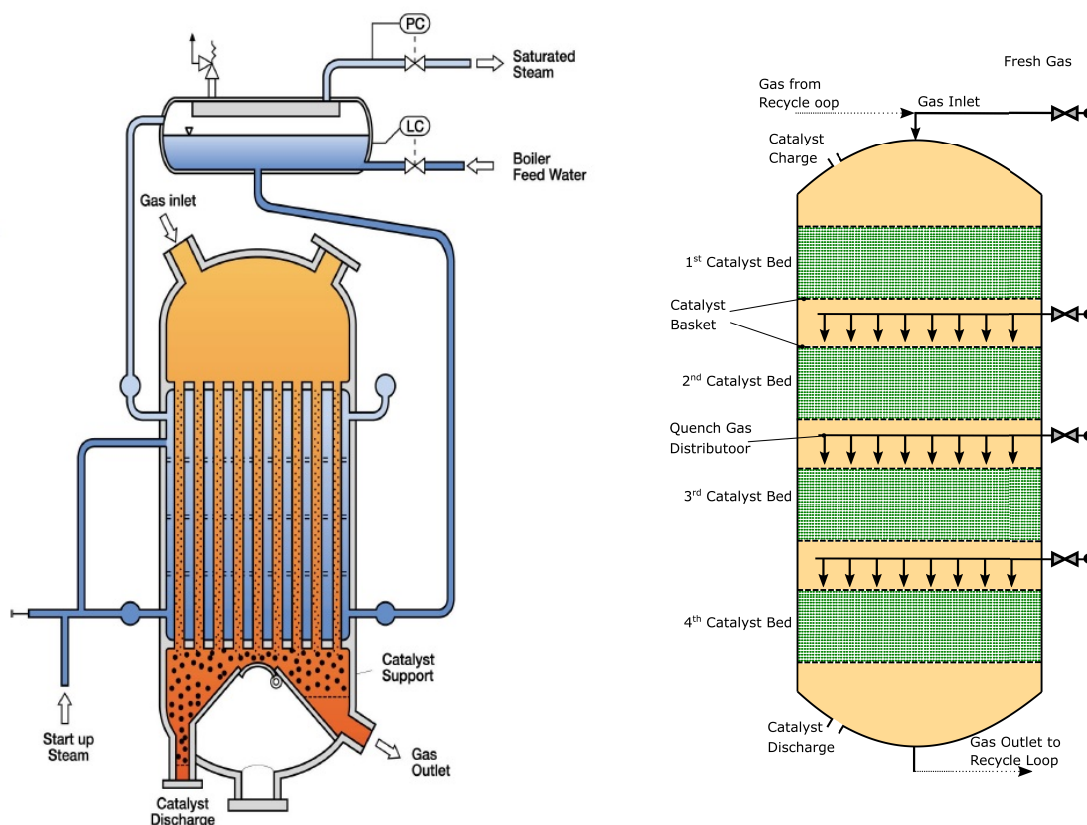
Figure 2.7: Scheme of the Lurgi isothermal reactor [65] (left) and ICI Synetix multi-bed quench reactor (right).

2.3.2.2 Isothermal Reactor / Single-Bed Converter

An isothermal reactor is designed as a shell and tube heat exchanger with a catalyst on the tube side and a cooling medium, mostly water, on the shell side. The heat of reaction is continuously removed through indirect heat exchange and recovered as steam on the shell side. An outer steam drum ensures a stable operation of the system, by controlling the temperature through an adjustment of the pressure and the flow rate of the boiling water. The cooling medium typically has a pressure in the range of 30 - 50 bar to ensure an operation temperature between 240 - 260 °C for high reaction rates. The produced medium pressure steam is further integrated into the process and may be used to reboil the bottom product in the distillation columns. Due to a complex mechanical design, the isothermal reactor has comparatively high investment costs and a limited capacity. Some reactor designs are equipped with an adiabatic top layer to avoid a preheating of the synthesis gas at the reactor inlet. The catalytic reaction in the adiabatic layer preheats the feed to a temperature above the cooling medium temperature to ensure an optimal heat

removal. This reduces the length of the tubes as they are used for heat removal rather than for preheating the feed gas. The application allows a decrease in size of 10 - 15%, resulting in an investment reduction by 15 - 25% [56].

Fig. 2.7 shows the pseudo-isothermal boiling water reactor developed by Lurgi GmbH, which has found wide distribution in industry [30, 47]. The reactor consists of a vertical shell and tube heat exchanger with fixed tube sheets. The design corresponds to the general description given above, whereby an adiabatic layer for preheating is missing. The typical operation conditions are in the range of 50 - 100 bar and 230 - 265 °C. Steam is produced at 40 - 50 bar and can be reused in the compression section or in the distillation unit. Air Liquide also offers a Dual-Reactor system (two-stage converter system) that is used to process syngas more effectively for high production capacities. The unit is a combination of two methanol converters. The isothermal water-cooled reactor is combined in a series with a gas-cooled reactor. In this work, the one-stage isothermal reactor system is applied on a large-scale, since the flow rates within the recycle loop are in an adequate range.
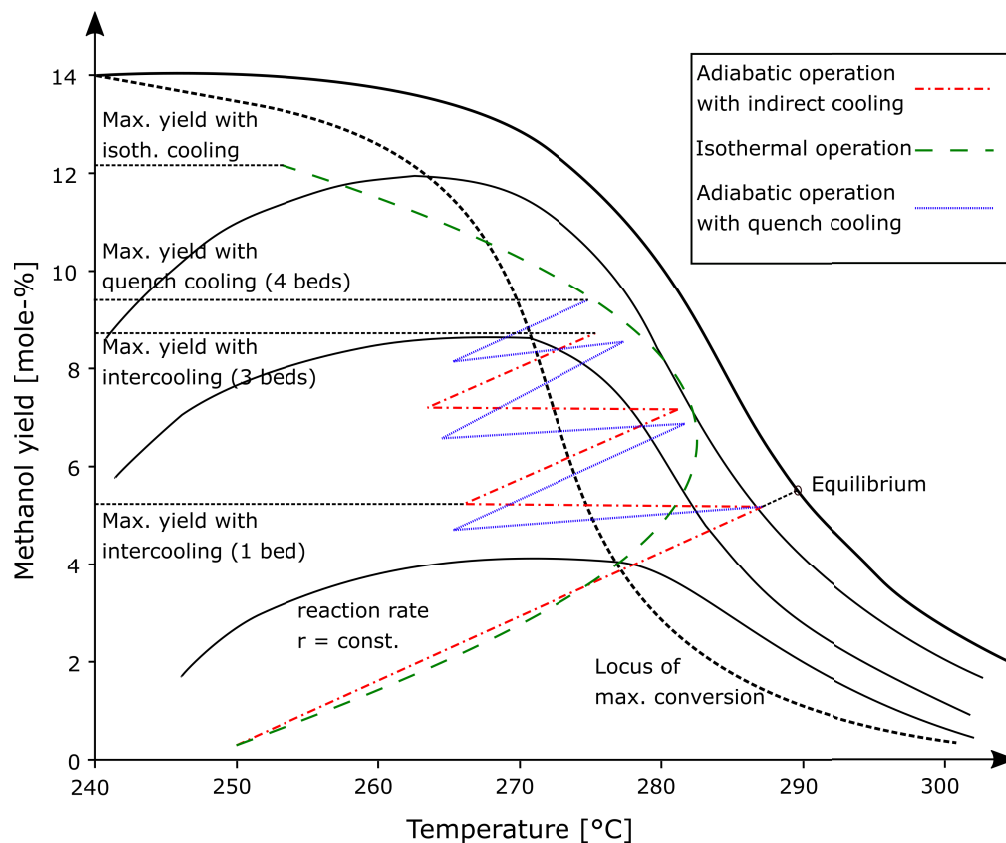
Figure 2.8: Process operation lines of an adiabatic reactor and an isothermal reactor.

2.4 Crude Methanol Purification

Although the industrial catalysts have a high selectivity of S > 99.5%, the reactor effluent may contain several impurities [83, 101]. The crude product not only contains water produced as a by-product in the hydrogenation reaction of CO_2, but also may include other impurities, such as dimethyl ether, methyl formiate, acetone, higher chained hydrocarbons (C_5 - C_{10}), ethanol and higher alcohols as well as dissolved gases (CH_4, CO, CO_2), termed as light ends. The amount of formed by-products depends on the type and the age of the catalyst and the operation conditions of the synthesis [6, 39]. The reactions over current copper catalysts hardly produce aldehydes and ketones, unlike the catalysts based on zinc-oxide which were used in high pressure processes in the past [39]. Furthermore, the low-pressure synthesis only generates minor quantities of formic and acetic acid. These chemical components have particularly led to corrosion problems in the high pressure synthesis.

The objective of methanol purification is to remove these impurities to generate a marketable product. The quality of methanol and the quantities of impurities allowed to be present are defined and classified by the ASTM D1152 specification [102]. Three different qualities of methanol can be distinguished according Table A.1 in Appendix A - fuel grade, grade A and grade AA Methanol. Methanol with fuel grade specification is used as burner or motor fuel, while grade A methanol in general serves as a solvent. Grade AA methanol is observed to become a standard for the methanol industry and is exclusively used for further processing to other bulk chemicals [3, 39, 42, 47].

Today, raw methanol is exclusively purified by distillation. According to the amount of impurities and the desired product quality, different distillation systems have to be applied [3, 39, 56]. In single-column systems, the light ends are removed overhead, while the product methanol is withdrawn above the reflux inlet. The process water and any heavy ends are discharged from the column bottom. A single-column is only sufficient to produce fuel grade methanol.

A two-column system comprises a topping column (extraction column) and a refining column and constitutes a cost-saving solution for the purification of crude methanol [6]. In order to reduce the heat duty of the reboiler, the refining column often is split into a first stage operating at elevated pressure (pressure column) and a second atmospheric stage (atmospheric column). The three-column system therefore represents an energy-saving alternative. In this configuration the topping column serves for the overhead removal of light ends and any DME present in the crude product, while methanol, water and heavy ends are withdrawn from the bottom. The bottom product is subsequently fed

to the pressure column to separate the water and the heavier ends from the methanol vapor, which is leaving the column at the top. The bottom waste product from the pressure column may still contain a considerable amount of methanol, which is fed to the atmospheric column for further recovery. Other by products of the atmospheric column include ethanol and higher alcohols (fusel oil). A schematic flowsheet of the two-column system and the three-column systems is shown in Fig. 2.9. Depending on the heat integration concept, the columns are heated by low or medium pressure steam. Generally, the methanol vapor of the pressure column is condensed in the reboiler of the atmospheric column to save energy. Typical features of the distillation columns can be found in [39, 101].
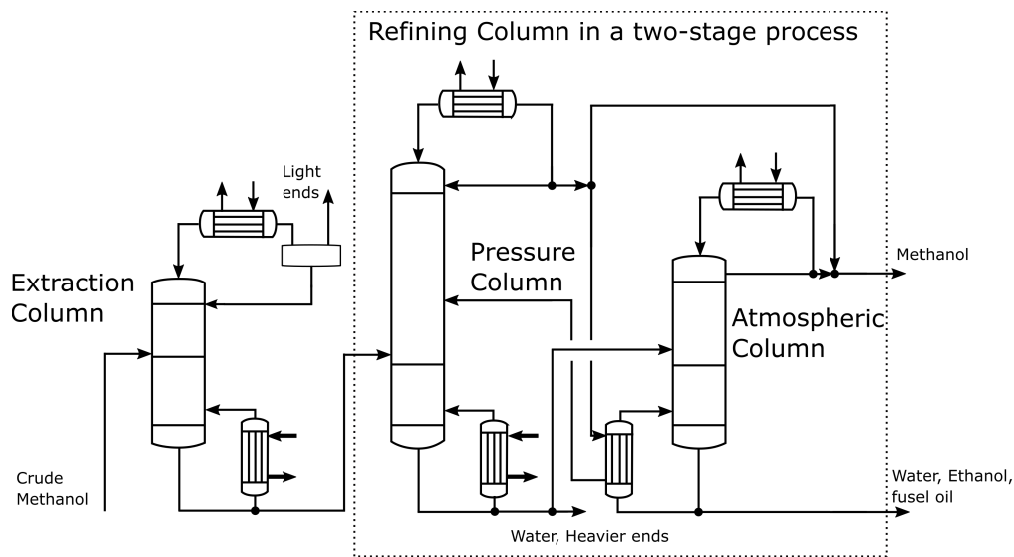
Figure 2.9: Flowsheet of a three-column distillation system.

Chapter 3

Methodology

3.1 Thermodynamic Analysis

This section presents the fundamentals of the energy analysis, the conventional exergetic analysis, the economic analysis, the exergoeconomic analysis and the advanced exergetic analysis. Additionally, Appendix E contains informations in regard to the definitions of the exergy of product and fuel as well as the calculation algorithm of the advanced exergetic analysis.

3.1.1 Energetic Analysis

According to the first law of thermodynamics energy is a conserved quantity which can be divided in various occurring forms. The energetic state variables can be determined by solving the overall energy balance in Eq. 3.1. In this work, the overall energy balance is simplified by assuming stationary processes and neglecting differences regarding the potential and kinetic energy. The remaining balance for an open system of the k-th component includes enthalpy flow rates $\dot{H}_j$ of the inlet (index in) and outlet (index out) streams, electrical or mechanical power $\dot{W}_{CV}$ and rate of heat transfer $\dot{Q}_{CV}$ of the control volume (index cv).

$$\frac{\mathrm{d}(U + KE + PE)}{\mathrm{d}\tau} = \dot{Q}_{j,CV} + \sum_{j=1} \dot{W}_{j,CV} + \sum_j \dot{m}_{j,in}(h + ke + pe)_{j,,in}$$
$$- \sum_j \dot{m}_{j,out}(h + ke + pe)_{j,out} \qquad (3.1)$$

$$0 = \dot{Q}_{j,\text{CV}} + \dot{W}_{j,\text{CV}} + \sum_j \dot{H}_{j,\text{in}} - \sum_j \dot{H}_{j,\text{out}} \tag{3.2}$$

Different characteristic parameters are used for a differentiation and evaluation of the processes investigated in this work. The chemical efficiency η_{ch} is calculated as the ratio of produced methanol and supplied fuel in Eq.3.3. Both, the energy content of methanol and fuel is determined by the lower heating value H_i^*. Accordingly, the electric efficiency η_{el} can be defined as the ratio of electric power output $\dot{W}_{\text{el}}$ and the supplied fuel in Eq. 3.4. The processes may generate two products which are of different energetic quality. In general, electrical power is energetically more valuable than methanol, so that the performance of the process cannot be evaluated solely by using the definition of the overall efficiency in Eq.3.5.

$$\eta_{\text{ch}} = \frac{(\dot{m} \cdot \dot{H}_{\text{i}})_{\text{Product}}}{(\dot{m} \cdot \dot{H}_{\text{i}})_{\text{Fuel}}} \tag{3.3}$$

$$\eta_{\text{el}} = \frac{\dot{W}_{\text{el,net}}}{(\dot{m} \cdot \dot{H}_{\text{i}})_{\text{Fuel}}} \tag{3.4}$$

$$\eta_{\text{tot}} = \eta_{\text{ch}} + \eta_{\text{el}} = \frac{\dot{W}_{\text{el,net}} + (\dot{m} \cdot \dot{H}_{\text{i}})_{\text{Product}}}{(\dot{m} \cdot \dot{H}_{\text{i}})_{\text{Fuel}}} \tag{3.5}$$

.

The characteristics of turbomachinery components, such as turbines (index T) and compressors (index C), are represented by the isentropic efficiency η_s. The term $h_{s,out}$ refers to the exit specific enthalpy determined by the inlet specific entropy and the outlet pressure.

$$\eta_{\text{s,T}} = \frac{\dot{W}_{\text{real}}}{\dot{W}_{\text{ideal}}} = \frac{h_{\text{in}} - h_{\text{out}}}{h_{\text{in}} - h_{\text{s,out}}} \tag{3.6}$$

$$\eta_{\text{s,C}} = \frac{\dot{W}_{\text{ideal}}}{\dot{W}_{\text{real}}} = \frac{h_{\text{s,out}} - h_{\text{in}}}{h_{\text{out}} - h_{\text{in}}} \tag{3.7}$$

---

*also abbreviated as *LHV*

3.1.2 Conventional Exergetic Analysis

The exergetic analysis is considered as a convenient and powerful tool to identify and quantify the inefficiencies and losses within chemical and energy conversion processes from a thermodynamic point of view. The methodology reveals the locations, the causes and the magnitude of the real thermodynamic inefficiencies. Exergy is defined as the maximum theoretical useful work obtainable as the system is brought into complete thermodynamic equilibrium with the thermodynamic environment while only interacting with this environment [103]. The methodology is well established and has proven to be advantegous for furthering the goal of a more effective use of resources [104]. The general exergy balance for an open (control-volume) system is representd by Eq. 3.8.

$$\frac{dE_{\text{cv}}}{d\tau} = \sum_j \left(1 - \frac{T_0}{T_j}\right) \cdot \dot{Q}_j + \dot{W}_{\text{CV}} + \sum_j \dot{E}_{j,\text{in}} - \sum_j \dot{E}_{j,\text{out}} - \dot{E}_{\text{D}} \tag{3.8}$$

The rate of exergy change $\frac{dE_{\text{cv}}}{d\tau}$ is calculated as the difference between exergy transfer across the boundary which is associated with mechanical or electric power $\dot{E}_{\text{W}}$, heat $\dot{E}_{\text{Q}}$, inlet and outlet material streams $\dot{E}_j$, and the rate of exergy destruction $\dot{E}_{\text{D}}$. The temperature T_j represents the average temperature of the rate of heat transfer at the boundary of the control volume, while T_0 refers to the temperature of the thermodynamic environment. Under steady state conditions, the rate of exergy destruction within the k-th component $\dot{E}_{\text{D},k}$ is given by Eq. 3.9. The term quantifies the irreversibilities within a component and is caused by mixing, chemical reaction, heat transfer and friction.

$$\dot{E}_{\text{D},k} = \dot{E}_{\text{Q}} + \dot{E}_{\text{W}} + \sum_j \dot{E}_{j,\text{in}} - \sum_j \dot{E}_{j,\text{out}} \tag{3.9}$$

The exergy flow rate of a stream of matter $\dot{E}_j$ is the sum of the physical, chemical, magnetic, kinetic, and potential exergy flow rate. In this work, the contribution of the magnetic, kinetic and potential exergies is neglected.

$$\dot{E}_j = \dot{E}_j^{\text{CH}} + \dot{E}_j^{\text{PH}} \tag{3.10}$$

$$\dot{E}_j^{\text{PH}} = \dot{n} \cdot \left((\overline{h} - \overline{h}_0) - T_0 \cdot (\overline{s} - \overline{s}_0)\right) \tag{3.11}$$

$$\dot{E}_j^{\text{CH}} = \dot{n} \cdot \left(\sum_i x_i \cdot \overline{e}_i^{\text{CH}} + \overline{R}T_0 \cdot \sum_i x_i \cdot \ln(x_i)\right) \tag{3.12}$$

With respect to the calculation of the chemical exergy, the model of Szargut is used as a reference environment [105]. The determination of the chemical exergy flow rate, according to 3.12, is only valid for a mixture of ideal gases. The chemical exergy of a stream, including a gas and a liquid phase, is calculated by their phase fractions if condensation occurs at ambient conditions (15 °C and 1 bar). The specific physical and chemical exergies are directly calculated by using the simulation sofware Aspen Plus® [106]. On the base of internal fortran routines, each stream is flashed to ambient conditions whereas the physical properties are taken from the simulation database.

An exergetic analysis often involves the calculation of measures of performance, such as the exergy destruction ratios and the exergetic efficiency. The use of dimensionless variables eases the interpretation of results, in particular when processes with different capacities are compared. For their determination, an exergy balance for the overall system and the k-th component can be written in the form of exergy fuel / exergy product in Eqs. 3.13 and 3.14. The exergy of fuel for the overall system $\dot{E}_{\mathrm{F},tot}$ is equal to the summation of the exergy of product $\dot{E}_{\mathrm{P},tot}$, the overall exergy destruction $\dot{E}_{\mathrm{D},tot}$ and the exergy loss $\dot{E}_{\mathrm{L},tot}$. On a component level an exergy loss is not defined. The SPECO approach is applied to define the exergy of fuel $\dot{E}_{\mathrm{F},k}$ and exergy of product $\dot{E}_{\mathrm{F},k}$ for a component [107].

$$\dot{E}_{\mathrm{F},tot} = \dot{E}_{\mathrm{P},tot} + \dot{E}_{\mathrm{D},tot} + \dot{E}_{\mathrm{L},tot} \tag{3.13}$$

$$\dot{E}_{\mathrm{F},k} = \dot{E}_{\mathrm{P},k} + \dot{E}_{\mathrm{D},k} \tag{3.14}$$

The exergy destruction ratio $y_{\mathrm{D},k}$ in Eq. 3.15 represents the ratio of the exergy destruction rate of the k-th component $\dot{E}_{\mathrm{D},k}$ and the exergy rate of the total system fuel $\dot{E}_{\mathrm{F},tot}$. Furthermore, $y_{\mathrm{D},k}^{*}$ in Eq. 3.16 represents the ratio of the exergy destruction rate of a component and the exergy destruction rate of the overall system. The exergetic efficiency ε_k defined in Eq. 3.17 constitutes a unique indicator for the performance and comparability of a system component [108].

$$y_{\mathrm{D},k} = \frac{\dot{E}_{\mathrm{D},k}}{\dot{E}_{\mathrm{F},tot}} \tag{3.15}$$

$$y_{\mathrm{D},k}^{*} = \frac{\dot{E}_{\mathrm{D},k}}{\dot{E}_{\mathrm{D},tot}} \tag{3.16}$$

$$\varepsilon_k = \frac{\dot{E}_{\mathrm{P},k}}{\dot{E}_{\mathrm{F},k}} \tag{3.17}$$

The exergetic analysis reveals information which is in general inaccessible through application of a thermodynamic analysis using energy and mass balances. Thereby, it provides a base to derive possible improvements, by identifying the major inefficiencies. However, no information is available, whether the suggested system modifications indeed will result in an improved overall system. Considering each component's improvement potential and the interactions among various system units in an advanced exergetic analysis will give realistic options for an improvement.

3.2 Economic Analysis

An economic analysis provides information about the economic feasibility of a construction and its operation while it is also a tool for the estimation of the cost associated with the generated products of a facility. In this thesis the method of the total revenue requirement (TRR) is applied. The levelized value TRR_L consists of the levelized annual carrying charges CC_L, the operating and maintenance costs OMC_L and the cost of the purchase of the fuel FC_L.

$$TRR_L = CC_L + FC_L + OMC_L \tag{3.18}$$

The levelized carrying charges represent the annuity of the total capital investment (TCI) calculated with the capital recovery factor (CRF). The TCI involves the fixed capital investment (FCI), the sum of allowances for funds during construction time ($AFUDC$) and start up costs. According to the approach described by Bejan et al. [104], the fixed capital investment (FCI) is calculated as the sum of direct and indirect cost. The direct costs include the onsite costs and offsite costs. Onsite costs (also referred to as bare module cost BMC or module cost C_M) comprise the purchased equipment cost (PEC), cost of installation, piping, instrumentation and control as well as cost for electrical equipment and materials. The offsite costs include expenditures for civil, structural and architectural work as well as service facilities. The calculation of the BMC is a challenging task, since a wide variety of data relating to cost and capacity of different types of components is available in the literature. The cost of equipment is determined by the capacity, the materials of construction, the design pressure and temperature. In the best case vendor quotations should be used for a cost estimation. When vendor cost quotations are missing, the PEC of various equipment items often are given in the form of estimating charts. In this thesis, the PEC for heat exchangers, compressors, expanders,

and pumps is based on data from [109–111], whereas the costs for distillation columns are also obtained from [112, 113]. Cost estimations for the SMR, ATR and DMR unit were obtained from [109, 110, 113]. For a calculation of the module cost C_M, effects of material, design temperature, design pressure and equipment features are taken into account. These effects are considered by factors (f_m, f_T, f_p, f_d) which correct the base cost C_B (PEC_k) of a component (modular method). In addition, the bare module factor f_{BM} can be applied to include the cost of any supporting equipment and connections as well as any indirect costs related to the equipment. Estimating charts in general already illustrate the bare module cost.

$$C_M = C_B f_d f_m f_T f_p f_{BM} \qquad (3.19)$$

- C_M = module cost of purchased equipment
- C_B = base cost of purchased equipment
- f_d = design factor
- f_m = material factor
- f_T = Temperature factor
- f_p = Pressure factor

An alternative to estimating charts are tables that provide component unit cost together with a scaling exponent α and a bare module factor f_{BM}. Although the scaling exponent for the same equipment can vary with the size and the reference year, the exponent is often assumed to remain constant. Due to the economies of scale effect, the values generally are below one, showing that the percentage increase in capacity is bigger than the percentage increase in cost [104, 105].

$$C_{PE,Y} = C_{PE,W} \left(\frac{X_Y}{X_W} \right)^{\alpha} \qquad (3.20)$$

With Equation 3.20 the unknown cost of a purchased equipment item $C_{PE,Y}$ at a specified capacity X_Y can be calculated from the known purchase cost of the same equipment item $C_{PE,W}$ at a different capacity X_W. The calculated cost of each equipment item must be brought to a common reference year, which is used as the base for all cost calculations. This is conducted by applying cost factors which represent inflation indicators for selected equipment at both, the year of the calculated known costs and the reference year [105]. In this work, the chemical engineering plant cost index (CEPCI) was used [114].

In contrast to the TCI, annually repeated expenditures for operation and maintenance as well as for fuel are subject to a cost increase. For their conversion to an annuity, the

constant escalation levelization factor (CELF) is applied, assuming a invariable nominal escalation rate r_n and effective interest rate i_{eff}.

$$CELF = \frac{k(1-k^n)}{(1-k)}CRF \qquad \text{with} \qquad k = \frac{1+r_n}{1+i_{eff}} \tag{3.21}$$

The operation and maintenance costs at the beginning of the operation are assumed to be 5% of the TCI and therefore mainly depend on the capacity of the plant.

$$OMC_L = TCI \cdot 0.05 \cdot CELF_{gen} \tag{3.22}$$

The fuel costs are calculated from fuel parameters, such as the mass flow rate, the heating value and the annual operation time τ. The levelization is conducted by applying a fuel specific levelization factor $CELF_{fuel}$.

$$FC_L = \dot{m}_{fuel} \cdot H_i \cdot \tau \cdot f_c \cdot CELF_{fuel} \tag{3.23}$$

Further specifications and assumptions of the economic analysis are summarized in Table 3.1. The construction is assumed to start in 2013. 40% of the investment is made in the mid-year 2014 and the remaining 60% in mid-year 2015. The plants are operated with 8000 full load hours a year. The prices for of the fuel natural gas and of the products methanol and electricity are subject to market fluctuations. Therefore, the profitability of the plants will be analysed in the context of typical price ranges. Regarding the fuel, the range is based on the Henry Hub spot price [115], while the price per ton of methanol is taken from world largest supplier Methanex$^{®}$, Canada [28]. For an economic assessment of processes with co-generation, prices for electricity are obtained from [116–118]. Expenditures for utilities such as catalysts and absorption materials are based on [119]. The economic estimation will be conducted using US$ 2016 as a currency.

The sum of the levelized carrying charges, operation and maintenance cost and fuel cost results in the annual total revenue requirement. The economic analysis provides a mean to evaluate the impact of market prices for fuels and products on the revenues and the economic feasibility. However, a clear distribution of the costs on the products is only possible through an exergoeconomic analysis.

Table 3.1: Specifications of the economic analysis.

Variable	Unit	Value	Variable	Unit	Value
Average capacity factor	%	91.3	Service facilities	% of C_M	30.0
CEPCI 2004 [114]	-	444.0	Architectural work	% of C_M	30.0
CEPCI 2010 [114]	-	532.9	Contingencies	% of C_M	15.0
CEPCI 2016 [114]	-	541.7	OMC	% of TCI	5.0
Eff. interest rate	%	8.0	MSR catalyst	\$/kg	2.2
Gen. inflation rate	%	2.5	SMR catalyst	\$/kg	10.0
Esc. rate fuel	%	1.0	ATR catalyst	\$/kg	10.0
Esc. rate comp.	%	4.0	WGS catalyst	\$/kg	3.0
Natural gas spot price	$\$_{2016}$/GJ	2.9	Pre-reform. cat.	\$/kg	10.0

3.3 Exergoeconomic Analysis

The exergoeconomic analysis combines the results of an exergetic- and an economic analysis and provides information which is not obtainable through the conventional analyses but essential for the design of a cost-effective system. The purpose of an exergoeconomic analysis is to identify the relative cost importance of each component. This is achieved by application of the exergy-costing principle, which requires costing equations for all components [105]. These equations consider cost rates $\dot{C}_j$ of entering and exiting exergy streams by assigning a specific monetary value c_j to each stream as well as cost rates due to capital investment $\dot{Z}_k^{CI}$ and operation and maintenance expenses $\dot{Z}_k^{OM}$ [104]. To obtain more precise information on the complex chemical systems, the cost rate of a stream is further split into the cost of the physical exergy $\dot{C}_j^{\mathrm{PH}} = c_j^{\mathrm{PH}}\dot{E}_j^{\mathrm{PH}}$ and the cost of the chemical exergy $\dot{C}_j^{\mathrm{CH}} = c_j^{\mathrm{CH}}\dot{E}_j^{\mathrm{CH}}$.

$$\sum_{j=1}^{n}(c_j \cdot \dot{E}_j)_{k,\mathrm{in}} + \underbrace{\frac{(CC_L + OMC_L) \cdot PEC_k}{\sum_n PEC \cdot \tau}}_{\dot{Z}_k = \dot{Z}_k^{CI} + \dot{Z}_k^{OM}} = \sum_{j=1}^{m}(c_j \cdot \dot{E}_j)_{k,\mathrm{out}} \tag{3.24}$$

The values of $\dot{Z}_k^{CI}$ and $\dot{Z}_k^{OM}$ are calculated by apportioning the CC_L and the OMC_L among the system components according to the contribution of the k-th component to the

purchased equipment cost for the overall system. Heat losses over system component's surface could also exhibit a cost stream, but are neglected in this work. If an exergetic fuel $\dot{E}_{\mathrm{F},k}$ and product $\dot{E}_{\mathrm{P},k}$ can be defined for a component, the cost balance can also be noted as in Eq. 3.25.

$$c_{\mathrm{P},k}\dot{E}_{\mathrm{P},k} = c_{\mathrm{F},k}\dot{E}_{\mathrm{F},k} + \dot{Z}_k \tag{3.25}$$

The terms $c_{\mathrm{F},k}$ and $c_{\mathrm{P},k}$ denote the average cost per exergy unit of fuel and product while $\dot{Z}_k$ refers to the cost rate associated with the investment and the operation and maintenance expenses. For dissipative components, such as condensers and valves, an exergy product is not defined. However, since these components are indispensible for the process operation, their costs, associated with the investment, the operation and maintenance and the exergy destruction (termed as $\dot{C}_{\mathrm{Diff}}$) will be charged to the overall systems' products.

A system of linear equations is obtained by setting up the component balances. In case the system is under-determined (the number of unknown cost streams is larger than the number of balances) auxiliary equations are required to assign a value to the unknown variables. In general, the inlet streams of a component are assumed to be known, while an information about the outlet streams is missing. If the number of exiting streams is higher than one ($m > 1$) a formulation of m-1 auxiliary equations is necessary to determine specific average cost of all streams. The F-principle (Fuel rule) on the fuel side and the P-principle (Product rule) are used to determine the auxiliary equations [105]. On one hand, the F-rule states that the specific cost associated with exergy removed from a component is equal to specific cost at which the exergy was supplied to the same stream in the upstream components. On the other hand, the P-rule states that each unit of exergy is supplied to all product streams at the same average cost $c_{\mathrm{P},k}$.

After the balance equations are solved, an exergoeconomic evaluation can be conducted by considering different exergoeconomic variables. One important outcome refers to the cost rate that is associated with the exergy destruction $\dot{C}_{\mathrm{D},k}$ of the k-th component.

$$\dot{C}_{\mathrm{D},k} = c_{\mathrm{F},k} \cdot \dot{E}_{\mathrm{D},k} \tag{3.26}$$

The exergoeconomic evaluation of a design reveals the components with the highest cost impact which includes the cost rate associated with the exergy destruction, as calculated in Eq. 3.26, and the investment cost of the respective component $\dot{Z}_k$. At first, the components are ranked in descending order according their cost significance

$\dot{C}_{D,k} + \dot{Z}_k$. By application of the exergoeconomic factor f_k in Eq. 3.27, the contribution of the investment cost (non-exergy related cost) to the cost rate $\dot{C}_{D,k} + \dot{Z}_k$ can be identified. Thus, the factor provides an information about the internal cost distribution within a component.

$$f_k = \frac{\dot{Z}_k}{\dot{Z}_k + \dot{C}_{D,k}} \tag{3.27}$$

The second important variable used in an exergoeconomic evaluation is the relative cost difference, denoted as r_k. The variable expresses the relative cost increase in the average cost per exergy unit between the product $c_{P,k}$ and the fuel $c_{F,k}$ of a component [104]. As shown in Eq. 3.28, the relative increase depends on the cost rate associated with the exergy destruction and the investment $\dot{C}_{D,k} + \dot{Z}_k$.

$$r_k = \frac{c_{P,k} - c_{F,k}}{c_{F,k}} = \frac{\dot{C}_{D,k} + \dot{Z}_k}{c_{F,k} \cdot \dot{E}_{P,k}} \tag{3.28}$$

The exergoeconomic factor f_k depends on the operation of a component and therefore has an individual value for each unit. However, for classes of components, such as heat exchangers, turbines and compressors, there are some common value ranges that usually apply. Consequently, an assessment by the factor must take into consideration the component type. Depending on the value of the exergoeconomic factor, a trade-off between investment cost and exergy destruction has to be made. High f values suggest a reduction in the investment costs of a component at the expense of its exergetic efficiency. On the other hand, low values indicate cost-savings that might be achieved for the overall system by a decrease of the irreversibilities (improving the exergetic efficiency) even if the component's capital cost will increase.

The results of the exergoeconomic evaluation are used to determine changes to the initial design in order to improve it from both, an economic and a thermodynamic point of view. The compromises between the investment cost and the cost rate of the exergy destruction can give indications for an iterative design improvement of the investigated system.

3.4 Advanced Exergetic Analysis

The conventional exergetic analysis indentifies the location, the magnitude and the cause of irreversibilities and indicates a general strategy for a thermodynamic improvement.

However, the method is not able to identify the interdependcies among the plant compo-
nents or to estimate the real potential for improvement. The advanced exergetic analysis
concept [120] provides detailed information on the interactions between each system
component and on their real improvement potential. To comply with this, the exergy
destruction within each component is split into its endogenous and exogenous parts
as well as avoidable and unavoidable parts, respectively. A combination of these two
splitting approaches provides further valuable information for an improvement of the
overall efficiency. A schematic of all options for splitting the exergy destruction of a
component is presented in Fig. 3.1, which was adopted from [121].
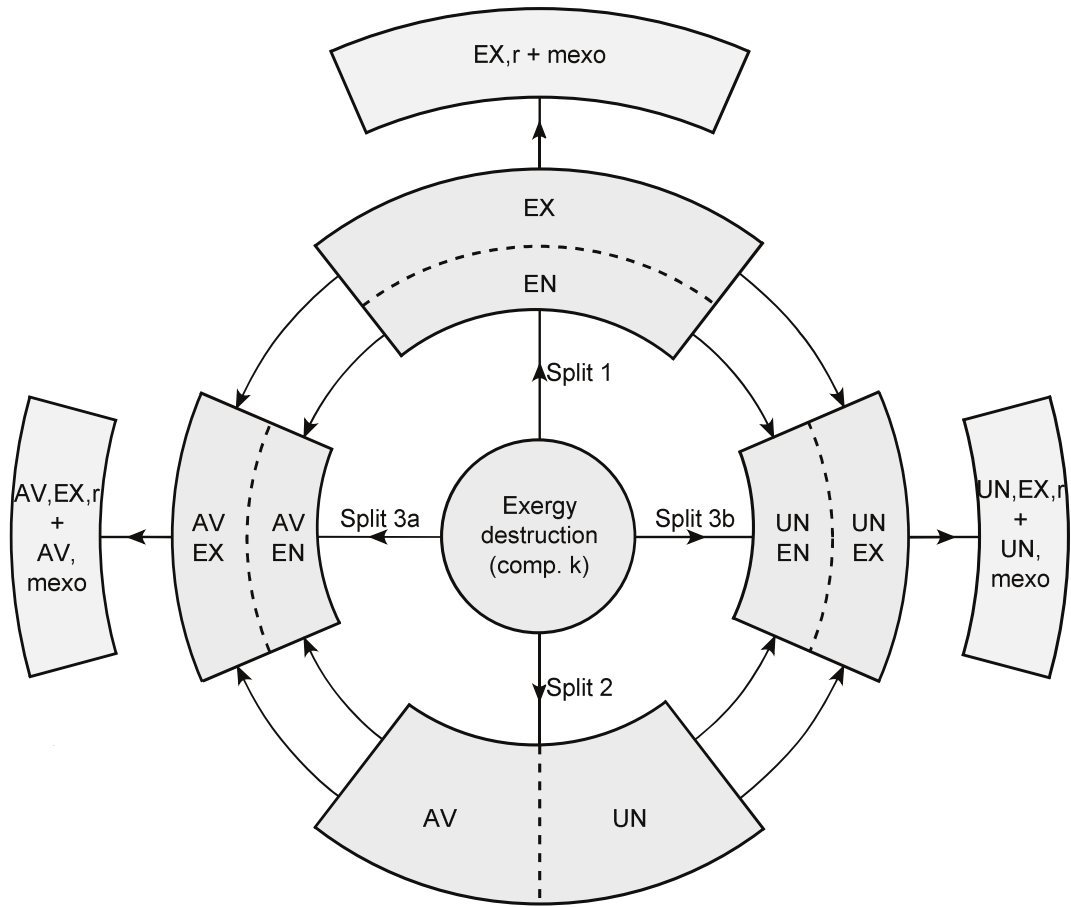
Figure 3.1: Overview of splitting options of the exergy destruction within a component in an
advanced exergy analsyis (adopted from [121]).

Splitting the exergy destruction of the k-th component into its avoidable (index AV) and
unavoidable (index UN) parts allows for an evaluation of the real improvement potential
of a component within a fixed process arrangement (Eq. 3.29). The main drawback
of this splitting approach is subjectivity: the calculation of unavoidable variables is
associated with the estimation of values based on the best knowledge and experience of

an engineer. The unavoidable exergy destruction of a component $\dot{E}_{\mathrm{D},k}$ can be directly calculated from a simulation in Aspen and is weighted by the default exergy rate of the product (Eq. 3.30).

$$\dot{E}_{\mathrm{D},k} = \dot{E}_{\mathrm{D},k}^{\mathrm{AV}} + \dot{E}_{\mathrm{D},k}^{\mathrm{UN}} \tag{3.29}$$

$$\dot{E}_{\mathrm{D},k}^{\mathrm{UN}} = \dot{E}_{\mathrm{P},k} \cdot (\dot{E}_{\mathrm{D},k}/\dot{E}_{\mathrm{P},k})^{\mathrm{UN}} \tag{3.30}$$

The unavoidable part of the exergy destruction refers to the amount of exergy destruction that cannot be further reduced because of technoeconomic limitations, such as manufacturing methods, cost of materials, and availability. The remaining avoidable exergy destruction represents the savings in irreversibilities of the k-th component that can be achieved through a technically feasible design or operational improvement.

The thermodynamic interdependencies among the components can be evaluated by splitting the exergy destruction of the k-th component into the endogenous and exogenous parts.

$$\dot{E}_{\mathrm{D},k} = \dot{E}_{\mathrm{D},k}^{\mathrm{EN}} + \dot{E}_{\mathrm{D},k}^{\mathrm{EX}} \tag{3.31}$$

The endogenous exergy destruction $\dot{E}_{\mathrm{D},k}^{\mathrm{EN}}$ is associated with the irreversibilities occurring within the k-th component operating with default exergetic efficiency while all other components are assumed to be reversible [108]. In contrast, the exogenous exergy destruction $\dot{E}_{\mathrm{D},k}^{\mathrm{EX}}$ within component k is caused by the irreversibilities of other system components. The endogenous exergy destruction can be calculated from a set of equations without the need for additional simulations. Several approaches for calculating the endogenous exergy destruction have been suggested [122–124]. These approaches face theoretical shortcomings and computational problems for chemical reaction systems [122].

The combination of the two splitting approaches results in four parts of the exergy destruction which are included in the final results of an advanced exergetic analysis. Only the endogenous avoidable and exogenous avoidable exergy destruction should be considered to find promising modifications for an improvement of the overall system [123]. The calculation algorithm for obtaining the unavoidable endogenous exergy destruction $\dot{E}_{\mathrm{D},k}^{\mathrm{UN,EN}}$ is given in Appendix F.

$$\dot{E}_{\mathrm{D},k} = \dot{E}_{\mathrm{D},k}^{\mathrm{UN,EN}} + \dot{E}_{\mathrm{D},k}^{\mathrm{UN,EX}} + \dot{E}_{\mathrm{D},k}^{\mathrm{AV,EN}} + \dot{E}_{\mathrm{D},k}^{\mathrm{AV,EX}} \tag{3.32}$$

$$\dot{E}_{\mathrm{D},k}^{\mathrm{UN,EX}} = \dot{E}_{\mathrm{D},k}^{\mathrm{UN}} - \dot{E}_{\mathrm{D},k}^{\mathrm{UN,EN}} \tag{3.33}$$

$$\dot{E}_{\mathrm{D},k}^{\mathrm{AV,EN}} = \dot{E}_{\mathrm{D},k}^{\mathrm{EN}} - \dot{E}_{\mathrm{D},k}^{\mathrm{UN,EN}} \tag{3.34}$$

$$\dot{E}_{\mathrm{D},k}^{\mathrm{AV,EX}} = \dot{E}_{\mathrm{D},k}^{\mathrm{AV}} - \dot{E}_{\mathrm{D},k}^{\mathrm{AV,EN}} \tag{3.35}$$

The remaining parts of the exergy destruction of the *k*-th component in Eq. 3.32 can be calculated by using equations 3.33 to 3.35. Based on simultaneous consideration of the four parts of exergy destruction within the *k*-th component, measures for improving the component and the overall system can be derived [120].

3.5 Simulation and Software

The simulations were conducted using the software Aspen Plus® (Aspen) version 9.1 [106]. Furthermore, for data analysis, data management, and additional calculations, Matlab® has been used. The analyses have been carried out at steady-state conditions. In Aspen, the property method Redlich-Kwong-Soave (RKS) was used to model the gas path. With respect to the acid gas removal system, the property method based on the Perturbed Chain Statistical Association Fluid Theory (PC-SAFT) equation of state was applied to the glycol Dimethyl Ether of Polyethylene Glycol (DEPG) representing the solvent in the Acid gas removal (Selexol®). This method is adequate to model liquid systems with large molecules for single components or in mixtures. Regarding the material properties, Aspen uses information from the NIST databank [125]. The properties of water and steam were calculated based on the steam table formulation IAPWS'95 [126].

In Aspen, the simulations have been performed in sequential modular mode. Internal routines named *design sepcification* are used to determine the conditions of several outlet streams. Furthermore, the embedded *sensitivity* function was used to determine favourable operation parameters for the key units of the process (see Section 4.1). The internal *calculator* module is used for a direct calculation of characteristic parameters, such as the stoichiometric measures and feed ratios. In particular, the module helps to monitor the operation of the sensitive chemical components. Another internal module called *transfer* can be useful for the calculations of the avoidable and unavoidable exergy destruction as well as for the simulations of loops which are induced by recycle streams. For all kinetically limited reactions, kinetics are implemented in the internal module *reactions*. This can be a challenging task, as the given reactions kinetics often

not suit the form that is required by Aspen. The program provides different types of kinetics in order to describe the reaction mechanism in the most suitable manner. Of particular importance are Langmuir-Hishlewood-Houston-Watson kinetics (LHHW) [82] and Power-Law kinetics. It may be challenging to implement kinetics from the literature in the form required by Aspen. A detailed description on the used kinetics and their implementation into Aspen is provided in Appendix B.

On a component level, several reactors are simulated by using the *RPLUG* reactor model, which is suitable to simulate a plug flow reactor. The model allows for an implementation of kinetics for an heterogenous catalysis and assumes a perfect mixture in the radial direction and no mixture in axial direction. A variety of kinetic models is implemented into the reactors to describe the occurring reactions properly. Power-Law kinetics based on a study by Luyben et al. [96] are implemented into the SMR and DMR model. The same kinetic type is used to model the WGS by using kinetic parameters from Choi and Stenger [127]. Regarding the methanol synthesis, the reaction kinetic inputs to the RPLUG model are taken from a study by van den Bussche et al. [128] and a study by Graaf et al. [129, 130] , in which a Cu/ZnO/Al$_2$O$_3$ and a Cu/Zn/Al/Zr catalyst is used for conversion, respectively. Finally, after conducting the sensitivity analyses, the model of van den Bussche was chosen for implementation.

Any combustion process was simulated by using the *RGIBBS* reactor model which calculates the outlet stream at chemical equilibrium conditions by minimizing the Gibbs free energy. With respect to pre-reformer and the desulphurizer, a fixed conversion rate is implemented into a *RSTOICH* model. The distillation columns are simulated by using the *RADFRAC* model.

Chapter 4

System Design and Modelling

The synthesis of a process design for a chemical plant is an important task. The decisions made in a design process significantly influence the future profitability, the environmental impact, flexibility in operation, and changes in system design. Therefore, in the first part of this chapter, parameter studies are conducted for the major units to generate new and advanced process designs for high conversion and efficiency. In the second part, six final process designs will be introduced which subsequently will be subject to the analyses.

4.1 Parameter Study for the Synthesis of Process Designs

The reforming unit and the methanol synthesis reactor are decisive for the overall performance of a methanol plant, since they are highly integrated from a chemical and thermal point of view. Due to a variety of impact parameters in conjunction with a complex reaction mechanism, the setting of favourable operation conditions is a challenging task. Sensitivity analyses are conducted for these units to show the impact of uncertain operation parameters. In conclusion, beneficial operation parameters for high conversion and methanol yield are identified taking into account existing technical limitations. Furthermore, information about the need for additional process steps can be derived from the results.

4.1.1 Reforming of Methane

The reforming unit is the key component within a natural gas-based methanol production process. The choice of a specific reforming technology influences the rate of conversion, the product yield, the overall efficiency of the process and consequently

also the economies of the plant. Therefore, profound investigations of the different syngas generation technologies are indispensable. In the following, the influence of operation parameters, such as the S/C ratio, O/C ratio, CO_2/C ratio, temperature and pressure on the conversion and the syngas composition will be investigated. The results of the sensitivity analyses are based on the assumption, that the reforming reactions reach chemical equilibirum. For all investigations, the natural gas feed has the same composition which is given in Appendix A.

4.1.1.1 Steam Reforming

Within the sensitivity analysis of the steam reformer, the influence of the S/C-ratio and the reactor temperature and pressure on the composition and the methane conversion is investigated.
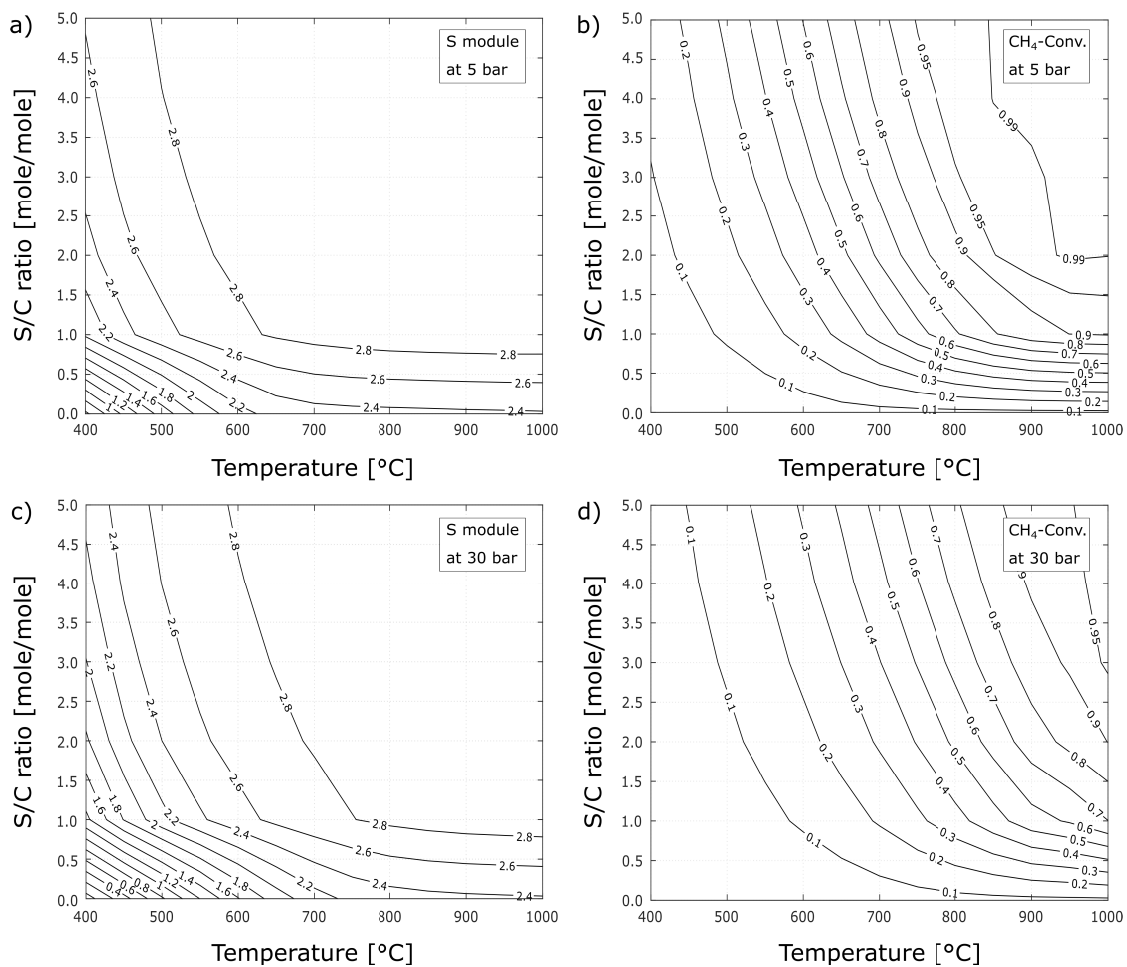
Figure 4.1: Sensitivity analysis of the steam methane reforming technology: a) and b) show the S module and the CH_4-conversion at 5 bar and c) and d) refer to the values at 30 bar.

Figure 4.1 shows the results of the stoichiometric S module and the CH_4-conversion at 5 and 30 bar, respectively. In general, when selecting the operation conditions of a reformer, a priority should be given to the conversion rate, since large methane slips are technologically not feasible for the synthesis unit. Considering the CH_4-conversion in Fig 4.1 b) and d), the contourplots suggest an operation at a temperature of at least above 900 °C and a S/C ratio above 2 for a high conversion rate. In this operation range the S module is fixed to a value of 3.

A comparison of a) with c) and b) with d) shows that the pressure has a less significant influence on the composition and the CH_4-conversion. With increasing pressure at constant temperature, hydrogen tends to react with CO_2 to produce CO according to the RWGS, resulting in lower values of the S module. On the other hand, the methane conversion decreases with increasing pressure due to the non-equimolar character of the SMR reaction. Thus, at elevated pressure a higher operation temperature is required to achieve a low methane slip. In the context of the overall process design the pressure should not be selected too low in order to limit the energy demand of the syngas compression unit.

4.1.1.2 Autothermal Reforming

The sensitivity of syngas composition and the CH_4-conversion to the supply of the reforming agents H_2O and O_2 as well as to the operation pressure is investigated. The results of the analysis are shown for a pressure of 10 bar in Figs. 4.2 a) and b) and for a pressure of 40 bar in Figs. 4.2 c) and d), respectively. For an O/C ratio of 0, pure SMR is presented, while POX is shown for an S/C ratio of 0. Based on the vertical lines, it can be concluded that combustion reactions in general has a higher impact than SMR on the composition and the conversion.

Also for the autothermal reformer, the operating conditions for a stoichiometric optimum and maximum conversion are different. As for the other reforming technologies, a high conversion rate has priority when selecting the operation parameters. Consequently, the reformer should be operated with an O/C-ratio of 0.6, which is currently the technological minimum [22, 66, 131]. For a high conversion of CH_4, the syngas composition can be adjusted via the O/C ratio. Accordingly, an increase in the O/C ratio will result in a syngas with reduced hydrogen content. Even if the Figs. 4.2 a) and c) could lead to the conclusion that the influence of the S/C-ratio is low, the composition strongly depends on the amount of integrated steam. A closer look at the composition reveals, that a S/C ratio of 0.5 - 0.7 (at an O/C ratio of 0.6) generates a syngas with favourable composition.
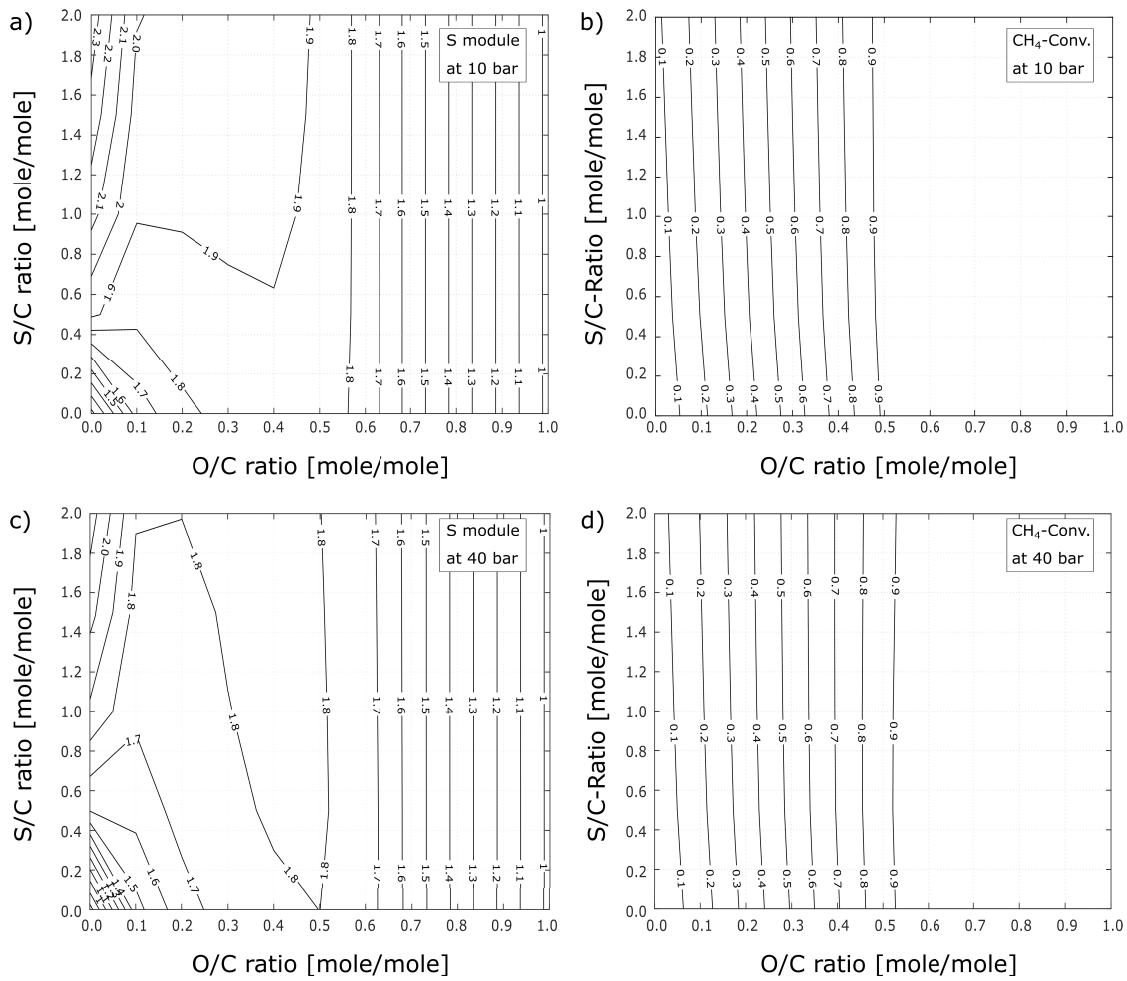
Figure 4.2: Sensitivity analysis of the autothermal reforming technology: a) and b) refer to the S module and the CH_4-conversion at 10 bar and c) and d) to the values at 40 bar.

4.1.1.3 Dry and Combined Reforming

The sensitivity of the S module and the CH_4-conversion to the S/C ratio and the CO_2/C ratio as well as to the operation temperature is presented for an operation pressure of 5 bar and 30 bar in Fig. 4.2. The contourplots a) and b) refer to the S module, while c) and d) show the conversion rate at the respective pressure. The plots in each Figure refer to an extremum in terms of the CO_2/C ratio - the solid lines represent the results for a low ratio of 0.5, while the dashed lines show the results for a high ratio of 2.5. The results of a pure operation as a DMR are shown on for a S/C ratio of zero.

For high CO_2/C ratio, 99% CH_4-conversion is achieved for an operation temperature in the range of 900 and 1050 °C. The course of the graphs in Figs. 4.2 b) and d) shows, that reforming by CO_2 is preferred at a high temperature level while the impact of the SMR dominates between 300 - 600 °C. Considering the syngas composition in a) and

c), the low S module shows that for high CO_2/C ratio a large amount of carbon dioxide leaves the reformer unconverted. For a low ratio syngas with a satisfactory composition in the range of S equals 1.6 - 1.7 can be produced. A comparison of 4.2 a) with c) and b) with d) shows that a pressure increase at constant operation temperature increases the conversion rate and the value of the S module.
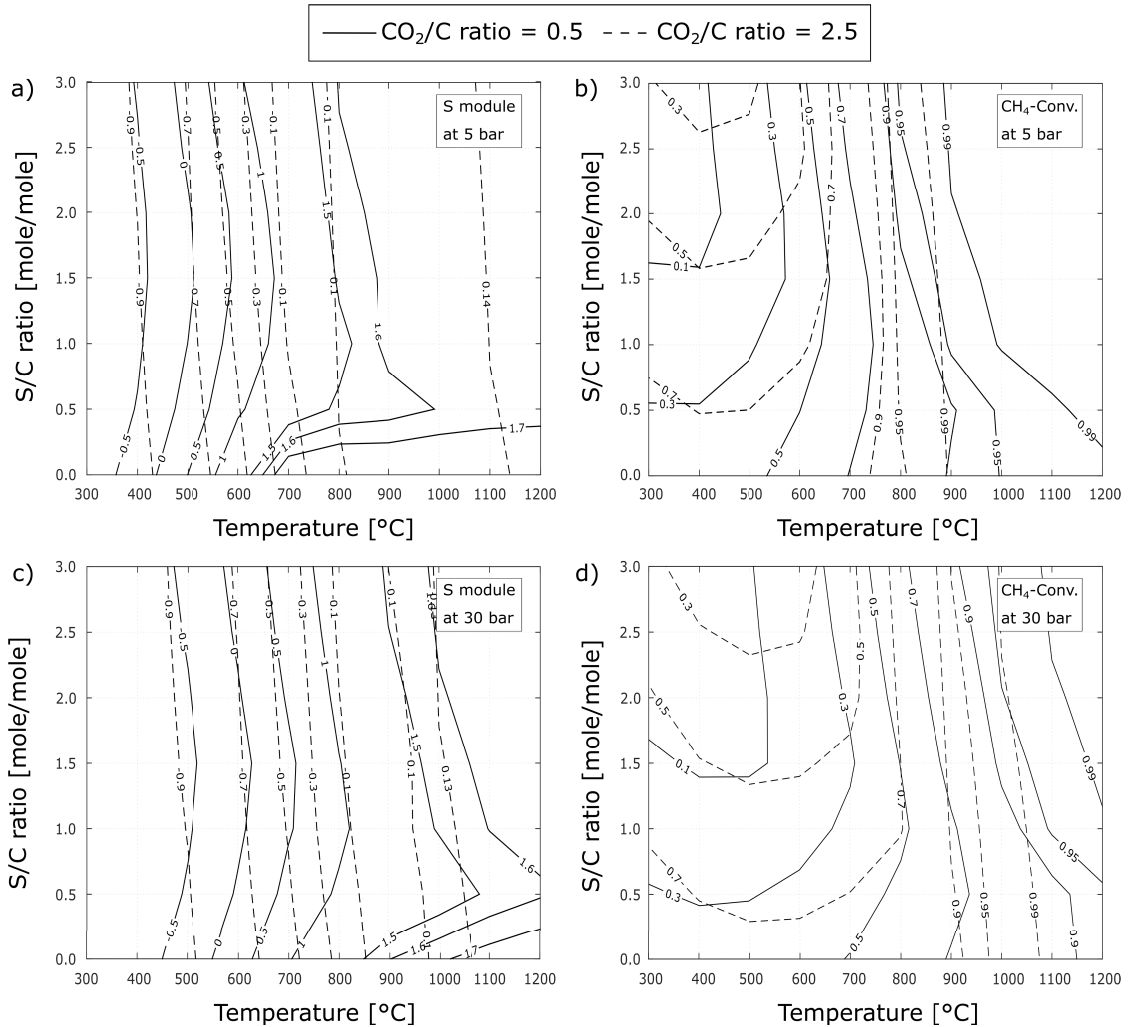
Figure 4.3: Sensitivity analysis of the dry methane reforming technology: a) and b) refer to the S-Module and the CH_4-conversion at 5 bar and c) and d) to the values at 30 bar.

In conclusion, the DMR should be operated in a temperature range of 900 - 1100 °C at a low pressure of 5 bar and a CO_2/C ratio of one. For an operation of a combined reformer (CMR), a slightly lower CO_2/C ratio of 0.8 and a S/C ratio between 0.6 and 0.7 is recommended.

4.1.1.4 Comparative Assessment of the Syngas Characteristics

The sensitivity analyses for the single reforming technologies have shown that the operation parameters for a stoichiometric optimum and a high conversion of CH_4 are different. Consequently the single reforming technologies are not capable of providing a syngas with an optimal composition for the methanol synthesis. However, as mentioned earlier in Section 3.1, the S module is not fully reliable for an assessment of the syngas quality. Therefore, the syngas composition shall also be assessed by using the other stoichiometric parameters.
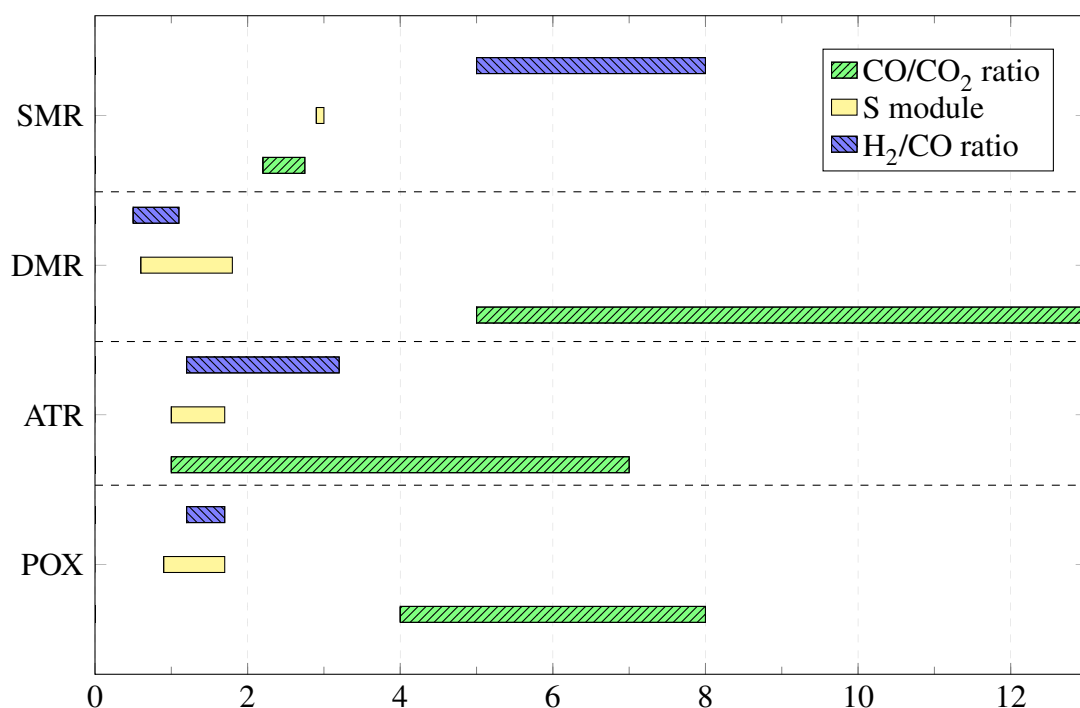
Figure 4.4: Range of the syngas composition for the commercially applied methane reforming technologies. The composition is expressed by three common stoichiomeric measures.

The bar chart in Fig. 4.4 shows the range of the common stoichiometric measures for the basic reforming technologies. The data has been recorded for the typical operation parameters which have been described in Section 3.1. Furthermore, the results are based on a high CH_4-conversion above 95%. The deviation of the stoichiometric measures from their ideal values means losses in terms of methanol yield and causes avoidable costs in the synthesis unit. The syngas from POX, ATR and DMR is highly reactive due to high CO/CO_2 ratio, but is deficient in hydrogen. In contrast, the syngas from SMR is characterized by excess hydrogen and comparatively low reactivity.

Although the characterization of the syngas indicates trends in regard to the efficiency of the synthesis reactor, no concrete conclusions can be drawn. Therefore, the output data of the sensitivity analyses for the reforming Section is used as an input information to an equilibrium synthesis reactor model with fixed temperature and pressure. The ternary plot in Fig. 4.5 shows the sensitivity of the methanol yield to the inlet composition of the synthesis gas at equilibrium conditions of 250 °C and 50 bar. Since the synthesis is also kinetically restricted by the catalyst, the methanol yield is much lower for the rate based models (see Fig. 4.6).
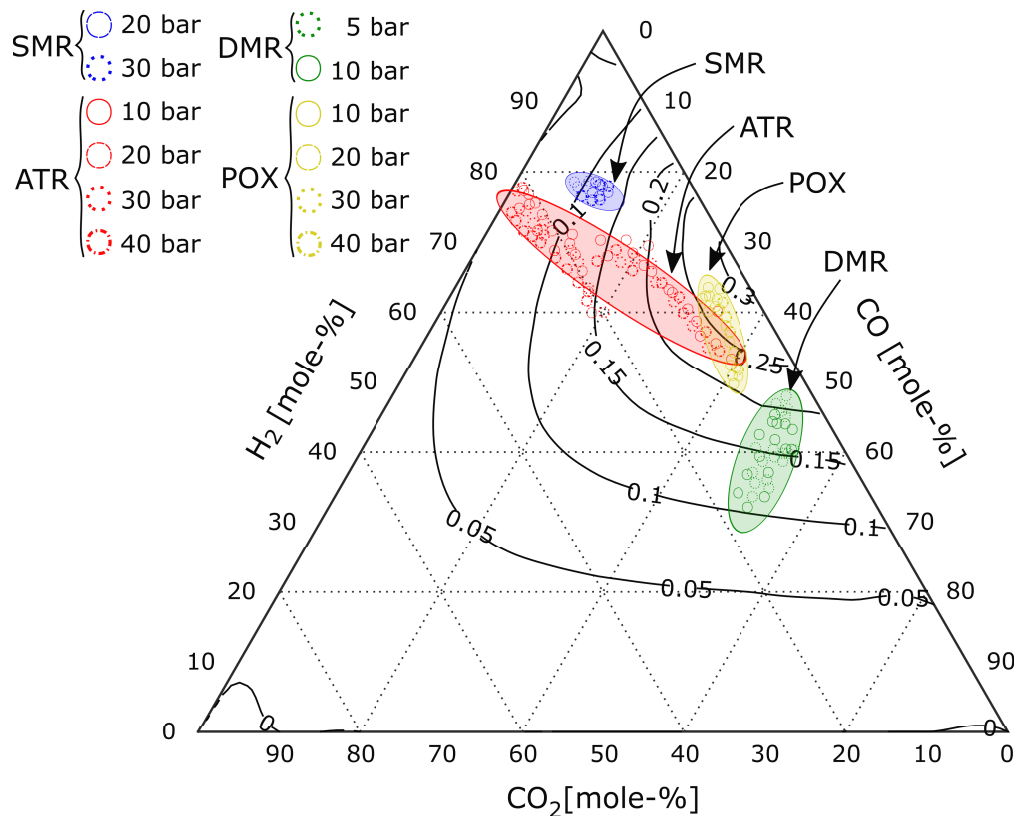
Figure 4.5: Ternary diagram for the methanol yield at equilibrium conditions of 50 bar and 250°C for a given inlet composition.

The selected equilibrium conditions are typical for the industrial used low-pressure methanol synthesis process. The ellipses indicate the agglomeration of recorded syngas compositions, that are obtained from the basic reforming technologies under the typical operation conditions. The key refers to the operation pressure of the respective reformer technology. A high methanol yield may be obtained by feeding a syngas generated by POX. However, this technology requires a large air separation unit for oxygen supply and has disadvantages in terms of heat integration [132]. The industrially most common SMR technology yields relatively small amounts of methanol due to hydrogen excess. In

regard to a syngas generated by ATR, the methanol yield can vary widely depending on the reformer operation. The methanol yield obtained for a typical syngas feed from DMR is in a moderate range. However, the analysis shows that DMR has a potential to be a competitive alternative to common reforming technologies. The results obtained from the sensitivity analysis suggest, that a combination of different reforming technologies can potentially improve the conversion and therefore also the efficiency of the overall system.

4.1.2 Methanol Synthesis

The synthesis reactor is the second core unit of a methanol process as it has high impact on the design and the performance of other system units. Downstream of the reactor, the number of distillation columns and flashing units, as well as the reboiler and condenser duties are determined by the conversion and the formation of by-products. Furthermore, the implementation of syngas conditioning technologies is determined by the performance of the reactor.

The previous analyses have shown that particularly the feed composition influences the conversion rate and thereby the product yield. As described in Section 2.3.2, the conversion is limited by the kinetics of the catalyst and the chemical equilibrium. So far, only chemical equilibrium has been considered as a restriction in the synthesis. To obtain more precise information on the synthesis, kinetics of the reactions have to be taken into account. A variety of models is available to describe the kinetics in methanol synthesis [47]. In this work, the two well-known kinetic models of Graaf et al. [129, 130] and Vanden Bussche et al. [128] have been selected for implementation. The first model describes the kinetics over a Cu/Zn/Al/Zr catalyst for a pressure range of 1 - 50 bar and a maximum temperature of 250 °C. The model of Vanden Bussche et al. uses a commercially available Cu/ZnO/Al$_2$O$_3$ catalyst that is applied in several modern plants. Both models are implemented into the same reactor model (*RPLUG*-Model in Aspen) for analysis of the methanol yield. The underlying operation conditions are very similar to those of the equilibrium model. The use of two models also serves as a validation of the models and as a control of their correct implementation in Aspen. The results of the two models show a very good agreement. Due to the widespread use of the catalyst, Vanden Bussche's model finally is used for the simulation of the processes.

The sensitivity of the methanol fraction to the inlet composition is depicted in the ternary composition diagrams in Fig. 4.6. In comparison with Fig. 4.5, the kinetic limitations become obvious. Furthermore, different conclusions can be drawn in regard

to the optimal syngas composition. As reported in [6, 46, 57, 133, 134] a maximum conversion results for a low CO_2 content of 2 - 10 % and a H_2/CO ratio of 2. Thus, for the design of new and efficient processes, syngas conditioning units have to be considered to decrease the CO_2 content while adjusting the H_2/CO ratio to a value of two. It should be noted that this sensitivity analysis identifies trends to make design decisions. The actual methanol yields of the processes may differ because the reaction rates depend on the components partial pressures and the temperature, and thus on the circulating mass flow, the reactor geometry and the heat flux.

Since methanol is synthesized from a mixture comprising primarily CO, CO_2 and H_2, it is of valuable knowledge which components actively participate in the synthesis. Therefore, the sensitivity of the component conversion rates to the feed composition was analysed for both models at approximately 250 °C and 50 bar. The obtained results which are shown in Appendix correspond to the findings of other studies [128–130, 134, 135].
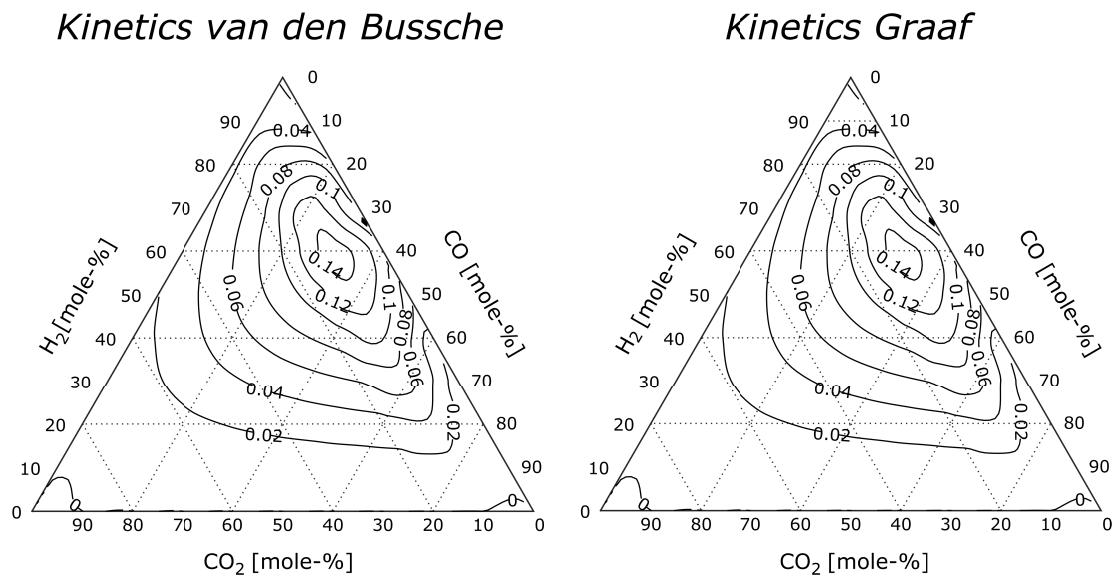
Figure 4.6: Sensitivity of the methanol yield to the inlet composition of the syngas for the kinetic models of Froment and Graaf under pseudo-isothermal conditions.

In the last step, one of the presented reactor models introduced in Section 2.3.2 had to be chosen for a system integration. All processes were simulated using both reactor models, including the synthesis loop for recirculation of unconverted syngas. Typical industrial design features and operation parameters were implemented into the models. With respect to the four-bed quench reactor system, the distribution of the quench gas was subject to an optimization to maximize the product yield at the reactor outlet [136]. The composition of the supplied syngas was taken from the simulation of the reformer technologies. Even if the characteristics of the synthesis have to be considered individually depending on the synthesis gas, the methanol yields correspond to the findings of other studies [86, 87, 137].
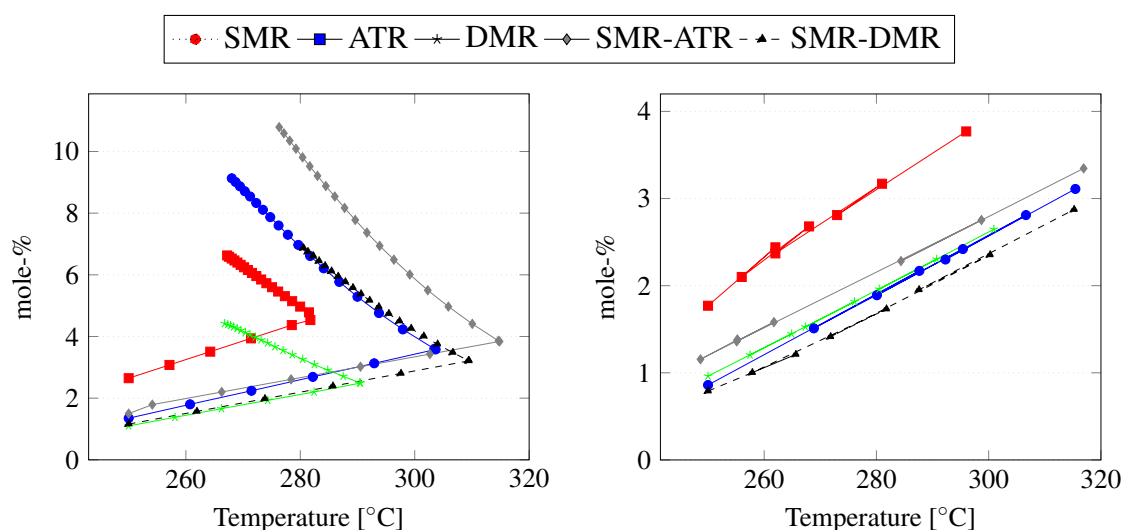
Figure 4.7: Methanol yield from the isothermal reactor and the adibatic quench reactor for different processes.

The results of the methanol yield for the isothermal reactor and the adiabatic quench reactor are shown in Fig D.3. Obviously, for all test cases, a larger amount of methanol is obtained for the isothermal reactor (left in Fig. D.3). The in-situ cooling minimizes the temperature rise inherent to the reaction, therefore allowing an advantegous operation characteristic (see Fig. 2.8). Thus, the isothermal reactor was chosen for all processes, which are subject to further investigations.

4.2 Overview of Processes and Subsystems

The thermodynamic and economic assessment is conducted for the processes in Table 4.1, which are further described in the following sections. Six different process designs are asssigned to the two categories *Base Processes* and *Advanced Processes*. The base processes are characterised by a single reforming technology - the SMR, ATR and DMR design use a stand-alone steam reformer, an autothermal reformer and a dry reformer, respectively. Except for the SMR case, no syngas conditioning steps are integrated into these designs.

The advanced process designs are the result of a carefully conducted design synthesis, which is based on detailed sensitivity analyses and heuristic optimization approaches, that were previously introduced in Section 4.1. In addition to a more complex design of the reforming unit, syngas conditioning steps may be integrated into synthesis path. In the CMR process, combined reforming by hydrogen and carbon dioxide is applied of the syngas stoichiometry. A CO_2 absorption based on the Selexol$^®$ process is implemented for further syngas adjustment. The SMR-ATR process includes a serial two-step reforming concept with downstream syngas conditioning by a reverse water gas shift. The SMR-DMR process features a parallel configuration of a steam methane reformer and a dry methane reformer.

Table 4.1: Specifications of the analysed processes.

Base Processes	SMR	ATR	DMR
Reformer	SMR	ATR	DMR
Syngas conditioning	CO_2-hydrogenation	none	none
Acid gas removal	none	none	none
Synthesis reactor	isothermal	isothermal	isothermal
Carbon utilization	yes	no	yes
Advanced Processes	**CMR**	**SMR-ATR**	**SMR-DMR**
Reformer	CMR	SMR and ATR	SMR and DMR
Syngas conditioning	WGS	RWGS	none
Acid gas removal	Selexol$^®$	none	none
Synthesis reactor	isothermal	isothermal	isothermal
Carbon utilization	yes	no	yes

In general, a methanol plant consists of the following subsystems: a pretreatment unit for the removal of sulfur impurities from natural gas, a reforming unit serving for the production of synthesis gas in conjunction with a syngas conditioning, a synthesis unit for the conversion of syngas to methanol, a purification section for refining of crude methanol in a set of distillation columns and a steam cycle for the heat integration of these subsystems (detailed information is provided in Chapter 2). The heat integration management system is designed for maximum electricity generation and is highly integrated into the other process units. Depending on the configuration, the steam cycle features a different design, whereby heat is recovered as steam in a two-pressure level HRSG. In general, steam must be provided to several process units, including the hydrogenation unit, the pre-reformer and in some cases to the reforming unit (SMR, CMR) and the syngas conditioning units (WGS). The amount of combustion fuel required for covering the heat duty mainly depends on the selection of the reforming unit. Further details will be given within the description of the configurations.

4.3 Basic Assumptions

Some of the major assumptions and design specifications used for the simulation of each process are presented in Table 4.2. The SMR, ATR, DMR, CMR process are designed for a medium capacity, while SMR-ATR and the SMR-DMR generate methanol on a large scale. In all process designs, a high calorific natural gas with a molar composition of of 94.9% CH_4, 2.5% C_2H_6, 0.2% C_3H_8, 0.06% C_4H_{10}, 0.02% C_5H_{12} 1.6% N_2, 0.7% CO_2, 0.02% COS [138] is used as a feedstock. The lower heating value H_i and the higher heating value H_s of the natural gas is 48.78 MJ/kg and 54.10 MJ/kg, respectively. Further assumptions for particular processes are given in the following sections.

Table 4.2: Basic assumptions for all processes.

Subsystem / Component	Unit	Value
General		
ambient temperature [139]	°C	15.0
ambient pressure [139]	bar	1.013
ambient air fractions	mole-%	21 / 79
mechanical efficiency of turbomachinery	%	99.0
electric generator efficiency	%	99.0
electric motor efficiency	%	96.0
syngas compressor isentropic efficiency	%	85.0
recycle compressor isentropic efficiency	%	87.0
Pretreatment		
H_2S absorption coefficient [113]	%	99.9
conversion rate of COS [113]	%	99.5
Methanol Synthesis		
catalyst density [96]	kg/m^3	1,775
void fraction [96]	-	0.5
diameter of tubes [96]	m	0.04
heat transfer coefficient [96]	kW/m^{2}K	0.3
Purification		
topping column		
condenser pressure [101]	bar	1.3
reboiler pressure [101]	bar	1.6
pressure column		
condenser pressure [101]	bar	1.9
reboiler pressure [101]	bar	2.8
Steam Cycle		
steam turbine isen. eff. LP/MP/HP [140, 141]	%	90/93/92
pumps isentropic eff.	%	85.0
condenser pressure	bar	0.05 - 0.4
max. live steam temperature	°C	620.0
pinch point temperature difference liquid/liquid,liquid/gas,gas/gas	°C	5,10,15
pressure drop liquid/gas per 100°C	%	2.0,3.0
pressure loss evaporation	%	4.0

4.4 SMR Process

Steam methane reforming is the most widely used technology for the industrial production of methanol. The first Base process (SMR process) therefore comprises a configuration which is based on commercial available processes for a capacity of 2,500 mtpd. The data was mainly obtained from [50, 96, 142]. A simplified flow diagram is presented in Fig. 4.8 and the corresponding data for a selection of flows from the simulation is given in Table 4.6. Further detailed information on the chemical composition of each stream is provided in Table D.1. The general assumptions in Table 4.2 are completed by the design specifications provided in Table 4.3.

Natural gas is entering the system with stream 1 and is first compressed to a pressure of 30 bar by CM-01. After desulphurization in R-01 and R-02, the sweet gas is entering an adiabatic pre-reformer, where higher hydrocarbons are cracked into methane. The product gas exits the reactor with a temperature of 510 °C and a pressure of 27 bar. Downstream, the effluent (stream 4) is mixed with steam at a S/C-ratio of 3.5 before entering a regenerative heat exchanger for preheating. The plant is equipped with a tubular fired steam reformer, where the heat (250 MW) for the endothermic steam reforming reaction is provided by the combustion of 28.7 kg/s natural gas (stream 7) and 16.5 kg/s tail gas. The tubular reformer consists of 3,500 tubes, each having a diameter of 0.01 meter and a length of 12 meter. The design specifications based on [142] were slightly adjusted to the required capacity. A large flow of combustion air (stream 8) is compressed in steam-turbine driven compressors to a pressure of 3.5 bar. The syngas leaves the steam reformer with a temperature of 950 °C and a pressure of 20.5 bar. The reaction parameters of the SMR section were selected according to the results of the sensitivity analyses in Section 4.1.

The air mass flow and the required fuel supply are determined by the high temperature heat demand of the SMR unit. Downstream, the low temperature heat needs to be integrated to increase the efficiency of the process. The combustion gases (stream 5) leave the furnace with a temperature of 884 °C and are fed to a heat recovery steam generator (HRSG). A part of the heat (approximately 30%) is integrated into the process by preheating the syngas in E-01 and by supply of steam to R-02, R-03 and R-04. The remaining heat (70%) is recovered as steam on two pressure levels. The low pressure level of 30 bar was selected for steam supply to the components within the syngas track. The high pressure level of 70 bar was the result of an iterative optimization process for maximum power generation of the steam turbines T-01 and T-02.

Table 4.3: Design specifications of the SMR process.

Subsystem / Component	Unit	Value
Reforming unit		
pre-reformer		
reactor pressure [50]	bar	28.0
reactor temperature [50]	°C	510.0
steam reformer		
catalyst density [142]	kg/m^3	2,000
void fraction [142]	-	0.5
number of tubes	-	3,500
length of tubes	m	12.0
diameter of tubes	m	0.01
heat transfer coefficient	kW/m^{2}K	0.5
S/C-ratio [33]	mole/mole	3.5
Methanol synthesis		
number of tubes	-	10,000
length of tubes [143]	m	18.0
purge ratio [96]	%	5.0
Purification		
topping column		
number of stages [101, 143]	-	42
reflux ratio	-	0.6
distillate to feed ratio	-	0.3
pressure column		
number of stages [101]	-	81
reflux ratio	-	0.8
distillate to feed ratio	-	0.9
atmospheric column		
number of stages	-	56
reflux ratio	-	0.9
distillate to feed ratio	-	0.7

    The synthesis gas leaving the reforming unit is compressed to 50 bar in multiple syngas compressor (CM-04 and CM-05) with intermediate cooling and water deduction. The compressed gas contains a surplus of hydrogen, which is represented by a stoichiometric module of S equal 3. Before entering the isothermal synthesis reactor, the fresh syngas (stream 6) is blended with three recycle streams of unconverted syngas. A special feature of this process is the stoichiometric adjustment of the syngas composition by

integration of a pure CO_2 stream for carbon utilization. The integration of CO_2 for direct hydrogenation in the synthesis unit was discussed in section 2.2.1. The increase of the carbon dioxide fraction in the syngas feed causes an increased methanol yield. However, an excessive amount of water is also produced via the reverse water-gas shift reaction, increasing the size and the energy demand of the distillation unit.

Table 4.4: Simulation results for selected flows of the SMR process.

Flow	Type	T °C	p [bar]	$\dot{m}$ [kg/s]	$\dot{E}$ [MW]
1	Natural gas	15.0	10.0	16.9	838.5
2	Natural gas	124.6	29.0	16.9	841.6
3	Steam	550.0	29.5	1.3	2.0
4	Clean gas	509.5	24.6	18.2	852.4
5	Exhaust gas	883.7	1.6	1631.9	996.6
6	Syngas	148.2	52.5	42.9	1012.6
7	Natural gas	15.0	16.0	28.7	1425.8
8	Air	15.0	1.0	1586.8	9.4
9	CO_2	45.0	52.5	13.4	8.8
10	Syngas	250.0	49.6	391.8	7099.4
11	Syn. $+ CH_3OH$	38.0	42.9	391.8	6979.8
12	Syngas	38.6	42.9	313.2	5558.5
13	Syngas	35.5	3.5	16.4	284.5
14	Crude methanol	38.0	2.0	60.5	1124.0
15	AAA methanol	71.0	1.3	30.0	672.3
16	Steam	440.0	58.7	358.0	501.8
17	Steam	300.0	27.1	81.1	93.5
18	Condensate	60.1	0.2	439.1	160.2
19	Water	15.0	1.0	65.4	3.26
20	Offgas	146.3	1.2	1630.5	107.8

Before entering the synthesis reactor, the syngas is preheated to 250 °C by recuperation of the thermal energy of the synthesis product. The use of a preheater is indispensable, since a minimum temperature of 220 °C is required for the activation of the reaction mechanism in the low-pressure synthesis. Due to moderate conversion rates and large recycle flow rates, the size of the reactor is relatively large. The reactor vessel contains 10,000 tubes, having a length of 18 meter and a radius of 0.04 meter each [143]. On the shell side, the heat of the exothermic reactions is recovered as steam having a constant
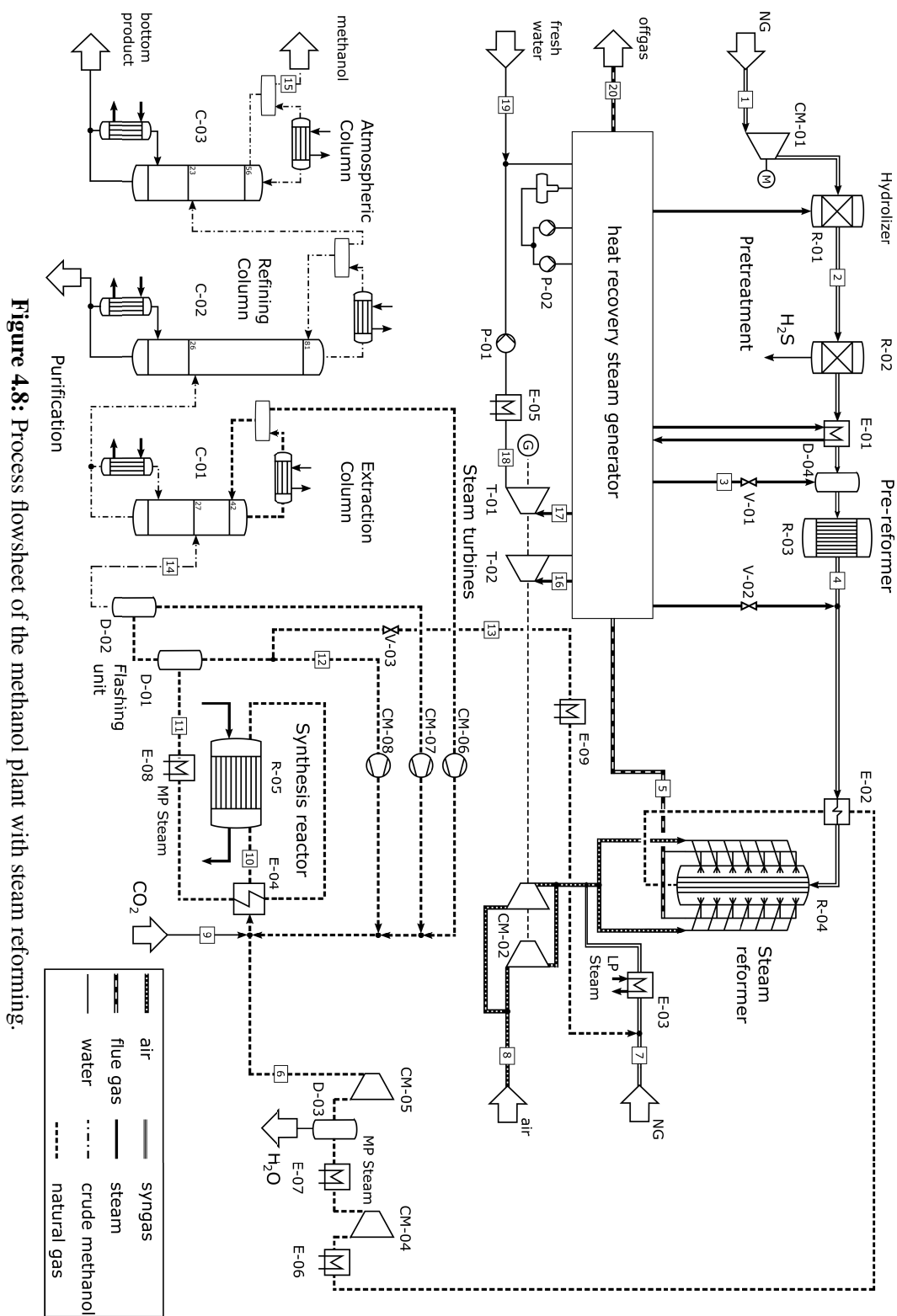
Figure 4.8: Process flowsheet of the methanol plant with steam reforming.

temperature of 262 °C and a pressure of 50 bar. The heat is returned to the process in the reboilers of the distillations columns. The effluent from the reactor (stream 11) consists of crude methanol, water and unconverted synthesis gas. The vapor phase and the liquid phase are separated in two flash drums D-01 and D-02. Three centrifugal compressors (CM-06, CM-07 and CM-08) are used to recycle unconverted syngas to the reactor inlet. Due to a pressure drop of 7 bar within the synthesis loop, the energy demand of the compressors is high. In order to avoid a build up of inert components in the cycle, 5 % of the mole flow rate of the fresh inlet gas is removed from the synthesis. The tail gas (stream 13) is used as a burner fuel in the SMR unit to reduce the consumption of natural gas.

Containing 73 mole-% methanol, the crude product still contains a considerable amount of water and other impurities, which are removed in a three-column distillation unit. Typical operation parameters were taken from [101, 143] and adjusted for high methanol purity. In the first column C-01 the light ends, H_2, CH_4, CO and N_2, are removed from the crude product and recycled to the reactor inlet. The bottom product is further purified in a refining and an atmospheric column (C-02 and C-03), which mainly serve to separate the large amount of water from the product.

4.5 ATR Process

The process based on autothermal reforming in general features a less complex design, but requires an air separation unit (ASU) as an additional subsystem. In comparison to the SMR process, the heat integration system is different, since the reforming unit represents a heat source instead of a heat sink. As a consequence, a combustion of the recycled tail gas is sufficient to cover the heat and electricity demand of the process. The specific assumptions for the simulation of the ATR process are given in Table 4.5. A flowsheet of the design is presented in Fig. 4.9 and the corresponding data for a selection of streams is given in Table 4.6. Further detailed information on the chemical composition of each stream is provided in Table D.2.

A flow of 22.8 kg/s natural gas is compressed to a pressure of 40 bar before desulphurization. Based on the sensitivity analyses in Section 4.1, a high operation pressure is required for high conversion in the combustion and catalytic zone of the ATR (R-03 and R-04). Despite of a low S/C ratio of 0.6, the flow rate of the syngas exiting from the reforming unit is higher than for the SMR process. However, due to elevated reforming pressure the electricity demand in the syngas compression unit is kept in a moderate

range. The conversion in the ATR is completed by supplying oxygen to the combustion zone at a O/C ratio of 0.55. As an additional subsystem an air separation unit (ASU) is required to provide oxygen with a purity of 95 mole-% (Stream 5).

Table 4.5: Design specifications of the ATR process.

Subsystem / Component	Unit	Value
Reforming unit		
pre-reformer		
reactor pressure	bar	34.8
reactor temperature	°C	550.0
autothermal reformer		
catalyst density	kg/m^3	2,500
void fraction	-	0.5
length	m	7.0
diameter [144]	m	1.0
O/C ratio [63]	mole/mole	0.55
S/C ratio [63]	mole/mole	0.6
Methanol synthesis		
number of tubes	-	10,000
length of tubes	m	12.0
purge ratio	%	11.0
Purification		
topping column		
reflux ratio	-	0.6
distillate to feed mole ratio	-	0.1
refining column		
reflux ratio	-	0.75
distillate to feed ratio	-	0.95
atmospheric column		
reflux ratio	-	0.8
distillate to feed ratio	-	0.95

The discharge from the reformer is first cooled in E-02 and E-03 before it is compressed in CM-04 and CM-05 to the operation pressure of the methanol synthesis. Liquid water is rejected from the system after the intercooler (E-05) to reduce the burden on downstream components. Due to a high conversion rate in the synthesis reactor (R-03) and a purge

ratio of 11%, the total circulating mass flow is only half as big as for SMR process. This is beneficial in regard to the size and cost for the reactor, the recuperator E-10 and the recycle compressors (CM-06, CM-07, CM-08). For instance, the length of the reactor tubes is only two-thirds of those in the SMR process. Apart from that, the design and operation of synthesis reactor is similar for the SMR and the ATR process.

Despite the moderate concentration of water in the crude product (8 mole-%), a three column distillation unit is required for the production of grade AA methanol. In comparison to the SMR process having a water content of 25% in the crude product, the heat duty of the reboiler heat exchangers is low.

Table 4.6: Simulation results for selected flows of the ATR process.

Flow	Type	T [°C]	p [bar]	$\dot{m}$ [kg/s]	$\dot{E}$ [MW]
1	Natural gas	15.0	10.0	22.8	1131.9
2	Natural gas	155.3	39.8	22.8	1137.7
3	Clean gas	558.8	34.8	36.7	1171.8
4	Syngas	922.63	33.3	60.2	1096.4
5	Oxygen	277.0	34.8	23.6	10.5
6	Syngas	157.0	25.2	60.2	1018.7
7	Air	15.0	1.0	418.3	2.5
8	Syngas	250.0	50.7	207.2	3763.3
9	Syn. + CH_3OH	38.0	44.8	207.2	3690.5
10	Purge gas	38.2	4.0	18.9	319.2
11	Crude methanol	38.0	2.0	33.8	711.4
12	Bottom product	133.0	2.8	0.9	0.1
13	AAA methanol	70.9	1.3	28.4	637.7
14	Water	15.0	1.0	13.9	0.7
15	Steam	600.0	175.3	61.3	104.9
16	Steam	218.3	15.0	130.2	131.2
17	Condensate	76.0	0.4	130.2	54.7
18	Offgas	110.0	1.9	437.2	35.1
19	Air	15.0	1.0	101.6	0.6
20	Nitrogen	17.9	3.3	76.9	9.7
21	Exhaust Gas	817.1	2.5	437.2	251.8
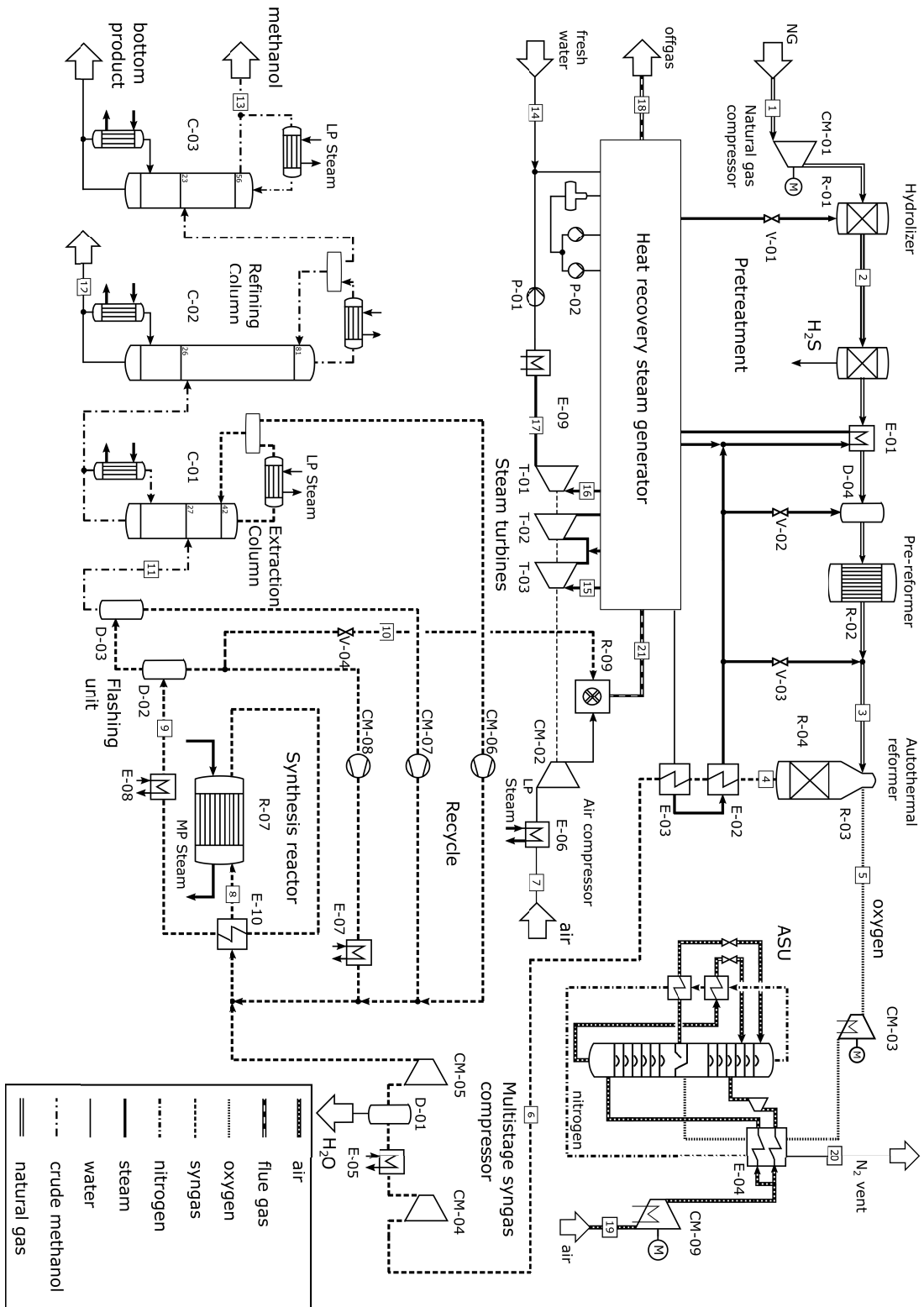
Figure 4.9: Process flowsheet of the methanol plant with autothermal reforming.

Process heat is mainly provided by cooling of the product stream from R-03 and by combustion of the purge gas from the synthesis unit in R-09. In contrast to processes with endothermic reforming, the capacity of the combustion unit is determined by the total electricity demand instead of the process heat demand. Within the HRSG heat is recovered on a medium pressure level (80 bar) and a high pressure level (200 bar) for electricity generation in a set of steam turbines (T-01 - T-03). Process steam with a low pressure between 35 - 40 bar is used for preheating the feed to the ATR and for supply to the components within the syngas track (R-01, R-02, R-03). The low-pressure ASU using an intercooled multistage air compressor does not favor a heat integration.

4.6 DMR Process

The process design with dry methane reforming (DMR) is similar to the design of the SMR process. The major design specifications and assumptions are given in Table 4.7. A process flowsheet is presented in Fig. 4.10 and the corresponding data for a selection of streams is given in Table 4.8. Further detailed information on the chemical composition of the streams is provided in Table D.3.

In contrast to the previously described processes, DMR is operated at a low pressure to attain a high conversion and a favourable syngas composition. Thus, the design is not equipped with a natural gas compressor. The dry reformer (R-04) is based on a tubular GHR design where convective heat is supplied by a flue gas from a combustion unit (R-05). With 360 MW, the process heat demand of the DMR is very large, since the endothermic reactions are carried out between 900 - 1000 °C. To decrease the demand for natural gas (stream 7), a large amount of tail gas is recycled from the synthesis unit (stream 12). The proportion in the total amount of combustion fuel is considerably higher than for the SMR process. A stream of 19.9 kg/s of natural gas is mixed with 60 kg/s of tail gas and combusted with air (stream 8). Before entering the tubes of the DMR, a pure CO_2 flow (stream 5) of 65.6 kg/s is mixed with desulphurized natural gas (stream 4) at a CO_2/C ratio of 1. The process parameters are selected to avoid carbon deposition on the catalyst surface.

The syngas from the reforming unit (stream 6) is characterized by a H_2/CO ratio of 1 and contains less than 3 mole-% of CO_2. Due to high pressure difference between the reforming and the synthesis unit, the electricity demand for the syngas compression (CM-04 and CM-05) is higher than in the alternative base processes. Furthemore, the processing of a large syngas flow additionally increases the energy consumption.

Table 4.7: Design specifications of the DMR process.

Subsystem / Component	Unit	Value
Reforming unit		
pre-reformer		
reactor pressure	bar	3.2
reactor temperature	°C	550.0
dry-reformer		
catalyst density	kg/m^3	2,000
void fraction	-	0.5
number of tubes	-	7,500
length of tubes	m	18.0
diameter of tubes	m	0.01
heat transfer coefficient	kW/m^{2}K	0.5
CO_2/C ratio	mole/mole	1.0
Methanol synthesis		
number of tubes	-	10,000
length of tubes	m	18.0
purge ratio	%	10.0
Purification		
topping column		
reflux ratio	-	0.6
distillate to feed ratio	-	0.1
pressure column		
reflux ratio	-	0.6
distillate to feed ratio	-	0.95

The stoichiometrically inappropriate composition of the untreated syngas results in a relatively low methanol yield. As a consequence, the circulated mass flow rate of unconverted syngas is twice as large design and three times larger than for the ATR design. The large mass flow rate leads to increased gas velocities, which in turn decrease the conversion rate. The components in the synthesis section accordingly are designed for a large capacity and therefore require a high capital investment. In comparison to the other base processes, the crude product shows a high methanol purity of 97.2 mole-%. Due to the low CO_2 content of the fresh syngas, the formation of excessive water in the synthesis unit is suppressed. The processing of the crude product to grade AAA

methanol can be conducted in a two-stage column system with comparatively low heat demand.

As in the SMR design, the capacity of the combustion unit is also determined by the process heat demand of the reforming unit. The combustion gases leaving the shell of the GHR still have a temperature of 950 °C (stream 15). On a lower temperature level, the excess heat is recovered on two pressure levels for electricity generation in a set of steam turbines (T-03, T-02 and T-01). The live steam parameters are given in Table 4.8 for stream 16, 17 and 18. A single reheating is used after T-02 to increase the steam content to 87 % at a condenser pressure of 0.05 bar.

Table 4.8: Simulation results for selected flows of the DMR process.

Flow	Type	T [°C]	p [bar]	$\dot{m}$ [kg/s]	$\dot{E}$ [MW]
1	Natural gas	15.0	7.0	25.3	1256.4
2	Natural gas	155.2	6.5	25.3	1257.7
3	Steam	565.0	67.9	90.1	144.1
4	Clean gas	546.7	5.5	33.2	1281.4
5	CO_2	15.0	5.5	65.6	35.6
6	Syngas	282.8	52.0	93.7	1557.5
7	Natural gas	15.0	5.0	19.9	1036.0
8	Air	15.0	1.0	1442.5	8.6
9	Syngas	250.0	51.7	632.9	8339.6
10	Syn. + CH_3OH	38.0	45.4	632.9	8231.6
11	Syngas	38.0	45.4	533.9	6647.2
12	Purge gas	29.9	4.0	59.3	723.4
13	Crude methanol	38.0	2.0	36.7	802.8
14	AAA methanol	80.4	1.9	31.5	706.3
15	Exhaust Gas	930.8	2.2	1521.8	1045.0
16	HP steam	600.0	178.6	306.3	524.3
17	MP Steam	414.8	64.5	388.5	532.6
18	LP steam	200.0	3.9	388.5	327.6
19	Condensate	32.9	0.05	388.5	68.0
20	Water	15.0	1.0	7.9	0.4
21	Offgas	120.0	1.6	1521.8	135.6
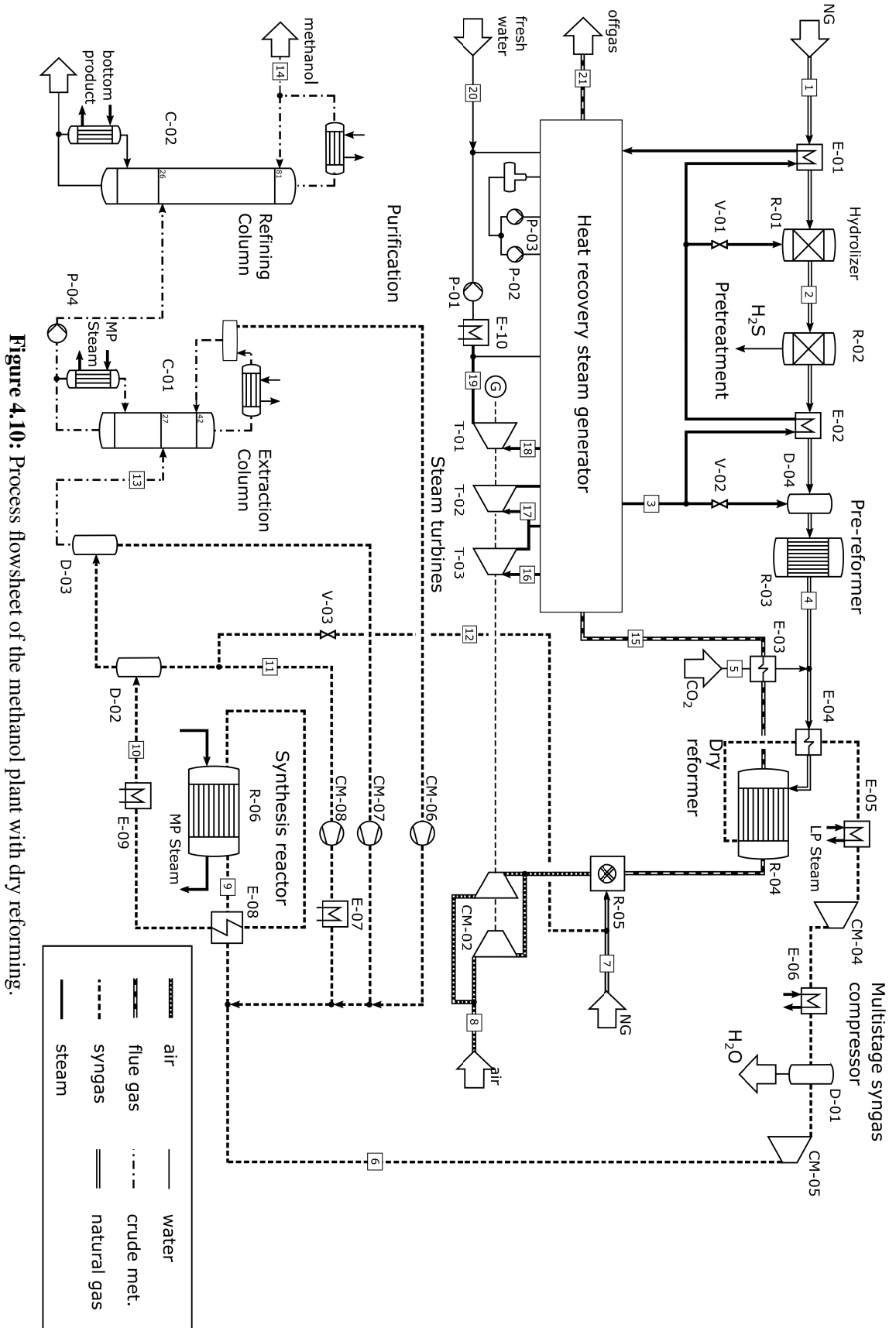
Figure 4.10: Process flowsheet of the methanol plant with dry reforming.

4.7 CMR Process

The bi-reforming concept (combined reforming) was introduced in Section 2.1.9 as an alternative for dry reforming with stoichiometrically more favourable syngas composition. The design is based on the specifications given in Table 4.9 and has methanol capacity of 2,800 mtpd. The process flowsheet and the corresponding data for a selection of streams is presented in Fig. 4.11 and Table 4.10, respectively. Further details on the chemical composition of the flows is provided in Table D.4 in Appendix D. Moreover, the temperature profiles of heat transfer are presented in Fig. 4.12.

Similar to the DMR design, the CMR process dispenses with the need for a natural gas compressor due to low operating pressure or the reformer. A steam flow of 90.1 kg/s (stream 3) and a CO_2 flow of 65.6 kg/s (stream 5) is supplied at a S/C and O/C ratio of 0.68 and 0.8, respectively. Due to the supply of steam the reaction mechanism is less endothermic than pure DMR, but still requires a considerable amount of heat. In comparison to the DMR process, 100 MW less heat is required for a conversion with low methane slip. Accordingly, the fuel demand for natural gas (stream 20) and tail gas (stream 10) is low. As in the other processes with endothermic reforming technology, the excess heat of the combustion gas (stream 15) is recovered as steam for electricity generation. The heat recovery steam generator comprises two pressure levels. The low pressure level mainly serves for steam supply to the reforming unit and for preheating of the reactants, while the high pressure level was chosen for maximum electricity generation. The flue gas (stream 21) leaves the process with a temperature of 120 °C.

The syngas exiting the reformer (stream 5) is characterized by a H_2/CO ratio of 1.4 and contains 4 mole-% CO_2. Downstream, the gas is processed in a low temperature water-gas shift (R-04) to adjust the H_2/CO ratio to the stoichiometric requirement (see Section 2.2.2). Simultaneously, the CO_2 content increases to more then 10%, which would result in an unacceptable low conversion and large recycle flows in the synthesis unit. Therefore, after cooling in E-06 and compression to 31 bar in CM-01, the syngas is fed to an AGR for CO_2 capture by absorption through Selexol$^®$ solvent. A stream of 20 kg/s CO_2 is rejected from the unit and is recycled to the reforming unit. The absorption leads to a reduction of the mass flow and therefore reduces the size and the investment cost of downstream process equipment.

Table 4.9: Design specifications of the CMR process.

Subsystem / Component	Unit	Value
Reforming unit		
pre-reformer		
S/C ratio	-	1.3
reactor pressure	bar	3.2
reactor temperature	°C	550.0
bi-reformer		
S/C ratio	-	0.68
CO_2/C ratio	-	0.8
Syngas conditioning unit		
water-gas shift		
gas temperature at inlet	°C	300.0
length	m	6.0
diameter	m	2.0
CO_2-absorption		
gas temperature at inlet	°C	31
lean solvent temperature [145]	°C	-1
solvent/gas mole ratio CO_2 absorber [145]	-	1.05
CO_2 compressor isen. stage efficiency [146]	%	77-78
Methanol synthesis		
number of tubes	-	10,000
length of tubes	m	18.0
purge ratio	%	10.0
Purification		
topping column		
reflux ratio	-	0.6
distillate to feed ratio	-	0.1
pressure column		
reflux ratio	-	0.9
distillate to feed ratio	-	0.95

The syngas leaving the AGR consists of 32.2 mole-% CO, 0.3 mole-% CO_2 and 66.7 mole-% H_2. The composition favors a high conversion and therefore allows for very small recycle flows in the synthesis loop (stream 8), reducing the size of the recycle compressors and the heat exchangers. The high methanol yield is also due to the generous geometrical design of the synthesis reactor. The crude product entering the distillation unit (stream 11) shows a high purity of 99.4 mole-%, since the formation of water is prevented by the low CO_2 content of the syngas. However, a two-stage column system is required to obtain methanol with grade AA quality. Thus the heat requirement of the distillation columns (C-01 and C-02) is comparatively low. In total, 32.5 kg/s methanol are generated.

Table 4.10: Simulation results for selected flows of the CMR process.

Flow	Type	T [°C]	p [bar]	$\dot{m}$ [kg/s]	$\dot{E}$ [MW]
1	Natural gas	15.0	5.0	16.9	836.8
2	Natural gas	155.0	3.5	16.9	837.0
3	CO_2	550.0	8.0	35.1	28.6
4	Clean gas	800.0	2.9	65.8	909.8
5	Syngas	950.0	2.0	65.8	1088.5
6	Syngas	80.0	31.0	64.5	1033.5
7	Syngas	60.0	24.0	41.5	990.5
8	Syngas	248.3	50.5	112.2	2698.5
9	Syn. + CH_3OH	38	45.5	112.2	2620.3
10	Purge gas	37.8	4.0	7.4	173.2
11	Crude methanol	38.0	2.0	37.9	846.3
12	AAA methanol	80.4	1.9	32.5	735.1
13	Water	15.0	1.0	13.8	0.7
14	Steam	600.0	41.6	166.6	267.7
15	Condensate	32.9	0.05	206.9	37.5
16	Water	20.0	1.0	549.0	27.6
17	Offgas	120.0	1.6	651.2	85.6
18	Exhaust gas	958.0	3.2	651.2	493.1
19	CO_2	183.0	15.0	20.0	40.9
20	Natural gas	15.0	4.0	14.9	735.9
21	Air	15.0	1.0	628.9	3.7
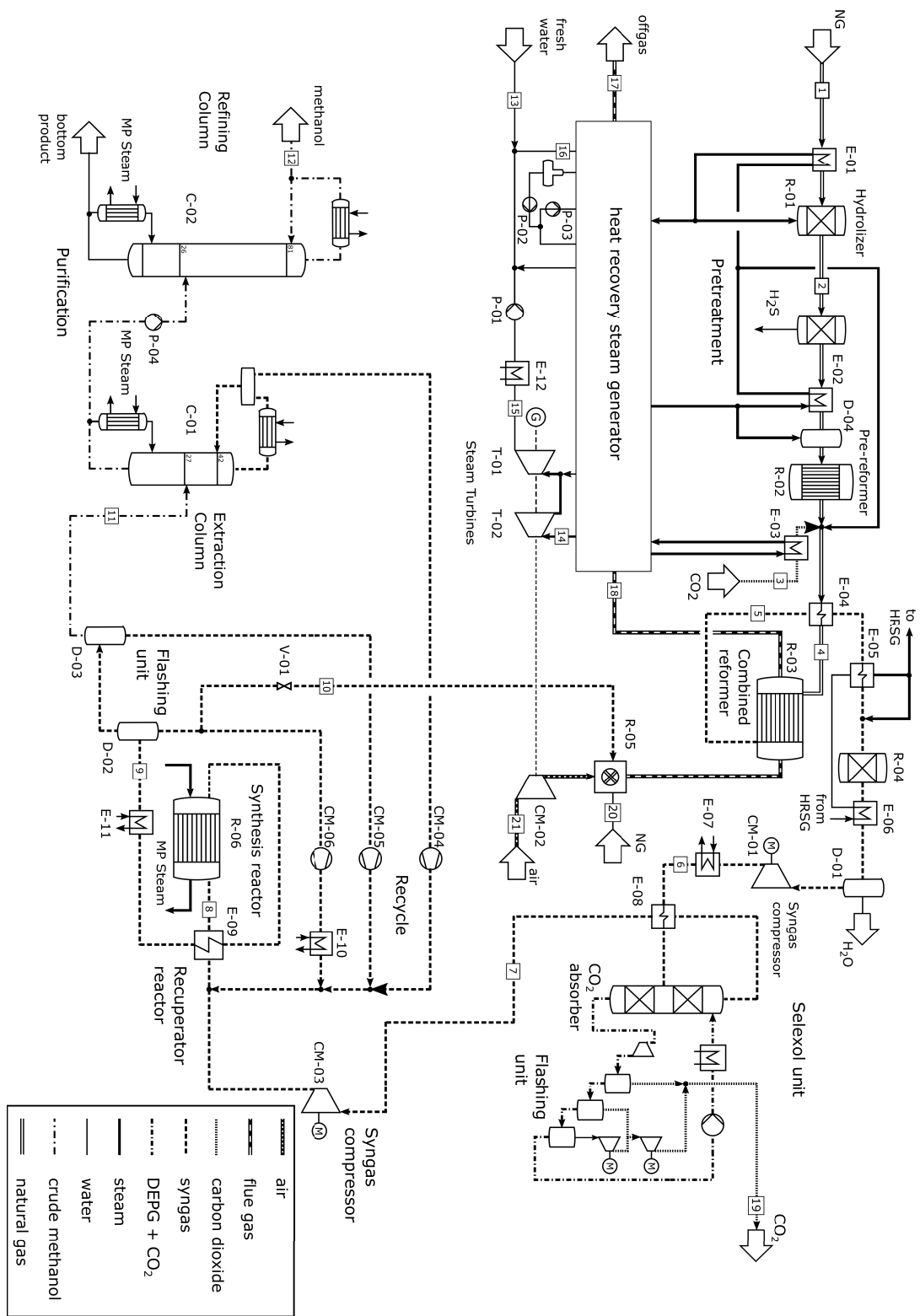
Figure 4.11: Process flowsheet of the methanol plant with combined reforming.
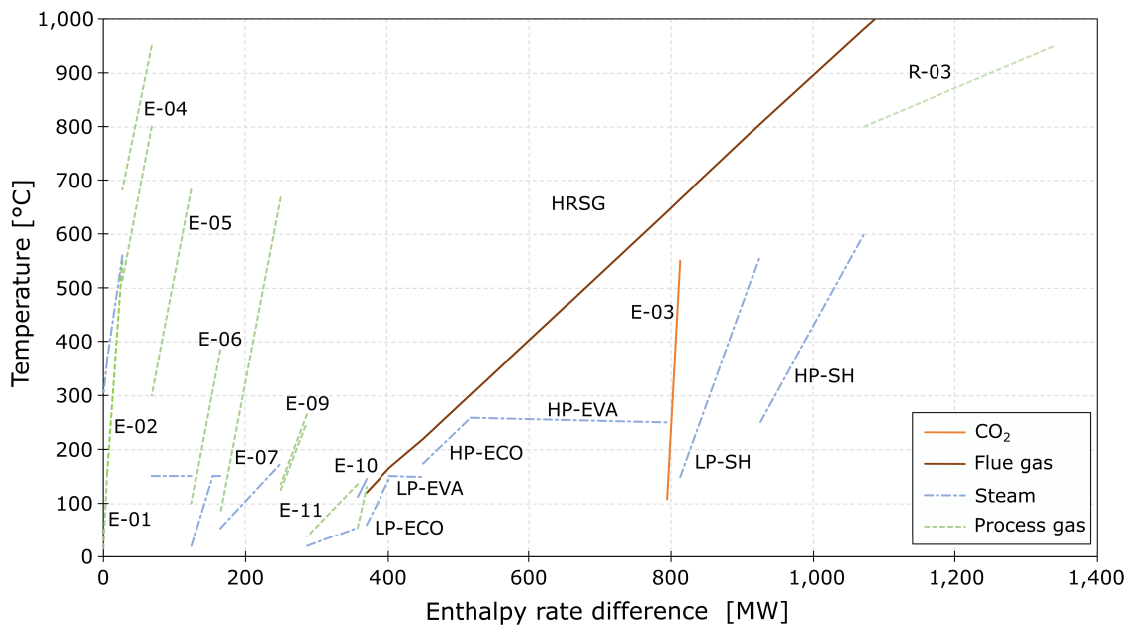
Figure 4.12: Temperature profiles of heat transfer within the CMR process.

4.8 SMR-ATR Process

The SMR-ATR process features a two-step reforming concept, comprising a serial configuration of a convective heated steam methane reformer (primary reformer) and an autothermal reformer (secondary reformer). The reforming concept has been applied on a commercial scale and is designed for a large capacity above 5,000 mtpd. A flowsheet of the system design is provided in Fig. 4.14 and the corresponding stream data is given in Table 4.12. The stream data is supplemented by Table D.5 in Appendix D. Furthermore, the temperature profiles of the heat transfer are presented in 4.13.

A flow of 43.9 kg/s natural gas is compressed in CM-01 to the operating pressure of the reformers (R-03 - R-05). After desulfurization and pre-reforming, methane is partially converted to syngas by SMR in a temperature range of 730 - 920 °C for an operating pressure of 38 bar (7% of methane feed). The remaining methane is subsequently combusted in the second autothermal reformer (R-04) at an O/C ratio of 0.51 to adjust the syngas composition for approaching the stoichiometric optimum. The integration of the secondary reformer reduces the load and the size of the primary reformer, having a low S/C ratio of only 0.5. The heat of the effluent (stream 6) from the secondary reformer is recovered as steam, which is provided to the shell side of the SMR to cover the heat demand of the endothermic reaction. In total, 70 MW of heat are transferred to the tubes of the SMR.

Table 4.11: Design specifications of the SMR-ATR process.

Subsystem / Component	Unit	Value
Reforming unit		
pre-reformer		
reactor pressure	bar	38.6
reactor temperature	°C	680.0
steam reformer		
catalyst density	kg/m^3	2,000
void fraction	-	0.5
number of tubes	-	5,000
length of tubes	m	11.0
diameter of tubes	m	0.01
heat transfer coefficient	kW/m^{2}K	0.5
S/C ratio	mole/mole	0.5
autothermal reformer		
catalyst density	kg/m^3	2,500
void fraction	-	0.5
length	m	7.0
diameter	m	3.0
O/C ratio	mole/mole	0.51
Water-gas shift		
inlet temperature	°C	1,040
length	m	14.0
diameter	m	4.0
Methanol synthesis		
number of tubes	-	10,000
length of tubes	m	18.0
purge ratio	%	10.0
Purification		
topping column		
reflux ratio	-	0.6
distillate to feed ratio	-	0.1
pressure column		
reflux ratio	-	0.6
distillate to feed ratio	-	0.95
atmospheric column		
reflux ratio	-	0.8
distillate to feed ratio	-	0.6

The operation of an autothermal reformer requires the application of an ASU as an additional and cost-intensive unit. A relatively large oxygen stream of 41.8 kg/s is supplied to the combustion zone of the autothermal reformer (R-04). As in the ATR process, the low-pressure ASU does not favor heat integration.

At the outlet of the reforming unit the syngas composition is characterized by a small hydrogen excess (H_2/CO ratio is 2.1). By water rejection in drum D-01 the composition is shifted to the product side of reaction 2.24 to drive the reverse water-gas shift reaction (RWGS) in R-06. Accordingly, a low amount of hydrogen reacts with carbon dioxide to increase the carbon monoxide content. The final syngas composition contains 0.8 mole-% CO_2, 63.6 mole-% H_2 and 31.0 mole-% CO.

Due to high pressure drop along the gas path, the syngas compression also represents a large energy consumer in this process. The pressure difference at the inlet and outlet of the syngas compression almost amounts to 40 bar. After synthesis is carried out at 50 bar and approximately 250 °C, the product stream from R-08 contains 10.4 mole-% methanol, which is separated from the gaseous phase in a flashing unit (D-03 and D-04). The corresponding recycle to feed ratio has a low value of 2.3. The crude product (stream 13) is characterized by a high purity of 97 mole-% methanol. However, three distillation columns are required to produce 63 kg/s methanol of the desired product quality.
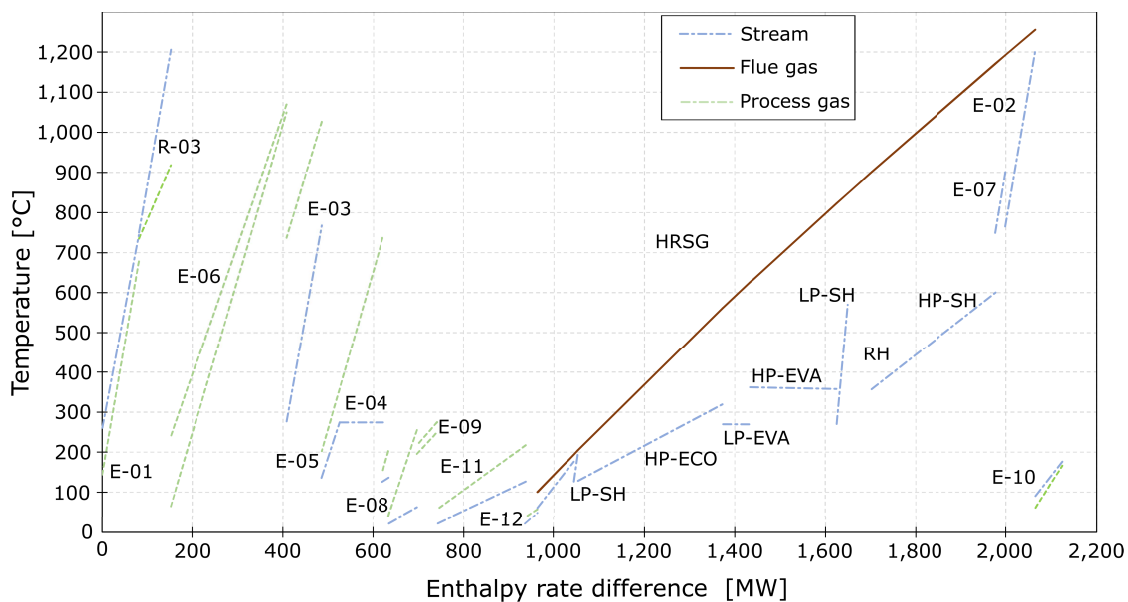
Figure 4.13: Temperature profiles of heat transfer within the SMR-ATR process.
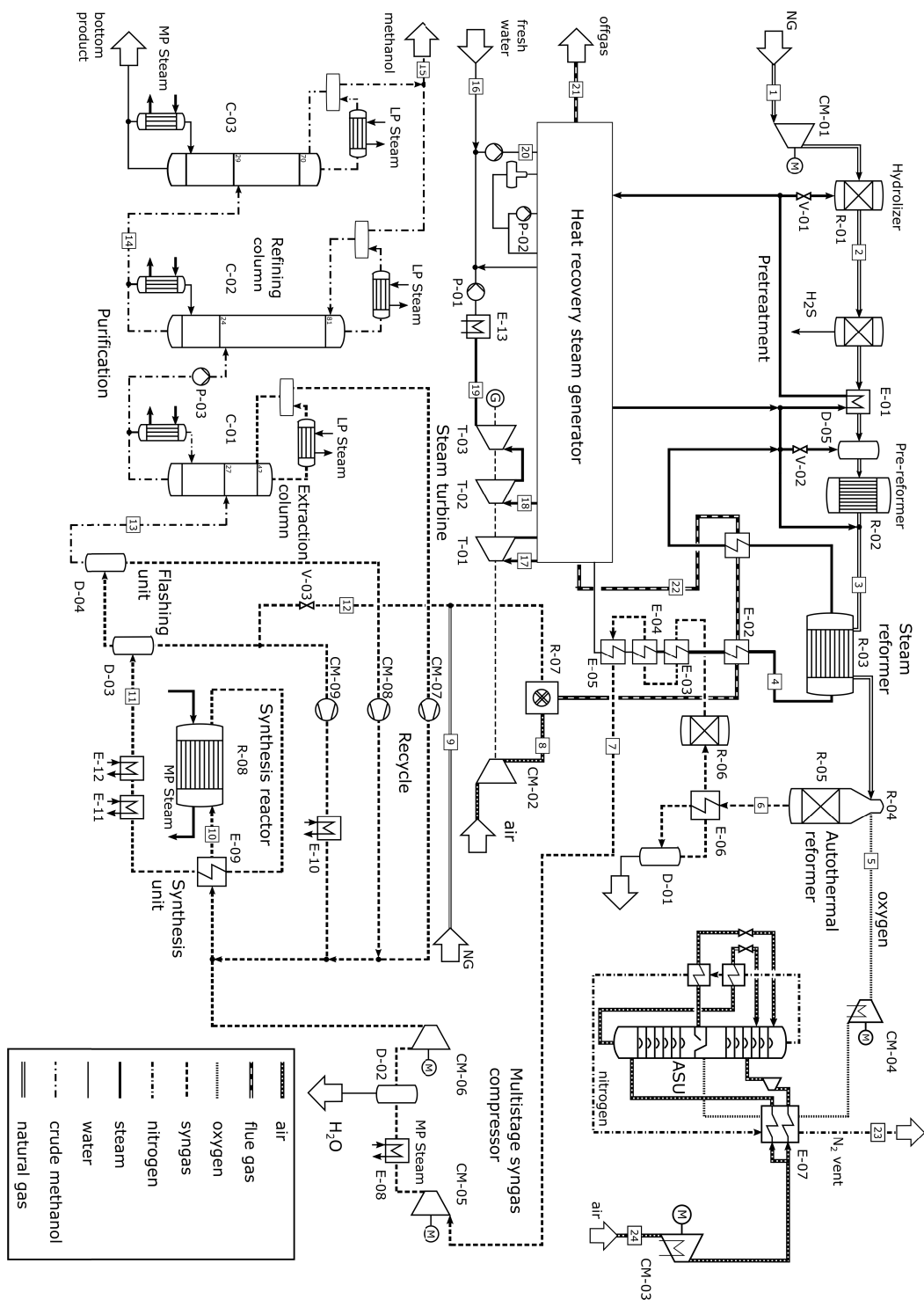
Figure 4.14: Process flowsheet of the methanol plant with two-step reforming.

The units of the entire process chain are embedded in a heat integration system. A moderate amount of additional natural gas (stream 9, 11.8 kg/s) is mixed with a purge of 25.2 kg/s of recycled syngas (stream 12) and is subsequently combusted with air. The air is exposed to a slight pressure elevation by CM-02. The heat of the combustion gases is recovered as steam in a two-pressure level HRSG for electricity generation, in order to cover the demand of the internal consumers. Only by using a single reheating, the steam quality at the oulet of the LP turbine is kept above a technological minimum feasible level of $x = 87.1\%$. The flue gas leaves the HRSG with stream 21 and has a temperature of 100 °C.

Table 4.12: Simulation results for selected flows of the SMR-ATR process.

Flow	Type	T [°C]	p [bar]	$\dot{m}$ [kg/s]	$\dot{E}$ [MW]
1	Natural gas	15.0	10.0	43.9	80.0
2	Natural gas	144.2	44.8	43.9	2191.4
3	Clean gas	734.2	37.8	71.4	2287.4
4	Steam	1219.1	48.5	61.3	169.9
5	Oxygen	273.0	34.0	41.8	18.6
6	Syngas	1059.1	31	113.2	2205.0
7	Syngas	150.0	11.2	93.0	1996.9
8	Air	176.4	4.0	750.1	115.5
9	Natural gas	15.0	4.0	11.8	585.4
10	Syngas	250	50.6	323.0	6700.5
11	Syn.+ CH_3OH	38.0	44.3	323.0	6535.9
12	Purge gas	36.9	4.0	25.2	485.0
13	Crude methanol	38.0	2.0	71.1	1565.3
14	Bottom product	100.8	3.0	2.7	47.9
15	AAA methanol	71.0	1.3	63.0	1423.9
16	Water	15.0	1.0	27.5	1.4
17	Steam	600.0	167.4	261.2	446.9
18	Steam	420.0	45.0	325.6	440.5
19	Condensate	45.8	0.1	325.6	82.1
20	Water	22.0	60.8	1062.9	59.9
21	Offgas	100	1.9	787.1	87.6
22	Exhaust gas	1170.8	2.4	787.1	750.7
23	Nitrogen	17.8	3.3	133.3	16.8
24	Air	15.0	1.0	175.1	1.0

4.9 SMR-DMR Process

The last process design comprises a parallel arrangement of a tubular gas-heated SMR and a tubular gas-heated DMR for a large capacity above 5,000 mtpd. A process flowsheet is presented in Fig. 4.16 and the corresponding data for selected streams is given in Table 4.14. Further details on the chemical composition of each stream are provided in Table D.6 in Appendix D. The underlying assumptions and design specifications are provided in Table 4.13. For a better understanding of the heat integration management, the temperature profiles of heat transfer are shown in Fig. 4.15.

A large mass flow rate of 45.6 kg/s natural gas is entering the system with stream 1 and is preheated and desulphurized in E-01 and R-01. The reforming unit is operated on two pressure levels, since the DMR (R-03) and SMR (R-04) favor a high conversion at significant different operating pressure. Only the subset of gas intended for the SMR (stream 3) is compressed in CM-01 while the gas grid pressure at the inlet is suitable for an efficient operation of the DMR. Downstream of R-03 the process gas requires a compression in CM-02 to allow a mixing with the syngas from the SMR. One quater of the total mole flow rate of natural gas is mixed with carbon dioxide (stream 5) at a CO_2/C ratio of 2 before entering the DMR. The conversion is carried out in a temperature range of 700 - 1050 °C and a pressure of 9 bar. The remaining natural gas (75 mole-%) is fed to the SMR unit and blended with steam at a S/C ratio of 1. The reactions are accomplished in a temperature range of 900 - 1100 °C and a pressure of 30 bar. The selected split fraction is the result of an iterative optimization approach for determination of a favourable syngas composition. However, after mixing the resulting product gas (stream 13) has a H_2/CO ratio of 1.8 and therefore is characterized by hydrogen deficiency.

The process gas having a pressure of 28 bar is subsequently dried and compressed in CM-05 and CM-06. The non-stoichiometric composition of the feed gas only allows a moderate conversion within the synthesis reactor resulting in relatively large mass flows in the recycle loop. Consequently, the recycle compressors and the product coolers are designed for a larger capacity resulting in a high investment cost. It is worth to mention, that the synthesis unit is operated with a high purge ratio of 20% to reduce the size of the loop components. Furthermore, a large recycle of syngas (stream 16) lowers the demand for combustion fuel (stream 12) to cover the internal energy consumption. However, the process heat demand of both reformers still requires the supply of 27.9 kg/s natural gas to the combustion unit. Large air compressors CM-03 and CM-04 operating with low pressure ratio are used to overcome the pressure drop within the flue gas line.

Table 4.13: Design specifications of the SMR-DMR process.

Subsystem / Component	Unit	Value
Reforming unit		
pre-reformer		
reactor pressure	bar	9.2
reactor temperature	°C	540.0
Steam reformer		
catalyst density	kg/m^3	1,775
void fraction	-	0.5
number of tubes	-	1,600
length of tubes	m	15.0
diameter of tubes	-	0.1
heat transfer coefficient	kW/m^{2}K	0.5
S/C-ratio	mole/mole	1.0
Dry methane reformer		
catalyst density	kg/m^3	2,000
void fraction	-	0.5
number of tubes	-	550
length of tubes	m	13.6
diameter of tubes	m	0.1
heat transfer coefficient	kW/m^{2}K	0.5
Methanol synthesis		
number of tubes	-	10,000
length of tubes	m	18.0
purge ratio	%	20.0
Purification		
topping column		
reflux ratio	-	0.6
distillate to feed ratio	-	0.1
refining column		
reflux ratio	-	0. 75
distillate to feed ratio	-	0.95

The crude product leaving the synthesis unit with stream 17 has a high methanol concentration of 96.3 mole-%. The desired product quality can be ensured by the

application of a two-stage column system. A flow of 65.9 kg/s methanol with Grade AA quality is generated within the process.

Similar to the base processes with DMR and SMR, the firing duty within the combustion unit is determined by the process heat demand of the two reforming reactors R-03 and R-04. A large flow of exhaust gas (stream 9) is splitted and passes through the shell-side of the tubular reactors, which are manufactured from high temperature resistant alloys. Downstream, the mixing stream still has a high temperature above 900 °C before entering the HRSG. The low-temperature heat is recovered on two pressure levels for electricity generation (see Figure 4.15). A single reheating is used to keep the steam content above $x = 87.3\%$ at the outlet of the LP steam turbine T-02. Exiting the HRSG the exhaust gas (stream 25) still has a temperature of 120 °C.
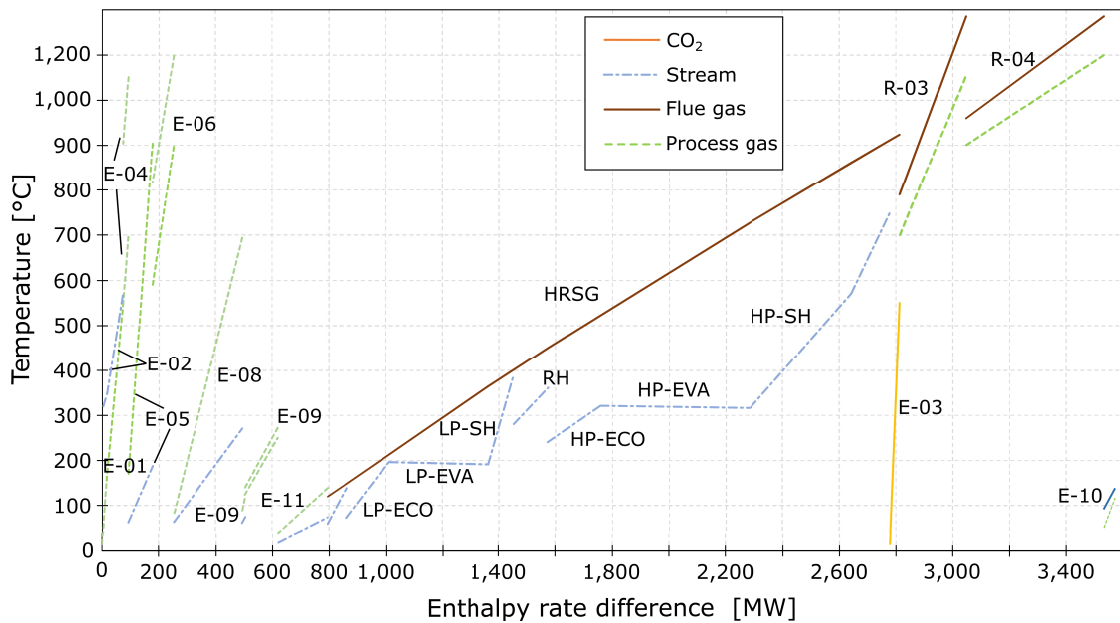
Figure 4.15: Temperature profiles of heat transfer within the SMR+DMR process.
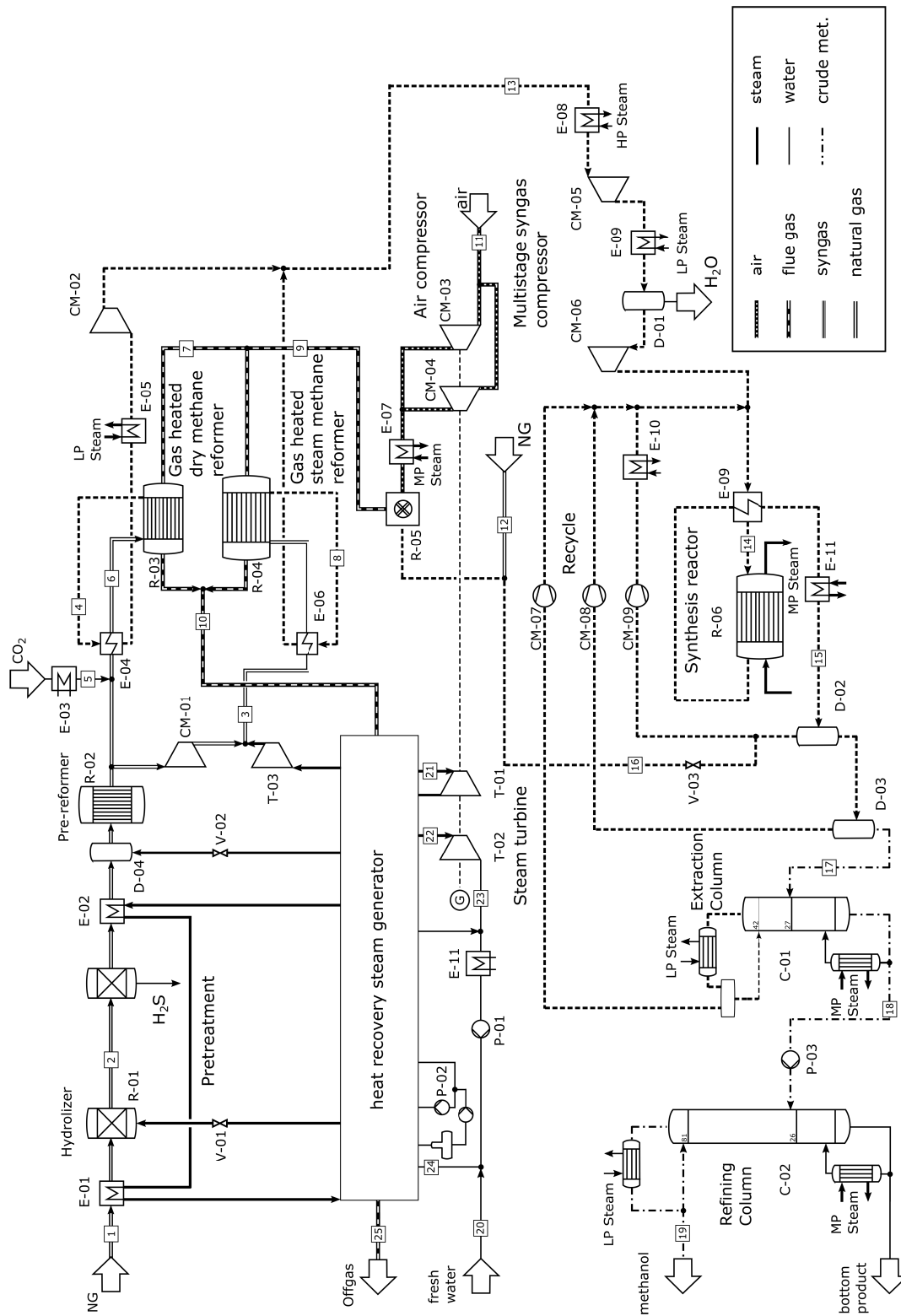
Figure 4.16: Process flowsheet of the methanol plant with steam and dry reforming.

Table 4.14: Simulation results for selected flows of the SMR-DMR process.

Flow	Type	T [°C]	p [bar]	$\dot{m}$ [kg/s]	$\dot{E}$ [MW]
1	Natural gas	15.0	10.0	45.6	2263.8
2	Natural gas	155.2	9.7	45.7	2266.5
3	Clean gas	590.1	33.0	73.8	1788.7
4	Syngas	1050.4	7.8	71.7	796.0
5	CO_2	550.0	9.2	59.3	48.7
6	Clean gas	700.0	8.8	71.7	632.4
7	Exhaust gas	1185.2	3.5	467.2	459.3
8	Syngas	1098.5	29.0	73.8	2191.6
9	Exhaust gas	1184.4	3.1	2172.9	2134.5
10	Exhaust Gas	923.8	3.1	2172.9	1544.7
11	Air	15.0	1.0	2077.3	12.3
12	Natural gas	15.0	5.0	27.9	1380.8
13	Syngas	693.6	28.7	145.5	2881.8
14	Syngas	250.0	50.2	417.7	7584.6
15	Syn. + CH_3OH	38.0	46.4	417.7	7404.2
16	Purge gas	35.0	5.0	67.8	1121.7
17	Crude methanol	38.0	2.0	76.4	1664.8
18	Bottom product	77.5	1.6	68.5	1509.1
19	AAA methanol	80.4	1.9	65.9	1492.6
20	Water	15.0	1.0	5.0	0.3
21	Steam	503.0	114.2	392.4	602.1
22	Steam	360.0	14.2	589.9	683.2
23	Condensate	32.9	0.05	589.9	103.7
24	Water	24.8	15.0	703.0	36.6
25	Offgas	120.0	1.8	2172.9	207.4

Chapter 5

Results and Discussion

This chapter presents the results obtained from the thermodynamic and economic analysis for the six processes that have been declared in the previous chapter 4. First, the process performance will be investigated on the basis of several chemical and thermodynamic indicators before an energetic analysis is carried out. Particular attention will be devoted to the CO_2 utilization potential by investigating the different integration concepts within the processes. Subsequently, a conventional exergetic analysis is conducted to identify the sources and the magnitude of the real inefficiencies occurring within the process units. An economic analysis is performed for an estimation of the investment cost and the variable cost involved in the projects. In this context, the impact of market prices of fuel and products on the revenue and the contribution margin of the analysed systems is also examined. Furthermore, an exergoeconomic analysis is conducted to determine the cost impact of each component on the overall system and the levelized cost of the generated products. Finally, for the most promising process, an advanced exergetic analysis is conducted to analyse the interdependencies among the components and their potential for an improvement.

5.1 Process Performance Analysis

In the following, characteristic parameters will be discussed to understand the main differences resulting from the design specifications of the analysed processes. Table 5.1 shows a selection of results for a comparison of the thermodynamic characteristics of the processes. Separately, Table 5.2 shows several chemical parameters which assess the performance of the reforming unit and the synthesis reactor. Furthermore, an energy distribution of the processes is presented in Figure 5.1.

Table 5.1: Selected results of the overall process.

		Base processes			Advanced processes		
		SMR	ATR	DMR	CMR	SMR-ATR	SMR-DMR
CH_3OH-capacity	mtpd	2590	2452	2719	2803	5440	5694
$\dot{W}_{el,net}$	MW	140.2	4.5	222.9	30.9	146.3	215.2
CH_4 process gas	kg/s	16.9	22.8	25.3	16.9	43.9	45.6
CH_4 comb. fuel	kg/s	28.7	-	19.9	14.9	11.8	27.9
Electric intensity	MJ/kg	1.78	1.06	3.23	3.06	1.73	1.52
CH_4-intensity[1]	kg/MWh	202.0	126.1	175.1	149.5	126.4	154.9
HP live steam temp.	°C	440.0	600.0	600.0	600.0	600.0	503.0
MP live steam temp.	°C	300.0	423.0	415.0	-	420.0	-
LP live steam temp.	°C	152.0	218.0	200.0	250.0	144.0	360.0
HP live steam pres.	bar	58.7	175.3	178.6	42	167	114.2
MP live steam pres.	bar	27.1	62.8	64.5	-	45	-
LP live steam pres.	bar	5.0	15.0	4.0	3.9	3.0	14.1
Exit temp. offgas	°C	146.0	110.0	120.0	120.0	100.0	120.0

[1] Ratio of total CH_4 intake to the total exergy of product

Taking into account technical limitations and scaling effects, the processes are designed for different methanol production capacities given in metric tons per day (mtpd). The base processes are designed for a methanol production of 2,450-2,720 mtpd, which is the typical capacity range for the majority of the plants in commercial operation. A single ATR unit may also cover a higher capacity of up to 5,000 mtpd [56]. The CMR process is designed for a slightly higher capacity, while the other two advanced prosesses represent large-scale applications above 5,000 mtpd. Furthermore, in all processes, electricity can be supplied to the grid as a second product. The net power $\dot{W}_{el,net}$ is particularly high for the processes with endothermic reforming technology. Here, the electricity generation is directly linked to the supply of process heat. In contrast, in the system with autothermal reforming technology, the steam cycle can be designed to cover only the internal electricity demand.

For all processes, heat is recovered as steam within a two-pressure level HRSG. Depending on the process design, the steam is expanded in two or three steam turbines. The differences in the steam cycle design are mainly influenced by the internal steam consumption of different units in the synthesis path and the pressure at which the steam

is required. In the SMR and SMR-DMR process, high temperature steam is primarily used as a reforming agent and for preheating the reactants, thus reducing the HP live steam temperature. The offgas temperature is similar for most of the processes. In the SMR process, low temperature heat is not integrated into the synthesis loop, resulting in a high offgas temperature.

Furthermore, the electric intensity and the CH_4-intensity are provided in Table 5.1. The electric intensity is calulated as ratio of the electrical duties, which are associated with synthesis process chain to generate the chemical product, to the mass flow rate of methanol. Thus, this number includes the power required for compression of the natural gas, the syngas and the recycle streams. The electric intensity is particularly high for the DMR and CMR process due to an energy-intensive syngas compression. The CH_4-intensity represents the ratio of the total natural gas intake, including the amount for syngas generation and for combustion, to the exergy of product of the overall system. For obvious reasons, the processes with single endothermic reforming technology are represented by a high CH_4-intensity. On the other hand, processes with autothermal reforming are characterized by a low intensity.
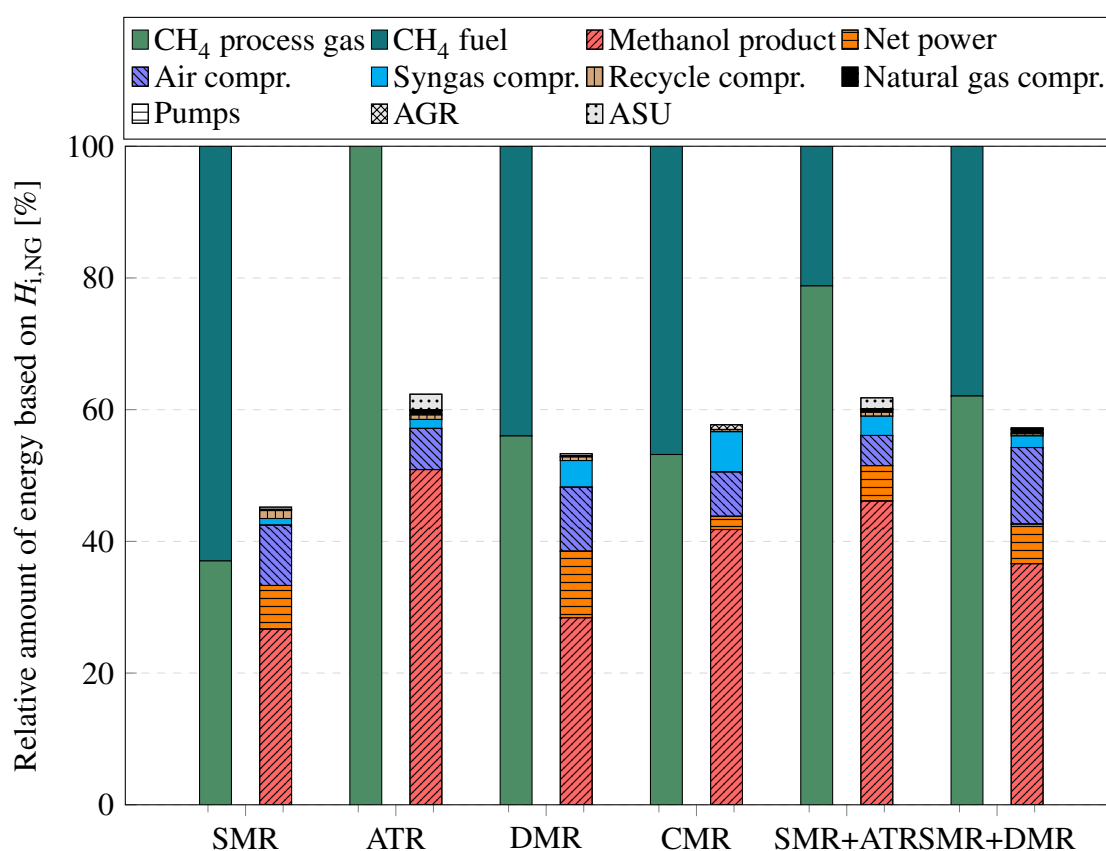
Figure 5.1: Energy distribution within the analysed processes.

The bar chart in Fig. 5.1 shows detailed information on the energy distribution within the processes. All values are given as relative data based on the lower heating value of the total methane intake. The left bar of each process represents the energy of the inlet streams, which refer to the amount of natural gas used for syngas generation and process heat supply, respectively. Furthermore, the right bar shows the product distribution (methanol and net electricity) and the internal electricity demand assigned to the main consumers.

Considering the left bars, the structure of the energy supply varies greatly for the processes. Due to the exothermic character of the ATR, sufficient process heat is generated directly in the syngas track, thereby eliminating the need to supply natural gas to the combustion unit. In contrast, the heat demand of the SMR and DMR technology is covered by the supply of natural gas as a combustion fuel. Accordingly, the proportion of natural gas intended for combustion is low for the SMR-ATR process. A clear assignment of the methane intake to the respective purpose is difficult, since the purge ratio varies for the processes.

The amounts of energy output (right bar) should be treated with care, since products of different energetic quality are produced. Most of the supplied energy obviously is converted into methanol, which is of lower energetic quality than electricity. In regard to the power generation, for all processes, the major part of electricity is consumed internally. The air compressor as the main consumer of electricity in particular has a large capacity for the processes with endothermic reforming technology. Here, the air intake is higher, as the demand for process heat is larger. The syngas compressor as the second largest consumer serves to overcome the pressure difference between the reforming unit and the synthesis unit. Especially for the processes with low-pressure DMR and CMR, the pressure difference and thus the energy consumption is high. On the other hand, an energy-intensive natural gas compressor is required for the high-pressure reforming processes based on ATR and SMR technology. Due to relatively low volume flows, a compression prior to reforming is less energy-intensive than downstream of the syngas generation unit. Fig. 5.1 shows, that the ASU in the ATR and the SMR-ATR process also constitutes a significant electricity consumer, caused by the multi-stage compression of very large air flows. Interestingly, the energy consumption of the recycle compressors in all processes is comparatively low, despite a high pressure drop in the synthesis loop. All other consumers, including the AGR in the CMR process, are also of minor significance.

An interpretation of the previous results requires an investigation of the key chemical components since their operation decisively influences the overall process characteristics.

Table 5.2 shows selected results for the reforming unit and the synthesis reactor. By providing information on the composition of the syngas after the reformer and at the inlet of the reactor, the impact of conditioning technologies and the recycle flows becomes visible. Regarding the synthesis reactor, the conversion rates of CO_2, CO and H_2 are represented by X_{CO_2}, X_{CO} and X_{H_2}. The mole ratio of the recycled flows to the syngas make-up flow is termed as recycle to feed ratio (RTFR). In general, the results are in line with the information obtained by the parameter studies.

Table 5.2: Selected results for the reforming unit and the synthesis reactor.

		Base processes			Advanced processes		
		SMR	ATR	DMR	CMR	SMR-ATR	SMR-DMR
		Syngas composition after reforming					
CO_2	mole-%	4.9	4.4	2.8	10.8	2.9	2.3
CO	mole-%	10.2	23.3	43.7	28.8	25.3	32.3
H_2	mole-%	49.0	56.1	42.4	58.4	58.2	57.6
CH_4	mole-%	0.3	1.1	3.6	0.0	0.0	0.9
H_2O	mole-%	35.2	14.1	7.5	1.6	12.8	6.5
		Syngas composition before the synthesis					
CO_2	mole-%	16.4	10.1	10.3	0.9	3.0	6.9
CO	mole-%	9.6	19.9	52.5	29.1	28.5	31.6
H_2	mole-%	68.5	61.4	28.2	66.7	63.5	56.8
CH_4	mole-%	1.4	2.9	6.5	0.3	0.3	1.9
H_2O	mole-%	0.5	0.4	0.6	0.0	0.2	0.8
		Synthesis Reactor					
RTFR	mole/mole	5.9	2.7	5.8	1.7	2.3	3.1
X_{CO_2}	%	8.0	2.1	6.9	17.3	2.4	6.0
X_{CO}	%	18.6	28.3	17.2	42.0	26.2	24.6
X_{H_2}	%	10.9	19.4	31.1	37.9	23.4	24.4
CH_3OH-yield	mole-%	6.0	8.0	5.0	15.0	10.4	9.9

As presented in Section 4.1, the composition of the syngas generated by the single reforming technologies in the base processes differs to a large extent. The syngas produced by SMR and ATR is characterized by a hydrogen surplus with reference to the stoichiometry of the methanol synthesis. A RWGS unit would be an adequate mean to

set a more favorable CO/H_2-ratio, while reducing the mole fraction of CO_2. In contrast, an unconditioned syngas provided by DMR has a high surplus of carbon monoxide and therefore would require a one-step WGS to improve the composition towards higher methanol yield. For all base processes, the CO_2 content is within an acceptable range. In particular the syngas from SMR contains a lot of steam, which causes an additional energy duty in the syngas compressor. In regard to the DMR process, a high methane slip of 3.6% results in large recycle flows of inert components in the synthesis loop. The methane conversion could be further increased by raising the mild operation conditions.

The syngas composition at the reactor inlet greatly deviates from the composition of the reforming product. According to the conversion rates X_{CO_2}, X_{CO} and X_{H_2}, the recycled syngas in the SMR and ATR is characterized by a lower mole fraction of CO and a higher mole fraction of H_2 and CO_2 (compared to the make-up syngas). Thus, through mixing of fresh and recycled syngas, the composition shifts to less favorable stoichiometric ratios. In regard to the DMR process gas, hydrogen is primarily active in the synthesis as indicated by the value of X_{H_2}. Accordingly, the syngas composition at inlet of the reactor is shifted to even lower values of H_2/CO ratio. Overall, comparatively low methanol yields in the range of 5 - 8 mole-% result for the base processes. Thus, a high RTFR of 5.9 and 5.8 results for the SMR and DMR process, while a moderate ratio of 2.7 is obtained for the ATR process.

With respect to the advanced processes, the reforming unit is designed for an improvement of the syngas composition for high methanol yield. At the reactor inlet the process gas has a value for the H_2/CO ratio in the range of 1.8 - 2.3. In the CMR process, the high CO_2 content of 10.8% would result in very large recycle streams. By application of an AGR with physical absorption, the CO_2 content is successfully reduced to a minimum. The highest conversion rates and accordingly the lowest RTFR result for the CMR process. The methanol yield for the advanced processes is in the range of 10 - 15 mole-%, reducing the RTFR to 1.7 - 3.1.

In general, a reduction of the circulated mass lowers the investment cost for the components of the synthesis unit. Furthermore, the amount of undesirable low temperature heat from the synthesis is decreased, reducing the capacity of several heat exchangers.

5.2 Potential Analysis for Carbon Dioxide Utilization

The potential for carbon dioxide utilization by different integration strategies is investigated. The direct hydrogenation of CO_2 as in the SMR process and the dry reforming by CO_2 as in the DMR, CMR, and SMR-DMR process constitute the two main measures for CO_2 utilization in methanol synthesis [84, 147]. The integration not only abates CO_2-emissions by valorization to a chemical intermediate, but also reduces the feedstock and combustion fuel that is required for the production. For the calculation of the CO_2-abatement and the CH_4-reduction, the processes are benchmarked against a conventional SMR process (Reference) without CO_2-hydrogenation.

Table 5.3 shows the main results of the CO_2-abatement within the analysed processes. For a comparison of processes generating two products of different energetic quality, the overall exergy of product $\dot{E}_{P,tot}$ seems to be the only reliable base for a comparison. The key figures provided in Table 5.3 have been defined in Section 2.2.1.

Table 5.3: Key figures of the CO_2-abatement potential within the analysed processes.

		Ref.	SMR	DMR	CMR	SMR-DMR
$\dot{E}_{P,tot}$	MW	693.78	812.54	929.13	765.97	1707.75
CH_4-consumption	t/h	159.13	148.00	162.78	114.26	238.42
CH_4-reduction	t/h	0	38.65	50.33	61.42	153.28
CO_2-feed	t/h	0	48.88	65.57	16.82	59.29
CO_2-feed inten.	kg/MWh	0	60.15	70.58	21.96	34.72
CO_2-emission	t/h	286.91	333.88	504.10	174.93	580.67
CO_2-emis. inten.	kg/MWh	413.54	410.91	542.55	228.37	340.02
CO_2-abatement	kg/MWh	0	62.79	-58.43	207.13	108.24
CO_2-abatement [1]	kg/MWh	0	191.53	89.27	425.80	352.97

[1] The key figure additionally considers the abated CO_2 associated with the CH_4-reduction. An emission factor of 55.9 t_{CO_2}/TJ is used for the calculation.

The results in Table 5.3 show that in all processes CO_2 can be successfully integrated for a reduction of the natural gas intake. However, other effects such as design improvements also have a significant influence on the fuel reduction and the other key figures. In particular for the SMR and the DMR process, a large amount of CO_2 is integrated per MWh exergy of product. Furthermore, the number of the total CO_2-emissions is provided to assess the true abatement potential of the processes. The amount of emitted CO_2 by

far exceeds the amount of integrated CO_2. The CO_2-abatement per MWh of exergy of product is calculated by substracting the difference of the emission intensity and the feed intensity of the considered process from emission intensity of the reference system. The integration measures by direct hydrogenation and partial CO_2 reforming successfully lead to an abatement of CO_2 per MWh of exergy of product. The highest CO_2-abatement with 207.1 kg/MWh results for the CMR process, followed by the SMR-DMR process and the SMR process with 108.3 kg/MWh and 62.8 kg/MWh, respectively. The DMR process offers no abatement potential since dry reforming requires a large amount of process heat (provided by combustion gases), thus resulting in high CO_2 emissions. If the abated CO_2 associated with the CH_4-reduction is taken into account with a factor of 55.9 t_{CO_2}/TJ [148], an abatement potential results for all processes. Depending on the CH_4-savings, the CO_2-abatement can reach considerably higher values.

5.3 Conventional Exergetic Analysis

The results obtained from the exergetic analysis for the overall system are given in Table 5.4. The processes are designed for different methanol production capacities and co-generate electricity in some cases. The exergy concept is the only reasonable base for a comparison of processes generating products of different energetic value. A distribution of the inefficiencies occurring within the major subsystems ($\dot{E}_{D,sys}$) is presented in Fig. 5.2. Since the processes have the same feedstock but produce different products, the inefficiencies for the aggregated subsystems are preferably related to the total exergy of fuel $\dot{E}_{F,tot}$ of the respective process. The corresponding amounts of the inefficiencies are shown in Figs. E.1 - E.6 and their absolute numvers are given in Tables E.1 - E.6. Furthermore, Table 5.5 shows a selection of the components with the highest exergy destruction rate for each process.

The base processes with single SMR, ATR and DMR technology have an exergetic efficiency of 31.1%, 56.9%, and 39.8%, respectively. The SMR and DMR design necessarily feature a co-production of electricity. Obviously, the exergy of fuel $\dot{E}_{F,tot}$ for processes with endothermic reforming technology is high due to the additional intake of natural gas as a combustion fuel. The exergy losses which are mainly associated with the offgases are correspondingly high. In contrast, the ATR design features a low exergy of fuel and relatively low exergy losses. Compared to the SMR and DMR design, having an exergy destruction ratio y_D of 63.5% and 53.3%, respectively, the major part of the exergy of fuel in the ATR process is used to generate the exergy of product ($y_{D,ATR} = 39.5\%$).

The advanced processes have a comparatively high exergetic efficiency, indicating a successful design selection from a thermodynamic point of view. The efficiency for the CMR, the SMR-ATR and the SMR-DMR design is 48.6%, 57.3% and 46.3%, respectively. Interestingly, the CMR process is of high exergetic efficiency, despite the fact that endothermic reforming technology is applied. This is due to the syngas conditioning technologies, which have a low exergy destruction, but allow a relatively large exergy of product. The SMR-ATR design has the highest exergetic efficiency of all studied processes. The thermoneutral combination of SMR and ATR only requires a small amount fuel and at the same time generates a synthesis gas which enables a high synthetic turnover and a large exergy of product. Regarding the SMR-DMR process, the numbers in Table 5.4 indicate that the equipment in general is of very large size. As a result, the process might require a large financial investment.

Table 5.4: Results obtained from the conventional exergetic analysis for the overall system.

No.	Process	$\dot{E}_{\text{F,tot}}$ [MW]	$\dot{E}_{\text{P,tot}}$ [MW]	$\dot{E}_{\text{D,tot}}$ [MW]	$\dot{E}_{\text{L,tot}}$ [MW]	ε [%]
1	SMR	2334.39	812.54	1327.88	194.81	34.8
2	ATR	1144.30	651.15	453.20	39.95	56.9
3	DMR	2336.87	929.13	1245.47	162.27	39.8
4	CMR	1576.45	765.97	653.66	156.83	48.6
5	SMR-ATR	2772.20	1587.02	1083.34	101.84	57.3
6	SMR-DMR	3689.79	1707.75	1735.50	246.54	46.3

For a comparison of the exergy destruction rate on a subsystem level, exergy destruction ratios $y_{\text{D,sys}}$ are presented in Fig. 5.2. On a subsystem level, all processes are characterized by the same exergetic hierarchy: The majority of the irreversibilities occurs within the reforming unit and the steam cycle, while the exergy destruction rate for the syngas compression, the methanol synthesis and the purification section is comparatively low. Irreversibilities related to the pretreatment, the ASU and the AGR are of minor significance.

In each process, more than 50% of the overall exergy destruction is attributable to the reforming unit ($y_{\text{D,sys}}^*$ in the range $50-59\%$). The subsystem includes the reforming reactors, the combustion unit and the air compression. The subsystem's irreversibilities are particularly high for the processes with endothermic technology. The main sources of inefficiencies refer to highly irreversible reactions occurring within the furnace (combus-

tion unit) and in the combustion zone of the autothermal reformer. The catalytic reactions in the SMR and DMR have a remarkable, albeit comparatively low exergy destruction.

The steam cycle which serves the overall heat integration exhibits the second highest irreversibilities, accounting for approximately 25-30% of the overall exergy destruction. The subsystem comprises various heat exchangers including the HRSG, a set of steam turbines and several pumps. Splitting the steam cycle into its components reveals that for the processes with endothermic reforming technology more than 60% of $\dot{E}_{D,sys}$ is caused by the heat transfer within the HRSG. In regard to the ATR and the SMR-ATR process, the exergy destruction within the HRSG is much lower (around 30% of the steam cycle's $\dot{E}_D$) due to lower process heat demand of the reforming unit. In general, irreversibilities within a heat exchanger are also caused by the consideration of pressure drop, which depends on the heat transfer area and the phsyical state of the flows. Based on high isentropic efficiencies, the steam turbines have a minor contribution to irreversibilities within the steam cycle. A significant exergy destruction rate occurs within the condenser since useless low temperature heat, coming from the cooling of the crude product stream in the synthesis loop, is rejected to the environment. This concerns in particular the processes with a high RTFR (SMR, DMR and SMR-DMR).

The syngas compression unit in general consists of several pre-coolers, two compressors and one intercooler and has an exergy destruction ratio $y_{D,sys}^*$ in the range of 4 - 7%. The irreversibilities are primarily caused by heat exchange at high temperature difference, by the pressure losses in the tubes of the heat exchangers and by friction during compression. In particular for the pre-coolers, the temperature difference between the process gas and the steam is high. The irreversibilities of the compressors are taken into account by an isentropic efficiency of 85%. The extent of irreversibilities for this subsystem is primarily determined by the quantitive influence of the mass flow rate of syngas and the pressure difference between the reforming unit and the synthesis unit.
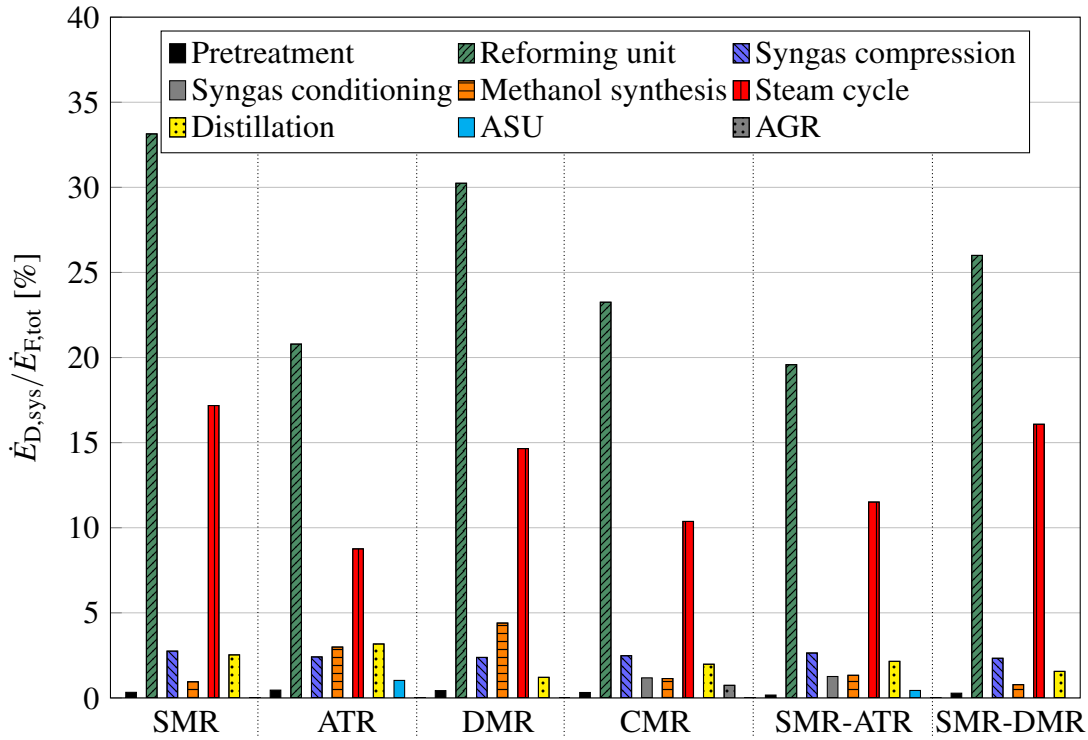
Figure 5.2: Results obtained from the conventional exergetic analysis for the aggregated subsystems.

The methanol synthesis unit has a small contribution to the overall inefficiencies. $y^*_{D,sys}$ is in the range of 2 - 8%. The subsystem includes a recuperator and several heat exchangers for crude product cooling as well as three recycle compressors and the synthesis reactor. Interestingly, the synthesis reactor only has a low exergy destruction rate which likely results from the heat transfer at low temperature difference between the process gas and the boiling water and from the low conversion rate. The major part of the system's irreversibilities occurs within the product coolers due to a large heat transfer rate. Because of a high isentropic efficiency of 87% and a moderate pressure drop in the synthesis unit, the exergy destruction of the recycle compressors is low.

Depending on the reformer technology and the corresponding conversion in the synthesis , the amount of impurities in the crude product varies. The number and size of the distillation columns in the purification section as well as the energy demand in the reboilers is particularly driven by the water content in the crude product. To a minor extent longer chained hydrocarbons (light ends) also play a role. In general, irreversibilities within a distillation column are caused by mixing of streams with non-equilibrium compositions and by differences of temperature and pressure within the column trays [149]. Additionally, heat transfer in the reboiler and the condenser also is associated with exergy destruction. High irreversibilities particularly occur in the SMR and ATR

process, due to a large water content in the crude product. Two-column distillation systems obviously have a lower exergy destruction. Depending on the column features and the crude product composition, the exergy losses which are discharged with the bottom product vary.

Due to minor significance, the ASU, the AGR and the conditioning unit will be discussed briefly. Irreversibilities within the ASU are mainly caused by friction and heat transfer within the intercooled multi-stage air compressor. With respect to the AGR, the absorption process in the column has the highest irreversibilities. The catalytic shift reactors in the syngas conditioning unit serve for a slight adjustment of the composition and therefore only cause a low exergy destruction.

The components in Table 5.5 are ranked by descending order of their exergy destruction rate. The combustion units have outstanding high irreversibilities. Additionally, several heat exchangers of the HRSG are ranked among the components. Their exergy destruction is caused by the large heat transfer rate at high temperature difference between the hot and the cold side. The distillation columns are also listed in the Table, while the recycle and syngas compressors are not associated with a high exergy destruction.

Table 5.5: Results obtained from the conventional exergetic analysis for the components with the highest exergy destruction.

SMR $\dot{E}_{\rm F}$=2334.4 MW		ATR $\dot{E}_{\rm F}$=1144.3 MW		DMR $\dot{E}_{\rm F}$=2336.9 MW		CMR $\dot{E}_{\rm F}$=1576.5 MW		SMR-ATR $\dot{E}_{\rm F}$=2772.2 MW		SMR-DMR $\dot{E}_{\rm F}$=3689.8 MW	
Comp. k	$y_{{\rm D},k}$[%]	Comp. k	$y_{{\rm D},k}$ [%]	Comp. k	$y_{{\rm D},k}$ [%]	Comp. k	$y_{{\rm D},k}$ [%]	Comp. k	$y_{{\rm D},k}$ [%]	Comp. k	$y_{{\rm D},k}$ [%]
R-04	29.97	R-09	11.64	R-05	25.54	R-05	18.62	R-07	12.92	R-05	21.77
HP-EVA	4.77	R-03	6.67	HP-ECO	3.16	HP-EVA	3.41	R-04	5.28	HP-EVA	3.56
HP-SH	1.59	C-02	1.79	HP-SH	2.46	R-03	2.58	HP-SH	2.11	LP-EVA	2.37
T-02	1.29	HP-EVA	1.16	E-09	2.09	HP-SH	1.90	E-13	1.37	HP-SH	1.65
E-05	1.32	E-03	1.12	R-04	2.08	E-07	1.51	C-02	1.30	E-11	1.30
C-02	1.27	E-08	0.96	LP-EVA	1.49	C-02	1.45	HP-EVA	1.29	LP-SH	1.29
CM02	0.95	C-03	0.92	E-05	1.36	E-05	1.13	HP-ECO	1.18	E-08	1.25
C-01	0.90	HP-SH	0.85	LP-RH	1.12	LP-SH	0.76	E-06	1.04	T-02	1.19
LP-SH	0.89	R-04	0.84	T-01	0.94	E-11	0.76	E-04	0.84	C-02	1.16
LP-EVA	0.59	E-09	0.70	C-02	0.89	CM-02	0.71	E-11	0.70	R-03	1.13
E-04	0.49	LP-EVA	0.69	T-02	0.59	T-01	0.67	E-03	0.51	RH	1.11
C-03	0.35	CM-02	0.65	E-06	0.58	E-06	0.60	C-01	0.49	E-05	0.85
E-08	0.34	T-01	0.62	E-03	0.52	LP-EVA	0.59	CM-02	0.48	R-06	0.59
E-01	0.24	E-02	0.55	MP-SH	0.47	C-01	0.50	T-03	0.48	CM-04	0.57
E-02	0.22	E-05	0.55	C-01	0.31	T-02	0.39	E-08	0.45	CM-03	0.57

5.4 Economic Analysis

An evaluation of the processes from a thermodynamic point of view allows a first classification and exclusion of unattractive designs. A holistic consideration, however, also requires an estimation of the major costs involved in a project. An economic assessment of the investigated processes is conducted by application of the total revenue requirement method (TRR). The assumptions underlying the analysis are given in Section 3.2. All monetary values are given in US-$ 2016. In regard to the economic sensitivity analysis, a pricing of the main product methanol and the by-product electricity is assumed. Furthermore, the costs for integrated and emitted CO_2 is first assumed to be zero, since the majority of methanol plants is located in regions without carbon pricing. The influence of CO_2 pricing on the levelized product cost is discussed in Section 5.5.

The results obtained from the economic analyses for the six processes are presented in Table 5.6. The values of the BMC, the FCI and the TCI mainly depend on the capacity of the respective system. The breakdown of the BMC shows that the investment is mainly assigned to the reforming unit (RE), having a share of 60 - 70% in the BMC. If the BMC of the ASU is added to the reforming unit, the proportion of the subsystem is similar high for the ATR and SMR-ATR process. The investment for the syngas compression unit (COMP) is determined by pressure difference between the chemical units and by the syngas volume flow. The synthesis unit (SYN) accounts for 7 - 13% of the BMC, whereby the investment costs are proportional to the circulating mass flow rate. In regard to the steam cycle, an increased investment share is exhibited for the processes with endothermic reforming technology.

The distribution of the levelized carrying charges CC_L, operation and maintenance cost OMC_L, and fuel costs FC_L shows that the annual revenue requirement TRR_L and therefore the economic feasibility is significantly influenced by the fuel costs. Considering the relative contribution per MWh of exergy of product, a dominating impact of the specific levelized fuel costs fc_L particularly is given for the processes with endothermic reforming technology. Especially for the SMR process, the fuel cost respresent a very high proportion in the cost of the end-products. The ATR and the SMR-ATR process profit from a high efficiency and therefore are associated with the low specific fuel cost.

At this point it should be emphasized that the specific costs per unit of exergy form an average value over two products and therefore cannot be equated with the levelized cost for electricity (LCOE) and methanol (LCOM). In most process designs, the specific carrying charges cc_L and operation and maintenance costs omc_L account for less than 50% of the total levelized cost per unit of exergy product. Slightly increased specific

costs for the investment arise for the SMR and the DMR process. The relatively low specific carrying charges for the large-scale processes SMR-ATR and SMR-DMR can be derived from effect of the economies of scale. Finally, the economic feasibility of the processes not only depends on the fuel cost but also on the future development of the market prices for the generated products methanol and electricity.

Table 5.6: Results obtained from the economic analysis for the overall systems.

		SMR	ATR	DMR	CMR	SMR-ATR	SMR-DMR
BMC	10^6 US$	507.37	308.87	505.24	358.29	594.93	642.03
PRE[1]	% BMC	2.09	5.06	0.92	0.71	4.87	0.88
RE[2]	% BMC	64.51	41.88	60.43	51.46	44.65	68.90
COMP[3]	% BMC	4.89	7.95	9.12	17.85	5.77	4.42
CON[3]	% BMC	-	-	-	0.08	5.30	-
SYN[4]	% BMC	13.04	11.47	8.35	7.89	10.07	7.33
SC[5]	% BMC	10.87	8.33	17.70	11.13	12.27	15.13
DISTL[6]	% BMC	4.61	7.83	3.47	4.49	3.94	3.34
ASU	% BMC	-	17.48	-	-	13.13	-
AGR	% BMC	-	-	-	6.39	-	-
FCI	10^6 US$	636.42	396.47	633.19	450.39	743.89	804.37
TCI	10^6 US$	674.73	420.34	671.31	477.50	788.66	852.79
CC_L	10^6 US$/a	68.72	42.81	68.37	48.63	80.37	86.86
OMC_L	10^6 US$/a	62.76	40.52	62.46	47.61	76.47	122.73
FC_L	10^6 US$/a	249.99	132.38	247.97	174.00	305.46	402.72
TRR_L	10^6 US$/a	381.5	215.72	378.80	270.25	462.26	612.31
cc_L[7]	US$/MWh	10.57	8.21	9.19	7.94	6.33	6.36
omc_L	US$/MWh	9.65	7.78	8.40	7.77	6.02	8.98
fc_L	US$/MWh	43.14	25.41	33.36	28.40	24.06	31.72

[1] Subsystem Pretreatment [2] Subsystem Reforming Unit [3] Subsystem Reforming Unit [3] Subsystem Syngas Conditioning [4] Subsystem Synthesis Unit [5] Subsystem Steam Cycle [6] Subsystem Distillation [7] The specific cost are related to $\dot{E}_{P,tot}$

In general, these economic decision parameters are subject to temporal and regional fluctuations. Thus, the estimation of the economic feasibility of a methanol plant is a complex task and difficult to predict. In the following, sensitivity analyses are carried out to show the impact of the levelized fuel cost on the revenues and on the contribution margin. From the investigations, the interdependence of the minimum selling prices of electricity and methanol for cost recovery can be deduced. Furthermore, the analyses result in a determination of break even points from which an economic favorability of a specific process can be derived under given market conditions.

An economic blackbox model is applied to analyse the relations between the inlet cost streams, the investment and the revenues from the selling of the products. Since one fuel stream and two product streams mean three degrees of freedom, two parameters must be specified - the specific fuel cost f_c and the sale price for electricity. Information about the exact cost distribution on the products is later obtained by the application of the exergoeconomic analysis.

All cost parameters included in the sensitivity analyses refer to levelized values to take into account temporal changes over an operation time of 20 years. The annual product cost for methanol and electricity (C_{Meoh} and C_{elec}) result from the calculation of the total annual revenue requirement and are obtained by solving the Eq. 5.1 -5.3.

$$TRR_L = CC_L + FC_L + OMC_L \tag{5.1}$$

$$C_{Meoh} + C_{Elec} = CC_L + FC_L + OMC_L \tag{5.2}$$

$$MC_{Meoh} = \frac{CC_L + \dot{m}_{fuel} \cdot LHV \cdot \tau \cdot f_c \cdot CELF_{fuel} + OMC_L - \dot{W}_{net} \cdot \tau \cdot MC_{elec}}{\dot{m}_{Meoh} * \tau} \tag{5.3}$$

The range of whole sale prices per MWh of generated electricity MC_{elec} was selected based on information reported in [116–118], while the cost range per GJ of natural gas was determined based on data obtained from [150, 151]. For an assessment of the economic feasibility, the calculated minimum price per metric ton of methanol is compared with market data published by the world's largest methanol production and distribution company Methanex Corporation (Methanex), Canada [28, 98]. The data basis includes monthly, continental wholesale contract prices for the last five years. The comparison with real market data also serves to validate the results of the economic analysis.

The Figs. 5.3 - 5.8 show the sensitivity of the minimum methanol price to the cost of natural gas and the selling price of electricity. The solid lines represent the process

specific isolines of constant methanol price to cover the TRR. Accordingly, their slope is a measure for the dependency of the minimum methanol price on the sale price of electricity. The dotted and dashed graphs represent the market data and show the 5-year high and low of the methanol wholesale price in selected continents. The graphs only serve as a reference for the isolines of the processes and should therefore not be related to the axis. Furthermore, the exact product cost distribution (for the reference price of 2.9 US$$_{2016}$/GJ), which is obtained from the exergoeconomic analysis, is broken down for the reference cases. In order to understand the graphics, the reference case of the SMR process will be exemplarily explained. For the sensitivity analysis, it is assumed that the respective plant participates in a market with electricity pricing.

In principle, a distinction can be made between two process types - those with endothermic reforming technology, in which a considerable amount of excess electricity is generated, and those with exothermic or mixed reforming technology. Regarding the first group of processes, Figs. 5.3, 5.5, 5.7, and 5.8 show that the wholesale price of electricity decisively influences the minimum product price for methanol to cover the TRR_L. For the processes with ATR and CMR technology in Figs. 5.4 and 5.6, the marginal influence results from the low power generation.

Figure 5.3: Impact of the natural gas cost and the sales price of electricity on the minimum sale price of methanol for the SMR process.

As shown in Table 5.6, the products generated in the SMR process are associated with high specific average cost per MWh. In addition to relatively large carrying charges, the product costs are high due to the large CH_4-intensity and thus to the fuel costs. For the reference case, the levelized fuel cost of approximately 3.9 US$/GJ result in levelized electricity cost (LCOE=$MC_{elec,ref}$) of 110 US$/MWh and levelized methanol cost (LCOM=$MC_{Meoh,ref}$) of 295 US$/mt. In case the levelized fuel cost $f_{c,A}$ increase to 7.8 US$/GJ at constant revenues from electricity $MC_{elec,ref}$, the minimum methanol price $MC_{Meoh,A}$ would amount to 590 US$/mt to cover the TRR. Under these conditions an economic operation in Europe most likely is not possible, while an economic feasibility of the project could be given in Asia and North America. With respect to case B, an increased levelized sale price of 168 US$/MWh for electricity at constant $f_{c,B}$ would result in reduced minimum cost of methanol $MC_{Meoh,B}$ of 216 US$/mt.

In general, for fuel cost above 7.5 US$/GJ, a ton of methanol cannot be produced at an economically competitive price. As for the other processes with endothermic reforming technology (e.g, DMR process in Fig. 5.5), the relatively steep incline of the isolines indicates a large dependence on selling price of electricty. Taking into account European electricity procurement prices between 50-80 US$/MWh [116] and an average European natural gas price of 4.5 - 5.5 US$/GJ [152] (6 - 7.5 US$/GJ on a levelized base), a cost-covering operation would require a minimum methanol price of 600 - 650 US$/mt. Based on this market data and the historical methanol prices [28], a domestic production would be associated with great economic uncertainties. With respect to the Asian and North American market, an economic feasibility could be given at levelized natural gas cost of up to 7 US$/GJ.

Fig.5.4 shows the results obtained from the sensitivity analysis of the ATR process. Due to low power generation, the revenues from the selling of electricity nearly have no influence on the minimum methanol price. In comparison with the endothermic reforming processes (SMR, DMR, CMR, SMR-DMR), methanol can be produced at relatively low cost. Even for levelized gas prices of up to 12 US$/GJ the plant could still be operated economically. The currently low natural gas prices of less than 3 US$/GJ in North America (4.1 US$/GJ on a levelized base) would result in methanol production cost of 250 - 260 US$/mt. Based on the European natural gas price of 4.5 - 5.5 US$/GJ in 2016 [152] (6 - 7.5 US$/GJ on a levelized base), minimum methanol cost of 330 - 400 US$/mt would result. A European production of methanol from natural gas by means of ATR technology therefore may be feasible.

The results obtained from the sensitivity analysis of the DMR process are presented in Figure 5.5. The process generates a large amount of excess electricity, which could

Figure 5.4: Impact of the natural gas price and the sales price of electricity on the minimum sale price of methanol for the ATR process.

Figure 5.5: Impact of the natural gas cost and the sales price of electricity on the minimum sale price of methanol for the DMR process.

constitute an additional source of income, thus influencing the minimum methanol price. Under the terms of a high electricity sale price above 80 US$/MWh and a low natural gas market price in the range of 0 - 3 US$/GJ, methanol could be offered for 0 US$/mt to cover the TRR of the plant. Thus, the plant could generate profits as a pure electricity market participant. For a MC_{elec} below 40 US$/MWh, the MC_{Meoh} is in the same range as for the SMR process in Figure 5.3. With increasing electricity prices, cost advantages for the DMR process arise due to the larger power capacity (see Tab. 5.1). Compared with the ATR process, the DMR process is economically only competitive for low cost of natural gas or a high sale price of electricity. The reference plant with fuel cost 2.9 US$_{2016}$/GJ generates electricity and methanol at levelized cost of 100 US$/MWh and 220 US$/mt. Considering current market conditions in Europe (see SMR process), a metric ton of methanol could be sold for a minimum price in the range of 400 - 500 US$/mt. The results of the sensitivity analysis show that a methanol production with CO_2-valorization can be economically feasible and competitive. However, the economic feasibility is essentially determined by the revenues from selling of electricity. In addition, the levelized product costs will increase if costs are assigned to the integrated CO_2.

Figure 5.6: Impact of the natural gas cost and the sales price of electricity on the minimum sale price of methanol for the CMR process.

Figure 5.6 illustrates the results of the sensitivity analysis for the CMR process. The slope of the isolines is less steep compared with the SMR and DMR process since the

power output is significantly lower. Above a natural gas price of 11 US\$/GJ, an operation of the plant may not be economically viable. Under the current market conditions, the production cost per ton or methanol are in the range of the respective continental contract price of Methanex. At MC_{elec} below 40 US\$/MWh, the ton of methanol can be sold for a lower price in comparison with the DMR process. Thus, bi-reforming constitutes a good alternative (to the DMR process) for CO_2-valorization at competitive product cost and with increased economic independence. The reference plant with fuel cost of 2.9 US\$$_{2016}$/GJ generates electricity at high levelized cost of 165 US\$/MWh and methanol at levelized product cost of 250 US\$/mt.
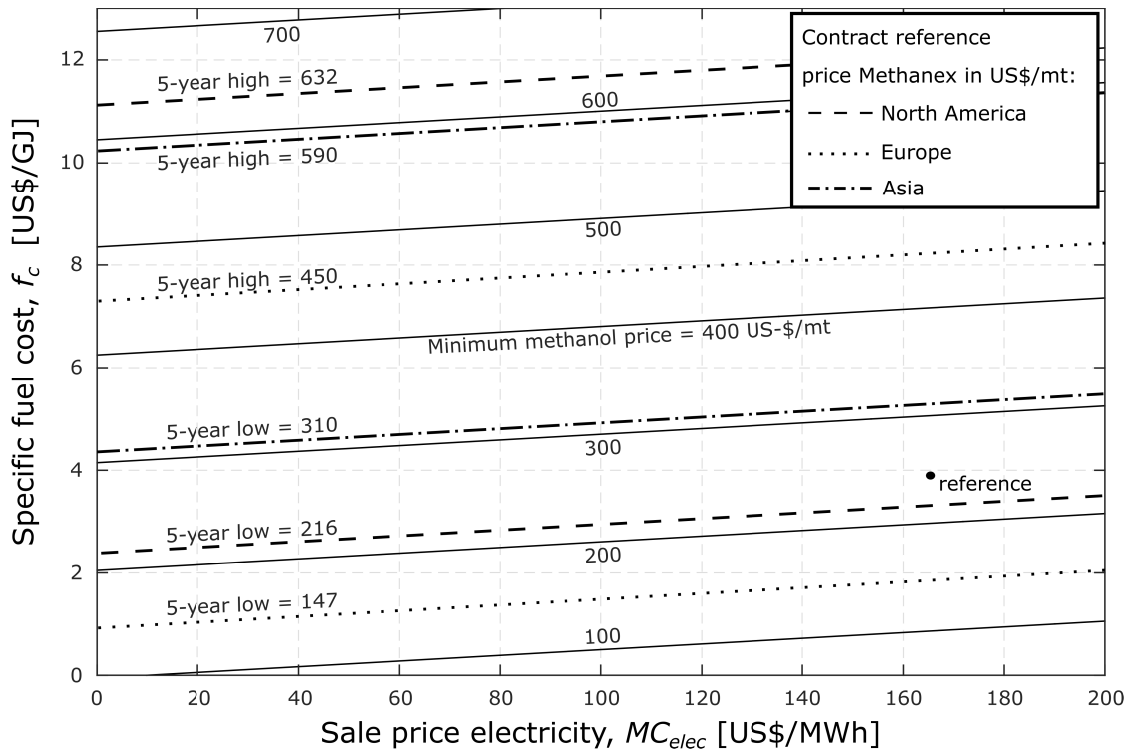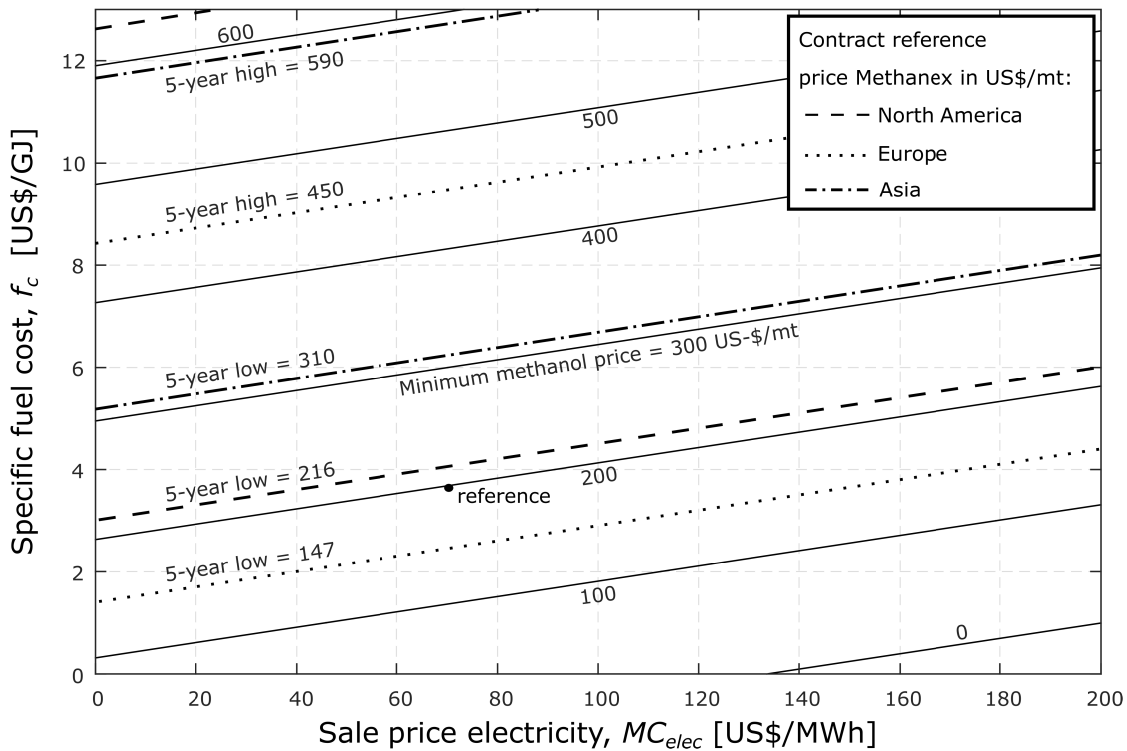
Figure 5.7: Impact of the natural gas cost and the sales price of electricity on the minimum sale price of methanol for the SMR-ATR process.

The SMR-ATR process was designed for a large capacity in order to use the effect of the economies of scale for decreasing the product cost. Regarding the product-related fixed cost (carrying charges cc_L) in Table 5.6, the process clearly shows a cost benefit over the processes with single reforming technology. Considering Fig. 5.7, the sale price of electricity has a considerable influence on MC_{Meoh} as indicated by the steep slope. Obviously, the SMR-ATR process can generate methanol at the lowest cost, regardless of the sale price for electricity. Similar to the DMR process, methanol could even be offered free of charge at low natural gas prices and high selling prices of electricity. For the

reference plant, the levelized cost of electricity amount to 75 US$/MWh while methanol is generated at product cost of approximately 200 US$/mt.
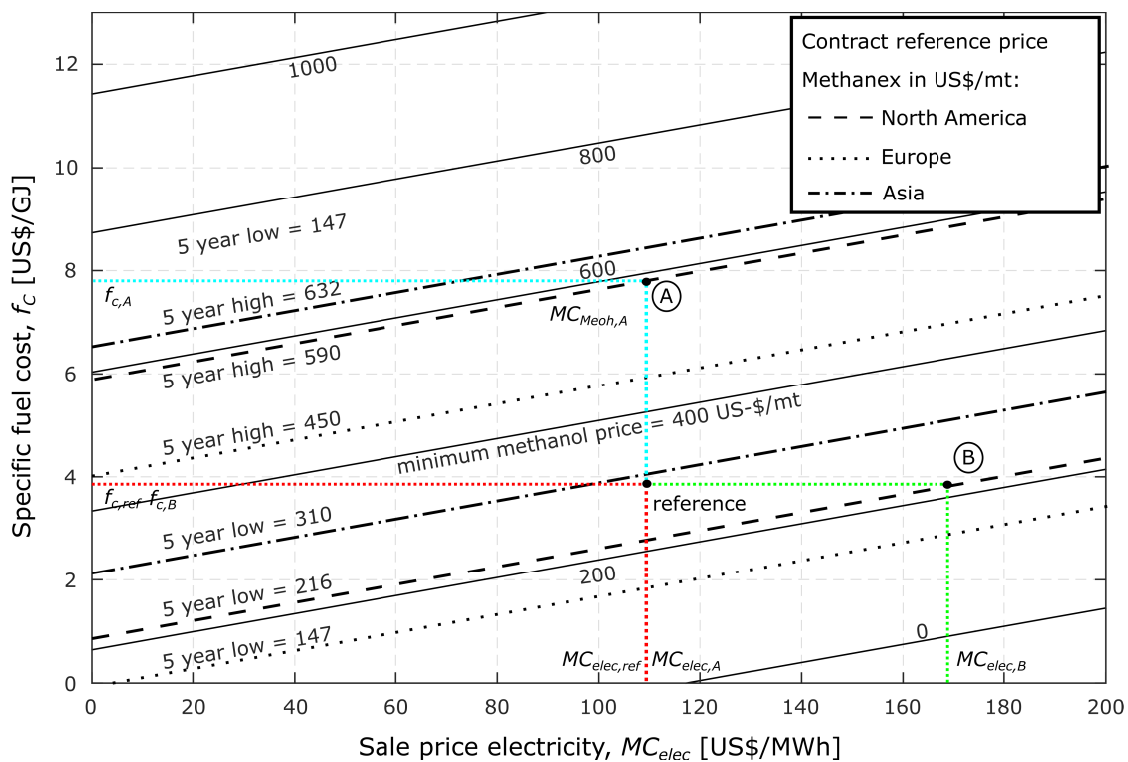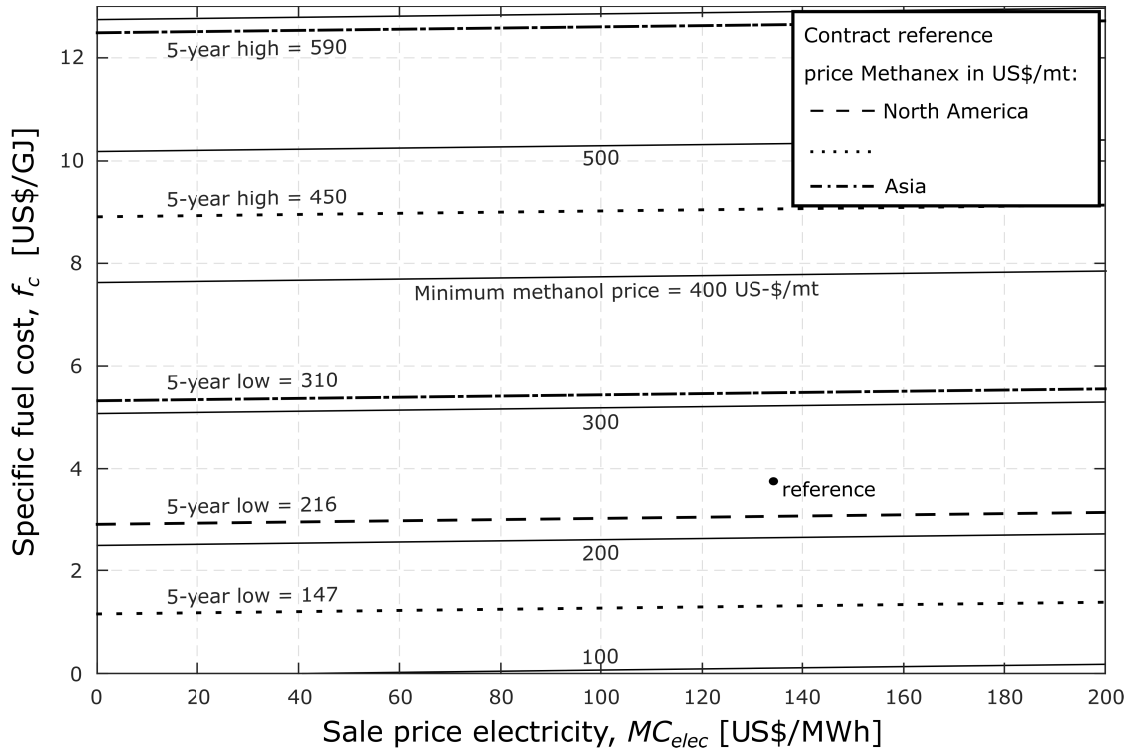

Figure 5.8: Impact of the natural gas cost and the sales price of electicity on the bottom price of methanol for the SMR-DMR process.

As shown in Table 5.1, the SMR-DMR process was also designed for a large capacity to reduce the capital cost by the effect of the economies of scale. The product-related carrying charges in Table 5.6 show that this attempt was successful. However, the average product cost are high due to the high fuel-intensity of the process. An operation above a natural gas price of 11 US$/GJ most likely would result in financial losses. Considering European market conditions, a minimum methanol price of 400 - 500 US$/mt would be necessary to recover the total cost. For the reference case, electricity is generated at levelized cost of 122 US$/MWh while the levelized product cost for methanol amount to 210 US$/mt.

In the economic consideration it may be useful to consider only the variable costs, while neglecting the fixed costs associated with the investment (sunk costs). The contribution margin CM is calculated as the difference between the revenues from the selling of the products $C_{Meoh} + C_{Elec}$ and the variable cost associated with the fuel procurement FC_L and the operation OMC_L. A positive contribution margin therefore represents the annual amount of income that is available to cover the fixed cost. In this analysis the operation and maintenance cost are exclusively added to the variable cost. The Figs. 5.9-5.11 show

the threshold, at which the revenues can be used to pay off the fixed costs. For each process, this threshold is represented by the isoline for a contribution margin of zero. The isolines are obtained by solving Eq. 5.4 and Eq. 5.5.

$$CM = C_{Meoh} + C_{Elec} - FC_L - OMC_L \qquad \text{with} \quad CM = 0 \tag{5.4}$$

$$MC_{Meoh} = \frac{\dot{m}_{\text{fuel}} \cdot LHV \cdot \tau \cdot f_c \cdot CELF_{\text{fuel}} + OMC_L - \dot{W}_{net} \cdot \tau \cdot MC_{elec}}{\dot{m}_{Meoh} * \tau} \tag{5.5}$$

Depending on the selling prices of the products, one area of the positive contribution margin results above and one area of the negative contribution margin below the respective isoline. The Figs. 5.9 - 5.11 therefore show at which levelized product market prices each of the plants can be operated economically under given levelized fuel cost of 3 US\$/GJ, 7 US\$/GJ, and 11 US\$/GJ, respectively. Furthermore, break even points can be read from the intersections of the isolines.
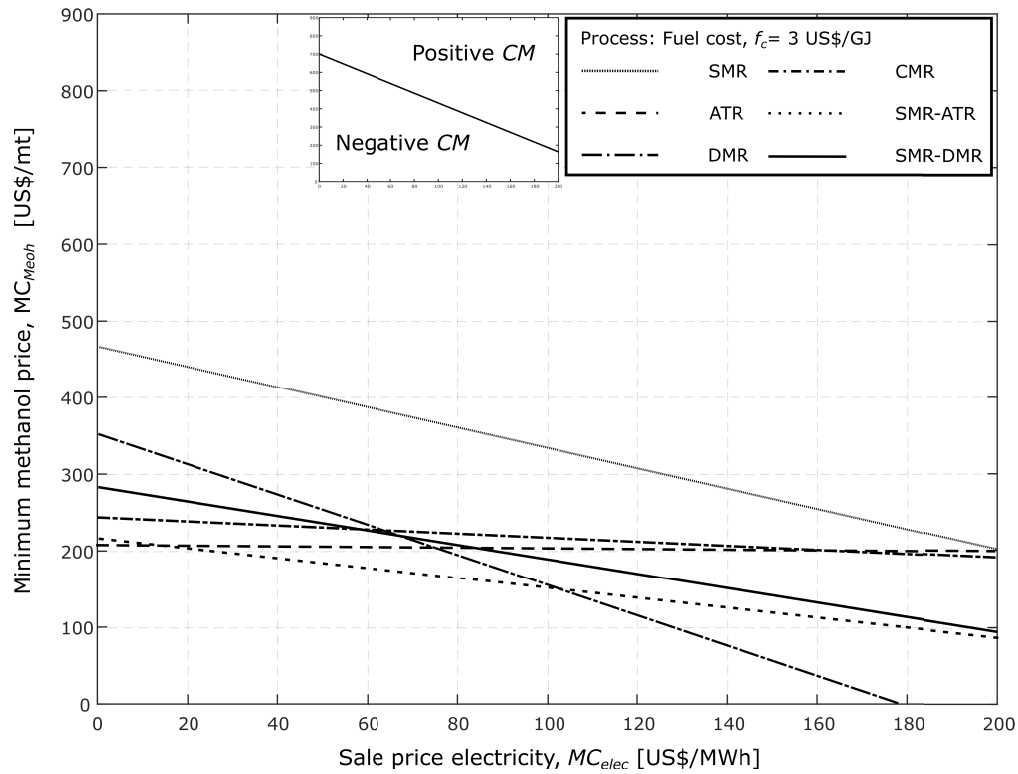
Figure 5.9: Sensitivity of the contribution margin depending on the minimum methanol price and the selling price of elecrtcity for fuel cost of 3 US\$/GJ.
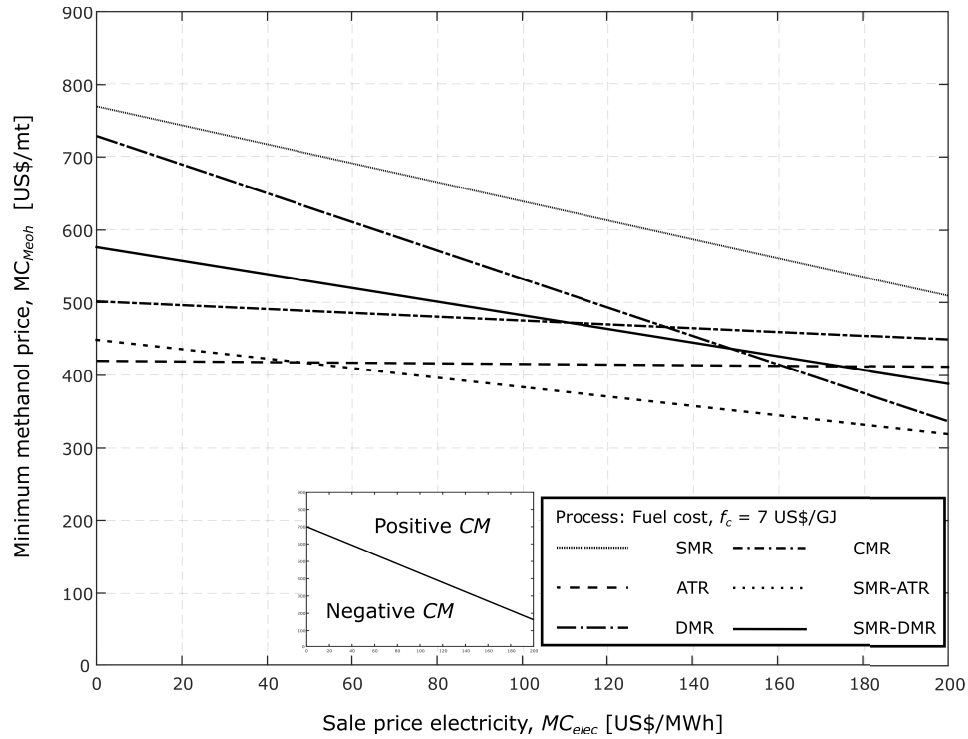
Figure 5.10: Sensitivity of the contribution margin depending on the minimum methanol price and the selling price of elecrtcity for fuel cost of 7 US$/GJ.

With rising fuel cost f_c, the minimum price per ton methanol MC_{Meoh} increases, assuming a constant levelized electricity selling price. Depending on the market conditions for methanol and electricity, different processes are economically more attractive. For fuel costs of 3 US$/GJ, the methanol can be sold in a range of 0 to 470 US$/mt to obtain a positive contribution margin for each process. The wide price range is determined by the fuel intensity and the pricing for electricity. For low revenues from the selling of electricity, the ATR and SMR-ATR process clearly have an economic advantage. On the other hand, for high revenues from the selling of electricity (above 100 US$/MWh), methanol from processes with endothermic reforming technology (DMR, SMR-DMR) could be offered for a cheaper price to recover the variable cost. Under consideration of historical methanol prices, an economic feasibility might be given for all considered processes.
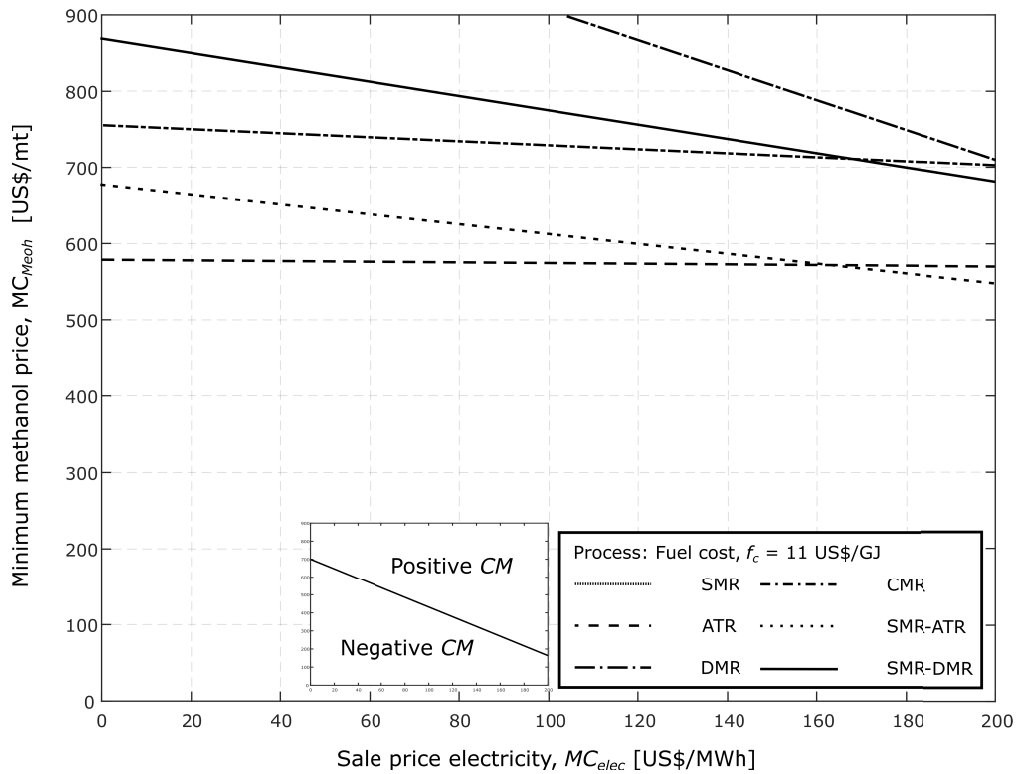
Figure 5.11: Sensitivity of the contribution margin depending on the minimum methanol price and the selling price of elecrtcity for fuel cost of 11 US$/GJ.

For fuel cost of 7 US$/GJ (see Fig. 5.10), methanol can be produced at cost of 300 - 800 US$/mt. The SMR and DMR process can only generate a positive contribution margin for very high product prices. Already for an electricity sale price of 40 US$/MWh the SMR-ATR reaches a break-even with the ATR process. Furthermore, the economic advantage of the ATR and SMR-ATR process increases compared to the designs with endothermic reforming technology. For fuel cost of 11 US$/GJ, only the processes with autothermal reforming (ATR and SMR-ATR) could possibly achieve a positive contribution margin. Now, these processes have a clear cost-advantage over the processes with endothermic reforming technology. In case of such high long-term prices, alternative syngas generation processes based on coal most likely would be the preferred option for methanol production. In these considerations, it should be noted, that a year-round sale of electricity at prices above 100 US$/MWh constitutes an unrealistic scenario. In conclusion, a clear economic hierarchy results for the investigated processes. The following ranking is obtained for ascending methanol product cost to cover the variable cost of the project: ATR process, SMR-ATR process, CMR process, followed by the SMR-DMR process, the DMR process and finally the SMR process. Cost advantages of the processes with endothermic technology especially arise for high electricity prices at low fuel cost.

5.5 Exergoeconomic Analysis

An exergoeconomic analysis is conducted in order to understand the formation and the flow of costs within the processes. Information on the cost distribution, the real levelized product cost and the economic significance of each component can be derived. Details on the application of the methodology are provided in Section 3.3. For each process, the results obtained from the exergoeconomic analysis are presented for a reference case using a natural gas is 2.9 US$${}_{2016}$/GJ. In Fig. 5.12 a relative cost distribution is given for the overall processes, whereby the investment cost $\dot{Z}_{tot}$ and the cost rates associated with the inefficiencies $\dot{C}_{L,tot}$ and $\dot{C}_{D,tot}$ are related to the total exergy product $\dot{E}_{P,tot}$.
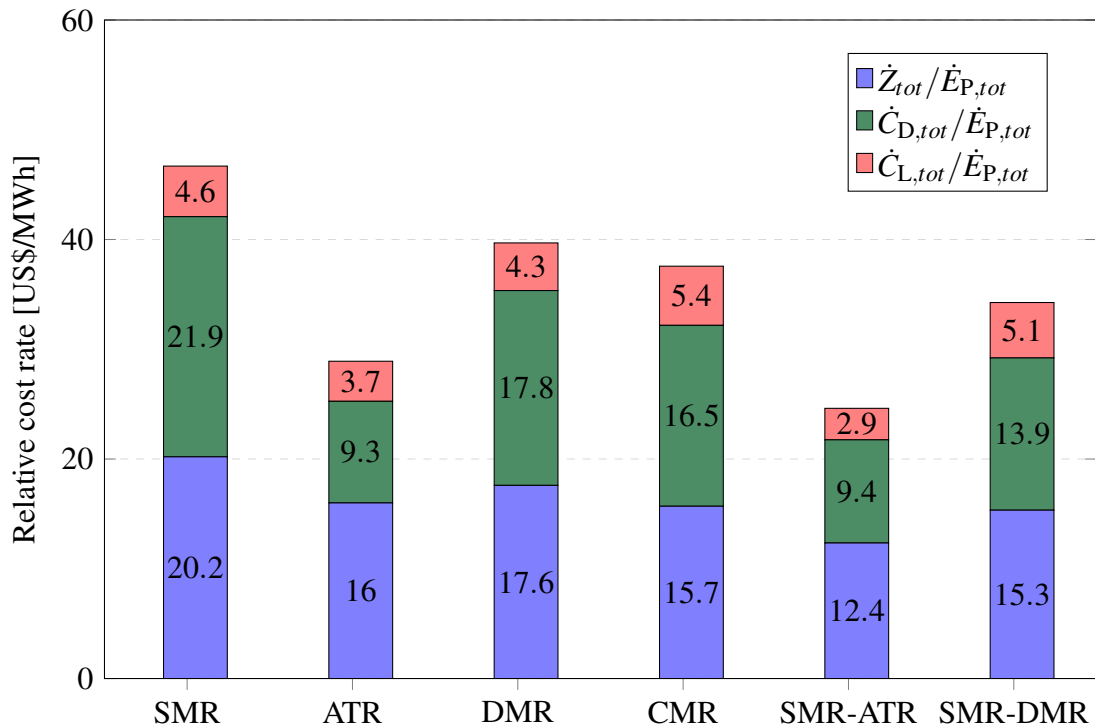
Figure 5.12: Relative cost rate associated with the investment and the inefficiencies of the overall processes.

The relative cost rate of the investment $\frac{\dot{Z}_{tot}}{\dot{E}_{P,tot}}$ includes the carrying charges and the operation and maintenance cost. In particular, the SMR and DMR process are capital intensive due to the large investment associated with the reforming unit. Regarding the advanced processes, the value of $\frac{\dot{Z}_{tot}}{\dot{E}_{P,tot}}$ is decreased due to a design improvement and the effect of the economies of scale.

Turning next to the relative cost rate associated with the exergy destruction $\frac{\dot{C}_{D,tot}}{\dot{E}_{P,tot}}$, the irreversibilities obviously exhibit the major cost source for the base processes with endothermic reforming technology. In regard to the ATR and the SMR-ATR process,

$\frac{\dot{C}_{D,tot}}{\dot{E}_{P,tot}}$ has a lower cost importance. The processes are of higher exergetic efficiency due to reduced irreversibilities within the reforming unit. Furthermore, the relative cost rate associated with the exergy losses of the overall system $\frac{\dot{C}_{L,tot}}{\dot{E}_{P,tot}}$ is shown in Fig. 5.12. The relative cost rate is particularly high for the SMR, DMR, CMR, SMR-DMR process since the exergy losses are mainly attributed to the off gases which are large for the endothermic reforming technologies. Accordingly, the influence of the cost rate is lower for the ATR and the SMR-ATR process.

In order to improve the cost effectiveness of a system, a detailed thermoeconomic evaluation has to be conducted on a component level. For each process, the results for a selection of components with the highest cost importance are presented in Tables 5.7 - 5.12. Accordingly, the components are ranked by descending order of their cost rate associated with the exergy destruction and the investment ($\dot{C}_{D,k} + \dot{Z}_k$). The exergoeconomic factor f_k and the relative cost difference r_k are used to evaluate the internal cost distribution and the relative cost increase between $c_{P,k}$ and $c_{F,k}$. By analysing the exergoeconomic variables, recommendations concerning changes of the design and of operation parameters can be made in order to decrease the levelized product cost within an iterative improvement process. From the results of all processes in Tables 5.7 - 5.12, some general conclusions can be drawn:

1. The combustion unit, the air compressors and several heat exchangers within the synthesis train and the steam cycle have a high cost impact. .

2. Regarding the heat exchangers, the exergy destruction $\dot{C}_{D,k}$ represents a dominant cost source, as indicated by a low exergoeconomic factor.

3. The compressors have a high value for the exergoeconomic factor, indicating that their investment $\dot{Z}_k$ constitutes the major cost source.

4. The circulating streams within the synthesis unit are associated with high average cost per unit of exergy.

5. The processes with CO_2 integration could be economically advantaged, since CO_2 was assumed to be free of cost.

6. The average cost per unit of exergy of the syngas strongly varies with the type of reforming agent. High average cost particularly result from the supply of costly oxygen in the process with autothermal reforming.

Regarding the reference SMR process, the detailed results obtained from the exergoeconomic analysis are presented in Table 5.7. The relative cost difference r for the overall plant amounts to 338.5%, whereby the average cost per unit of exergy product $c_{p,tot}$ includes the cost of dissipative components and the cost rate associated with exergy losses. The relative cost difference for electricity ($r_{elec} = 747.1\%$) is much higher than the one for methanol ($r_{Meoh} = 253.1\%$). The exergoeconomic factor f_{tot} has a value of 46.7%, indicating that the levelized product cost can potentially be decreased by an improvement in the exergetic efficiency at the expense of higher investment cost.

On a component base, the steam reformer R-04, the air compressor CM-02 and the high temperature syngas cooler E-06 have the highest value of the sum $\dot{Z}_k + \dot{C}_{D,k}$ and therefore represent the most important components from a thermoeconomic point of view. In regard to the reformer, the low exergoeconomic factor shows that the costs are almost exclusively due to the exergy destruction. Thus, the cost impact of the SMR can be reduced by an increase in the exergetic efficiency. Corresponding measures concern the use of an advanced burner technology to reduce the irreversibilities associated with the combustion reactions (by lowering the air to fuel ratio) and the reduction of the S/C ratio to decrease irreversibilities due to mixing. Furthermore, a preheating of the combustion reactants might also lower the exergy destruction within R-04. The air compressor unit CM-02 is the most expensive component of the process and has the second highest value of the sum $\dot{Z}_k + \dot{C}_{D,k}$. The high value of the exergoeconomic factor f suggests a reduction of the capital investment at the expense of larger irreversibilities. For this purpose, the high isentropic efficiency ($\eta_s = 0.86$) and the pressure ratio could be reduced. The pressure ratio, however, is fixed by the outlet pressure of the off gases and the pressure drop within the HRSG.

The high temperature syngas cooler E-06 in the syngas compression unit also has a remarkable high value of $\dot{Z}_k + \dot{C}_{D,k}$ causing a high cost difference r_k. Considering the low f value, the cost increase is exclusively due to exergy destruction. Thus the irreversibilities should be reduced at the expense of an increase of the capital investment and the O&M cost. The cost rate $\dot{C}_{D,k}$ is due to large irreversibilities and the high average cost at which exergy is supplied to the component $c_{F,k}$. The exergy destruction is mainly caused by heat transfer at high temperature difference of up to 400 °C. An integration into the heat management system at a higher temperature level (increase in thermodynamic average temperature on the cold side) would decrease the impact of $\dot{C}_{D,k}$, but is impossible due to internal heat distribution of the process and the corresponding design specifications of the steam cycle. An extension of the heat transfer area or an use of materials with a higher heat transfer coefficient may reduce the cost rate $\dot{C}_{D,k}$ to a

certain extent. The high-pressure evaporator HP-EVA in the HRSG is also characterized by large irreversibilities, which constitute the main cost source for this component. An increase in the steam pressure in order to reduce the irreversibilities would require major changes within the heat integration management system, since the vapor fraction at the outlet of the low-pressure turbine is already at the lower boundary. By an increase of the heat supply, the steam parameters could be increased to reduce the irreversibilities due to heat transfer. However, the cost rate associated with the exergy losses of the off gases would increase. The recuperator E-04 in the synthesis unit also has a high cost importance for the SMR process. According to the low exergoeconomic factor of 28.5%, a cost reduction might be achieved by an increase in the exergetic efficiency of the component. However, The large cost rate $\dot{C}_{D,k}$ is rather caused by the high average cost per unit of exergy of fuel, which results from the costly recycle streams of unconverted syngas. Thus, approaches to reduce the sum $\dot{C}_{D,k} + \dot{Z}_k$ should consider a reduction of the cost that were supplied upstream to the process gas.

The main condenser E-05 is rated to position number six and has a low f value. The cost rate $\dot{C}_{D,k}$ results from the large irreversibilities and the high average cost $c_{F,k}$ of useless steam. By changing the live steam parameters, the temperature of the inlet steam could be reduced, thus decreasing the exergy destruction. The irreversibilities also constitute the major cost source for the high-pressure superheater (HP-SH). The live steam temperature is limited to 600 °C, while the combustion gases from the radiative zone of the SMR enter the heat exchanger with a temperature of approximately 900 °C. The key decision variables include the steam pressure, the live steam temperature and the inlet temperature of the combustion gases. By an increase of the HP pressure level and the live steam temperature, the exergy destruction rate could be reduced. Interestingly, despite a high isentropic efficiency η_s, the irreversibilities also have a high impact on the cost of the high-pressure steam turbine T-02. A further increase of η_s and a reduction of the pressure ratio would reduce the exergy destruction.

The other components are only briefly discussed since their cost influence on the overall process is of lower significance. The highly inefficient distillation columns C-01, C-02 and C-03 lead to a significant increase in the average cost per unit of exergy as indicated by a relative cost difference of each above 250%. Their cost importance is mainly attributed to the inefficiencies which result from the heat transfer within the condenser and the reboiler. By reducing the formation of water in the synthesis, the impurities of the crude product and thus the irreversibilities could be lowered. Due to a low steam mass flow rate within the low pressure level of the HRSG, the sum of $\dot{C}_{D,k} + \dot{Z}_k$ is comparatively low for the LP-SH and LP-EVA.

Table 5.7: Results obtained from the exergoeconomic analysis for a selection of components of the reference SMR process.

Comp. k	$\dot{E}_{\mathrm{F},k}$	$\dot{E}_{\mathrm{P},k}$	$\dot{E}_{\mathrm{D},k}$	ε_k	$y_{\mathrm{D},k}$	$c_{\mathrm{F},k}$	$c_{\mathrm{P},k}$	$\dot{C}_{\mathrm{D},k}$	$\dot{Z}_k$	$\dot{C}_{\mathrm{D},k} + \dot{Z}_k$	f_k	r_k
	[MW]	[MW]	[MW]	[%]	[%]	[\$/GJ]	[\$/GJ]	[\$/h]	[\$/h]	[\$/h]	[%]	[%]
R-04	1,669.71	970.20	699.51	58.1	30.0	3.97	7.53	10,004.95	2,410.65	12,415.60	19.4	89.5
CM-02	203.86	181.70	22.16	89.1	1.0	25.49	40.87	2,033.07	8,027.91	10,060.98	79.8	60.4
E-06	97.77	40.14	57.64	41.1	2.5	38.61	94.32	8,012.08	36.47	8,048.55	0.5	144.3
HP-EVA	436.16	324.87	111.29	74.5	4.8	12.95	17.40	5,187.03	21.73	5,208.76	0.4	34.4
E-04	64.69	53.25	11.44	82.3	0.5	54.99	71.52	2,264.60	904.02	3,168.62	28.5	30.1
E-05	34.64	-	30.84	-	1.3	21.33	-	2,368.42	9.15	2,377.56	0.4	-
HP-SH	129.89	92.85	37.04	71.5	1.6	12.95	18.18	1,726.46	21.87	1,748.34	0.0	40.4
T-02	380.36	350.22	30.14	92.1	1.3	22.77	25.49	2,470.44	956.34	3,426.80	27.9	11.9
E-08	23.14	15.20	7.94	65.7	0.3	54.99	84.42	1,571.29	39.00	1,610.29	2.4	53.4
C-02	42.53	12.95	29.58	30.5	1.3	12.10	45.73	1,288.26	279.83	1,568.09	17.9	278.0
LP-SH	28.14	7.36	20.78	26.2	0.9	12.95	50.35	968.28	22.97	991.25	0.0	288.9
C-01	26.21	5.14	21.07	19.6	0.9	12.10	64.86	917.66	58.22	975.89	6.0	436.1
E-02	50.54	45.45	5.09	89.9	0.2	38.61	43.36	707.25	69.0	776.21	8.9	12.3
CM-08	15.97	14.01	1.95	87.8	0.1	23.95	37.56	168.52	518.07	686.59	75.5	56.8
LP-EVA	79.17	65.30	13.86	82.5	0.6	12.95	15.80	646.05	23.99	670.03	3.6	22.0
Total	2,334.39	812.54	1,327.88	34.8	56.9	3.72	16.31[*]	17,776.30	16,435.73	34,212.04	46.7	338.5

[*] includes $\dot{C}_{\mathrm{L}}$ and $\dot{C}_{Diff}$

The results obtained from the exergoeconomic analysis of the ATR process are presented in Fig. 5.8. The relatively low value of the sum $\dot{C}_{D,tot} + \dot{Z}_{tot}$ indicates that the process enables a more cost-effective provision of exergy of product compared with the SMR or DMR process. Both, the capital investment and the cost of the irreversibilities are essentially lower than for the other base processes with similar methanol capacity. Accordingly, the relative cost difference r_{tot} only amounts to 204.5%. A special feature of this process is the high average cost of the exergy streams which are due to the supply of costly oxygen to the ATR.

The air compressor CM-02, the combustion unit R-09, the condenser E-09 and the ATR R-03 have the highest cost importance within the system. As for the other processes, the air compressor exhibits the highest $\dot{Z}_k$ among all components. The large f value of 86.9% clearly suggests a reduction of $\dot{Z}_k$ by accepting larger irreversibilities. Key design variables for a reduction of the investment cost include the pressure ratio and the isentropic efficiency. Since the offgases leave the HRSG at 1.9 bar and the isentropic efficiency is high, significant savings could be achieved by a reduction of both parameters.

In contrast to all other processes, the combustion unit R-09 has a lower cost importance for the overall system due to smaller capacity. A part of the required process heat is internally provided by the partial oxidation of methane in the autothermal reformer R-03, compensating the heat supply of the combustion unit. However, R-09 has the second highest value of the sum $\dot{C}_{D,k} + \dot{Z}_k$. Similar to the combustion units in the other systems, the cost rate associated with the exergy destruction represents the major cost source (low f value). A reduction of the excess air not only might help to reduce cost rate associated with the irreversibilities in R-09 but also the capital investment for CM-02. In regard to the ATR, being ranked to position number 4, the irreversibilities also constitute the major cost source as indicated by the low f value. The decision variables include the S/C ratio and the O/C ratio. By a reduction of the O/C ratio, the exergy destruction due to highly irreversible combustion reactions could be reduced. However, parameter changes should be conducted carefully as they strongly influence the exergy destruction of other components.

The steam cycle condenser E-09 and the crude product cooler are also rated among the components with the highest cost importance. Both heat exchangers serve to remove low temperature heat from the synthesis unit and the entire process. The respective value of the exergoeconomic factor is low, due to a large cost rate associated with the irreversibilities. The exergy destruction rate is in a moderate range, so that the costs are rather caused by the high average cost at which exergy is supplied to the components. An effective measure to decrease $\dot{C}_{D,k}$ is the reduction of the RTFR in the synthesis unit.

This could be achieved by an increase of the synthesis unit pressure at the expense of a higher investment for the syngas compression unit.

The refining column C-02 is rated position number 7, whereby the low f factor indicates that the irreversibilities, related to the large heat transfer rate in the reboiler and in the condenser, are crucial to the cost of the component. The key decision parameters include the water content in the crude product and the reflux ratio of the reboiler. The water content could only be reduced by major parameter and design changes in the reforming and the synthesis unit. A decrease of the reflux ratio would effectively help in decreasing the exergy destruction but also increase the exergy losses associated with the rejection of the bottom product to the environment.

The HP-EVA and the intermediate cooler E-05 in the syngas compression unit are ranked to position number 8 and 9, both having a low f value. The cost rate $\dot{C}_{D,k}$ is less due to exergy destruction by heat transfer at large temperature difference, but rather caused by the high average cost per unit of exergy of fuel. A decrease of the average temperature difference between the hot and the cold side (thus of the outlet temperature of the process gas) by an increase of the heat transfer area would effectively reduce exergy detruction but inevitably increase the cost of the synthesis unit recuperator E-10, which is also listed in Table 5.7. Similar to the other components of the synthesis unit, the large value of $\dot{Z}_k + \dot{C}_{D,k}$ results from high average cost per unit of exergy of the process gas.

With respect to the turbomachinery, the specific cost for the internally supplied electricty (or mechanical work) are in the same range as for the SMR process. Also for this process, the turbines show unexpected low f values. The low-pressure turbine T-01 is among the components with the highest cost significance. Although the isentropic efficiency is already high, a further increase would lead to a reduction of the exergy destruction. Further measures to decrease $\dot{C}_{D,k}$ concern an improvement of the live steam parameters to decrease the irreversibilities due to friction by an increase of the steam quality within the last stages of the turbine.

Table 5.8: Results obtained from the exergoeconomic analysis for a selection of components of the reference ATR process.

Comp. k	$\dot{E}_{F,k}$	$\dot{E}_{P,k}$	$\dot{E}_{D,k}$	ε_k	$y_{D,k}$	$c_{F,k}$	$c_{P,k}$	$\dot{C}_{D,k}$	$\dot{Z}_k$	$\dot{C}_{D,k}+\dot{Z}_k$	f_k	r_k
	[MW]	[MW]	[MW]	[%]	[%]	[$/GJ]	[$/GJ]	[$/h]	[$/h]	[$/h]	[%]	[%]
CM-02	69.41	61.92	7.48	89.2	0.7	23.45	45.14	631.70	4,203.71	4,835.41	86.9	92.5
R-09	308.90	175.74	133.16	56.9	11.6	4.32	8.87	2,070.85	809.19	2,880.04	28.1	105.4
E-09	8.05	0.00	8.05	-	0.7	80.63	-	2,336.82	50.62	2,387.44	2.1	-
R-03	1,032.23	955.89	76.34	92.6	6.7	7.08	7.76	1,944.82	398.23	2,343.05	17.0	9.6
E-08	15.52	4.59	10.93	29.6	1.0	40.08	136.71	1,577.24	20.11	1,597.35	1.3	241.1
E-03	52.37	39.54	12.83	75.5	1.1	30.23	40.07	1,396.58	3.90	1,400.47	0.3	32.6
C-02	28.48	7.98	20.50	28.0	1.8	15.36	63.53	1,133.46	251.12	1,384.58	18.1	313.6
HP-EVA	61.15	47.84	13.31	78.2	1.2	18.85	24.12	903.40	3.88	907.28	0.4	28.0
E-05	14.34	8.07	6.27	56.3	0.6	32.91	58.89	742.43	12.14	754.57	1.6	78.9
E-06	27.60	23.53	4.07	85.3	0.4	43.15	51.94	632.38	112.49	744.87	15.1	20.4
CM-04	10.09	9.12	0.98	90.3	0.1	23.56	45.65	82.98	642.11	725.08	88.6	93.8
T-01	76.43	69.31	7.12	90.7	0.6	20.41	23.18	523.22	168.84	692.05	24.4	13.6
E-02	25.33	19.03	6.30	75.1	0.6	30.23	40.30	685.86	4.20	690.06	0.6	33.3
HP-SH	48.26	38.50	9.76	79.8	0.9	18.85	23.70	662.27	9.83	672.10	1.5	25.7
CM-01	7.27	5.78	1.48	79.6	0.1	23.45	52.55	125.37	480.42	605.79	79.3	124.1
C-03	17.14	6.65	10.49	38.8	0.9	9.50	33.53	358.87	216.31	575.18	37.6	252.8
MP-EVA	51.80	43.96	7.84	84.9	0.7	18.85	22.34	532.19	20.66	552.86	3.7	18.5
Total	1,144.30	651.15	453.2	56.9	39.6	3.79	11.24[*]	6,183.46	10,416.54	16,600.00	62.8	204.5

[*] includes $\dot{C}_L$ and $\dot{C}_{Diff}$

Regarding the DMR process, the results obtained from the exergoeconomic analysis are given in Table 5.9. The value of the sum $\dot{C}_{D,tot} + \dot{Z}_{tot}$ is of a similar magnitude as for the SMR process. The relative average cost difference r_{tot}, however, only amounts to 284.3% in comparison to 338.5% in the SMR process due to larger exergy rate of product. In regard to the products, the relative cost difference for electricity and methanol is 640.1% and 171.4%, respectively. The cost rates associated with the capital investment (and O&M costs) and the exergy destruction have a similar cost impact on the overall process, as shown by an exergoeconomic factor of $f_{tot} = 49.8\%$.

In regard to the cost distribution and the cost importance of the components, similar characteristics as for the SMR process can be identified. Also for the DMR process, the combustion unit R-05, the air compressors CM-02, and the condenser E-10 are the most important components from a thermoeconomic point of view. Due to the high process heat demand, these units are designed for a large capacity. The combustion unit has the highest value of the sum $\dot{C}_{D,k} + \dot{Z}_k$ and shows a typical low f value of 25%. The cost rate $\dot{C}_{D,k}$ might be decreased by lowering the air-to-fuel ratio and thus the excess air for the combustion. However, the mass flow rate of the excess air is determined by the outlet temperature and therefore by the operation of the DMR reactor. A lower air mass flow rate would also result in a reduction of the capacity of the air compressor CM-02, which is ranked to the second position among the components with the highest cost significance. The high value of f shows, that the capital investment and the O&M costs are the main source of cost. A reduction of the isentropic efficiency would decrease $\dot{Z}_k$ at the expense of a lower exergetic efficiency. Furthermore, the pressure ratio might be slightly decreased for a design improvement since the pressure of the offgases is still high with 1.6 bar. In particular for the DMR process, the circulating mass flow rate in the synthesis unit is high. The removal of a large amount of low temperature heat from the synthesis unit is responsible for the large irreversibilities within the crude product cooler E-09 and the condenser E-10. Both components have a low value of f, suggesting an increase in the exergetic efficiency. A reduction of the RTFR by an increase of the synthesis unit pressure exhibits the most effective measure to decrease the irreversibilities in these heat exchangers. Additionally, the heat transfer area can be increased to reduce the average temperature difference of heat transfer and thus the component's exergy destruction. The large value of the relative cost difference for E-09 is due to the high spcific cost of the circulating water between the condenser and the crude product cooler.

Another component with a high cost significance refers to the water-cooled high temperature syngas cooler E-05. According to the low value of f, a reduction of $\dot{C}_{D,k}$ should be achieved by decreasing the average temperature difference (up to 500 °C) of

heat transfer. An intervention in the operation of the reformer could lead to a reduction of the temperature of the process gas on the hot side. On the other hand, the syngas cooler could be exposed to a higher temperature level on the steam side, which would require a rearrangement of the components in the steam cycle.

Considering the value of the sum $\dot{C}_{D,k} + \dot{Z}_k$ in Table 5.9, all other components (down from position 6) obviously have a lower cost importance. In regard to the high-pressure economizer HP-ECO, the superheater HP-SH and the reheater LP-RH in the HRSG, the irreversibilities play a major role for their cost significance. The high exergy destruction is predominantly caused by large mass flow rates of the high-pressure steam and the exhaust gas. A reduction of the operation temperature of the DMR would effectively reduce the irreversibilities due to heat transfer within the HP-SH and thus the associated cost rate $\dot{C}_{D,k}$.

The low and medium-pressure turbines T-01 and T-02 are also listed in the Table 5.9, being ranked to position 8 and 11. As for the steam turbines in the other processes, the irreversibilities also constitute the major cost source for these components. A change of the live steam parameters and a slight decrease in the pressure ratio in order to increase the steam quality at the outlet of T-01 constitute effective measures to reduce $\dot{C}_{D,k}$.

As for the other processes, the refining column C-02 is also among the components with a highest cost impact due to a large cost rate associated with the irreversibilities. A decrease of the reflux ratio would potentially lower $\dot{C}_{D,k}$ at the expense of an increase of the cost rate associated with exergy losses. Additionally, the temperature of the steam in the reboiler could be lowered to reduce the exergy destruction due to heat transfer.

Table 5.9: Results obtained from the exergoeconomic analysis for a selection of components of the reference DMR process.

Comp. k	$\dot{E}_{F,k}$	$\dot{E}_{P,k}$	$\dot{E}_{D,k}$	ε_k	$y_{D,k}$	$c_{F,k}$	$c_{P,k}$	$\dot{C}_{D,k}$	$\dot{Z}_k$	$\dot{C}_{D,k} + \dot{Z}_k$	f_k	r_k
	[MW]	[MW]	[MW]	[%]	[%]	[\$/GJ]	[\$/GJ]	[\$/h]	[\$/h]	[\$/h]	[%]	[%]
R-05	1,709.69	1,112.97	596.72	65.1	25.5	4.07	7.00	8,753.34	2,966.85	11,720.18	24.8	71.3
CM-02	214.62	190.72	23.90	88.9	1.0	21.74	35.21	1,870.65	7,372.72	9,243.36	79.5	61.1
E-10	58.84	-	36.94	-	1.6	53.06	-	7,057.01	149.36	7,206.37	0.0	-
E-09	65.16	16.36	48.80	25.1	2.1	31.90	128.81	5,603.31	106.26	5,709.58	1.8	303.8
E-05	59.81	28.00	31.82	46.8	1.4	45.73	98.26	5,237.65	56.90	5,294.55	1.1	114.8
HP-ECO	341.42	267.66	73.75	78.4	3.2	11.01	14.07	2,924.37	20.86	2,945.23	0.7	27.8
HP-SH	254.46	196.94	57.52	77.4	2.5	11.01	14.29	2,280.66	39.84	2,320.50	1.7	29.7
T-01	259.59	237.54	22.04	91.5	0.9	19.72	22.29	1,564.99	635.45	2,200.44	28.5	13.0
CM-04	49.75	44.39	5.37	89.2	0.2	21.74	33.38	420.16	1,438.90	1,859.06	77.1	52.8
E-06	24.26	10.80	13.46	44.5	0.6	36.40	82.70	1,763.79	36.05	1,799.83	2.0	127.2
T-02	232.60	218.88	13.72	94.1	0.6	19.51	21.49	963.45	595.69	1,559.15	37.8	10.1
LP-EVA	108.94	74.16	34.78	68.1	1.5	11.02	16.21	1,380.49	4.82	1,385.31	0.3	47.1
LP-RH	53.60	27.54	26.06	51.4	1.1	11.01	21.86	1,033.16	42.50	1,075.66	3.9	98.4
C-02	27.12	6.28	20.84	23.2	0.9	10.23	57.16	767.67	293.21	1,060.88	27.4	457.1
R-03	68.29	65.31	2.98	95.6	0.1	81.32	85.06	873.37	4.59	877.96	0.5	4.6
CM-05	39.46	34.85	4.61	88.3	0.2	21.74	28.27	360.88	457.83	818.71	55.5	29.7
RECUP	69.15	53.64	15.50	77.6	0.7	11.01	15.22	614.64	197.13	811.77	23.9	37.9
Total	2,336.87	929.13	1,245.47	39.8	53.3	3.68	14.14[*]	16,487.07	16,350.55	32,837.63	49.8	284.2

[*] includes $\dot{C}_L$ and $\dot{C}_{Diff}$

Table 5.10 presents the results obtained from the exergoeconomic analysis of the CMR process. For a similar methanol capacity, the sum of the cost rates $\dot{C}_{D,tot} + \dot{Z}_{tot}$ is lower than for the SMR and DMR process. This reduction is mainly caused by a lower power capacity of the system (see Table 5.1). According to the product capacities (with a focus on methanol), the average relative cost difference r_{tot} is comparatively low. A special feature of this process is the integrated Selexol$^{\circledR}$ unit which causes relatively high average cost of the syngas by recycling CO_2 of high specific cost to the reforming unit. This in turn causes a sharp increase of the cost rate associated with the inefficiencies of the components in the synthesis unit. The combustion of unconverted and costly synthesis gas (stream 10 in Fig. 4.11) results in high average cost per unit exergy of the exhaust gas and finally in high specific cost of the steam and electricity. Thus, in comparison to other processes, electricity is provided internally to the consumers at high average cost $c_{F,k}$ of 27.0 US\$/GJ. For the overall process, $\dot{Z}_{tot}$ has a larger impact than the cost rate associated with the irreversibilities $\dot{C}_{D,tot}$.

As with the other processes, the combustion unit R-05 and the air compressor CM-02 also have the highest cost importance for the CMR process. In comparison to the endothermic DMR and SMR process, the demand for process heat is low, thus reducing the size of these components. The most important design variables and their impact on the components' costs have already been explained in detail for the other processes. Interestingly, the refining column C-02 is rated to position number three. The steam supplied to the reboiler of the column has large average cost per unit of exergy, causing a high value of $\dot{C}_{D,k}$. A reduction of the irreversibilities due to a decrease of the reflux ratio would cause an unacceptable low product purity and high exergy losses. In this case a third column would be required to guarantee AA methanol product quality. Furthermore, the steam temperature on the hot side of the reboiler could be reduced to lower the exergy destruction related to heat transfer.

The crude product cooler E-11 in the CMR process is comparatively small, since the circulating mass flow is low due to a high conversion rate in the synthesis unit. However, the component is ranked to position number four, having irreversibilities as the major cost source. The high cost rate $\dot{C}_{D,k}$ is caused by a combination of a low exergetic efficiency and high average cost per unit of exergy of fuel. An increase of the synthesis pressure could reduce the circulating mass flow rate (and the heat transfer rate) and thus the inefficiencies within E-11. In addition, further cost reduction might be achieved by exposing the component to higher steam temperatures to reduce the high temperature difference of heat transfer.

The syngas cooler E-07 is rated to position number 6 and has a low value for the variable f due to a high cost rate associated with the irreversibilities. Considering Fig. 4.12, it is highly recommended to relocate the heat exchanger within the heat integration system to reduce the exergy destruction due to heat transfer. Turning next to the combined reformer R-03, the relatively low value of the factor f suggests a decrease of the cost rate associated with the irreversibilities. A decrease of the heat transfer rate achieved through a reduction of the inlet temperature of the combustion gases results in a lower conversion rate of methane. Alternatively, the S/C ratio could be increased and the CO_2/C ratio decreased to reduce the heat demand of the reforming reactions.

The syngas compressor CM-01 has a high cost significance due to a large cost rate associated with the capital investment ($f_k = 83.7\%$). The component is designed for a large capacity due to high pressure ratio of 15 between the AGR and the reforming unit. The cost rate $\dot{Z}_k$ could be reduced by increasing the operation pressure of the combined reformer or by a reduction of the isentropic efficiency of CM-01. A change of the operation parameters of the reformer, however, should be treated with care.

The high-pressure evaporator (HP-EVA) is also important from a thermoeconomic point of view due to a high value of the sum $\dot{C}_{D,tot} + \dot{Z}_{tot}$. The exergy destruction constitutes the major cost source and results from the heat transfer at a temperature difference of up to 400 °C (see Fig. 4.12). An increase of the steam pressure may decrease $\dot{C}_{D,k}$, but requires major design changes in the steam cycle.

The syngas cooler E-05 is also listed in Table 5.10. The component serves to cool the syngas for the WGS unit while preheating simultaneously steam for the shift reaction. The low value for the variable f results from a low exergetic efficiency of 50.1% in conjunction with relatively high average cost of the exergy of fuel. Comparing the values of the sum $\dot{C}_{D,k} + \dot{Z}_k$ in Table 5.10, the other components obviously have a relatively low cost significance. The water gas shift reactor R-04 is operated with low conversion rate, thus exhibiting low irreversibilities. However, the f factor shows that the cost rate associated with the irreversibilities is dominating. As with the other processes, the irreversibilities are also the major cost source for the turbines T-01 and T-02.

Table 5.10: Results obtained from the exergoeconomic analysis for a selection of components of the reference CMR process.

Comp. k	$\dot{E}_{\mathrm{F},k}$	$\dot{E}_{\mathrm{P},k}$	$\dot{E}_{\mathrm{D},k}$	ε_k	$y_{\mathrm{D},k}$	$c_{\mathrm{F},k}$	$c_{\mathrm{P},k}$	$\dot{C}_{\mathrm{D},k}$	$\dot{Z}_k$	$\dot{C}_{\mathrm{D},k}+\dot{Z}_k$	f_k	r_k
	[MW]	[MW]	[MW]	[%]	[%]	[$/GJ]	[$/GJ]	[$/h]	[$/h]	[$/h]	[%]	[%]
R-05	890.55	597.04	293.51	67.0	18.6	4.30	7.07	4,538.87	1,421.47	5,960.34	23.9	64.6
CM-02	103.31	93.10	10.21	90.1	0.7	27.02	40.65	992.93	3,572.59	4,565.52	78.3	50.4
C-02	33.17	10.24	22.93	30.9	1.5	35.62	124.04	2,940.05	320.98	3,261.02	9.8	248.3
E-11	18.72	6.81	11.92	36.6	0.8	72.04	199.23	3,090.80	25.84	3,116.64	0.8	176.6
E-12	17.32	-	17.32	0.00	1.1	39.6	-	2,466.63	63.99	2,530.63	2.5	-
E-08	46.27	22.51	23.75	48.7	1.5	34.58	71.58	2,956.59	42.27	2,998.86	1.4	107.0
R-03	219.33	178.70	40.62	81.5	11.8	15.82	2.76	1,728.77	840.33	2,569.10	32.7	33.8
CM-01	82.08	78.13	3.94	95.2	0.3	27.02	35.37	383.74	1,962.64	2,346.38	83.7	30.9
HP-EVA	179.95	126.22	53.73	70.1	3.4	11.82	16.88	2,286.64	11.30	2,297.94	0.5	42.8
E-05	35.78	17.91	17.87	50.1	1.1	28.57	57.11	1,837.60	2.98	1,840.58	0.2	99.9
T-01	139.02	128.50	10.52	92.4	0.7	25.25	28.10	956.14	365.61	1,321.75	27.7	11.3
HP-SH	111.59	81.62	29.97	73.1	1.9	11.82	16.22	1,275.37	16.44	1,291.81	1.27	37.19
CM-03	11.23	10.08	1.15	89.8	0.1	27.02	56.67	111.86	964.17	1,076.02	89.6	109.7
C-01	8.90	1.04	7.86	11.7	0.5	35.62	320.16	1,007.48	58.82	1,066.29	5.5	798.9
T-02	127.28	121.16	6.12	95.2	0.4	22.83	24.77	502.92	343.65	846.58	40.6	8.5
E-06	18.55	9.08	9.47	49.0	0.6	24.21	49.56	825.21	3.44	828.66	0.4	104.7
R-04	87.58	85.20	2.38	97.3	0.2	72.80	74.84	623.95	3.21	627.16	0.5	2.8
Total	1,576.45	765.97	653.66	48.6	41.5	3.83	12.41[*]	12,621.10	12,033.39	24,654.48	56.9	224.0

[*] includes $\dot{C}_{\mathrm{L}}$ and $\dot{C}_{Diff}$

The results obtained from the exergoeconomic analyis of the SMR-ATR process are presented in Table 5.11. The process is designed for a large capacity, thus requiring a higher capital investment and increased O&M costs ($\dot{Z}_{tot}$) compared to other processes. Due to relatively low exergy destruction (see Table 5.4), the capital investment and O&M cost have a dominating impact on the cost of the overall process. The exergy streams have low average cost, since the reforming agent oxygen can be supplied cheaply due to the effect of the economies of scale concerning the ASU. As a result, the internally consumed electricity is of low cost which generally decreases the cost rate associated with the exergy destruction of the electricity consuming units. In comparison with other processes the relative cost increase r_{tot} is the lowest, having a value of 154.0%

Considering the component level, the combustion unit R-07, the air compressor CM-02 and the ATR R-05 are the most important components from a thermoeconomic point of view. Taking into account the plant capacity and the process heat demand, the size of R-07 and CM-02 is relatively small. The heat of the effluent from the ATR is recovered in the primary tubular steam reformer R-03, thus lowering the heat duty that needs to be covered by the combustion of fuel in R-07. Furthermore, the process benefits from a low heat requirement of the SMR, since the conversion must be limited for stoichiometric reasons. Similar to the combustion unit, the autothermal reformer R-04 is characterized by a low f value, showing a dominating impact of $\dot{C}_{D,k}$. The irreversibilities, caused by the highly irreversible POX reactions, might be reduced by adjusting the S/C and the O/C ratio.

Also for this process, the condenser E-13 has a high cost significance due to the cost related to the irreversibilities. However, compared with the other processes, the steam has low average cost per unit exergy, resulting in a comparatively low value of $\dot{C}_{D,k} + \dot{Z}_k$. All high-pressure heat exchangers of the HRSG are present in Table 5.11 and have a low exergoeconomic factor. The large value of $\dot{C}_{D,k}$ results from large heat transfer rates and high temperature differences between the process gas, the exhaust gas and the steam (see Fig. 4.13).

Obviously, the large steam flows also cause large cost rates $\dot{C}_{D,k}$ in the medium and low-pressure turbine, which are rated to position ten and eleven. Interestingly, the capital investment and O&M costs play a more important compared to the turbines in the other processes. The refining column C-02 also has a high cost importance in this process given by cost rate $\dot{C}_{D,k}$. Although a three column distillation system is applied, a large heat transfer rate is given for the reboiler of column C-02. A decrease of the reflux ratio might reduce the value of the sum $\dot{C}_{D,k} + \dot{Z}_k$ for C-02. However, if the exergy losses

should be maintained at the same level, a more intensive operation of the atmospheric column C-03 would be required, thus shifting the irreversibilities downstream.

Due to large syngas mass flow rates, a variety of components within the syngas track appears among the units with the highest cost importance. These include the main recycle compressor CM-09, the syngas compressors CM-05 and CM-06 as well as the recuperator of the shift unit E-06. Common to all these compressors is the dominant cost influence of $\dot{Z}_{D,k}$.

The results obtained from the exergoeconomic analysis of the SMR-DMR process are presented in Table 5.12. The process has the highest methanol and electric capacity among all analysed processes. Accordingly, the value of the sum $\dot{C}_{D,tot} + \dot{Z}_{tot}$ is much higher than for the other processes. The relative cost difference of the overall system amounts to 229.3% which is lower than for the DMR and SMR process but higher compared to the SMR-ATR, the ATR, and the CMR process. As for the other systems, the relative cost difference for electricity is much higher than for methanol. The corresponding values for r_{elec} and r_{Meoh} amount to 777.7% and 150.2%, respectively.

The combustion unit R-05, the air compressors CM-03 and CM-04, the high-pressure economizer HP-ECO, and the low-pressure turbine T-02 are the most important components from a thermoeconomic perspective. Comparing the values of the sum $\dot{C}_{D,k} + \dot{Z}_k$, an outstanding cost importance of the combustion unit is revealed. The component is designed for huge capacity due to the high process heat demand of both endothermic reforming units R-03 and R-04. The relatively low f value of 25.0% suggests an increase of the exergetic efficiency at the expense of higher investment costs. The irreversibilities are mainly caused by the chemical reactions, the heat transfer and the mixture of streams at different temperature. A decrease of $\dot{C}_{D,k}$ can be achieved by lowering the unit cost of the exergy of fuel $c_{F,k}$ through an increase of the share of natural gas in the total amount of fuel. In general, the recycled syngas from the purge (stream 16) has higher specific cost than natural gas. Furthermore, actions can be taken to increase ε_k. These measures include a preheating of reactants and the reduction of the excess air for combustion. The latter measure would simultaneously reduce the investment cost and therefore the cost importance of the air compressors, which are ranked to position two and three. In addition, a further decrease of $\dot{Z}_k$ of the most capital-intensive units could be achieved by reducing the isentropic efficiency η_s.

Table 5.11: Results obtained from the exergoeconomic analysis for a selection of components of the reference SMR-ATR process.

Comp. k	$\dot{E}_{F,k}$	$\dot{E}_{P,k}$	$\dot{E}_{D,k}$	ε_k	$y_{D,k}$	$c_{F,k}$	$c_{P,k}$	$\dot{C}_{D,k}$	$\dot{Z}_k$	$\dot{C}_{D,k} + \dot{Z}_k$	f_k	r_k
	[MW]	[MW]	[MW]	[%]	[%]	[\$/GJ]	[\$/GJ]	[\$/h]	[\$/h]	[\$/h]	[%]	[%]
R-07	1,044.63	686.59	358.04	65.7	12.9	5.13	8.70	6,610.10	2,208.43	8,818.53	25.0	69.6
CM-02	124.45	111.04	13.42	89.2	0.5	16.46	30.43	794.83	4,793.02	5,587.86	85.8	85.0
R-04	2,087.82	1,941.35	146.48	93.0	5.3	5.10	5.63	2,687.60	1,053.41	3,741.01	28.2	10.5
HP-SH	220.19	161.60	58.60	73.4	2.1	11.29	15.43	2,382.59	24.05	2,406.64	1.0	36.6
E-13	37.93	-	37.93	-	1.4	13.44	-	1,834.77	79.07	1,913.84	4.1	-
HP-ECO	176.76	143.93	32.83	81.4	1.2	11.29	14.28	1,334.98	214.23	1,549.21	13.8	26.5
HP-EVA	139.51	103.87	35.65	74.5	1.3	11.29	15.18	1,449.48	4.81	1,454.29	0.3	34.4
C-02	52.28	16.30	35.98	31.2	1.3	7.12	31.33	922.77	497.75	1,420.52	35.0	339.8
CM-09	12.85	11.48	1.37	89.3	0.1	16.62	45.79	82.19	1,123.25	1,205.44	93.2	175.5
T-02	196.59	184.77	11.82	94.0	0.4	14.58	16.31	620.42	530.62	1,151.04	46.1	11.9
T-03	161.73	148.45	13.28	91.8	0.5	14.58	16.70	696.95	435.75	1,132.70	38.5	14.5
CM-01	12.60	11.43	1.18	90.7	0.00	16.46	43.85	69.70	1,057.18	1,126.88	93.8	166.5
CM-03	12.97	11.27	1.69	87.0	0.1	16.78	41.23	102.22	890.13	992.36	89.7	145.7
E-06	175.18	146.33	28.85	83.5	1.0	5.25	7.10	545.29	426.37	971.66	43.9	35.1
CM-05	26.03	24.31	1.73	93.4	0.1	16.62	27.19	103.23	821.66	924.89	88.8	63.6
CM-06	52.38	48.86	3.52	93.3	0.1	16.62	21.71	210.72	684.72	895.44	76.5	30.6
R-02	115.92	113.20	2.72	97.7	0.1	83.07	85.08	812.94	4.81	817.74	0.6	2.4
Total	2,772.20	1,587.02	1,083.34	57.3	39.1	3.83	9.73[*]	14,924.19	19,600.33	34,524.52	56.8	154.0

[*] includes $\dot{C}_L$ and $\dot{C}_{Diff}$

Due to the high mass flow rate of the exhaust gas, very large amounts of heat need to be recovered as steam in the HRSG in order to achieve a high overall efficiency. According to the large heat transfer rates, a variety of heat exchangers (HP-EVA, LP-EVA, HP-SH, LP-SH and RH) has a high cost significance caused by the cost rate associated with their irreversibilities. For a deeper understanding of the inefficiencies, Fig. 4.15 should be considered. A reduction in the temperature difference between the hot and cold side would reduce the exergy destruction within the HRSG and thus the cost rate $\dot{C}_{D,k}$ of the heat exchangers. The temperature profiles in Fig. 4.15 show that a third pressure level or a pressure increase of the HP level could be an effective measure to reduce the irreversibilities. Furthermore, a temperature drop of the exhaust gas (T_{10}) would also reduce $\dot{C}_{D,k}$. However, this would result in a high methane slip from the reformer and increase the cost of downstream components.

Despite the high exergetic efficiency of the high- and low-pressure turbines T-01 and T-02, the irreversibilities exhibit the major cost source. The low-pressure turbomachinery is designed for a large power output of 530 MW, resulting in relatively large irreversibilities. A change of the live steam parameters might decrease the exergy destruction caused by friction of water droplets in the last expansion stages (improvement of steam quality). The extraction column C-01 and the refining column C-02 are also among the components with the highest cost significance. Large process streams have to be processed at low exergetic efficiency, which causes a predominating cost rate of the irreversibilities (f_k = 10 - 20%). Effective measures for a reduction of the irreversibilities have been introduced before.

Table 5.12: Results obtained from the exergoeconomic analysis for a selection of components of the reference SMR-DMR process.

Comp. k	$\dot{E}_{F,k}$	$\dot{E}_{P,k}$	$\dot{E}_{D,k}$	ε_k	$y_{D,k}$	$c_{F,k}$	$c_{P,k}$	$\dot{C}_{D,k}$	$\dot{Z}_k$	$\dot{C}_{D,k} + \dot{Z}_k$	f_k	r_k
	[MW]	[MW]	[MW]	[%]	[%]	[\$/GJ]	[\$/GJ]	[\$/h]	[\$/h]	[\$/h]	[%]	[%]
R-05	2,429.67	1,626.51	803.16	66.9	21.8	5.02	8.33	14,527.56	4,847.73	19,375.29	25.0	65.9
CM-04	207.25	186.20	21.05	89.8	0.6	26.20	39.19	1,985.32	6,717.43	8,702.76	77.2	49.6
CM-03	209.33	188.15	21.19	89.9	0.6	26.20	37.97	1,998.46	5,972.62	7,971.08	74.9	44.9
HP-EVA	490.40	358.98	131.42	73.2	3.6	14.32	19.58	6,773.87	28.30	6,802.17	0.4	36.8
T-02	579.51	535.75	43.76	92.5	1.2	23.62	26.42	3,721.07	1,671.93	5,393.00	31.0	11.8
LP-EVA	268.33	180.95	87.38	67.4	2.4	14.32	21.29	4,503.94	39.75	4,543.69	0.9	48.7
E-11	47.82	-	47.82	-	1.3	23.43	-	4,066.85	195.40	4,262.25	3.0	-
E-08	127.58	81.52	46.06	63.9	1.3	23.84	37.39	3,952.65	24.00	3,976.65	0.60	56.8
C-02	61.19	18.45	42.74	30.2	1.2	18.35	69.83	2,822.74	597.03	3,419.77	17.5	280.6
HP-SH	269.93	209.10	60.83	77.5	1.7	14.32	18.56	3,135.39	55.64	3,191.03	1.7	29.6
LP-SH	89.57	41.90	47.67	46.8	1.3	14.32	31.15	2,457.18	81.41	2,538.58	3.2	117.5
E-11	35.01	16.99	18.02	48.5	0.5	33.61	74.73	2,180.66	333.43	2,514.09	13.3	122.3
RH	68.22	27.28	40.94	40.0	1.1	14.32	36.48	2,110.23	66.04	2,176.27	3.0	154.8
E-05	54.28	22.88	31.40	42.2	0.9	17.89	42.78	2,022.80	27.16	2,049.96	1.3	139.1
T-01	201.68	190.05	11.63	94.2	0.3	23.25	25.65	973.26	663.85	1,637.11	40.6	10.3
E-10	46.28	39.42	6.86	85.2	0.2	33.61	41.73	829.55	322.49	1,152.04	28.0	24.2
C-01	16.91	2.75	14.16	16.3	0.4	18.35	123.85	935.42	109.26	1,044.68	10.5	575.0
Total	3,689.79	1,707.75	1,735.50	46.3	47.0	3.79	12.48[*]	23,678.22	26,199.11	49,877.33	52.5	229.3

[*] includes $\dot{C}_L$ and $\dot{C}_{Diff}$

The calculated levelized cost of electricity (LCOE) and methanol (LCOM) are consistent with the results of the economic sensitivity analysis in Section 5.4. However, the exact breakdown of costs by allocation of monetary values to each unit of exergy of a stream allows for advanced and alternative conclusions regarding the economic use of the processes. Figs. 5.13 and 5.14 present the levelized cost of methanol and the levelized cost of electricity in dependence of the specific fuel cost f_c. The linear slope illustrates the sensitivity of the cost of the respective product to a change of the fuel cost.

Considering the results in Fig. 5.13, the SMR process obviously cannot produce methanol at competitive cost. Crucial is the supply of large quantities of expensive high temperature steam as a reforming agent, which increases the average cost per unit exergy of the syngas. Furthermore, this high temperature steam therefore cannot be used for electricity generation. In addition, the process is not as highly integrated into the steam cycle as the other synthesis routes, resulting in a higher cost rate associated with the exergy losses. The cost of the losses are assigned to the products relative to their exergy rate. A third reason refers to the direct hydrogenation of CO_2 in the methanol synthesis. The integration results in an excessive water production by the reverse water gas shift reaction (see reaction Eq. 2.27), which increases the capacity of the components in the synthesis loop and the distillation unit. Downstream a large amount of heat is provided by costly steam within the reboilers, thus additionally increasing the cost of the main product.

In regard to the other processes, the levelized methanol cost are in a similar range. Obviously, the SMR-DMR and the SMR-ATR process profit from the economies of scale and the corresponding low fixed cost. The SMR-ATR process can produce methanol at the lowest levelized cost. As the specific fuel cost increase, the cost advantage of producing methanol increases. It should be noted that CO_2 for dry reforming and hydrogenation is assumed to be free of charge (concerning the SMR, DMR, CMR, and SMR-DMR process). Under these terms, the SMR-DMR process can generate methanol at the second lowest cost. If costs are assigned to the incoming CO_2 stream, the levelized methanol cost will be higher. For fuel cost of 8 US$/GJ the ATR and CMR process reach break even with the DMR process. The product related low fixed cost of the DMR process are crucial for the cost advantage at low fuel cost. On the other hand, the increased product cost for the ATR at specific fuel cost of 0 US$/GJ can be attributed to the costly supply of oxygen. At a high natural gas price above 8 $/GJ, the fuel cost have a higher influence on the LCOM of the DMR (compared with the ATR and CMR process) due to high CH_4-intensity. The methanol product of the CMR and the ATR process shows a similar price sensitivity to changes in the fuel cost.
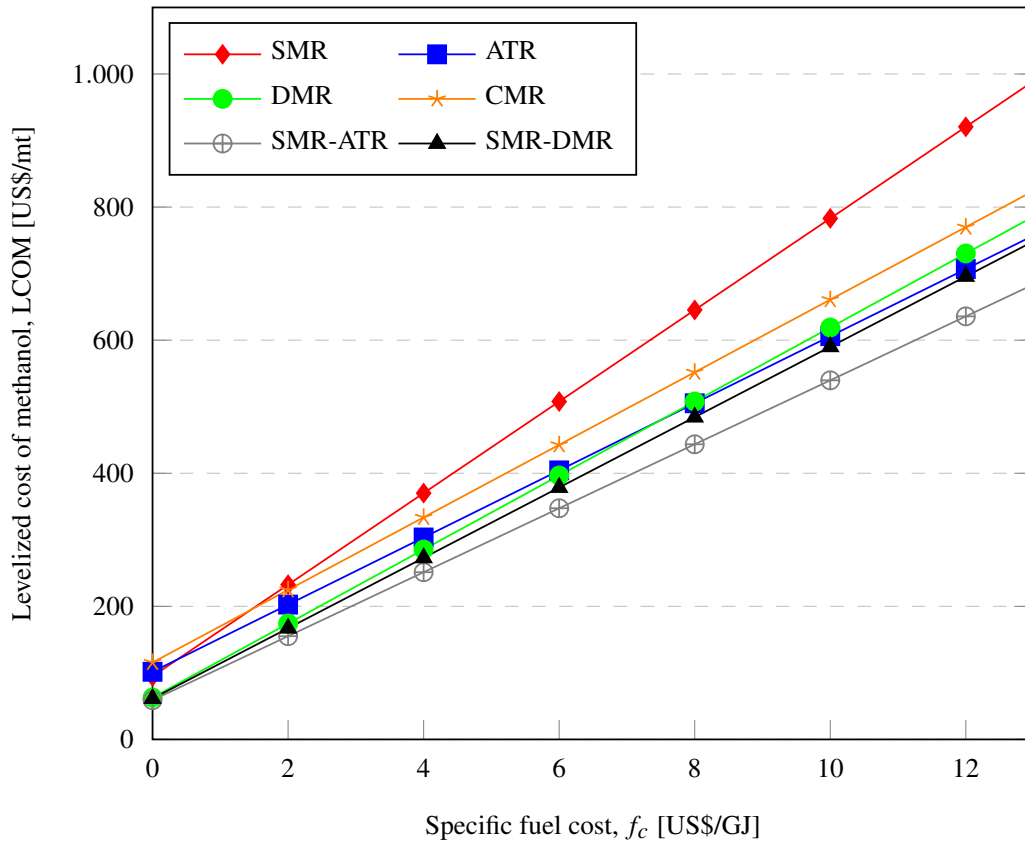
Figure 5.13: Levelized cost of methanol (LCOM) as a function of the fuel cost.

The levelized cost of electricity (LCOE) directly depend on the average cost at which exergy is supplied to the steam cycle. Thus, the LCOE depend on the average cost of the exhaust gas from the combustion unit and on the specific cost of the process gas. Depending on the system design, the combustion fuel contains a different proportion of syngas which is determined by the purge ratio in the synthesis unit. The syngas is of higher average cost per unit exergy than the supplied natural gas. Consequently, the LCOE of a process increases with an increasing supply of purge gas to the combustion unit. Considering Fig. 5.14, a clear trend becomes apparent. For the processes with endothermic reforming technology, the LCOE show a high sensitivity to changes in the specific fuel cost, while it is low for the processes with autothermal reforming.

The CMR process generates electricity at the highest levelized cost among all processes. The syngas recycled to the combustion unit is more expensive than for other processes causing high specific cost of the exhaust gases. The high price sensitivity can be explained by the high proportion of natural gas (66 mass-%) in the total amount of combustion fuel.

A pecularity arises for the ATR process. Since exclusively syngas is used as a combustion fuel, the LCOE directly depend on the specific cost of the process gases. Therefore, for low natural gas prices, the LCOE is already high due to expensive syngas generation caused by the use of a costly reforming agent. For the same reason a low price sensitivity results for the LCOE. The remaining processes (SMR, DMR, SMR-DMR, SMR-ATR) have lower LCOE at low specific fuel cost, since heat is rather provided by the combustion of natural gas instead of using the process gas. Accordingly the sensitivity of the LCOE to price changes is higher than for the ATR process. For fuel cost of 5.3 US$/GJ the ATR process reaches break even with the SMR and the SMR-DMR process. The SMR-ATR process can clearly generate electricity at the lowest cost. The SMR-ATR process shows a significant advantage in terms of the levelized electricity generation cost. Interestingly, the process has low LCOE at low specific fuel cost although costly oxygen is used as a reforming agent. In comparison to the ATR process, the SMR-ATR process obviously can profit from the effect of the economies of scale of the ASU. In addition, the LCOE show a low sensitivity to changes in the specific cost due to low CH_4-intensity.
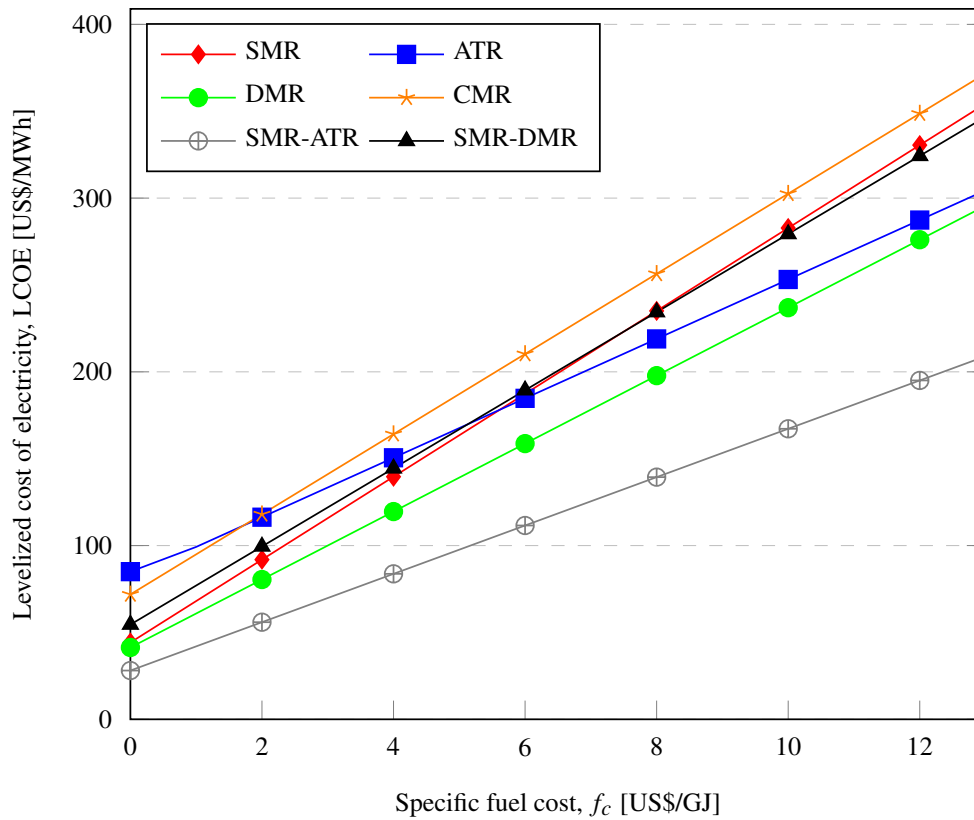
Figure 5.14: Levelized cost of electricity (LCOE) as a function of the fuel cost.

Within the economic analysis, the cost rate of integrated CO_2 streams was assumed to be zero since it was considered as a waste product (e.g., from a power plant with carbon capture), which could cause additional cost if it would be emitted. However, high-purity CO_2 might constitute a resource of value since process equipment inevitably would be required for the supply. Consequently, the processes with CO_2 integration could have been favored in the cost estimation. A sensitivity analysis is performed to investigate the impact of possible CO_2 cost on the levelized product cost. Figure 5.15 presents the levelized cost of methanol as a function of the specific fuel cost, taking into account the uncertainty of the cost of CO_2. Accordingly, Figure 5.16 shows the sensitivity of the levelized cost of electricity. For the analysis, the cost for CO_2 were assumed to be in the range of 0 - 100 US$/t. The graphs of the cases with maximum CO_2 cost (SMR100, DMR100 and SMR-DMR100) are shown in Figs. 5.15 and 5.16. Furthermore, the graphs for the cases without CO_2 cost are presented as a reference. Consequently, the two related graphs (e.g. DMR and DMR100) limit the range of the cost influence of the CO_2 on the methanol cost (e.g. $\Delta LCOM_{SMR}$) for a constant cost of natural gas.
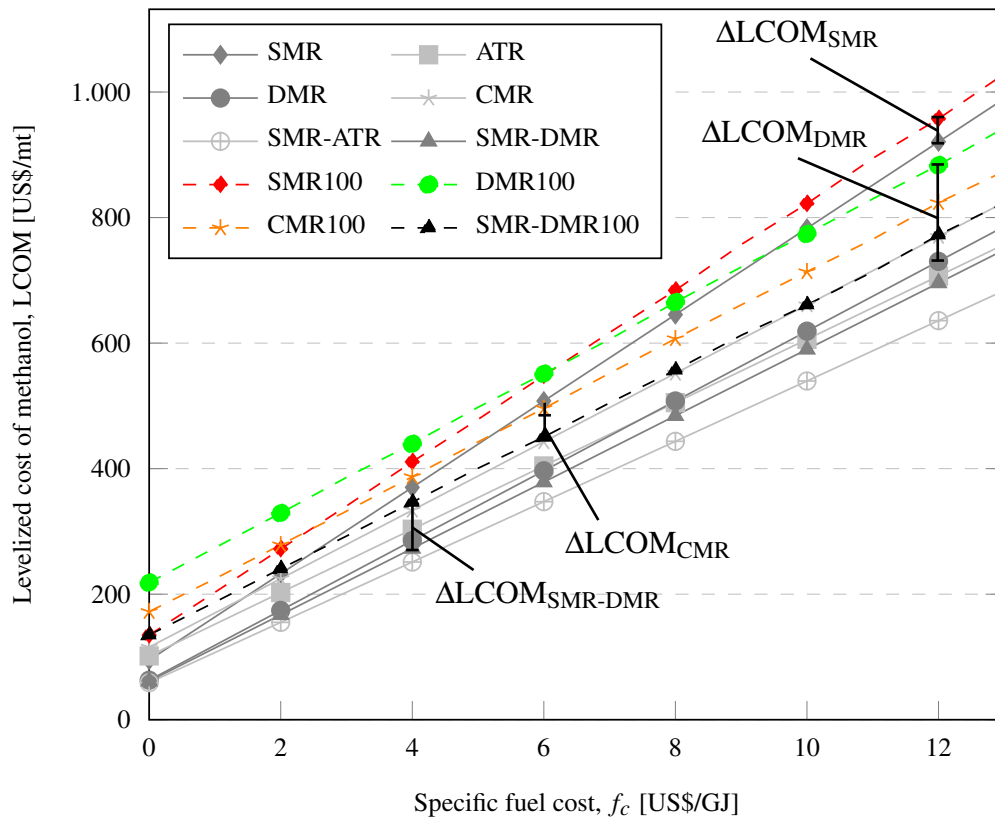
Figure 5.15: Levelized cost of methanol as a function of the fuel cost under uncertainty of the cost for CO_2.

The increase of the levelized cost of electricity and methanol by monetization of CO_2 is proportional to the amount of integrated CO_2. Consequently, the LCOM and LCOE show the highest sensitivity to a change in the CO_2 cost for the DMR process, followed by the SMR-DMR process, the CMR process, and the SMR process. Under the assumption of a monetization of CO_2, a different cost hierarchy results for the processes.

In regard to the LCOM, the processes with CO_2 integration already lose their cost advantage for low costs of CO_2. For maximum CO_2 cost of 100 US$/t, the LCOM for the DMR process is higher than for the SMR process at low fuel cost. Taking into account the cost increase $\Delta\text{LCOM}_{\text{CMR}}$ and $\Delta\text{LCOM}_{\text{SMR-DMR}}$, the LCOM of the CMR and SMR-DMR process is still lower than for the SMR process. In comparison to the ATR process, methanol is generated at higher levelized cost in the CMR and in the SMR-DMR process.
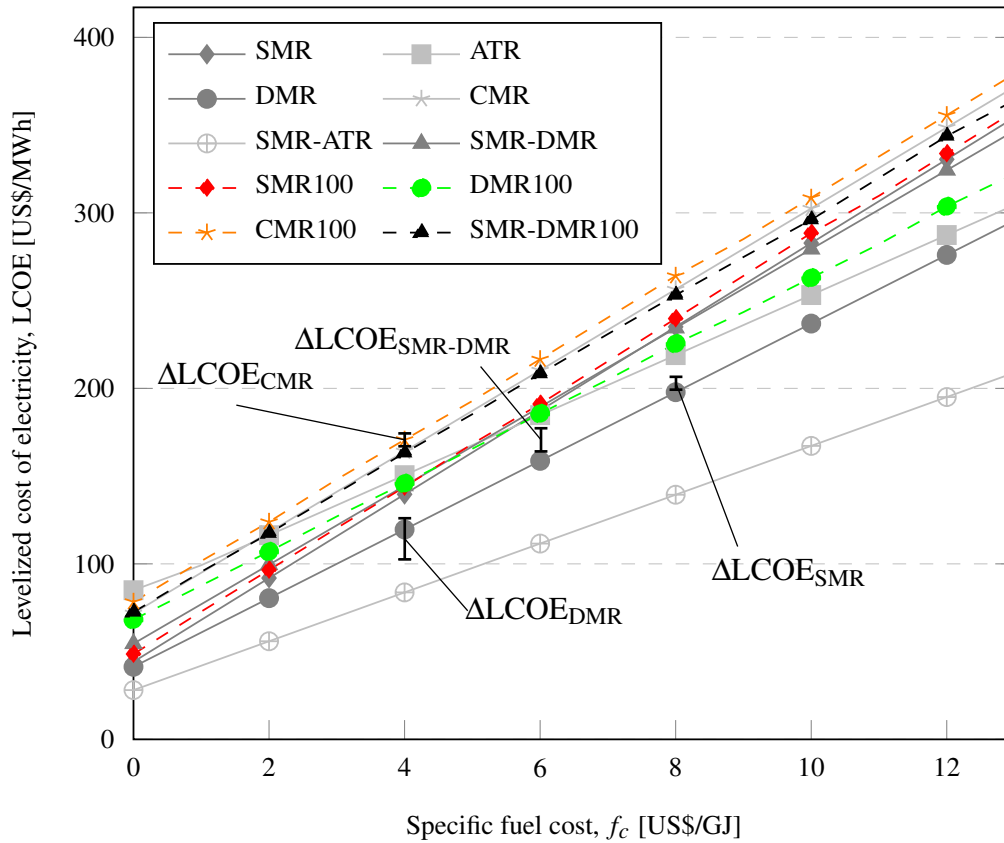
Figure 5.16: Levelized cost of electricty as a function of the fuel cost under uncertainty of the cost for CO_2.

With respect to the sensitivity of the LCOE in Fig. 5.16, similar conclusions can be drawn. The LCOE in particular increase for the DMR process. At low fuel cost of up to 4 US$/GJ, the LCOE is higher for the DMR process than for the SMR process. Furthermore, electricity generated by the ATR process is of lower levelized cost compared to the electricity from SMR-DMR process. The CMR process still has the highest LCOE, although the CO_2 costs only have a small impact. In regard to the SMR process, CO_2 cost have a marginal influence.

5.6 Advanced Exergetic Analysis

The results obtained from the exergetic, the economic and the exergoeconomic analysis showed that the SMR-ATR process is the most attractive from a thermodynamic and economic point of view. In order to allow a better understanding of the component interactions and the improvement potential, an advanced exergetic analysis is applied to the system configuration. The methodology of the advanced exergetic analysis was introduced in Section 3.4 and a flowsheet of the process was presented in Figure 4.14. The results of the conventional and advanced exergetic analysis on a component level are provided in Table F.1 in Appendix F.

Unavoidable and Avoidable Exergy Destruction

An improvement of the operating conditions of the studied components in the scope of technical and economic limitations helps to decrease their exergy destruction rate. Doing so, the unavoidable part of a component's exergy destruction $\dot{E}_{D,k}^{UN}$ quantifies the amount of exergy destruction that cannot be further reduced. Even though the assumptions made are subjective, general trends for an improvement can be identified. For the present analysis, a generous approach with increased heat exchange areas and high isentropic efficiencies was applied. Regarding the reactors, the changes mainly refer to a decreased pressure drop and an increased heat transfer coefficient k. The unavoidable exergy destruction of the columns is estimated through consideration of the minimum reflux ratio [149] and minimum temperature difference in the utility heat exchangers. The complete set of assumptions is presented in Table 5.13. The results of the modifications for a selection of components with the highest $\dot{E}_{D,k}$ are presented in Figure 5.17.

Table 5.13: Assumptions for the determination of the unavoidable exergy destruction.

Comp. k	$\dot{E}_{D,k}$	$\dot{E}_{D,k}^{UN}$
R-01	$\Delta p = 0.2$ bar	$\Delta p = 0$ bar
R-02	$\Delta p = 0.2$ bar	$\Delta p = 0$ bar
R-03	$l = 11$m, $n = 5000$, $k = 0.5$ kW/m^{2}K	$l = 12.1$ m, $n = 6300$, $k = 0.6$ kW/m^{2}K
R-04	$\Delta p = 2$ bar	$\Delta p = 0$ bar
R-05	$\Delta p = 1$ bar	$\Delta p = 0$ bar
R-06	$\Delta p = 1$ bar	$\Delta p = 0$ bar
R-07	$\Delta p = 1$ bar, $\lambda = 2.42$	$\Delta p = 0$ bar, $\lambda = 1.00$
R-08	$\Delta p_{pg} = 3$ bar, $\Delta p_{st} = 1$ bar	$\Delta p_{pg} = 0$ bar, $\Delta p_{st} = 0$ bar
C-01	$\Delta T_{con} = 40$K, $\Delta T_{re} = 180$ K, $R_{C\text{-}01} = 0.6$	$\Delta T_{con} = 10$ K, $\Delta T_{re} = 10$ K, $R_{C\text{-}01} = 0.45$
C-02	$\Delta T_{con} = 40$K, $\Delta T_{re} = 160$ K, $R_{C\text{-}01} = 0.6$	$\Delta T_{con} = 10$ K, $\Delta T_{re} = 10$ K, $R_{C\text{-}02} = 0.45$
C-03	$\Delta T_{con} = 20$K, $\Delta T_{re} = 170$ K, $R_{C\text{-}03} = 0.8$	$\Delta T_{con} = 40$ K, $\Delta T_{re} = 10$ K, $R_{C\text{-}03} = 0.6$
E-01 - E-13	$\Delta T_{min} = 10$ - 500 K, $\Delta p = 0.2$ - 4 bar	$\Delta T_{min} = 0.5$K $\Delta p = 0$
ECO, EVA, SH	$\Delta T_{min} = 10$ - 500 K, $\Delta p = 0.2$ - 5 bar	$\Delta T_{min} = 0.5$K $\Delta p = 0$
T-01,T-03	$\eta_s = 0.92$, $\eta_{mech} = 0.99$	$\eta_s = 0.95$, $\eta_{mech} = 1$
T-02	$\eta_s = 0.93$, $\eta_{mech} = 0.99$	$\eta_s = 0.95$, $\eta_{mech} = 1$
CM-01,CM-05-06	$\eta_s = 0.88$, $\eta_{mech} = 0.99$	$\eta_s = 0.92$, $\eta_{mech} = 1$
CM-02	$\eta_s = 0.85$, $\eta_{mech} = 0.99$	$\eta_s = 0.92$, $\eta_{mech} = 1$
CM-07 - CM-09	$\eta_s = 0.87$, $\eta_{mech} = 0.99$	$\eta_s = 0.92$, $\eta_{mech} = 1$
P-01 - P-03	$\eta_s = 0.85$, $\eta_{mech} = 0.99$	$\eta_s = 0.89$, $\eta_{mech} = 1$

Even though the process is of high exergetic efficency, the results obtained from the conventional exergetic analysis in Section 5.3 and Table F.1 show that the simulated process still has a high improvement potential. In general, the larger the absolute value of the irreversibilities within a component is, the higher its improvement priority must be.

The furnace R-07 and the combustion zone of the autothermal reformer R-04 have the highest exergy destruction based on the results of the conventional exergetic analysis. In general, it is reasonable to assume that every reactor system is unique in terms of operating conditions and technical features. In particular, the catalyst activity, the selectivity of a reaction and the operation mode are likely to be kept constant. Therefore, a low improvement potential of several reactors only results from slight changes in terms of operating conditions. With respect to R-07 and R-04, a lower pressure drop was assumed, reducing the thermodynamic irreversibilities due to friction. Furthermore, the mass flow rate of air and thus the combustion ratio λ has been adjusted to stoichiometric consumption of the combustion reactions. By application of this measures, a large improvement potential for R-07 is given, which is represented by the relatively high share of avoidable exergy destruction. In contrast, R-04 only shows a marginal potential for improvement. A relative high improvement potential is obtained for the SMR unit R-03, although the component is not shown in Figure 5.17. An extension of the tube length l in conjunction with an increase of the heat transfer coefficient k and the number of tubes n results in a reduction of irreversibilities due to heat transfer at lower temperature difference.

Several heat exchangers are rated among the components with the highest exergy destruction (see Table 5.5). The unavoidable part $\dot{E}_{\mathrm{D},k}^{\mathrm{UN}}$ results after a reduction of the pressure drop and a minimization of the temperature difference, respectively. Several heat exchangers of the high pressure level in the HRSG have a large potential for improvement. In particular for the HP-SH and the HP-EVA, the major amount of irreversibilities can be avoided (70% and 87%). In regard to the high-pressure economizer HP-ECO and the recuperator E-06, the avoidable exergy destruction also has a high share of 53% and 55% in total $\dot{E}_{\mathrm{D},k}$, respectively. The improvement potential of the intercooler E-04 is restricted, since a large difference in the hot and cold thermodynamic average temperature is still present after modification. The exergy destruction of the crude product gas cooler E-11 is primarily caused by a large heat transfer rate. Thus, the major part of the irreversibilities can be avoided by application of the modifications.

Considering Figure 5.17, the refining column C-02 and the extraction column C-01 exhibit a large improvement potential. In regard to the refining column C-02 82% of the component's total exergy destruction can be avoided. For the extraction column this values even amounts to 89%. The turbomachinery is characterized by high exergetic efficiencies and thus only plays a subordinate role in regard to the avoidable exergy destruction. However, a moderate improvement potential arises, although the isentropic efficiencies η_s are high in the design case. Increasing the isentropic stage efficiencies of

the air compressors CM-02 and CM-03, the absolute exergy destruction decreases by 45% and 46%, respectively. Among the steam turbines, the low-pressure expander T-03 exhibits the largest potential for improvement.

In conclusion, the avoidable part of exergy destruction is relatively large for the majority of components, which indicates a considerable improvement potential for the overall process. In particular, the furnace R-04, the distillation columns C-01 and C-02, and the high-pressure heat exchangers of the HRSG offer a potential for improvement.

Endogenous and Exogenous Exergy Destruction

The component interactions are quantified by differentiation in endogenous and exogenous exergy destruction. The corresponding values for $\dot{E}_{D,k}^{EN}$ and $\dot{E}_{D,k}^{EX}$ are provided in Table F.1. Furthermore, the definitions of the exergetic efficiencies required by the calculation of the endogenous exergy destruction are shown in Table E.1.

Two-thirds of the overall exergy destruction is endogenous with a varying distribution among the system components. Therefore, an improvement strategy should first consider the internally caused inefficiencies, before modifications in the system design are studied. A variety of components has a significant large exogenous exergy destruction, having a share of 35 - 40% in the components total exergy destruction. This characteristic results from a highly integrated system design with several recycle streams and highlights the importance of component interactions within the process.

The furnace R-07 and the autothermal reformer R-04 are the most important components exhibiting a high endogenous exergy destruction due to highly irreversible oxidation reactions taking place. The mode of operation of both components has a large impact on the exergy destruction within the other components. In particular, the heat exchangers in the HRSG (HP-ECO, HP-EVA, HP-SH) are affected by the performance of the furnace R-07 and therefore by the heat demand of the SMR in R-03. The exogenous exergy destruction of the components in the syngas compression unit (CM-05 and CM-06), the synthesis unit (E-09 - E-10, CM-07 - CM-09) and the purification section (C-01 - C-03) is largely determined by the mode of operation of the reformer units R-03, R-04 and R-05. The irreversibilities within these components is strongly affected by the recycle gas flow and the composition of the crude product, which in turn depend on the composition of the syngas feed. In addition, the synthesis reactor R-08 also has a significant impact on the exogenous exergy destruction of several components as its operating conditions and the catalyst type affect the conversion rate and thus the recycle

flow in the synthesis loop. The results suggest, that a careful selection and operation of the reformer and synthesis reactor technology contributes to a reduction of the exergy destruction of other components.

Combined Splitting of Exergy Destruction

Based on combined splittings of the avoidable and unavoidable as well as the endogenous and exogenous parts of exergy destruction (see Eq. 3.29- Eg. 3.35), the most promising components for an improvement within the existing design and for possible modifications in system layout are identified. The avoidable and unavoidable endogenous and exogenous parts of exergy destruction are illustrated in Figure 5.17 for the components with the highest irreversibilities.

Considering only modifications in the operating range ($\dot{E}_\mathrm{D}^{\mathrm{AV,EN}}$), the autothermal reformer R-07, the refining column C-02 as well as the high-pressure heat exhangers in the HRSG (HP-EVA and HP-SH) exhibit an independent improvement potential as shown by a large value for the endogenous exergy destruction. Isolated improvement attempts should also be applied to the syngas cooler E-04, the recuperator E-06 as well as to the crude product cooler E-03. The improvement potential of the autothermal reformer is of minor significance. Taking into account design modifications ($\dot{E}_\mathrm{D}^{\mathrm{AV,EX}}$), reductions in exergy destruction can particularly be achieved for the HP-SH, the HP-EVA and C-02 by changing their system location and their mode of operation. Considering the limitations arising from the highly integrated system design, suggested modifications have to be investigated carefully. One approach would be an analysis of the binary component interactions.

Figure 5.17: Results of splitting the exergy destruction into its unavoidable and avoidable endogenous and exogenous parts (UN EN, UN EX, AV EN, AV EX).
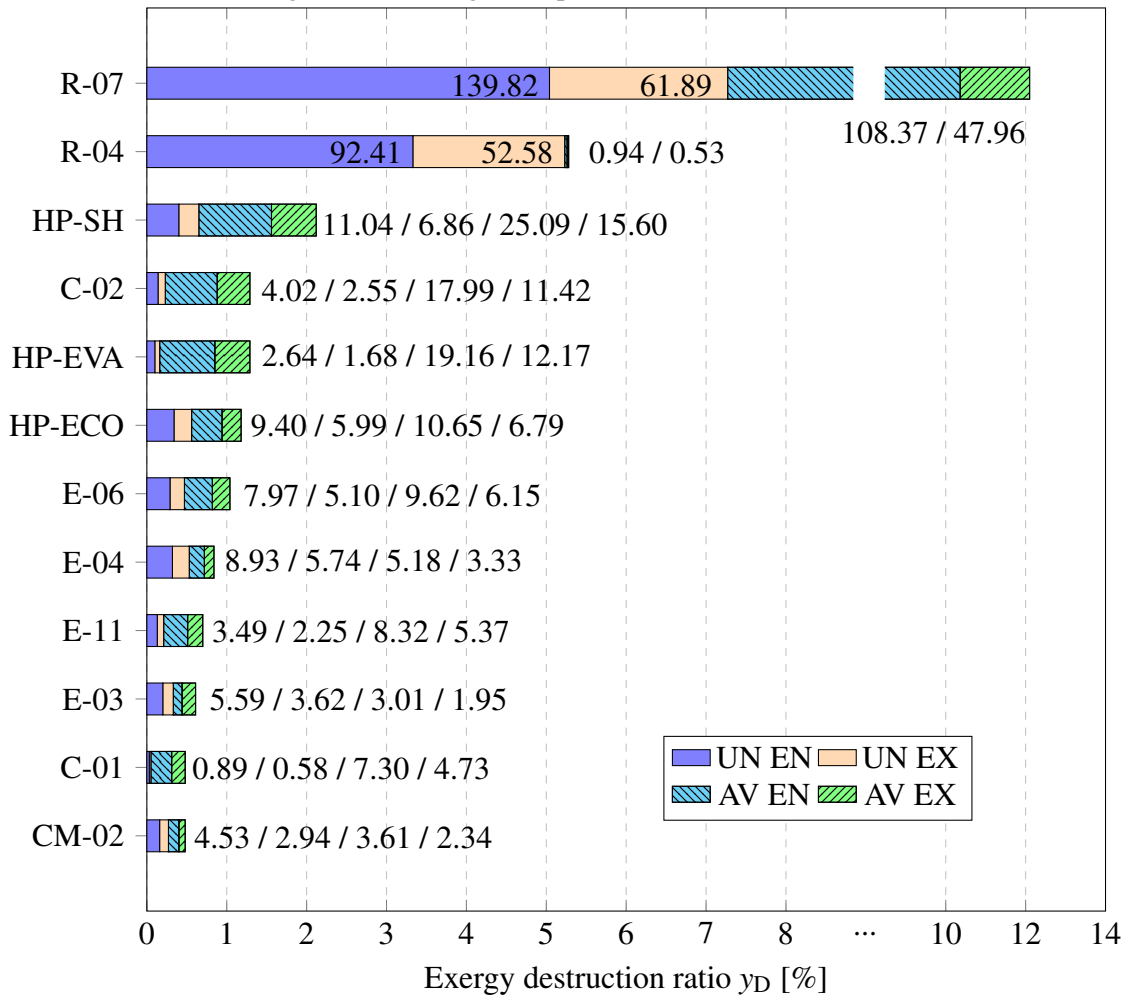
Chapter 6

Conclusions and Outlook

In this thesis, six different processes for the production of the bulk chemical methanol from natural gas have been evaluated and compared. Based on sensitivity analyses for the crucial process units of the synthesis reactor and the reformer, their interactions and influence on the performance of the overall process is investigated. Processes equipped with a stand-alone SMR, ATR and DMR unit represent the *Base processes* which are designed for a medium methanol capacity of approximately 2,500 mtpd. The SMR and ATR processes are commercially available, while the innovative process with dry reforming is considered as a pre-commercial technology. The SMR process is featured with an innovative CO_2-integration for carbon utilization by direct hydrogenation in the synthesis unit. The operation of an autothermal reformer requires the use of an air separation unit for oxygen supply. The results of the sensitivity analysis show that the basic reforming technologies are inadequate for high conversion rates in methanol synthesis.

Taking into account the conclusions of the sensitivity analyses, innovative and more efficient process designs are developed (*advanced Processes*). The CMR process features mixed reforming by steam and carbon dioxide to generate a synthesis gas with a favourable composition for the stoichiometry of the methanol reactions. However, an AGR based on the Selexol$^{®}$ process is required to reduce the large CO_2 mole fraction in the synthesis gas, which would lead to unacceptable low conversion rates. The implementation of an AGR causes an energy penalty and increases the investment cost of the overall process. The SMR-ATR process comprises a serial configuration of a primary tubular steam reformer and a secondary autothermal reformer. This reforming unit particularly is commercialized for large scale applications with a methanol capacity above 5,000 mtpd to reduce the investment cost due to the effect of the economies of scale. In this process a water-gas shift unit is used for further syngas conditioning. The SMR-DMR process comprises a parallel arrangement of a gas heated steam reformer and a gas heated dry

reformer. In this process configuration, the generated syngas does not require any further treatment to achieve a high methanol yield. For all processes, two commercial methanol synthesis technologies, including an isothermal reactor and a quench reactor, have been implemented and assessed. The results show, that the isothermal reactor clearly allows for a higher methanol yield, thus beeing the technology of choice for the subsequent analyses of the processes.

6.1 Process Performance Analysis

A first assessment of the different synthesis routes is conducted by using several thermodynamic and chemical key figures, such as the CH_4-intensity, the S-module, the electric intensity, the methanol yield and the recycle to feed ratio. The selection of a specific reforming technology is decisive for a co-production of methanol and electricity. Depending on the process design, the electricity generation varies in the range of 4 - 220 MW. Exothermic ATR is the preferred option among the stand-alone reforming technologies in the Base processes, if a high methanol yield shall be achieved. The process is highly efficient without a co-production of electricity. The processes equipped with an endothermic DMR and SMR unit are in demand for high temperature process heat, which is supplied by the combustion of natural gas. Only a part of the heat from the combustion gases is integrated into the reforming unit, while the remainder is recovered as steam for electricity generation. Thus, all processes with endothermic reforming technology feature a co-generation of methanol and electricity. Correspondingly, the SMR, DMR and SMR-DMR process have a high CH_4-intensity of 202, 175, and 155 kg/MWh of exergy product, respectively. In contrast, processes with autothermal reforming (ATR, SMR-ATR) have a low CH_4-intensity of 126 kg/MWh.

Because of their high significance for the process, the reforming and synthesis unit are examined more closely. Depending on the syngas composition at the reactor inlet, large differences in terms of methanol yield arise. The highest yield of 15 mole-% is obtained for the CMR process, having the most complex syngas conditioning unit. The other advanced processes with a stoichiometrically adjusted composition of the syngas achieve a yield of 10.4 mole-% (SMR-ATR) and 9.9 mole-% (SMR-DMR), respectively. For comparison, yields of 6.0, 8.0, and 5.0 mole-% are obtained for the SMR, ATR and DMR process.

Furthermore, the energy distribution within the processes is investigated by considering the input and output streams as well as the internal electricity consumers. The energy

input includes natural gas as a fuel for generating process heat and as a feedstock for syngas generation. In the endothermic processes, 40 - 60% of the total energy input is used to generate process heat and electricity, while it is less than 25% in the ATR and SMR-ATR process. The air compressor is the main electricity consumer in all processes since a large flow rate of air is required by the combustion unit. Depending on the configuration, the compressor consumes 50-70% of the generated energy. The syngas compression unit also represents a large consumer, whereby the energy demand greatly varies with the reforming technology. A low consumption in particular arises for the processes with ATR and SMR technology.

Special attention is paid to the CO_2-abatement potential of the processes with carbon utilization by two different integration strategies - direct hydrogenation of CO_2 within the synthesis unit and dry reforming of methane. The motivation of carbon utilization not only refers to the valorisation of CO_2, but also to the saving of feedstock. For a calculation of the abatement potential and the fuel reduction, the processes are benchmarked against a conventional SMR process. The investigation shows, that CO_2 can be successfully integrated for a reduction of the fuel demand. The highest CO_2-abatement potential is identified for the CMR process, emitting 207.1 kg less CO_2 per MWh exergy of product. Regarding the SMR and the SMR-DMR process 62.8 kg and 108.2 kg less CO_2 are emitted, respectively.

6.2 Conventional Exergetic Analysis

Considering the results obtained from the exergetic analysis, large differences arise in regard to the overall exergetic efficiency. The conventional process with commercial steam methane reforming has the lowest exergetic efficiency of 34.8%. The innovative process with dry reforming by CO_2 achieves an efficiency of 39.8%. The low efficiencies result from a large consumption of fuel for process heat supply and from the low conversion rates in the synthesis unit. For the ATR process, a high exergetic efficiency of 56.9% results due to low fuel consumption and high synthesis conversion. The three advanced processes CMR, SMR-ATR and SMR-DMR also exhibit a high efficiency of 48.6%, 57.3% and 46.3%, resulting from integration of improved syngas generation and conditioning.

The exergy destruction is particularly high for the processes with endothermic reforming technology, due to highly irreversible reactions that occur during combustion for generating the process heat. Accordingly, the inefficiencies of processes with ATR

technology are low. On a subsystem level, the highest exergy destruction is attributed to the reforming unit, in particular to the combustion unit and the steam cycle. The components of the syngas compression and the synthesis unit also exhibit irreversibilities, but on a smaller scale. Inefficiencies related to the pretreatment unit and the syngas conditioning play a minor role.

On a component level, the combustion unit has the largest significance, having an exergy destruction ratio y_D in the range of 10-30% for the different processes. Further components with a high exergy destruction include the reformer and several heat exchangers within the steam cycle.

6.3 Economic Analysis

The economics of the processes were investigated by application of the total revenue requirement method. The levelized TRR for the SMR, ATR, DMR, CMR, SMR-ATR and SMR-DMR process amounts to 476 US$ million, 216 US$ million, 379 US$ million, 270 US$ million, 462 US$ million, and 612 US$ million, respectively. The cost per MWh of generated product highly depend on the fuel cost and therefore on the market price of natural gas. For the reference scenario with a low market price of 2.9 US$/GJ, the fuel cost account for 61-66% of the average exergy product cost in the different processes. In regard to the fixed cost, 45 - 65% of the total investment is asscociated with the syngas generation unit.

In addition to high fluctuations in the natural gas price, the selling price of the by-product electricity represents another uncertainty which influences the revenues and thus the minimum methanol selling price. Due to high net power, the electricity price particularly has an impact on the economics of the processes with endothermic reforming technology. Considering historical methanol market prices, the continental natural gas cost and the electricity production cost allows to draw some interesting conclusions. Methanol from conventional SMR cannot be produced economically for levelized fuel cost above 7 US$/GJ, with varying cost for the different continents. In regard to the process with dry methane reforming an economic feasibility is given for fuel cost of up to 11 US$/GJ. The ATR and the SMR-ATR process are economically viable on specific markets even at high fuel cost above 13 US$/GJ.

Furthermore, the threshold of the contribution margin has been investigated for the six processes. For fuel cost of 3 US$/GJ, the majority of the processes may generate a positive contribution margin, while for 7 US$/GJ only the CMR, the ATR and the

SMR-ATR process may generate revenues to cover the fixed cost. For fuel cost of 11 US\$/GJ, only the ATR and SMR-ATR process can be operated without an economic deficit.

By application of the analysis, information about the economic feasibility and the dependence of the revenues on given market conditions is obtained. However, in order to get an information about the cost distribution within the processes and the exact levelized product cost, an exergoeconomic analysis is conducted.

6.4 Exergoeconomic Analysis

The exergoeconomic analysis for the six processes is conducted for a reference fuel price of 2.9 US\$$_{2016}$/GJ. For all processes, the capital investment and the cost rate of the irreversibilities have a significant impact on the final product cost. In regard to the processes with endothermic reforming technology, the relative impact of the cost rate associated with the irreversibilities and the losses is higher than for the processes with autothermal reforming.

On a component level, the combustion units have a dominant cost influence due to the cost rate associated with the large irreversibilities. Furthermore, the air compressor, as the most capital intensive component in the processes, also has a high cost significance. Several heat exchangers a considerable high cost importance due to the irreversibilities related to large heat transfer rates. The exergoeconomic analysis reveals that a variety of components offers a high potential for a thermoeconomic improvement to decrease the levelized cost of the products. The levelized cost of electricity for the SMR, ATR, DMR, CMR, SMR-ATR, and SMR-DMR process amount to 113.4 US\$/MWh , 135.5 US\$/MWh , 98.1 US\$/MWh, 138.0 US\$/MWh, 68.4 US\$/MWh, and 119.8 US\$/MWh. The levelized cost of methanol are 294.6 US\$/mt, 248.6 US\$/mt, 224.3 US\$/mt, 274.9 US\$/mt, 198.4 US\$/mt and 214.8 US\$/mt for the SMR, ATR, DMR, CMR, SMR-ATR and SMR-DMR process, respectively. In these consideration, the processes with CO_2-integration are favoured since the inlet CO_2 was assumed to be free of charge. In fact, the economic benefits through integration measures of CO_2 are lost in case the CO_2 is monetized. The increase of the LCOM and the LCOE is particularly high for the DMR and SMR-DMR process.

The results of the exergoeconomic analysis show that the process with two-step reforming is the most attractive design from a thermoeconomic point of view, having the lowest LCOE and LCOM.

6.5 Advanced Exergetic Analysis

An advanced exergetic analysis is conducted for the SMR-ATR process to gain a deeper understanding of the component interactions and their improvement potential. For this purpose, the exergy destruction is split into its characteristic parts. A large amount of the exergy destruction of the overall system is endogenous and for a variety of components avoidable which is due to the generous assumptions that were made. Thus, an improvement potential lies on the internal operating parameters, while component interactions have a lower significance. The reforming unit and the synthesis reactor have a high influence on the irreversibilities within the components of the purification section and the steam cycle. The analysis reveals, that particularly the combustion unit and the high-pressure heat exchangers of the HRSG offer a large potential for improvement under current technological limitations.

6.6 Outlook

For future work, further measures need to be taken to drive the progress towards a more sustainable and less energy-itensive production of methanol. These measures include, among others, investigations on new catalyst materials for increased conversion under high CO_2 concentration to remedy the limited use of carbon utilization. In addition, the further development (and scaling to an industrial level) of alternative reactor technologies for high methanol yield, such as membrane reactors, will be in the focus of interest. Efficiency improvements in general can be achieved by application of mathematical optimization to the highly non-linear system, in particular to the heat integration management system. Especially for the processes with autothermal reforming, a combined cycle power plant instead of a simple steam-cycle could be integrated for electricity generation, since high temperature process heat is not required. Furthermore, considerations can be made to further use the large amount of low-temperature waste heat, for example by integration into a district heating network. In regard to the co-production processes, investigations on a product flexibility by variation of the synthesis operation parameters might be conducted to increase the profitability.

In general, the low natural gas price of the recent years has formed the basis to keep pace with the ever-increasing demand for methanol. However, small coal-based plants are widespread in some regions, in particular in China as the main consumer of methanol. Therefore, further investigations will be conducted to assess the economic competition between natural gas-based and coal-based processes.

Bibliography

[1] World energy outlook 2017. U.S. Energy Information Administration, 2017.

[2] BP energy outlook 2017. British Petroleum, 2017.

[3] G. Olah, A. Goeppert, and G. Prakash. *Beyond Oil and Gas: The Methanol Economy*. Wiley-VCH, 2009.

[4] Tracking clean energy progress. International Energy Agency, 2017.

[5] R. Cuellar-Franca and A. Azapagic. Carbon capture, storage and utilisation technologies: a critical analysis and comparison of their life cycle environmental impacts. *Journal of CO_2 utilization*, 9:82 –102, 2015.

[6] M. Bertau, H. Offermanns, L. Plass, F. Schmidt, and H. Wernicke. *Methanol: The Basic Chemical and Energy Feedstock of the Future*. Springer-Verlag Berlin Heidelberg, 2014.

[7] C. Zhang, K. Jun, R. Gao, G. Kwak, and H. Park. Efficient utilization of carbon dioxide in a gas-to-methanol process composed of CO_2/steamâmixed reforming and methanol synthesis. *Journal of CO_2 Utilization*, 16:1 –7, 2016.

[8] P. Markewitz, W. Kuckshinrichs, W. Leitner, J. Linssen, P. Zapp, R. Bongartz, A. Schreibera, and T. Müller. Worldwide innovations in the development of carbon capture technologies and the utilization of CO_2. *Energy Environmental Science*, 5:7281 –7305, 2012.

[9] M. Luu, D. Milani, A. Bahadori, and A. Abbas. A comparative study of CO_2 utilization in methanol synthesis with various syngas production technologies. *Journal of CO_2 Utilization*, 12:62 –76, 2015. ISSN: 2212-9820.

[10] D. Milani, R. Khalilpour, G. Zahedi, and A. Abbas. A model-based analysis of CO_2 utilization in methanol synthesis plant. *Journal of CO_2 Utilization*, 10 (2015):12 –22, 2015.

[11] M. Luu, D. Milani, and A. Abbas. Analysis of CO_2 utilization for methanol synthesis integrated with enhanced gas recovery. *Journal of Cleaner Production*, 112:3540 –3554, 2016.

[12] B. Cañnete, C. Gigola, and N. Brignole. Synthesis gas processes for methanol production via CH_4 reforming with CO_2, H_2O, and O_2. *Industrial & Engineering Chemistry Research*, 53:7103 –7112, 2014.

[13] G. Olah. Beyond oil and gas: the methanol economy. *Angewandte Chemie International Edition*, 44:2636 –2639, 2005.

[14] G. Olah. The methanol economy. *Chemical & Engineering News*, 81:5, 2003.

[15] G. Olah. Hydrocarbons in the 21st century. In *Chemical Research - and Beyond: Challenges and Vision*. American Chemical Society, Washington DC, USA, 1998.

[16] M. Berggren. Methanol and derivates analysis 11th volume, 2015.

[17] M. Alvarado. The changing face of the global methanol industry. *IHS Chemical Bulletin insights*, 3, 2016.

[18] M. Alvarado. Global methanol outlook 2016. IHS Markit, Methanol Market Services Asia, May 2016.

[19] Methanex investor presentation, Mar. 2017. URL: `https://www.methanex.com/sites/default/files/MEOH%20March_April%202017_0.pdf`. Accessed: June 2017.

[20] J. Späth. Analyse des globalen methanolmarktes im allgemeinen und des chinesischen marktes im besonderen. BASF AG, 2007. URL: `https://www.steinbeis-sibe.de/wp-content/uploads/2016/12/Spaeth_Jan.pdf`. Accessed: March 2017.

[21] The methanol industry. Methanol Institute. URL: `http://www.methanol.org/the-methanol-industry/`. Accessed: January 2017.

[22] K. Aasberg-Petersen, C. Stub Nielsen, I. Dybkjær, and J. Perregaard. Large scale methanol production from natural gas. Haldor Topsœ, 2014.

[23] J. Hansen. Methanol production technology: todays and future renewable solutions. Methanol Workshop, Lund University, 2015.

[24] Methanol plants. ThyssenKrupp Industrial Solutions AG, 2017. URL: `https://www.thyssenkrupp-industrial-solutions.com/de/produkte-und-services/chemical-plants-und-processes/organic-chemicals-und-petrochemicals/methanol-plants/`. Accessed: March 2018.

[25] A. Riaza, G. Zahedi, and J. Klemeš. A review of cleaner production methods for the manufacture of methanol. *Journal of Cleaner Production*, 57:19 –37, 2013.

[26] I. Dybkjær and K. Aasberg-Petersen. Synthesis gas technology large-scale applications. *The Canadian Journal of Chemical Engineering*, 94:607 –612, 2016.

[27] A. Galadima and O. Muraza. From synthesis gas production to methanol synthesis and potential upgrade to gasoline range hydrocarbons: a review. *Journal of Natural Gas Science and Engineering*, 25:303 –316, 2015.

[28] Methanex regional contract methanol prices for north america, europe and asia. online. URL: `https://www.methanex.com/sites/default/files/methanol-price/MxAvgPrice_Jan%2030%2C%202018.pdf`. Accessed: June 2018.

[29] M. Alvarado. Methanol. Information Handling Service (IHS), 2016.

[30] J. Ott, V. Gronemann, F. Pontzen, E. Fiedler, G. Grossmann, B. Kersebohm, G. Weiss, and C. Witte. *Methanol*. Wiley VCH Verlag GmbH & Co. KGaA, June 2012.

[31] C.-J. Yang and R. Jackson. China's growing methanol economy and its implications for energy and the environment. *Energy Policy*, 41:878 –884, 2012.

[32] D. Kourkompas. Power to fuel concept: process analysis and economic evaluation. In *Proceedings of the 28th International Conference on Efficiency, Costs, Optimization, Simulation and Environmental Impact of Energy Systems - ECOS2015*, 2015. Pau, France.

[33] J. Balsutraitis and W. L. Luyben. Methane conversion to syngas for gas-to-liquids (GTL): is sustainable CO_2 reuse via dry methane reforming (DMR) cost competitive with SMR and ATR processes? *ACS Sustainable Chemical Engineering*, 3:2100 –2111, 2015.

[34] M. Ravi, M. Ranocchiari, and J. van Bokhoven. The direct catalytic oxidation of methane to methanol - a critical assessment. *Angewandte Chemie*, 56 (52):16417–16676, 2017.

[35] M. da Silva. Synthesis of methanol from methane: challenges and advances on the multi-step (syngas) and one-step routes (dmtm). *Fuel Processing Technology*, 145(42):42 –61, 2016.

[36] K. Otsuka and Y. Wang. Direct conversion of methane into oxygenates. *Applied Catalysis A: General*, 222:145 –161, 2001.

[37] C. Hammond et al. Direct catalytic conversion of methane to methanol in an aqueous medium by using copper-promoted Fe-ZSM-5. *Angewandte Chemie International Edition*, 51:5129 –5133, 2012.

[38] Selective monohalogenation of methane over supported acid or platinum metal catalysts and hydrolysis of methyl halides over alumina-supported metal oxide/hydroxide catalysts: a feasible path for the oxidative conversion of methane into methyl alcohol/dimethyl ether. *Journal of the American Chemical Society*, 105:6529, 1983.

[39] E. Supp. How to produce methanol from coal. Springer Verlag, 1990.

[40] P. Tijm, F. Waller, and D. Brown. Methanol technology developments for the new millennium. *Applied Catalysis A*, 221:275 –282, 2001.

[41] I. Wender. Reactions of synthesis gas. *Fuel Processing Technology*, 48:189 –297, 1996.

[42] W. Cheng and H. Kung. *Methanol production and use*. CRC Press, 1994.

[43] P. Biedermann, T. Grube, and B. Höhlein. Methanol as an energy carrier. Forschungszentrum Jülich, 2006.

[44] C. Machado, J. de Medeiros, O. Araújo, and R. Alves. A comparative analysis of methanol production routes: synthesis gas vs. CO_2 hydrogasification. In *Proceedings of the 2014 International Conference on Industrial Engineering and Operations Management*, 2014. Bali, Indonesia.

[45] H. Shahhosseini, D. Iranshahi, S. Saeidi, E. Pourazadi, and J. Klemeš. Multiobjective optimisation of steam methane reforming considering stoichiometric ratio indicator for methanol production. *Journal of Cleaner Production*, 180:655 –665, 2018.

[46] P. Spath and D. Dayton. Preliminary Screening âTechnical and Economic Assessment of Synthesis Gas to Fuels and Chemicals with Emphasis on the Potential for Biomass-Derived Syngas. Technical report, National Energy Laboratory NREL, 2003.

[47] G. Bozzano and G. Manenti. Efficient methanol synthesis: perspectives, technologies and optimization strategies. *Progress in Energy and Combuston Science*, 56:71 –105, 2016.

[48] S. Zhao, H. Yi, X. Tang, S. Jiang, F. Gao, B. Zhang, Y. Zuo, and Z. Wang. The hydrolysis of carbonyl sulfide at low temperature: a review. *The Scientific World Journal*, 2013(739501), 2013.

[49] K. Antoniak, P. Kowalik, R. Narowski, M. Konkol, and J. Ryczkowski. Investigations on hydrogenation of selected organic sulfur compounds on the Ni-Mo/Al$_2$O$_3$ catalyst in terms of natural gas desulfurization. *Annales universitatis mariae curie-sklodowska.*, 2011.

[50] J. Molburg and R. Doctor. Hydrogen from steam-methane reforming with CO$_2$-capture. Argonne National Laboratory and U.S. Department of Energy, 2003.

[51] J. Cross, G. Jones, and M. A. Kent. Pre-reforming in syngas plants - an introduction to pre-reforming catalysts. *Nitrogen+Syngas*, 341, 2016.

[52] M. Wesenberg. *Gas Heated Steam reformer modelling*. PhD thesis, Norwegian University of Science and Technology, 2006.

[53] S. Angeli, G. Monteleone, A. Giaconia, and A. Lemonidou. State-of-the-art catalysts for ch4 steam reforming at low temperature. *International Journal of Hydrogen Energy*, 39:1979 –1997, 2014.

[54] J. Baltrusaitis and W. Luyben. Methane conversion to syngas for gas-to-liquids (gtl): is sustainable CO$_2$ reuse via dry methane reforming (dmr) cost competitive with smr and atr processes? *ACS Sustainable Chemical Engineering*, 3:2100–2111, 2015.

[55] K. Aasberg-Petersen, J.-H. Bak Hansen, T. Christensen, I. Dybkjær, P. Seier Christensen, C. Stub Nielsen, S. Winter Madsen, and J. Rostrup-Nielsen. Technologies for large-scale gas conversion. *Applied Catalysis*, 221:379 –387, 2001.

[56] P. Dahl, T. Christensen, S. Winter-Madsen, and S. King. Proven autothermal reforming for modern large-scale methanol plants. In *Proceedings of the Nitrogen + Syngas International Conference & Exhibition*, 2014. Paris, France.

[57] K. Klier, V. Chatikavanij, R. G. Herman, and G. W. Simmons. Catalytic synthesis of methanol from CO/H$_2$: iv. the effects of carbon dioxide. *Journal of Catalysis*, 74(2):343 –360, 1982.

[58] I. Dybkjær. Synthesis gas technology. *Hydrocarbon Engineering*, 2006. URL: https://www.topsoe.com/sites/default/files/topsoe_synthesis_gas_technology.ashx__2.pdf.

[59] A. De Groote and G. Froment. Simulation of the catalytic partial oxidation of methane to synthesis gas. *Applied Catalysis A: General*, 138:245 –264, 1996.

[60] P. Arku, B. Regmi, and A. Dutta. A review of catalytic partial oxidation of fossil fuels and biofuels: recent advances in catalyst development and kinetic modelling. *Chemical Engineering Research and Design*. accepted manuscript.

[61] B. Enger, R. Lødeng, and A. Holmen. A review of catalytic partial oxidation of methane to synthesis gas with emphasis on reaction mechanisms over transition metal catalysts. *Applied Catalysis A: General*, 346:1–27, 2008.

[62] J. Lerou. The changing landscape of hydrocarbon feedstocks for chemical production - implications for catalysis: a workshop. The National Academic Press, Washington D.C. 2016.

[63] E. Sorensen. Autothermal reforming for efficient and versatile syngas production. In *2017 Syngas Technologies Conference*, 2017. URL: https://www.globalsyngas.org/uploads/downloads/S1-2-%20Haldor%20Topsoe-Esben%20Sorensen.pdf. Accessed: June 2018.

[64] M. Nikoo and N. Amin. Thermodynamic analysis of carbon dioxide reforming of methane in view of solid carbon formation. *Fuel Processing Technology*, 92:678 –691, 2011.

[65] T. Wurzel. Lurgi megamethanol technology - delivering the building blocks for future fuel and monomer demand, 2006.

[66] Lurgi megamethanol, 2010.

[67] Topsœ methanol technology: tailor-made design for optimal operation, 2011.

[68] D. Pakhare and J. Spivey. A review of dry (CO_2) reforming of methane over noble metal catalysts. *Chemical Society Reviews*, 43(22):7813 –7837, 2014.

[69] S. Arora and R. Prasad. An overview on dry reforming of methane: strategies to reduce carbonaceous deactivation of catalysts. *RSC Advances*, 6:108668 – 108688, 2016.

[70] T. Blumberg, T. Morosuk, and G. Tsatsaronis. Exergy-based analyses applied to the CO_2 utilization strategies in the synthesis of methanol from fossil fuels. In *21st Conference on Process Integration for Energy Saving and Pollution Reduction*, 2018. Prag, Czech.

[71] H. Holm-Larsen. CO_2 reforming for large scale methanol plants- an actual case. *Studies in Surface and Science and Catalysis*, 136:441–446, 2001.

[72] H. Wang and C. Au. CH_4/ CD_4 isotope effects in the carbon dioxide reforming of methane to syngas over SiO_2-supported nickel catalysts. *Catalysis Letters*, 38(1 - 2):77 –79, 1996.

[73] C. Zhang, K. Jun, R. Gao, G. Kwak, and H. Park. Carbon dioxide utilization in a gas-to-methanol process combined with CO_2/steam-mixed reforming: techno-economic analysis. *Fuel*, 190:303 –311, 2016.

[74] M. Ravanchi and S. Sahebdelfar. Carbon dioxide capture and utilization in petrochemical industry potentials and challenges. *Applied Petrochemical Research*, 4(1):63 –77, 2014.

[75] B. Nematollahi, M. Rezaei, L. E.N., and M. Khanjenoori. Thermodynamic analysis of combined reforming process using gibbs energy minimization method: in view of solid carbon formation. *Journal of Natural Gas Chemistry*, 21(6):694 –702, 2012.

[76] F. Samimi, R. M.R., and A. Shariati. Development of an efficient methanol production process for direct CO_2 hydrogenation over a $Cu/ZnO/Al_2O_3$ catalyst. *Catalysts*, 7(11):332, 2017.

[77] S. Van-Dal and C. Bouallou. Design and simulation of a methanol production plant from CO_2 hydrogenation. *Journal of CO_2 Utillization*, 57:38 –45, 2013.

[78] Carbon Recycling International. URL: http://carbonrecycling.is/.

[79] Mitsui Chemicals Group. URL: https://www.mitsuichem.com.

[80] M. Perez-Fortes, J. Schöneberger, A. Boulamanti, and E. Tzimas. Methanol synthesis using captured CO_2 as raw material: techno-economic and environmental assessment. *Applied Energy*, 161:718 –732, 2016.

[81] Y. Daza and J. Kuhn. CO_2 conversion by reverse water gas shift catalysis: comparison of catalysts, mechanisms and their consequences for CO_2 conversion to liquid fuels. *RSC Advances*, 6(55):49675 –49691, 2016.

[82] S. S. Iyer, T. Renganathan, S. Pushpavanam, M. Vasudeva Kumar, and N. Kaisare. Generalized thermodynamic analysis of methanol synthesis: effect of feed composition. *Journal of CO$_2$ Utilization*, 10:95–104, 2015.

[83] R. De María, I. Díaz, M. Rodríguez, and A. Sáiz. Industrial methanol from syngas: kinetic study and process simulation. *International Journal of Chemical Reactor Engineering*, 11(1):469 –477, 2013.

[84] T. Blumberg, M. Morosuk, and G. Tsatsaronis. Exergy-based evaluation of methanol production from natural gas with CO$_2$ utilization. *Energy*, 141:2528 –2539, 2017.

[85] E. Heydorn and B. Diamond. Commercial-scale demonstration of the liquid phase methanol (LPMEOH^{TM}) process. Air Products and Chemicals, Inc. and Eastman Chemical Company, 2003.

[86] L. Chen, L. Jiang, Q. Z. Song, and D. Posarac. Optimization of methanol yield from a lurgi reactor. *Chemical Engineering & Technology*, 34,(5):817 –822, 2011.

[87] S. Sinadinovic Friser, M. Jankovic, and R. Radicevic. Simulation of the fixed-bed reactor for methanol synthesis. *Petroleum and Coal*, 43(1):31 –34, 2001.

[88] The Linde Group. URL: `http://www.linde-engineering.de/de/process_plants/hydrogen_and_synthesis_gas_plants/gas_products/methanol/index.html`. Accessed: June 2018.

[89] Lurgi MegaMethanol / Air Liquide S.A. URL: `https://www.engineering-airliquide.com/de/lurgi-megamethanol`. Accessed: June 2018.

[90] S. Almeland, K. Meland, and D. Edvardsen. Process Design and Economical Assessment of a Methanol Plant. Technical report, Norwegian University of Science and Technololy, Department of Chemical Engineering, 2009.

[91] S. Ozturk and Y. Shah. I-c methanol synthesis process. U.S. Department of Energy, 1984.

[92] M. Badano and F. Zardi. Casale group experience in revamping ammonia, methanol and urea complexes. In *Proceedings of Nitrogen Conference*, 1999. Caracas, Venezuela.

[93] G. Hawkins. Methanol converter types. GBH Enterprises Ltd.

[94] Casale SA. URL: `https://www.casale.ch/business-areas/methanol/distinctive-technology.html`. Accessed: June 2018.

[95] Toyo Engineering Corporation. URL: http://www.toyo-eng.com/jp/en/products/petrochmical/methanol/. Accessed: June 2018.

[96] W. Luyben. Design and control of a methanol reactor/column process. *Industrial & Engineering Chemistry Research*, 49(13):6150 –6163, 2010.

[97] Johnson Matthey plc. URL: http://www.jmprotech.com. Accessed: June 2018.

[98] Air Liquide S.A. URL: https://www.airliquide.com/. Accessed: June 2018.

[99] G. Eigenberger. *Ullmanns Encyclopedia of chemical Engineering - Chapter Fixed-Bed Reactors*. Wiley VCH Verlag GmbH & Co. KGaA, 1992.

[100] J. Lange. Methanol synthesis: a short review of technology improvements. *Catalysis Today*, 64:3 –8, 2001.

[101] G. B. Hawkins. Methanol plant theory of distillation. GBH Enterprises Ltd.

[102] Standard specification for methanol (methyl alcohol), ASTM international.

[103] G. Tsatsaronis. Definitions and nomenclature in exergy analysis and exergoeconomics. *Energy*, 32:249 –253, 2007.

[104] A. Bejan, G. Tsatsaronis, and M. Moran. *Thermal Design and Optimization*. New York: John Wiley & Sons, Inc., 1996.

[105] J. Szargut, D. Morris, and F. Steward. *Exergy Analysis of thermal, chemical and metallurgical processes*. New York: Hemisphere Publishing Corporation, 1988.

[106] Aspen Tech., Inc., Aspen Plus. URL: https://www.aspentech.com/.

[107] A. Lazaretto and G.Tsatsaronis. SPECO: a systematic and general methodology for calculating efficiencies and costs in thermal systems. *Energy*, 31(8):1257 –1289, 2006.

[108] G. Tsatsaronis. *Thermodynamic optimization of complex energy systems,* in A. Bejan and E. Mamut, editors. Kluwer Academic Publishers, 1999. Chapter Strength and Limitation of Exergy Analysis.

[109] G. Ulrich and P. Vasudevan. *Chemical Engineering: Process Design and Economics. A Practical Guide.* Hampshire Durham, 2nd edition, 2002.

[110] H. Loh. Process Equipment Cost Estimation Final Report. Research report DOE/NETL 2002/1169. National Energy Laboratory, U.S. Department of Energy, 2002.

[111] G. Towler and R. Sinnott. *Chemical Engineering Design: Principles, Practice and Economics of Plant and Process Design.* Oxford: Elsevier Ltd., 2nd edition, 2007.

[112] W. Luyben. Design and control and of a methanol and reactor/column process. *Industrial & Engineering Chemistry Research*, 49:6150 –6163, 2010.

[113] Cost and performance baseline for fossil energy plants volume 2: coal to synthetic natural gas and ammonia. DOE/NETL-2010/1402, National Energy Technology Laboratory, 2011.

[114] Chemical engineering plant cost index. URL: http://www.chemengonline.com.

[115] Henry hub natural gas spot price. U.S. Energy Information Administration. URL: https://www.eia.gov/dnav/ng/hist/rngwhhdm.htm. Accessed: June 2018.

[116] Levelized cost and levelized avoided cost of new generation resources in the annual energy outlook 2017. U.S. Energy Information Administration, 2018. URL: https://www.eia.gov/outlooks/aeo/pdf/electricity_generation.pdf.

[117] Electricity price statistics. Eurostat, 2017. URL: http://ec.europa.eu/eurostat/statistics-explained/index.php/Electricity_price_statistics. Accessed: January 2018.

[118] Global electricity prices by selected countries in 2017. Statista, Statistic, 2018. URL: http://ec.europa.eu/eurostat/statistics-explained/index.php/Natural_gas_price_statistics.

[119] D. Green and R. Perry. *Perry's Chemical Engineers Handbook*. McGraw-Hill, 8th edition, 2007.

[120] T. Morosuk and G. Tsatsaronis. Strengths and limitations of advanced exergetic analysis. In *Proceedings of the ASME 2013 International Mechanical Engineering Congreed & Exposition*, pages 1 –11, 2013.

[121] M. Sorgenfrei. *Analysis of IGCC-Based Plants with Carbon Capture for an Efficient and Flexible Electric Power Generation*. PhD thesis, Technische Universität Berlin, 2016.

[122] S. Kelly, G. Tsatsaronis, and T. Morosuk. Advanced exergetic analysis: approaches for splitting the exergy destruction into endogenous and exogenous parts. *Energy*, 34(3):284 –391, 2009.

[123] T. Morosuk and G. Tsatsaronis. A new approach to the exergy analysis of absorption refrigeration machines. *Energy*, 33(6):890 –907, 2008.

[124] T. Morosuk and G. Tsatsaronis. Advanced exergy analysis for chemically reacting systems - application to a simple open gas-turbine system. In volume 12 of number 3, pages 105 –111, 2009.

[125] National Institute of Standards and Technology. URL: http://www.nist.gov/.

[126] International Association for the Properties of Water and Steam. URL: http://www.iapws.org/.

[127] Y. Choi and H. Stenger. Water gas shift reaction kinetics and reactor modeling for fuel cell grade hydrogen. *Journal of Power Sources*, 124(2):432 –439, 2003.

[128] K. M. Vanden Bussche and G. F. Froment. A steady-state kinetic model for methanol synthesis and the water gas shift reaction on a commercial $Cu/ZnO/Al_2O_3$ catalyst. *Journal of catalysis*, 161:1 –10, 1996.

[129] G. Graaf, E. Stamhuis, and A. Beenackers. Kinetics of low pressure methanol synthesis. *Chemical Engineering Science*, 43(12):3185 –3195, 1988.

[130] G. Graaf, H. Scholtens, E. Stamhuis, and A. Beenackers. Intra-particle diffusion limitations in low-pressure methanol synthesis. *Chemical Engineering Science*, 45(4):773 –783, 1990.

[131] K. Aasberg-Petersen, T. Christensen, C. Stub Nielsen, and I. Dybkjær. Recent developments in autothermal reforming and prereforming for synthesis gas production in gtl applications. *Fuel Chemistry Division Preprints*, 47(1):96 –97, 2002.

[132] M. Korobitsyn, F. van Berkel, and G. Christie. Review of synthesis gas processes. Extracted from report: SOFC as a gas separator, 2000.

[133] S. Iyer, T. Renganathan, S. Pushpavanam, M. Kumar, and N. Kaisare. Generalized thermodynamic analysis of methanol synthesis: effect of feed composition. *Journal of CO_2 Utilization*, 10:95 –104, 2015.

[134] G. Graaf, P. Sijtsema, E. Stamhuis, and G. Joosten. Chemical equilibria in methanol synthesis. *Chemical Engineering Science*, 41(11):2883 –2890, 1986.

[135] T. Chang, R. Rousseau, and P. Kilpatrick. Methanol synthesis reactions: calculations of equilibrium conversions using equations of state. *Industrial & Engineering Chemistry Process Design and Development*, 25(2):477 –481, 1986.

[136] T. Blumberg, M. Morosuk, and G. Tsatsaronis. A comparative exergoeconomic evaluation of the synthesis routes for methanol production from natural gas. *Applied Sciences*, 7(12):1213, 2017.

[137] N. Rezaie, A. Jahanmiri, B. Moghtaderi, and M. Rahimpour. A comparison of homogenous and heterogenous dynamic models for industrial methanol reactors in the presence of catalyst deactivation. *Chemical Engineering and Processing*, 44(8):911 –921, 2005.

[138] Union Gas. URL: `https://www.uniongas.com/about-us/about-natural-gas/Chemical-Composition-of-Natural-Gas`. Accessed: December 2016.

[139] ISO 2533, standard atmorsphere.

[140] M. Deckers. CFX aids design of world's most efficient steam turbine, 2003.

[141] F. Deidewig. Steam turbines. Presentation of lecture Kraftwerkstechnik.

[142] W. Luyben. Control of parallel dry methane and steam methane reforming processes for fischer-tropsch syngas. *Journal of Process Control*, 39:77 –87, 2016.

[143] W. Luyben. *Chemical reactor Design and Control*. New Jersey: John Wiley & Sons, inc., 2006.

[144] J. Piña and D. Borio. Modeling and simulation of an autothermal reformer. *Latin American Applied Research*, 36:289 –294, 2006.

[145] R. Doctor, J. Molburg, and P. Thimmapuram. Oxygen-blown gasification combined cycle: carbon dioxide recovery, transport, and disposal. Energy Systems Divison, Argonne National Laboratory, 1997.

[146] E. Ludwig. *Applied Process Design for Chemical and Petrochemical Plants*, volume 1. Gulf Professional Publishing, 3rd edition, 2001.

[147] T. Blumberg, T. Morosuk, and G. Tsatsaronis. Exergy-based evaluation of methanol production from natural gas. In *4th international conference on contemporary problems of thermal engineering - CPOTE*, 2016. Katowice, Poland.

[148] CO_2 emissionsfaktoren für fossile brennstoffe. Umwelt Bundesamt, 2016.

[149] Z. Wei, B. Zhang, S. Wu, Q Chen, and G. Tsatsaronis. Energy-use analysis and evaluation of distillation systems through avoidable exergy destruction and investment costs. *Energy*, 42(1):424 –433, 2012.

[150] Wholesale gas price survey 2017 edition - a global review of price formation mechanisms. International Gas Union, 2017.

[151] Natural gas price in the united states and europe from 1980 - 2030. Statista and World Bank, 2018.

[152] World bank commodities price forecast. Statistics of the worldbank, 2017. URL: `http://pubdocs.worldbank.org/en/678421508960789762/CMO-October-2017-Forecasts.pdf`. Accessed: June 2018.

[153] Federal specification methanol (methyl alcohol), 1998.

[154] A. Kiss, J. Pragt, H. Vos, G. Bargeman, and M. de Groot. Novel efficient process for methanol synthesis by CO_2 hydrogenation. *Chemical Engineering Journal*, 284:260 –269, 2016.

Appendix A

Specification of Industrial Methanol and Composition of Natural Gas

Table A.1: U.S. Federal grade specification for Methanol (adopted from [153]).

Component	Fuel Grade	Grade A	Grade AA
Ethanol mg/kg		-	< 10
Acetone, mg/kg		< 30	< 20
Total acetone and aldehyde, mg/kg		<30	<30
Acid (as acetic acid), mg/kg			<30
Color index (APHA)		< 5	< 5
Sulfuric acid test (APHA)		< 30	< 30
Boiling point range		< 1	< 1
Dry residue, mg/L		< 10	< 10
Density (20 °C), g/cm3		0.7928	0.7928
Permanganate number, min			> 30
Methanol content, wt%		99.85	> 99.85
Water content, wt%		< 0.15	< 0.10

Table A.2: Composition of natural gas assumed for the simulations (in mole-%).

Component	This study [mole-%]	Range [mole-%]	$\overline{LHV}$ [MJ/kmole]	$\bar{e}^{CH}$ [MJ/kmole]
Methane	94.3	87.0 - 97.0	802.3	831.65
Ethane	2.5	1.5 - 7.0	1,437.2	1,265.8
Propane	0.2	0.1 - 1.5	2,044.2	2,154.0
Iso-Butane	0.03	0.01 - 0.3	2,659.3	2,668.9
Normal Butane	0.03	0.01 - 0.3	2,044.2	2,805.8
Iso-Pentane	0.01	0 - 0.04	3,272.6	3,463.3
Normal Pentane	0.01	0 - 0.04	3,272.6	3,463.3
Nitrogen	1.6	0.2 - 5.5	0.0	0.7
Carbon Dioxide	0.7	0.1 - 1.0	-	275.1
Carbonyl Sulfide	0.02	0 - 0.05		

Appendix B

Reaction Kinetics

Methanol Synthesis - Vanden Bussche and Froment   The reaction kinetics implemented into the methanol synthesis reactor are based on expressions developed by vanden Bussche and Froment [128]. The kinetic steady state model considers the hydrogenation of CO_2 in Eq. B.1 and the water-gas shift reaction in Eq. B.2

$$CO_2 + 3H_2 \rightleftharpoons CH_3OH + H_2O \tag{B.1}$$

$$CO_2 + 2H_2 \rightleftharpoons CO + H_2O \tag{B.2}$$
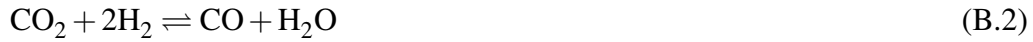
The proposed model is subject to the assumption, that the main carbon source of methanol is CO_2. In contrast, another accepted model by Graaf et al. [129] takes into account the hydrogenation of CO_2 and CO. The reactions are carried out on a commercial ICI 51-2 $Cu/Zn/Al_2O_3$ catalyst. The parameters are estimated for a pressure range of 1-51 bar and a temperature range of 180 - 280 °C. The reaction rates R_j for Eq. B.1 and Eq. B.2 are given by Eq. B.3 and Eq. B.4, respectively.

$$R_1 = (k_4 p_{CO_2} p_{H_2}) \frac{\left[1 - \frac{1}{K_{E1}} \frac{p_{CH_3OH} p_{H_2O}}{p_{CO_2} p_{H_2}^3} \right]}{\left[1 + k_3 \left(\frac{p_{H_2O}}{p_{H_2}} \right) + k_1 \sqrt{p_{H_2}} + k_2 p_{H_2O} \right]^3} \tag{B.3}$$

$$R_2 = (k_5 p_{CO_2}) \frac{\left[1 - \frac{1}{K_{E1}} \frac{p_{CO} p_{H_2O}}{p_{CO_2} p_{H_2}} \right]}{\left[1 + k_3 \left(\frac{p_{H_2O}}{p_{H_2}} \right) + k_1 \sqrt{p_{H_2}} + k_2 p_{H_2O} \right]^3} \tag{B.4}$$

The reaction rates are given as a summarized form deviated by Luyben et al. [112] for implementation in Aspen. The kinetics are described by LHHW-type equations (Langmuir-Hinshelwood-Hougen-Watson), which are adequate to model exothermic reactions over a solid catalyst. The LHHW structure has the form

$$R = (\text{kinetic term})\frac{(\text{driving-force term})}{(\text{adsorption term})} \tag{B.5}$$

The conversion of the reaction rate equations from the original paper into the required form by Aspen is challenging. The translated input parameters can be found in [112]. The rate and adsorption coefficients $k_i, (i = 1 - 5)$ as well as the equilibrium constants K_{E1} and K_{E2} are given as a function of the temperature according to the Arrhenius und vanÂ´t Hoff equations.

$$k_i = k_i^0 \cdot exp\left(-\frac{E_A, i}{RT}\right) \tag{B.6}$$

$$K_j = k_j^0 \cdot exp\left(-\frac{\Delta H_{Ads,j}}{RT}\right) \tag{B.7}$$

E_A refers to the activation energy and $\Delta H_{Ads,j}$ to adsorption enthalpy. The coefficients and constants in equations B.6 and B.7 have to be implemented in the form of equation B.8. Accordingly, the coefficients A and B can be drived by transforming equations B.6 and B.7 to the shape of equation B.8. In general, the coefficients C and D are not needed to describe the kinetics.

$$ln(K_n) = A_n + \frac{B_n}{T} + C_n \cdot \ln T + D_n \cdot T \tag{B.8}$$

Methanol Synthesis - Graaf   In contrast to the model of vanden Bussche and Froment, the kinetic model of Graaf et al. [129, 130] also considers methanol production by hydrogenation of CO in Eq.B.10.

$$CO + 2H_2 \rightleftharpoons CH_3OH \tag{B.9}$$

$$CO_2 + 2H_2 \rightleftharpoons CO + H_2O \tag{B.10}$$

$$CO_2 + 3H_2 \rightleftharpoons CH_3OH + H_2O \tag{B.11}$$

The experiments in their studies were carried out for a temperature range of 210 - 245 °C at pressures between 15 and 50 bar on a commercial $CuO/ZnO/Al_2O_3$ catalyst manufactured by Haldor Topsøe (MK101). Furthermore, the scope of validity is constrained by the composition of the inlet gas: 0.0 - 22.0 mole-% CO, 2.1 - 26.1 mole-% CO_2, 67.4 - 90.0 mole-% H_2. The reaction rates R_j resulting from the experiments of Graaf et al. [129, 130] are given by:

$$R_1 = (k_1) \frac{\left[k_2 p_{CO} p_{H_2}^{3/2} - k_3 p_{CH_3OH} p_{H_2}^{-1/2} \right]}{\left[k_10 \sqrt{p_{H_2}} + k_11 p_{H_2O} + k_12 p_{CO} \sqrt{p_{H_2}} + k_13 p_{CO} p_{H_2O} + k_14 p_{CO_2} \sqrt{p_{H_2}} + k_15 p_{CO_2} p_{H_2O} \right]}$$

(B.12)

$$R_2 = (k_4) \frac{\left[k_5 p_{CO_2} p_{H_2} - k_6 p_{H_2O} p_{CO} \right]}{\left[k_10 \sqrt{p_{H_2}} + k_11 p_{H_2O} + k_12 p_{CO} \sqrt{p_{H_2}} + k_13 p_{CO} p_{H_2O} + k_14 p_{CO_2} \sqrt{p_{H_2}} + k_15 p_{CO_2} p_{H_2O} \right]}$$

(B.13)

$$R_3 = (k_7) \frac{\left[k_8 p_{CO_2} p_{H_2}^{3/2} - k_9 p_{H_2O} p_{CH_3OH} p_{H_2}^{-3/2} \right]}{\left[k_10 \sqrt{p_{H_2}} + k_11 p_{H_2O} + k_12 p_{CO} \sqrt{p_{H_2}} + k_13 p_{CO} p_{H_2O} + k_14 p_{CO_2} \sqrt{p_{H_2}} + k_15 p_{CO_2} p_{H_2O} \right]}$$

(B.14)

The Rate expressions are already given in the form as required by Aspen. The rate coefficients ($k_i, i = 1, 4, 7$), the adsorption coefficients ($i = 10 - 15$), and the coefficients of the driving terms ($i = 2, 3, 5, 6, 7, 8$) have to be implemented into Aspen by using equation B.8. The parameters A-D can be found in [129] and [154]

Steam Methane Reforming   The model of steam methane reforming incorporates power-law, first-order kinetics implemented in the steady state simulation to represent the processing reaction mechanisms in an adequate way. The kinetic expressions for implementation is Aspen are obtained from [142] and consider forward and reverse SMR and WGS reactions respectively. The kinetics of the SMR are given as:

$$R_{SMR,f} = k_f p_{CH_4} p_{H_2O} = 0.1 e^{-275,000/RT} p_{CH_4} p_{H_2O} \tag{B.15}$$

$$R_{SMR,r} = k_r p_{CO} p_{H_2} = 9.7 \cdot 10^{-14} e^{-47,000/RT} p_{CO} p_{H_2} \tag{B.16}$$

The kinetics for the WGS are given as:

$$R_{WGS,f} = k_f P_{CO} p_{H_2O} = 2.6 \cdot 10^{-7} e^{-47,000/RT} p_{CO} p_{H_2O} \tag{B.17}$$

.

$$R_{WGS,r} = k_r p_{CO_2} p_{H_2} = 1.575 \cdot 10^{-5} e^{-85,460/RT} p_{CO_2} p_{H_2} \tag{B.18}$$

The pressures are provided in Pascals, temperatures in Kelvin, the reaction is conducted in the vapor phase and the reaction rate R has the unit kmol/m^3. The parameter k refers to the pre-exponential coefficient. The activation energy is given in kJ/kmol and R refers to the ideal gas constant. Since SMR is an highly endothermic reaction, the activation energy of the forward reaction is much larger in comparison to the reverse reaction. Accordingly, the activation energies for the slighly exothermic WGS can be interpreted.

Dry Methane Reforming The kinetic model of dry methane reforming is also based on power-law, first-order kinetics given by equation B.19 and B.20. The import parameters and units correspond to the import parameters and units of the SMR kinetics and were also obtained from [142].

$$R_{DMR,f} = k_f p_{CO_2} p_{CH_4} = 2000 e^{-300,000/RT} p_{CO_2} p_{CH_4} \tag{B.19}$$

$$R_{DMR,r} = k_r p_{CO} P_{H_2} = 2.738 \cdot 10^{-11} e^{-48,513/RT} p_{CO} p_{H_2} \tag{B.20}$$

In addition, a small amount of water is formed by the reaction of the reverse water gas shift.

$$R_{RWGS} = k_r p_{CO} p_{H_2} = 10^{-11} e^{-50,000/RT} p_{CO_2} p_{H_2} \tag{B.21}$$

Appendix C

Sensitivity Analyses of the Methanol Reactor
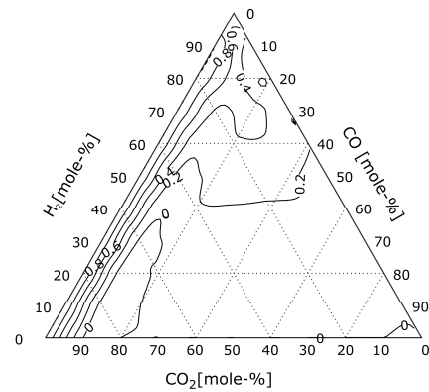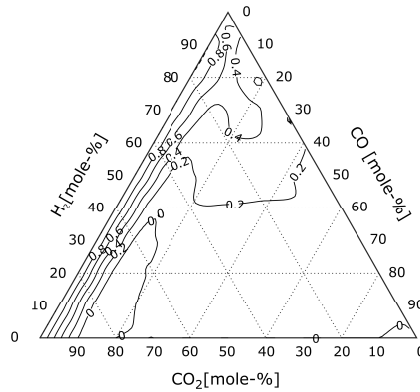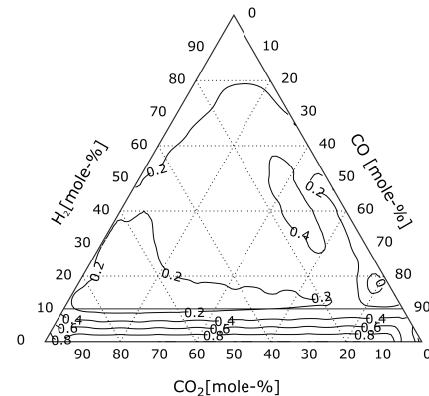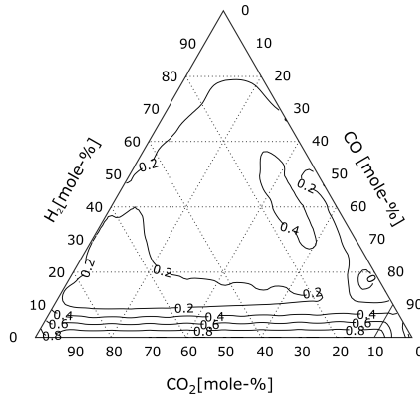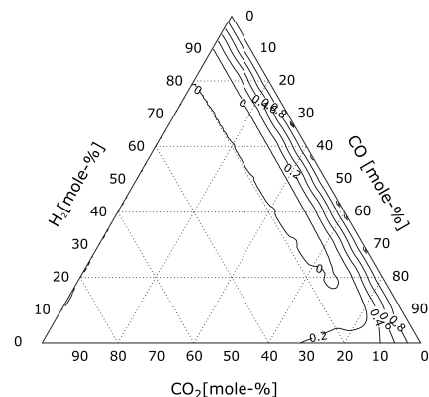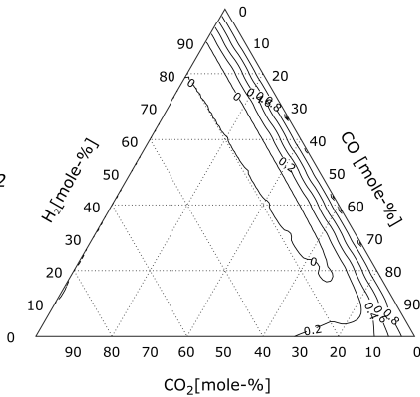
Figure C.1: Contour plot of the conversions of CO, H_2 and CO_2 at 250°C and a pressure of 50 bar.

Appendix D

Detailed Stream Data for the Processes
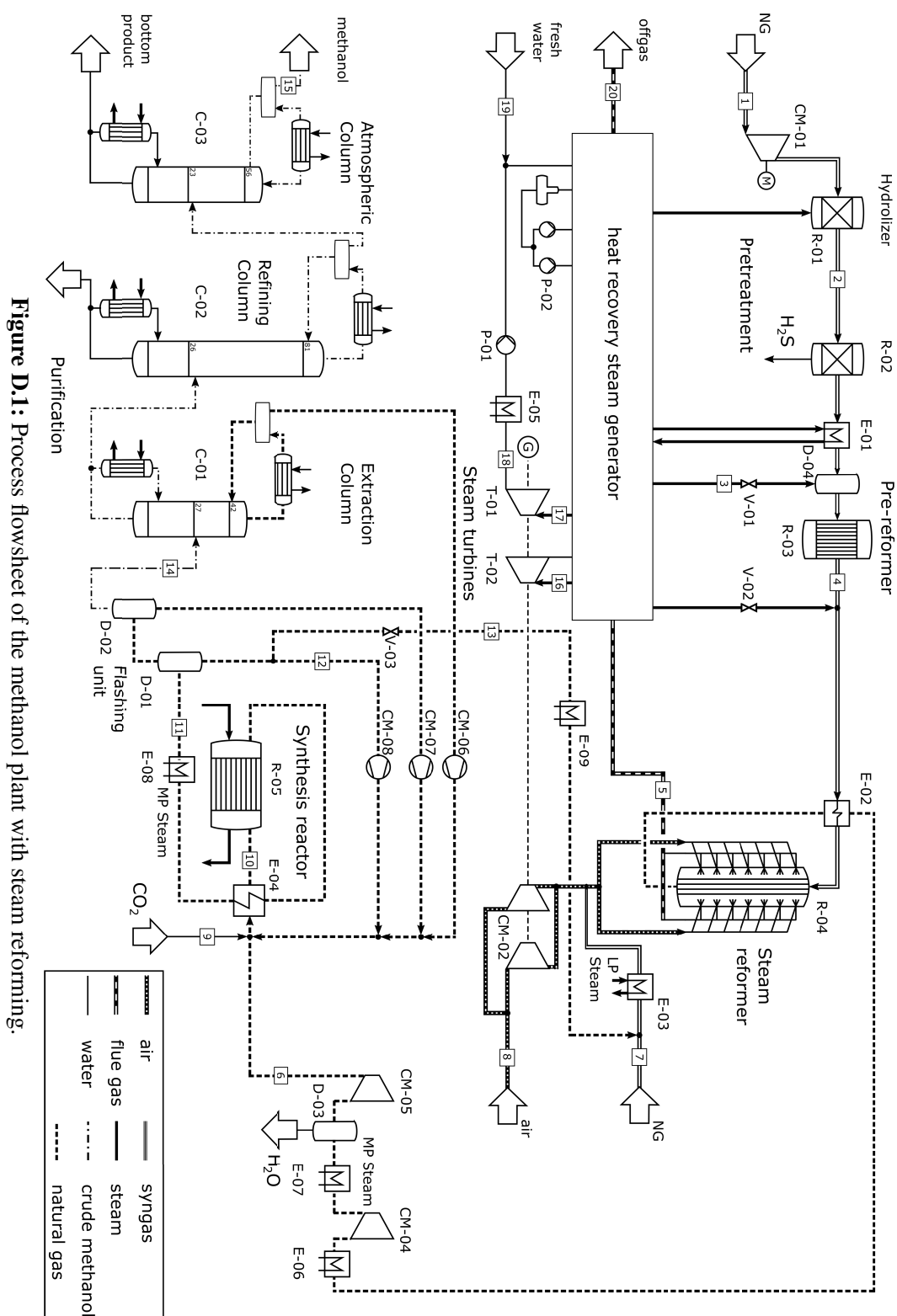
Figure D.1: Process flowsheet of the methanol plant with steam reforming.

Table D.1: Stream data obtained from the simulation of the SMR process.

Stream No.		1	2	3	4	5	6	7	8	9	10
Temperature	°C	15.00	124.57	550.00	509.54	883.73	148.21	15.00	15.00	45.00	250.00
Pressure	bar	10.00	29.00	29.49	24.59	1.61	52.50	10.00	1.01	52.50	49.59
Mass flow	kg/sec	16.88	16.90	1.31	18.20	1631.94	42.88	28.71	1586.77	13.55	391.76
CO	mole-%	0.00	0.00	0.00	0.96	0.00	15.18	0.00	0.00	0.00	9.60
CO_2	mole-%	0.70	0.72	0.00	0.66	3.66	7.33	0.70	0.00	100.00	16.41
H_2O	mole-%	0.00	0.08	100.00	5.74	7.60	3.17	0.00	0.00	0.00	0.52
H_2	mole-%	0.00	0.00	0.00	0.00	0.00	73.47	0.00	0.00	0.00	68.46
CH_4	mole-%	94.90	94.81	0.00	91.18	0.00	0.49	94.90	0.00	0.00	1.41
CH_4O	mole-%	0.00	0.00	0.00	0.00	0.00	0.00	0.00	0.00	0.00	2.57
$\dot{E}^{CH}$	MW	833.00	832.99	0.07	832.49	32.08	967.30	1416.51	9.41	6.12	6747.62
$\dot{E}^{PH}$	MW	5.44	8.60	1.89	19.90	964.50	45.34	9.25	0.00	2.70	351.79
$\dot{E}^{TOT}$	MW	838.45	841.59	1.95	852.39	996.58	1012.64	1425.76	9.41	8.82	7099.40

Stream No.		11	12	13	14	15	16	17	18	19	20
Temperature	°C	38.00	38.67	35.52	38.00	70.95	440.00	300.00	60.08	15.00	146.25
Pressure	bar	42.94	42.94	3.50	2.00	1.30	58.74	27.12	0.20	1.01	1.21
Mass flow	kg/sec	391.79	312.84	16.47	60.48	29.98	358.00	81.07	439.10	65.36	1631.94
CO	mole-%	8.32	9.00	9.00	0.00	0.00	0.00	0.00	0.00	0.00	0.00
CO_2	mole-%	16.11	17.22	17.22	0.58	0.00	0.00	0.00	0.00	0.00	3.66
H_2O	mole-%	1.94	0.06	0.06	25.70	0.00	100.00	100.00	100.00	100.00	7.60
H_2	mole-%	64.98	70.26	70.26	0.00	0.00	0.00	0.00	0.00	0.00	0.00
CH_4	mole-%	1.50	1.62	1.62	0.00	0.00	0.00	0.00	0.00	0.00	0.00
CH_4O	mole-%	6.03	0.65	0.65	73.72	100.00	0.00	0.00	0.00	0.00	0.00
$\dot{E}^{CH}$	MW	6732.64	5329.29	280.49	1123.78	671.77	17.88	4.05	21.93	3.27	32.08
$\dot{E}^{PH}$	MW	247.13	229.17	4.00	0.22	0.55	483.94	89.45	138.94	0.00	75.78
$\dot{E}^{TOT}$	MW	6979.77	5558.46	284.49	1124.00	672.33	501.82	93.5	160.17	3.27	107.86
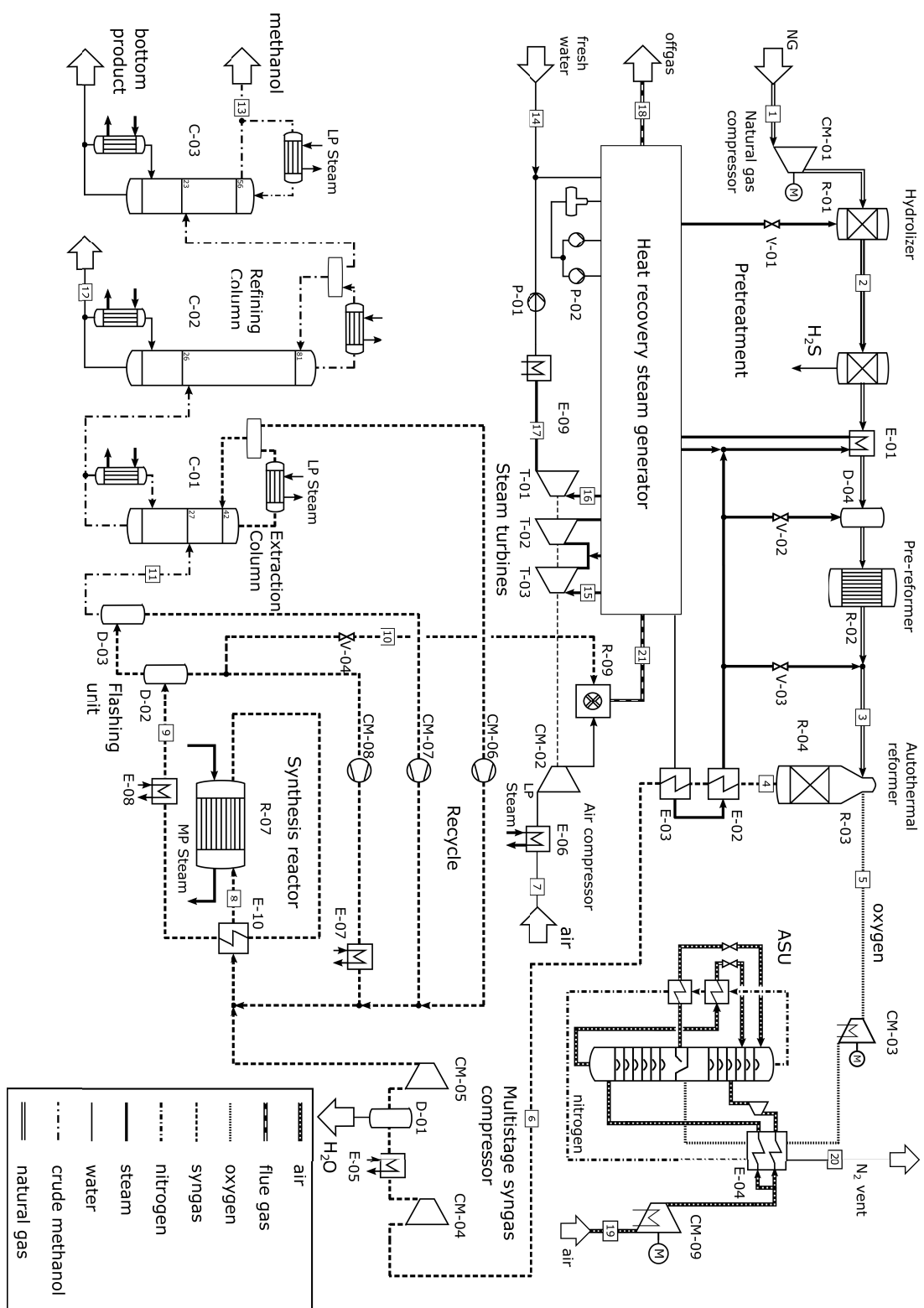
Figure D.2: Process flowsheet of the methanol plant with autothermal reforming.

Table D.2: Stream data obtained from the simulation of the ATR process.

Stream No.		1	2	3	4	5	6	7	8	9	10
Temperature	°C	15.00	155.31	558.79	922.63	277.00	156.98	15.00	250.00	38.00	34.9
Pressure	bar	10.00	39.80	34.82	32.32	34.82	25.19	1.01	50.69	44.80	4.00
Mass flow	kg/sec	22.79	22.81	36.68	60.24	23.55	60.24	418.33	207.21	207.51	18.91
CO	mole-%	0.00	0.00	0.03	23.22	0.00	23.22	0.00	19.90	16.18	17.62
CO_2	mole-%	0.70	0.72	0.46	4.43	0.00	4.43	0.00	10.86	12.01	12.84
H_2O	mole-%	0.00	0.05	36.30	14.05	0.00	14.05	0.00	0.38	0.68	0.02
H_2	mole-%	0.00	0.00	0.00	56.09	0.00	56.09	0.00	61.42	56.07	61.10
CH_4	mole-%	94.90	94.83	60.51	1.05	0.00	1.05	0.00	2.97	3.36	3.66
CH_4O	mole-%	0.00	0.00	0.00	0.00	0.00	0.00	0.00	1.21	8.00	0.73
$\dot{E}^{CH}$	MW	1124.56	1124.54	1124.92	975.37	2.50	975.37	2.48	3586.98	3573.52	314.67
$\dot{E}^{PH}$	MW	7.35	13.13	46.90	120.99	7.99	43.28	0.00	176.34	116.92	4.56
$\dot{E}^{TOT}$	MW	1131.90	1137.67	1171.82	1096.36	10.49	1018.65	2.48	3763.31	3690.45	319.23

| Stream No.		11	12	13	14	15	16	17	18	19	20
Temperature	°C	38.00	133.09	70.95	15.00	600.00	218.33	75.88	110.00	15.00	17.85
Pressure	bar	2.00	2.80	1.30	1.01	175.25	15.00	0.40	1.98	1.01	3.27
Mass flow	kg/sec	33.78	0.89	28.44	13.90	61.25	130.22	130.22	437.24	101.55	76.86
CO	mole-%	0.00	0.00	0.00	0.00	0.00	0.00	0.00	0.00	0.00	0.00
CO_2	mole-%	0.87	0.00	0.00	0.00	0.00	0.00	0.00	3.12%	0.00%	0.00%
H_2O	mole-%	8.32	100.00	0.00	100.00	100.00	100.00	100.00	6.26	0.00	0.00
H_2	mole-%	0.00	0.00	0.00	0.00	0.00	0.00	0.00	0.00	0.00	0.00
CH_4	mole-%	0.00	0.00	0.00	0.00	0.00	0.00	0.00	0.00	0.00	0.00
CH_4O	mole-%	90.80	0.00	100.00	0.00	0.00	0.00	0.00	0.00	0.00	0.00
$\dot{E}^{CH}$	MW	711.30	0.04	637.20	0.69	3.06	6.51	6.51	7.08	0.60	1.98
$\dot{E}^{PH}$	MW	0.12	0.08	0.52	0.00	101.79	124.64	48.21	32.62	0.00	7.69
$\dot{E}^{TOT}$	MW	711.42	0.13	637.72	0.69	104.85	131.15	54.72	35.10	0.60	9.67

Figure D.3: Process flowsheet of the methanol plant with dry reforming.

Table D.3: Stream data obtained from the simulation of the DMR process.

Stream No.		1	2	3	4	5	6	7	8	9	10
Temperature	°C	15.00	155.21	565.00	546.65	15.00	282.78	15.00	15.00	250.00	38.00
Pressure	bar	7.00	6.51	67.90	5.53	5.53	52.00	5.00	1.01	51.73	45.39
Mass flow	kg/sec	25.32	25.34	90.08	33.19	65.57	93.66	19.89	1442.52	632.90	632.90
CO	mole-%	0.00	0.00	0.00	0.80	0.00	45.80	0.00	0.00	52.58	52.52
CO_2	mole-%	0.70	0.72	0.00	0.55	100.00	2.96	0.00	0.00	10.26	11.47
H_2O	mole-%	0.00	0.05	100.00	21.40	0.00	2.91	0.00	0.00	0.58	0.08
H_2	mole-%	0.00	0.00	0.00	0.00	0.00	44.49	0.00	0.00	28.15	23.14
CH_4	mole-%	94.90	94.84	0.00	76.03	0.00	3.41	100.00	0.00	6.50	6.94
CH_4O	mole-%	0.00	0.00	0.00	0.00	0.00	0.00	0.00	0.00	1.12	5.00
$\dot{E}^{CH}$	MW	1249.51	1249.49	4.50	1249.03	29.61	1488.62	1031.25	8.56	8001.90	7989.53
$\dot{E}^{PH}$	MW	6.90	8.23	139.58	32.34	5.97	68.90	4.72	0.00	337.73	242.03
$\dot{E}^{TOT}$	MW	1256.41	1257.72	144.08	1281.37	35.57	1557.52	1035.97	8.56	8339.64	8231.56

| Stream No.		12	13	14	15	16	17	18	19	20	21
Temperature	°C	29.88	38.00	80.38	930.78	600.00	414.81	200.00	32.90	15.00	120.00
Pressure	bar	4.00	2.00	1.86	2.21	178.63	64.51	3.93	0.05	1.01	1.60
Mass Flows	kg/sec	59.32	36.66	31.48	1521.73	306.26	388.45	388.45	388.45	7.88	1521.8
CO	mole-%	54.58	0.00	0.00	0.00	0.00	0.00	0.00	0.00	0.00	0.00
CO_2	mole-%	11.96	0.93	0.00	6.03	0.00	0.00	0.00	0.00	0.00	6.02
H_2O	mole-%	0.00	1.82	0.00	6.70	100.00	100.00	100.00	100.00	100.00	6.70
H_2	mole-%	24.31	0.00	0.00	0.00	0.00	0.00	0.00	0.00	0.00	0.00
CH_4	mole-%	7.29	0.01	0.00	0.00	0.00	0.00	0.00	0.00	0.00	0.00
CH_4O	mole-%	0.93	97.24	100.00	0.00	0.00	0.00	0.00	0.00	0.00	0.00
$\dot{E}^{CH}$	MW	714.84	802.68	705.47	44.95	15.30	19.41	19.41	19.41	0.39	44.87
$\dot{E}^{PH}$	MW	8.59	0.13	0.78	1000.03	509.04	513.24	308.18	48.60	0.00	90.67
$\dot{E}^{TOT}$	MW	723.43	802.81	706.26	1044.98	524.34	532.64	327.59	68.00	0.39	135.54
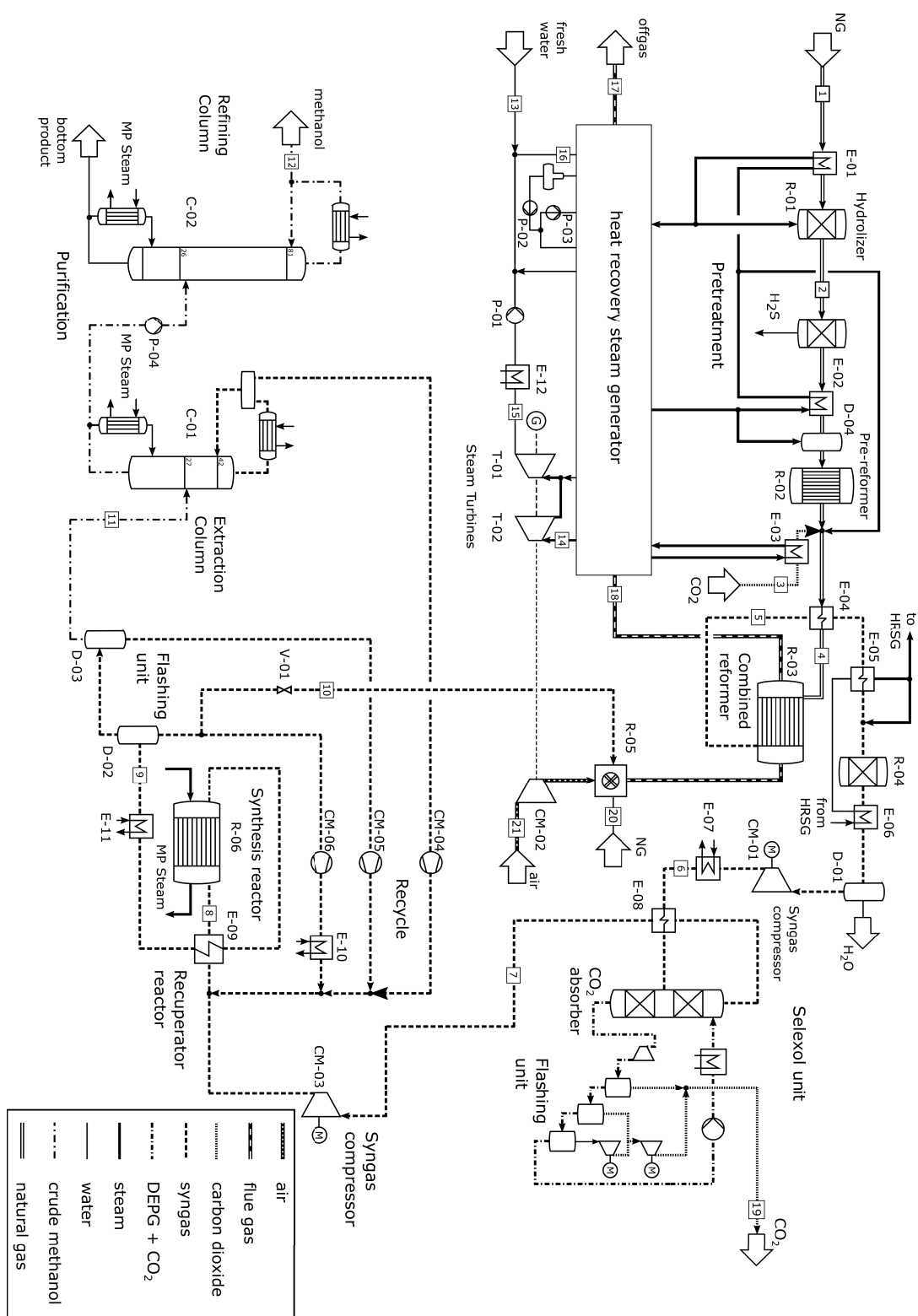
Figure D.4: Process flowsheet of the methanol plant with combined reforming.

Table D.4: Stream data obtained from the simulation of the CMR process.

Stream No.		1	2	3	4	5	6	7	8	9	10	11
Temperature	°C	15.00	155.01	550.00	800.00	950.00	80.00	60.00	248.26	38.00	37.76	38.00
Pressure	bar	5.00	3.54	8.00	2.86	2.00	31.00	24.00	50.50	45.53	4.00	2.00
Mass flow	kg/sec	16.88	16.90	35.13	65.82	65.82	64.53	41.54	112.22	112.22	7.41	37.95
CO	mole-%	0.00	0.00	0.00	0.41	35.58	29.22	32.25	29.04	23.63	27.61	0.01
CO_2	mole-%	0.70	0.72	100.00	31.15	4.00	10.98	0.30	0.87	1.06	1.18	0.26
H_2O	mole-%	0.00	0.08	0.00	29.24	8.38	0.00	0.00	0.00	0.04	0.00	0.27
H_2	mole-%	0.00	0.00	0.00	0.00	51.63	59.37	67.00	66.73	58.04	67.85	0.00
CH_4	mole-%	94.90	94.81	0.00	38.59	0.06	0.06	0.06	0.25	0.31	0.36	0.00
CH_4O	mole-%	0.00	0.00	0.00	0.00	0.00	0.00	0.00	1.60	15.03	0.79	99.46
$\dot{E}^{CH}$	MW	833.00	832.99	15.86	846.03	1003.25	995.63	960.36	2581.36	2554.21	170.84	846.70
$\dot{E}^{PH}$	MW	3.80	4.03	12.71	63.80	85.29	37.91	30.11	117.15	66.09	2.33	0.13
$\dot{E}^{TOT}$	MW	836.81	837.02	28.57	909.83	1088.54	1033.54	990.47	2698.50	2620.30	173.17	846.83

| Stream No.		12	13	14	15	16	17	18	19	20	21
Temperature	°C	80.38	15.00	600.00	32.90	20.00	120.08	957.97	183.00	15.00	15.00
Pressure	bar	1.86	1.013	41.96	0.05	1.013	2.55	3.13	15.00	4.00	1.01
Mass flow	kg/sec	32.46	13.82	166.64	206.87	549.00	651.21	651.21	20.00	14.86	628.94
CO	mole-%	0.00	0.00	0.00	0.00	0.00	0.00	0.00	10.69	0.00	0.00
CO_2	mole-%	0.00	0.00	0.00	0.00	0.00	4.79	4.79	78.34	0.70	0.00
H_2O	mole-%	0.00	100.00	100.00	100.00	100.00	9.71	9.71	0.00	0.00	0.00
H_2	mole-%	0.00	0.00	0.00	0.00	0.00	0.00	0.00	10.82	0.00	0.00
CH_4	mole-%	0.00	0.00	0.00	0.00	0.00	0.00	0.00	0.05	94.90	0.00
CH_4O	mole-%	100.00	0.00	0.00	0.00	0.00	0.00	0.00%	0.00	0.00	0.00
$\dot{E}^{CH}$	MW	727.36	0.69	8.33	10.33	27.45	17.07	17.07	36.82	733.04	3.73
$\dot{E}^{PH}$	MW	7.73	0.00	259.37	27.14	0.10	68.49	476.01	4.13	2.88	0.00
$\dot{E}^{TOT}$	MW	735.09	0.69	267.70	37.47	27.55	85.56	493.08	40.94	735.93	3.72
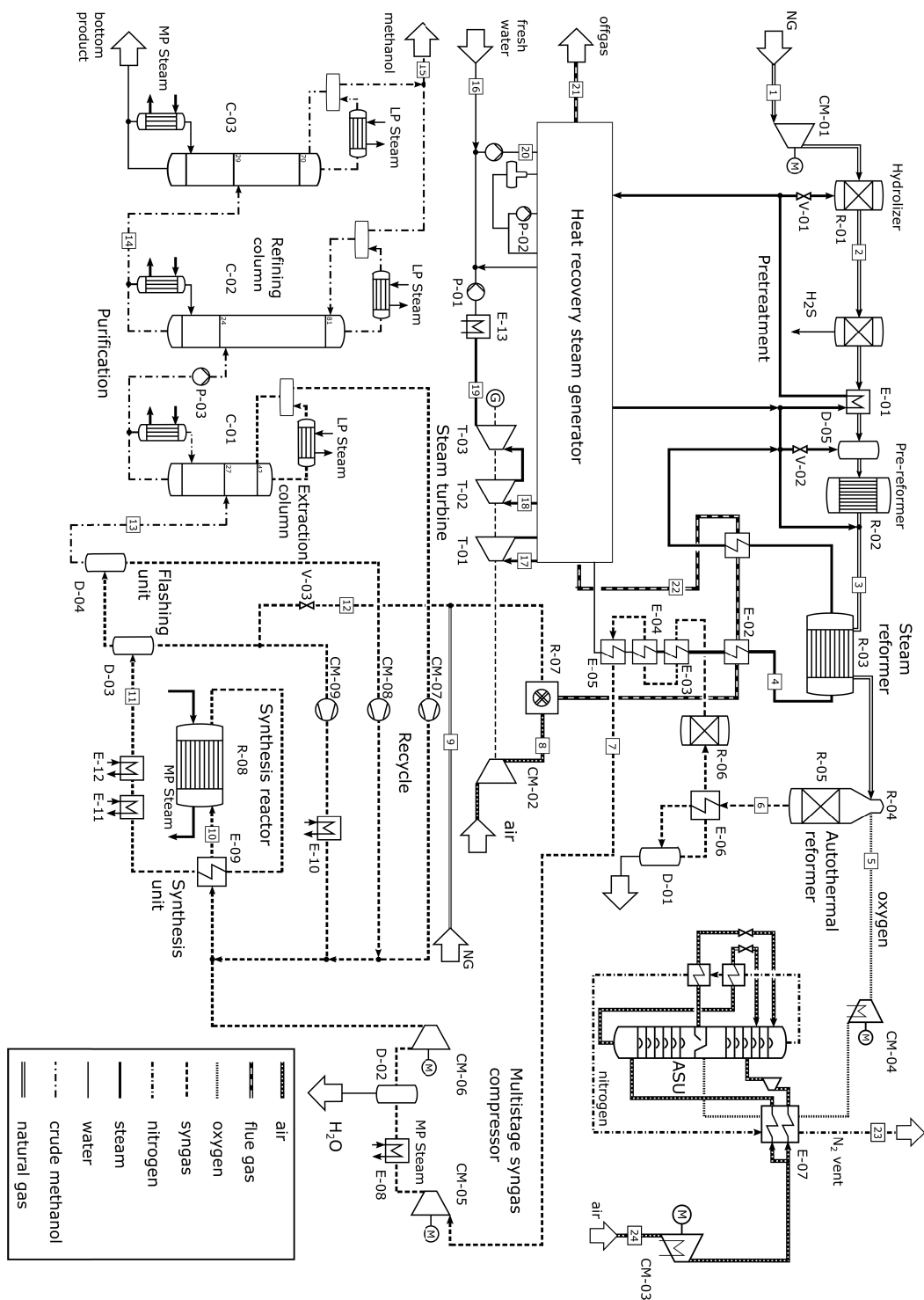
Figure D.5: Process flowsheet of the methanol plant with two-step reforming.

Table D.5: Stream data obtained from the simulation of the SMR-ATR process.

Stream No.		1	2	3	4	5	6	7	8
Temperature	°C	15.00	144.15	734.20	1219.13	273.00	1059.13	150.00	176.43
Pressure	bar	10.00	44.80	37.80	48.50	34.00	31.00	11.15	4.00
Mass flow	kg/sec	43.89	43.91	71.35	61.25	41.85	113.20	93.02	750.11
CO	mole-%	0.00	0.00	0.66	0.00	0.00	25.17	31.03	0.00
CO_2	mole-%	0.70	0.72	0.45	0.00	0.00	2.85	0.78	0.00
H_2O	mole-%	0.00	0.02	35.83	100.00	0.00	12.81	3.46	0.00
H_2	mole-%	0.00	0.00	0.00	0.00	0.00	58.18	63.60	0.00
CH_4	mole-%	94.90	94.86	62.08	0.00	0.00	0.09	0.11	0.00
CH_4O	mole-%	0.00	0.00	0.00	0.00	0.00	0.00	0.00	0.00
$\dot{E}^{CH}$	MW	2165.81	2165.79	2165.67	3.06	4.62	1938.00	1943.08	4.45
$\dot{E}^{PH}$	MW	14.15	25.56	121.72	165.82	14.02	267.01	53.87	111.02
$\dot{E}^{TOT}$	MW	2179.96	2191.35	2287.40	168.88	18.64	2205.01	1996.94	115.47
Stream No.		9	10	11	12	13	14	15	16
Temperature	°C	15.00	250.00	38.00	36.94	38.00	100.88	70.96	15.00
Pressure	bar	4.00	50.57	44.26	4.00	2.00	3.00	1.30	1.01
Mass flow	kg/sec	11.82	323.00	323.19	25.15	71.09	2.74	62.97	27.48
CO	mole-%	0.00	28.55	24.76	27.45	0.00	0.00	0.00	0.00
CO_2	mole-%	0.70	3.13	3.75	4.05	0.66	0.00	0.00	0.00
H_2O	mole-%	0.00	0.20	0.15	0.00	1.52	33.73	0.01	100.00
H_2	mole-%	0.00	63.28	56.93	63.14	0.00	0.00	0.00	0.00
CH_4	mole-%	94.90	0.31	0.37	0.40	0.00	0.00	0.00	0.00
CH_4O	mole-%	0.00	1.37	10.33	0.85	97.80	66.27	99.99	0.00
$\dot{E}^{CH}$	MW	583.10	6396.33	6344.66	478.16	1565.08	47.74	1410.96	1.37
$\dot{E}^{PH}$	MW	2.29	304.12	191.23	6.82	0.24	0.12	12.97	0.00
$\dot{E}^{TOT}$	MW	585.40	6700.45	6535.89	484.98	1565.32	47.86	1423.94	1.37
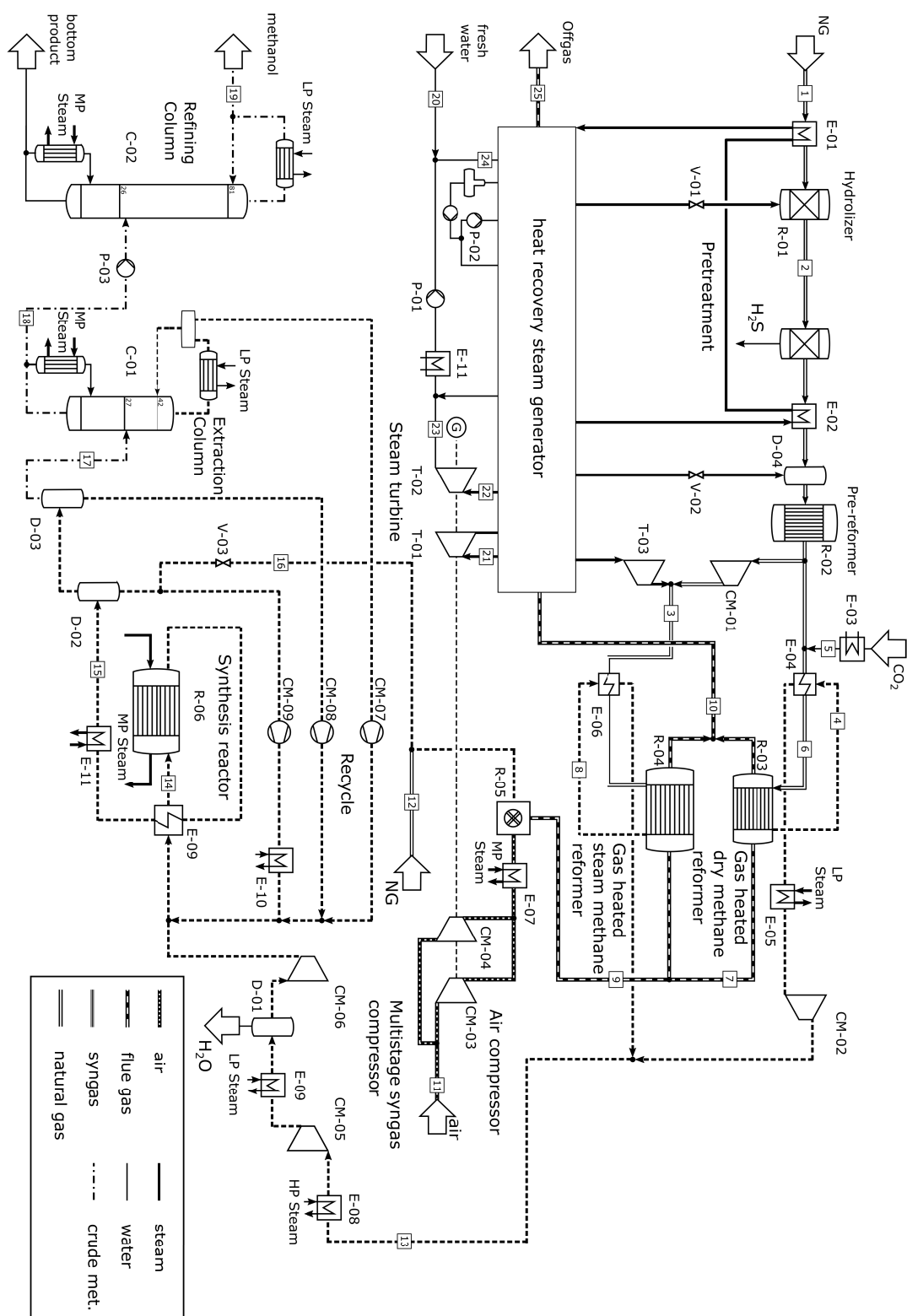
Figure D.6: Process flowsheet of the methanol plant with steam and dry reforming.

Table D.5 continued: Stream data obtained from the simulation of the SMR-ATR process.

Stream No.		17	18	19	20	21	22	23	24
Temperature	°C	600.00	420.00	45.83	21.95	100.00	1170.74	17.79	15.00
Pressure	bar	167.40	45.00	0.10	60.82	1.90	2.44	3.27	1.01
Mass Flows	kg/sec	261.22	325.62	325.62	1062.90	787.09	787.07	133.25	175.12
CO	mole-%	0.00	0.00	0.00	0.00	0.00	0.00	0.00	0.00
CO_2	mole-%	0.00	0.00	0.00	0.00	4.97	4.97	0.00	0.00
H_2	mole-%	100.00	100.00	100.00	100.00	9.84	9.84	0.00	0.00
H_2O	mole-%	0.00	0.00	0.00	0.00	0.00	0.00	0.00	0.00
CH_4	mole-%	0.00	0.00	0.00	0.00	0.00	0.00	0.00	0.00
CH_4O	-mole-%	0.00	0.00	0.00	0.00	0.00	0.00	0.00	0.00
$\dot{E}^{CH}$	MW	13.05	16.27	16.27	53.10	21.08	21.08	3.42	1.04
$\dot{E}^{PH}$	MW	433.86	424.19	65.93	6.83	66.52	729.62	13.34	0.00
$\dot{E}^{TOT}$	MW	446.91	440.46	82.21	59.93	87.6	750.70	16.77	1.04

Table D.6: Stream data obtained from the simulation of the SMR-DMR process.

Stream No.		1	2	3	4	5	6	7	8
Temperature	°C	15.00	155.17	590.12	1050.14	550.00	700.00	1185.15	1098.53
Pressure	bar	10.00	9.70	33.00	7.79	9.20	8.79	3.50	28.99
Mass flow	kg/sec	45.58	45.60	73.77	71.74	59.29	71.74	467.17	73.77
CO	mole-%	0.00	0.00	0.50	52.66	0.00	0.34	0.00	23.62
CO_2	mole-%	0.70	0.72	0.34	6.39	100.00	64.52	4.80	0.46
H_2O	mole-%	0.00	0.02	51.03	14.86	0.00	2.48	8.01	2.98
H_2	mole-%	0.00	0.00	0.00	25.75	0.00	0.00	0.00	71.20
CH_4	mole-%	94.90	94.86	47.37	0.02	0.00	32.14	0.00	1.33
CH_4O	mole-%	0.00	0.00	0.00	0.00	0.00	0.00	0.00	0.00
$\dot{E}^{CH}$	MW	2249.11	2249.09	1687.64	706.89	26.77	585.57	11.57	1963.55
$\dot{E}^{PH}$	MW	14.69	17.36	101.11	89.08	21.90	46.85	447.73	228.06
$\dot{E}^{TOT}$	MW	2263.80	2266.45	1788.74	795.97	48.67	632.42	459.30	2191.61
Stream No.		9	10	11	12	13	14	15	16
Temperature	°C	1184.36	923.83	15.00	15.00	693.57	250.00	38.00	35.03
Pressure	bar	3.50	3.09	1.00	5.00	28.69	50.19	46.43	5.00
Mass flow	kg/sec	2172.88	2172.88	2077.32	27.86	145.52	417.68	417.68	67.79
CO	mole-%	0.00	0.00	0.00	0.00	32.29	62.95	27.91	30.90
CO_2	mole-%	4.80	4.80	0.00	0.70	2.23	21.48	8.72%	9.37%
H_2O	mole-%	8.01	8.01	0.00	0.00	6.52	1.03	0.27	0.01
H_2	mole-%	0.00	0.00	0.00	0.00	57.64	8.12%	50.21%	55.60%
CH_4	mole-%	0.00	0.00	0.00	94.90	0.94	2.10	2.15	2.38%
CH_4O	mole-%	0.00	0.00	0.00	0.00	0.00	2.87%	9.90%	0.80%
$\dot{E}^{CH}$	MW	53.80	53.80	12.32	1374.46	2668.09	7247.54	7188.58	1104.11
$\dot{E}^{PH}$	MW	2080.70	1490.91	0.00	6.28	213.69	337.10	215.63	17.62
$\dot{E}^{TOT}$	MW	2134.50	1544.72	12.32	1380.74	2881.78	7584.63	7404.22	1121.73

Table D.6 continued: Stream data obtained from the simulation of the SMR-DMR process.

Stream No.		17	18	19	20	21	22	23	24	25
Temperature	°C	38.00	77.52	80.38	15.00	503.04	360.00	32.90	24.77	120.00
Pressure	bar	2.00	1.64	1.86	1.01	114.18	14.17	0.05	15.00	1.77
Mass flow	kg/sec	76.43	68.46	65.91	5.00	392.36	589.87	589.87	702.96	2172.88
CO	mole-%	0.00	0.00	0.00	0.00	0.00	0.00	0.00	0.00	0.00
CO_2	mole-%	0.94	0.00	0.00	0.00	0.00	0.00	0.00	0.00	4.80
H_2O	mole-%	2.73	3.03	0.00	100.00	100.00	100.00	100.00	100.00	8.01
H_2	mole-%	0.00	0.00	0.00	0.00	0.00	0.00	0.00	0.00	0.00
CH_4	mole-%	0.00	0.00	0.00	0.00	0.00	0.00	0.00	0.00	0.00
CH_4O	mole-%	96.33	96.97	100.00	0.00	0.00	0.00	0.00	0.00	0.00
$\dot{E}^{CH}$	MW	1664.49	1507.56	1476.91	0.25	19.60	29.47	29.47	35.12	53.80
$\dot{E}^{PH}$	MW	0.26	1.57	15.70	0.00	582.51	653.70	74.20	1.51	153.60
$\dot{E}^{TOT}$	MW	1664.75	1509.13	1492.61	0.25	602.11	683.17	103.66	36.63	207.40

190

Appendix E

Exergetic Analysis

Table E.1: Definitions of the exergetic efficiency for selected components.
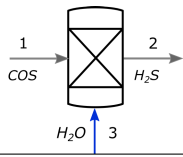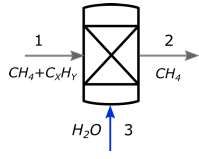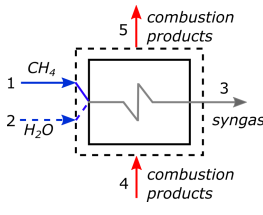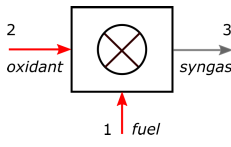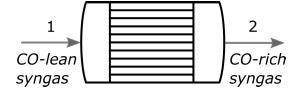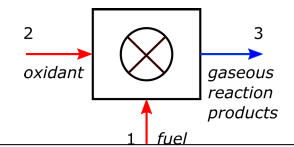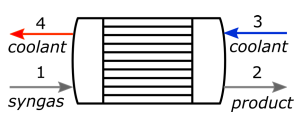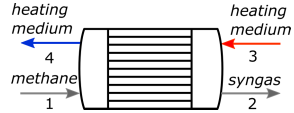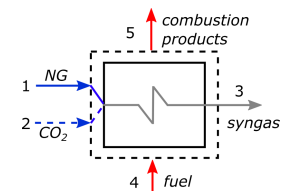
Component	$\dot{E}_\mathrm{F}$	$\dot{E}_\mathrm{P}$
Hydrolizer	$\dot{E}_1^{\mathrm{CH}} - \dot{E}_1^{\mathrm{CH,H_2S}} + \dot{E}_1^{\mathrm{PH}} - \dot{E}_2^{\mathrm{PH}} + \dot{E}_3^{\mathrm{PH}} - (\dot{E}_2^{\mathrm{CH}} - \dot{E}_2^{\mathrm{CH,H_2S}})$	$\dot{E}_2^{\mathrm{CH,H_2S}} - \dot{E}_1^{\mathrm{CH,H_2S}}$
Pre-reformer	$(\dot{E}_1^{\mathrm{CH}} - \dot{E}_1^{\mathrm{CH,CH_4}} - \dot{E}_1^{\mathrm{CH,CO}}) + \dot{E}_1^{\mathrm{PH}} + \dot{E}_3 - \dot{E}_2^{\mathrm{PH}} - (\dot{E}_2^{\mathrm{CH}} - \dot{E}_2^{\mathrm{CH,CH_4}} - \dot{E}_2^{\mathrm{CH,CO}})$	$(\dot{E}_2^{\mathrm{CH,CH_4}} + \dot{E}_2^{\mathrm{CH,CO}}) - (\dot{E}_1^{\mathrm{CH,CH_4}} - \dot{E}_1^{\mathrm{CH,CO}}$
Steam methane reformer	$\dot{E}_1^{\mathrm{CH}} - \dot{E}_1^{\mathrm{CH,CO}} - \dot{E}_1^{\mathrm{CH,CO_2}} - \dot{E}_1^{\mathrm{CH,H_2}} - (\dot{E}_3^{\mathrm{CH}} - \dot{E}_3^{\mathrm{CH,CO}} - \dot{E}_3^{\mathrm{CH,CO_2}} - \dot{E}_3^{\mathrm{CH,H_2}}) + \dot{E}_4^{\mathrm{PH}} - \dot{E}_5^{\mathrm{PH}} + \dot{E}_2$	$\dot{E}_3^{\mathrm{PH}} - \dot{E}_1^{\mathrm{PH}} + \dot{E}_3^{\mathrm{CH,CO}} + \dot{E}_3^{\mathrm{CH,CO_2}} + \dot{E}_3^{\mathrm{CH,H_2}} - \dot{E}_1^{\mathrm{CH,CO}} - \dot{E}_1^{\mathrm{CH,CO_2}} - \dot{E}_1^{\mathrm{CH,H_2}}$
Autothermal reformer combustion zone	$\dot{E}_1^{\mathrm{CH}} - \dot{E}_1^{\mathrm{CH,CO}} - \dot{E}_1^{\mathrm{CH,CO2}} - \dot{E}_1^{\mathrm{CH,H_2}} - \dot{E}_2^{\mathrm{CH}} - (\dot{E}_3^{\mathrm{CH}} - \dot{E}_3^{\mathrm{CH,CO}} - \dot{E}_3^{\mathrm{CH,CO_2}} - \dot{E}_3^{\mathrm{CH,H_2}})$	$\dot{E}_3^{\mathrm{PH}} - \dot{E}_1^{\mathrm{PH}} - \dot{E}_2^{\mathrm{PH}} + \dot{E}_3^{\mathrm{CH}} + \dot{E}_3^{\mathrm{CH,CO}} + \dot{E}_3^{\mathrm{CH,CO_2}} - \dot{E}_1^{\mathrm{CH,CO}} - \dot{E}_1^{\mathrm{CH,CO_2}} - \dot{E}_1^{\mathrm{CH,H2}}$
Autothermal reformer catalytic zone	$(\dot{E}_2^{\mathrm{CH}} - \dot{E}_2^{\mathrm{CH,CO}} - \dot{E}_2^{\mathrm{CH,H_2}} - \dot{E}_2^{\mathrm{CH,CO_2}}) - (\dot{E}_3^{\mathrm{CH}} - \dot{E}_3^{\mathrm{CH,CO}} - \dot{E}_3^{\mathrm{CH,H_2}} - \dot{E}_3^{\mathrm{CH,CO_2}})$	$(\dot{E}_3^{\mathrm{CH,CO}} + \dot{E}_3^{\mathrm{CH,H_2}} + \dot{E}_3^{\mathrm{CH,CO_2}}) - (\dot{E}_1^{\mathrm{CH,CO}} - \dot{E}_1^{\mathrm{CH,H2}} - \dot{E}_1^{\mathrm{CH,CO_2}})$

Table E.1 continued: Definitions of the exergetic efficiency for selected components.

Component	$\dot{E}_F$	$\dot{E}_P$	
Reverse water-gas shift reactor	$(\dot{E}_1^{CH} - \dot{E}_1^{CH,CO}) - (\dot{E}_2^{CH} - \dot{E}_2^{CH,CO}) + \dot{E}_1^{PH} - \dot{E}_2^{PH}$	$\dot{E}_2^{CH,CO} - \dot{E}_1^{CH,CO}$	
Furnace	$\dot{E}_1^{CH} + \dot{E}_2^{CH} - \dot{E}_3^{CH}$	$\dot{E}_3^{PH} - \dot{E}_2^{PH} - \dot{E}_1^{PH}$	
Synthesis reactor	$(\dot{E}_1^M - \dot{E}_2^M) + (\dot{E}_1^{CH} - \dot{E}_1^{CH,CH_3OH}) - (\dot{E}_2^{CH} - \dot{E}_2^{CH,CH_3OH})$	$(\dot{E}_2^T - \dot{E}_1^T) + (\dot{E}_2^{CH,CH_3OH} - \dot{E}_1^{CH,CH_3OH}) + (\dot{E}_4^{PH} - \dot{E}_3^{PH})$	
Heated reformer	$(\dot{E}_1^{CH} - \dot{E}_1^{CH,CO} - \dot{E}_1^{CH,H_2} - \dot{E}_1^{CH,CO_2}) - (\dot{E}_2^{CH} - \dot{E}_2^{CH,CO} - \dot{E}_2^{CH,H_2} - \dot{E}_2^{CH,CO_2}) + \dot{E}_3^{PH} - \dot{E}_4^{PH}$	$(\dot{E}_2^{CH,CO} + \dot{E}_2^{CH,H_2} + \dot{E}_2^{CH,CO_2}) - (\dot{E}_1^{CH,CO} - \dot{E}_1^{CH,H2} - \dot{E}_1^{CH,CO_2}) + \dot{E}_2^{PH} - \dot{E}_1^{PH}$	
Dry reformer	$(\dot{E}_1^{CH} - \dot{E}_1^{CH,CO} - \dot{E}_1^{CH,CO_2} - \dot{E}_1^{CH,H_2}) - (\dot{E}_3^{CH} - \dot{E}_3^{CH,CO} - \dot{E}_3^{CH,CO_2} - \dot{E}_3^{CH,H_2}) + \dot{E}_4^{PH} - \dot{E}_5^{PH} + \dot{E}_2$	$\dot{E}_3^{PH} - \dot{E}_1^{PH} + \dot{E}_3^{CH,CO} + \dot{E}_3^{CH,CO_2} + \dot{E}_3^{CH,H_2} - \dot{E}_1^{CH,CO} - \dot{E}_1^{CH,CO_2} - \dot{E}_1^{CH,H_2}$	

Results of the Exergetic Analysis of the SMR process

Figure E.1: Exergy destruction rate $\dot{E}_D$ for the aggregated subsystems of the SMR process

Table E.1: Results obtained from the conventional exergetic analysis for the aggregated subsystems of the SMR process.

	$\dot{E}_D$ [MW]	y_D[%]	$\dot{E}_L$ [MW]
Pretreatment	7.7	0.33	0.2
Reforming Unit	773.6	33.14	-
Syngas Compression	64.3	2.75	3.1
Synthesis Unit	22.2	0.95	-
Purification	59.1	2.53	46.9
Steam Cycle	401.0	17.18	144.7
Total	1327.9	56.88	194.8

Results of the Exergetic Analysis of the ATR process

Figure E.2: Exergy destruction rate $\dot{E}_D$ for the aggregated subsystems of the ATR process.

Table E.2: Results obtained from the conventional exergetic analysis for the aggregated subsystems of the ATR process.

	$\dot{E}_D$ [MW]	y_D [%]	$\dot{E}_L$ [MW]
Pretreatment	5.3	0.46	0.2
Reforming Unit	237.9	20.79	-
Syngas Compression	27.5	2.41	0.8
Synthesis Unit	34.2	2.99	-
Purification	36.3	3.17	3.8
Steam Cycle	100.2	8.76	35.1
Air Separation	11.8	1.0	
Total	453.2	39.6	39.9

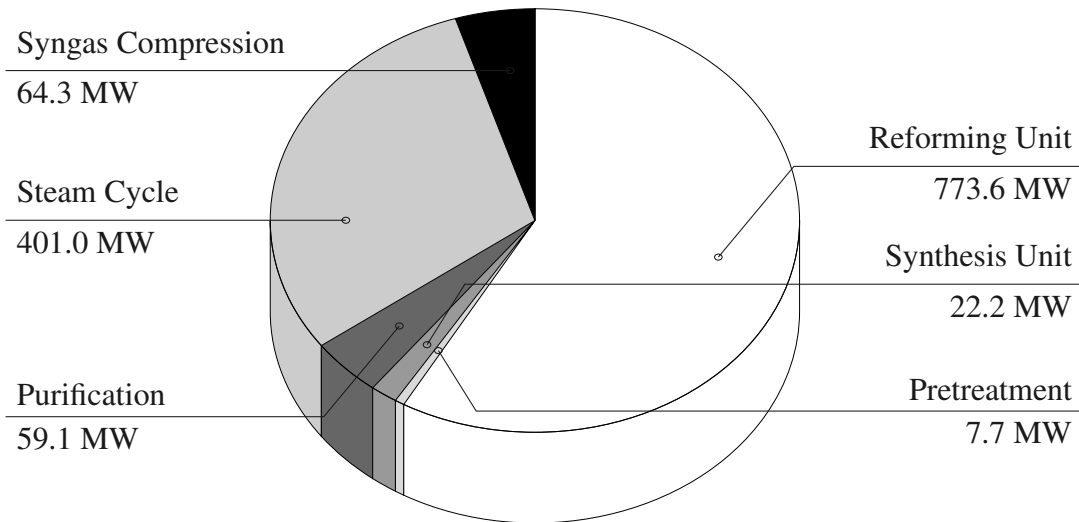# Results of the Exergetic Analysis of the DMR Process

Figure E.3: Exergy destruction rate $\dot{E}_\mathrm{D}$ for the aggregated subsystems of the DMR process.

Table E.3: Results obtained from the conventional exergetic analysis for the aggregated subsystems of the DMR process.

	$\dot{E}_\mathrm{D}$ [MW]	y_D [%]	$\dot{E}_\mathrm{L}$ [MW]
Pretreatment	10.0	0.43	0.3
Reforming Unit	706.7	30.24	-
Syngas Compression	55.5	2.38	0.4
Synthesis Unit	102.73	4.39	-
Purification	28.2	1.21	26.0
Steam Cycle	342.3	14.7	135.6
Total	1245.5	52.13	162.3

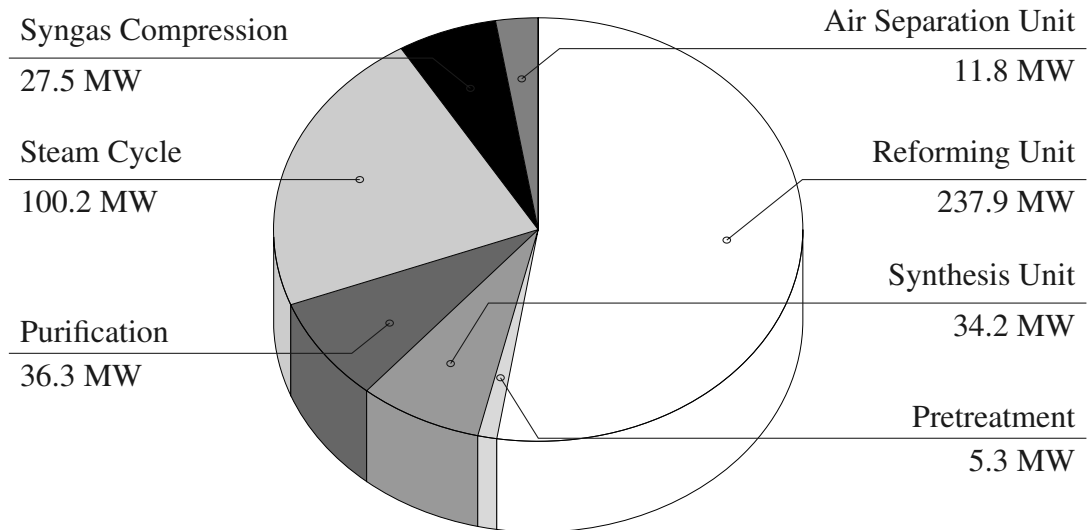# Results of the Exergetic Analysis of the CMR Process

Figure E.4: Exergy destruction rate $\dot{E}_D$ for the aggregated subsystems of the CMR process.

Table E.4: Results obtained from the conventional exergetic analysis for the aggregated subsystems of the CMR process.

	$\dot{E}_D$ [MW]	y_D [%]	$\dot{E}_L$ [MW]
Pretreatment	5.0	0.32	0.2
Reforming Unit	366.5	23.25	-
Syngas Conditioning	18.6	1.18	-
Syngas Compression	39.0	2.52	0.1
Selexol	11.7	0.85	34.8
Synthesis Unit	18.0	1.14	-
Purification	31.3	1.98	36.1
Steam Cycle	163.4	10.37	85.6
Total	653.7	40.06	156.8

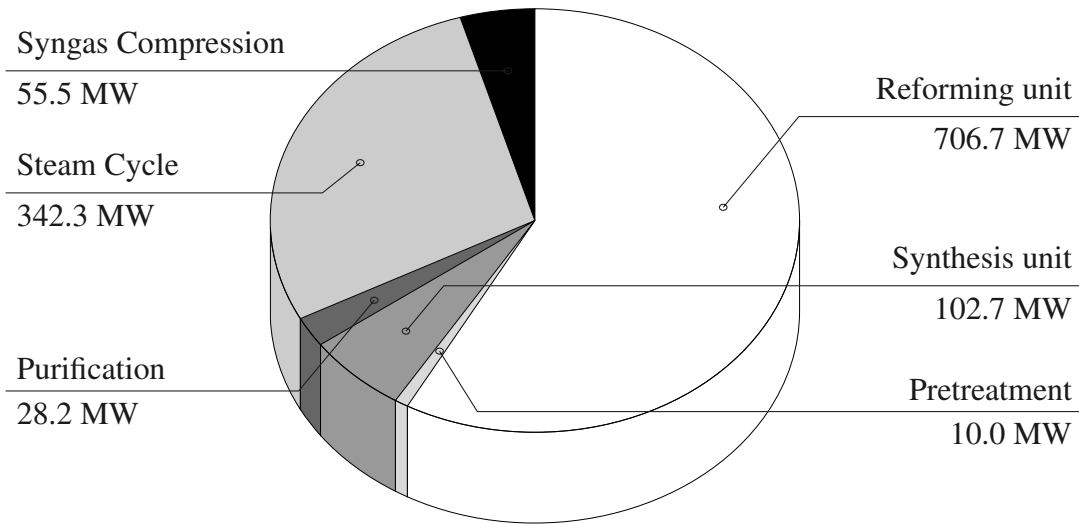# Results of the Exergetic Analysis of the SMR-ATR Process
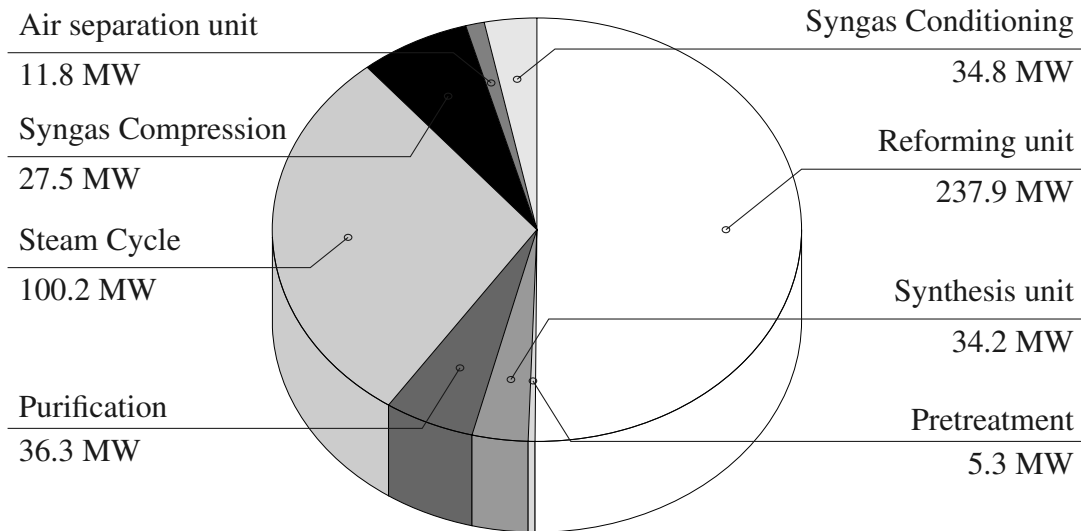
Figure E.5: Exergy destruction rate $\dot{E}_D$ for the aggregated subsystems of the SMR-ATR process.

Table E.5: Results obtained from the conventional exergy analysis for the aggregated subsystems of SMR-ATR process.

	$\dot{E}_D$ [MW]	y_D [%]	$\dot{E}_L$ [MW]
Pretreatment	4.6	0.17	0.4
Reforming Unit	542.8	19.58	-
Syngas Conditioning	34.8	1.26	1.5
Syngas Compression	73.3	2.64	0.2
Synthesis Unit	36.9	1.33	-
Purification	59.7	2.15	12.1
Steam Cycle	319.0	11.5	87.6
Air Separation	12.3	0.44	-
Total	1083.3	39.08	101.8

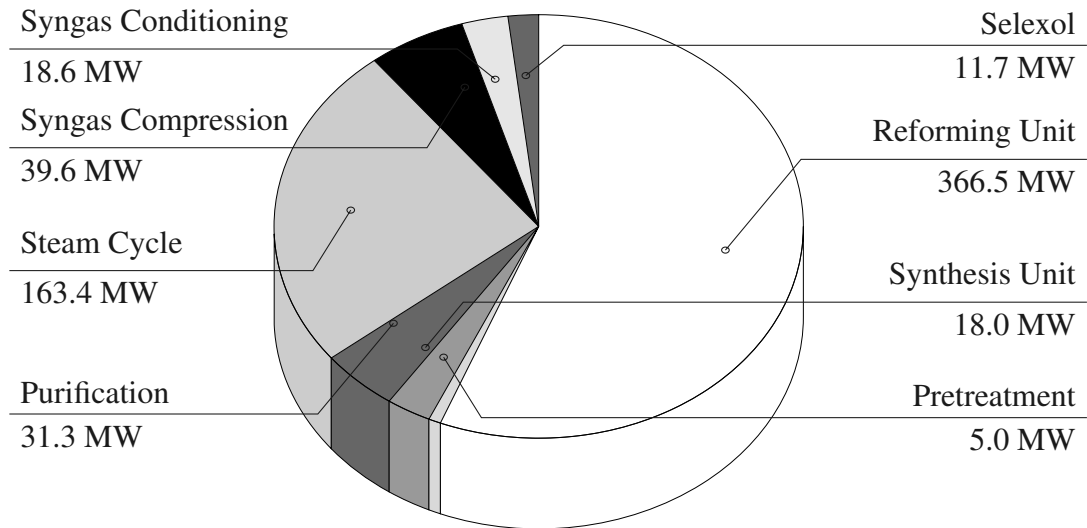# Results of the Exergetic Analysis of the SMR-DMR Process
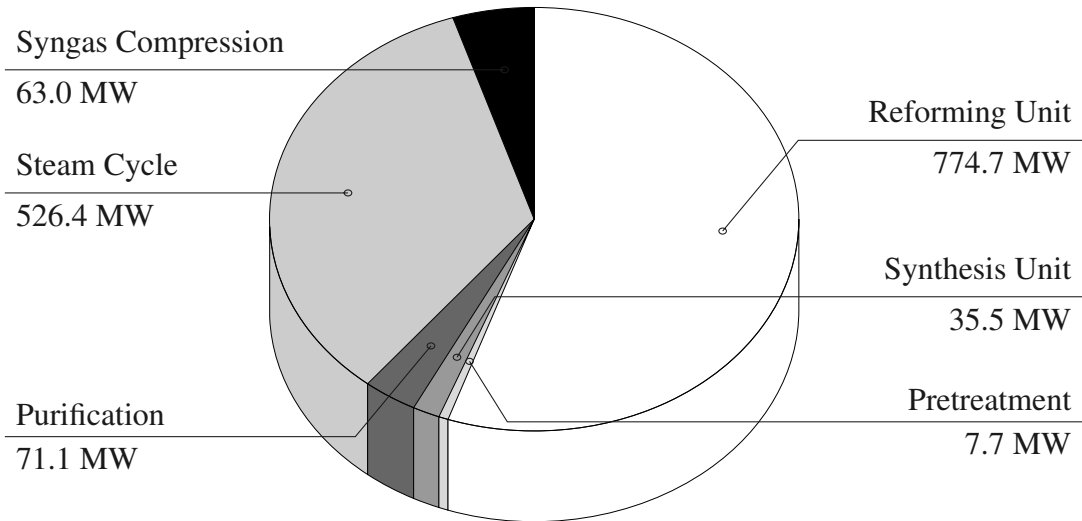
Figure E.6: Exergy destruction rate $\dot{E}_D$ for the aggregated subsystems of the SMR-DMR process.

Table E.6: Results obtained from the conventional exergy analysis for the aggregated subsystems of the SMR-DMR process.

	$\dot{E}_D$ [MW]	y_D [%]	$\dot{E}_L$ [MW]
Pretreatment	10.3	0.28	0.4
Reforming Unit	959.3	26.00	-
Syngas Compression	86.04	2.33	0.7
Synthesis Unit	28.84	0.8	-
Purification	57.6	1.56	38.0
Steam Cycle	593.4	16.08	207.4
Total	1735.5	47	246.5

Appendix F

Advanced Exergetic Analysis

Calculation Algorithm for the Advanced Exergy Analysis

1. Endogenous Exergy Destruction

The endogenous exergy destruction $\dot{E}_{D,k}^{EN}$ is calculated from a set of equations assuming that all components except the k-th component are working with an exergetic efficiency of one.

2. Exogenous Exergy Destruction

$$\dot{E}_{D,k}^{EX} = \dot{E}_{D,k} - \dot{E}_{D,k}^{EN} \tag{F.1}$$

3. Unavoidable Exergy Destruction

$$\dot{E}_{D,k}^{UN} = \dot{E}_{P,k} \cdot \left(\frac{\dot{E}_{D,k}}{\dot{E}_{P,k}} \right)^{UN} \tag{F.2}$$

4. Avoidable exergy destruction

$$\dot{E}_{D,k}^{AV} = \dot{E}_{D,k} - \dot{E}_{D,k}^{UN} \tag{F.3}$$

5. Unavoidable endogenous exergy destruction

$$\dot{E}_{D,k}^{UN,EN} = \frac{\dot{E}_{D,k}^{EN} \cdot \varepsilon_k}{1 - \varepsilon_k} \cdot \left(\frac{\dot{E}_{D,k}}{\dot{E}_{P,k}} \right)^{UN} \tag{F.4}$$

6. Avoidable endogenous exergy destruction

$$\dot{E}_{\mathrm{D},k}^{\mathrm{AV,EN}} = \dot{E}_{\mathrm{D},k}^{\mathrm{EN}} - \dot{E}_{\mathrm{D},k}^{\mathrm{UN,EN}} \tag{F.5}$$

7. Avoidable exogenous exergy destruction

$$\dot{E}_{\mathrm{D},k}^{\mathrm{AV,EX}} = \dot{E}_{\mathrm{D},k}^{\mathrm{AV}} - \dot{E}_{\mathrm{D},k}^{\mathrm{AV,EN}} \tag{F.6}$$

8. Unavoidable exogenous exergy destruction

$$\dot{E}_{\mathrm{D},k}^{\mathrm{UN,EX}} = \dot{E}_{\mathrm{D},k}^{\mathrm{UN}} - \dot{E}_{\mathrm{D},k}^{\mathrm{UN,EN}} \tag{F.7}$$

Component Results for the SMR-ATR Process

Table F.1: Results obtained from the conventional and the advanced exergetic analyses for selected component groups.

| | Conventional Exergy Analysis | | | | | Advanced Exergy Analysis | | | |
	$\dot{E}_D$ [MW]	$\dot{E}_F$ [MW]	$\dot{E}_P$ [MW]	y_D [%]	ε [%]	$\dot{E}_D^{UN}$ [MW]	$\dot{E}_D^{AV}$ [MW]	$\dot{E}_D^{EN}$ [MW]	$\dot{E}_D^{EX}$ [MW]
R-01	0.05	0.47	0.42	0.0	88.8	0.02	0.03	0.03	0.02
R-02	2.72	115.92	113.20	0.1	97.7	2.68	0.04	1.64	1.08
R-03	5.93	141.98	136.06	0.2	95.8	3.03	2.90	3.59	2.34
R-04	146.48	2087.82	1941.35	5.3	93.0	145.0	1.48	93.36	53.12
R-05	0.66	1.08	0.41	0.0	38.6	0.01	0.65	0.40	0.26
R-06	1.49	58.24	56.75	0.1	97.4	0.28	1.21	0.90	0.59
R-07	358.04	1044.63	686.59	12.9	65.7	139.8	61.9	108.4	47.96
R-08	1.36	1545.53	1544.17	0.1	99.9	1.16	0.2	1.3	0.06
E-01	3.33	48.89	45.56	0.1	93.2	1.20	2.13	2.01	1.32
E-02	4.91	58.99	54.08	0.2	91.7	2.46	2.45	2.97	1.94
E-03	14.17	59.28	45.11	0.5	76.1	9.21	4.96	8.60	5.57
E-04	23.18	84.32	61.14	0.8	72.5	14.68	8.50	14.11	9.07
E-05	1.20	5.02	3.81	0.0	76.0	0.65	0.55	0.73	0.48
E-06	28.85	175.18	146.33	1.0	83.5	13.07	15.77	17.60	11.25
E-07	0.84	21.13	20.29	0.0	84.1	0.84	0.00	0.83	0.01
E-08	12.41	17.87	5.46	0.5	30.6	10.31	2.10	7.53	4.89
E-09	4.85	21.66	16.81	0.2	77.6	0.12	4.73	2.93	1.92
E-10	2.31	17.30	14.99	0.1	86.7	0.56	1.74	1.39	0.91
E-11	19.42	51.66	32.24	0.7	62.4	5.74	13.68	11.81	7.61
E-12	1.27	2.93	1.66	0.1	56.6	0.34	0.93	0.77	0.50
E-13	5.26	18.11	12.85	0.2	71.0	1.15	4.11	3.18	2.08
LP-ECO	7.25	3.02	4.23	0.2	41.7	3.44	0.78	2.56	1.76
LP-EVA	41.56	27.72	13.84	0.5	66.7	8.73	5.11	8.40	5.44
LP-SH	18.21	13.79	4.42	0.2	75.7	4.70	0.28	2.67	1.75
HP-ECO	176.76	143.93	32.83	1.2	81.4	15.39	17.44	20.06	12.77
HP-EVA	139.51	103.87	35.65	1.3	74.5	4.32	31.32	21.80	13.85
HP-SH	220.19	161.60	58.60	2.1	73.4	17.90	40.69	36.14	22.46
RH	41.42	30.08	11.34	0.4	72.6	1.13	36.80	6.88	4.47
T-01	4.90	105.19	100.29	0.2	95.4	3.37	1.53	2.96	1.94
T-02	11.82	196.59	184.77	0.4	94.0	8.83	2.99	7.17	4.65
T-03	13.28	161.73	148.45	0.5	91.8	8.51	4.77	8.05	5.22

Table F.1 continued: Results obtained from the conventional and the advanced exergetic analyses for selected component groups of the SMR-ATR process.

| | Conventional Exergy Analysis | | | | | Advanced Exergy Analysis | | | |
| | $\dot{E}_\mathrm{D}$ | $\dot{E}_\mathrm{F}$ | $\dot{E}_\mathrm{P}$ | y_D | ε | $\dot{E}_\mathrm{D}^\mathrm{UN}$ | $\dot{E}_\mathrm{D}^\mathrm{AV}$ | $\dot{E}_\mathrm{D}^\mathrm{EN}$ | $\dot{E}_\mathrm{D}^\mathrm{EX}$ |
	[MW]	[MW]	[MW]	[%]	[%]	[MW]	[MW]	[MW]	[MW]
CM-01	1.18	12.60	11.42	0.0	90.7	0.81	0.37	0.71	0.47
CM-02	13.42	124.45	11.04	0.5	89.2	7.47	5.95	8.14	5.28
CM-03	9.40	36.44	27.04	0.0	74.2	4.37	5.03	4.77	4.63
CM-04	0.93	10.19	9.26	0.0	90.9	0.53	0.40	0.56	0.37
CM-05	1.73	26.03	24.31	0.1	93.4	1.39	0.34	1.04	0.68
CM-06	3.52	52.38	48.86	0.1	93.3	2.83	0.69	2.13	1.39
CM-07	0.21	3.57	3.36	0.0	94.1	0.16	0.05	0.13	0.08
CM-08	0.02	0.27	0.25	0.0	94.2	0.01	0.01	0.01	0.01
CM-09	1.37	12.85	11.48	0.1	89.3	0.98	0.39	0.83	0.54
P-01	0.40	2.48	2.08	0.0	84.1	0.29	0.11	0.24	0.16
P-02	0.68	4.73	4.05	0.0	85.6	0.35	0.33	0.41	0.27
P-03	0.00	0.02	0.02	0.0	87.1	0.00	0.00	0.00	0.00
D-01	3.97	29.12	25.14	0.1	86.4	3.97	0.00	3.97	0.00
D-02	17.01	2003.38	1986.37	0.6	99.2	17.01	0.00	17.01	0.00
D-03	0.00	12.57	12.57	0.0	99.9	0.00	0.00	0.00	0.00
D-04	0.14	0.51	0.37	0.0	72.6	0.14	0.00	0.14	0.00
C-01	13.50	16.15	2.65	0.5	16.4	1.47	12.03	8.19	5.13
C-02	35.98	52.28	16.30	1.3	31.2	6.57	29.41	22.00	13.97
C-03	1.40	1.81	0.41	0.1	20.5	0.64	0.76	0.85	0.55

$\dot{E}_\mathrm{F,Tot} = 2772.2$